EFFECTS OF AMBIENT CROSSFLOWS AND DENSITY STRATIFICATION ON THE CHARACTERISTIC BEHAVIOR OF ROUND, TURBULENT BUOYANT JETS

Thesis by

Steven Jay Wright

In Partial Fulfillment of the Requirements

for the Degree of

Doctor of Philosophy

California Institute of Technology

Pasadena, California

1977

(Submitted May 17, 1977)

ACKNOWLEDGMENTS

I hardly know where to begin. To acknowledge everyone who helped me out at critical points would be difficult, if not impossible. This is especially true since I may not realize how much the help of others has contributed to my reaching this point. Let me try anyway.

Even though I have thanked him many times, I would like to take this opportunity to acknowledge the efforts of Dr. John Roberson on my behalf. It was at his suggestion that I first decided to apply to Caltech, so I can truly say that without him, I would not be here today.

I would also like to recognize the efforts of Dr. Norman Brooks, especially in helping to turn this manuscript into something readable. I just hope that I can do as much for someone else sometime in the future. It was also Dr. Brooks' suggestion that I pursue this area of research and he provided the impetus for my getting started in the right direction.

At the time that many of the ideas presented in this manuscript were only halfway thought out, several valuable discussions with Dr. E. John List helped me to understand the problem. These discussions, class lectures, and an unpublished manuscript were helpful in providing the framework on which my understanding of the research was developed. Without Dr. List's guidance, it is safe to say that this research would be incomplete.

I also want to thank Dr. Fredric Raichlen for his help and interest at various stages of my research. In particular, he helped me to get started developing the light probe, and this help is greatly appreciated.

There are, of course, many others whose general comments and advice helped me out along the way. I would especially like to recognize Greg Gartrell, Phil Roberts, and Bob Koh for the contributions that they made to this research.

The National Science Foundation supported this research under Grant Numbers GK-35774X and ENG 75-02985. This financial support is greatly appreciated along with the assistance from the California Institute of Technology, both in the form of research facilities and financial support. The laboratory experiments could not have been performed without the help of several individuals. Elton Daly and Joe Fontana had to turn my half-completed sketches into final products, and their ability to do so never ceased to amaze me. In addition, Elton taught me enough along the way so that it will be easier for me to develop laboratory experiments in the future. Several others helped out during the course of the experiments including Linda Figueroa, Bob Shultz, Dave Byrum, and Rich Eastvedt. It makes me realize just how dependent on others I was just to list those names.

Then there was the preparation of the manuscript. I would like to especially thank Joan Mathews for her patience and ability in deciphering the material that I gave to her and putting it in a presentable form. The same goes for Dave Byrum with respect to the drafting of the figures. Adelaide Massengale also assisted in the preparation of the manuscript.

Finally, I would like to acknowledge the efforts of two special people who helped me so much, especially in getting through the difficult times. Vito Vanoni was a constant source of encouragement to me and there were times that I really needed encouragement. Some of his enthusiasm for his profession and life in general rubbed off along the way and I am grateful for the interactions that I had with Vito. I am

also grateful for the support and patience of my wife, Dayle. There were difficult times and times when I have been very busy, and I am afraid that I have neglected her in those situations. Now it's her turn to do the same to me as she begins work on her degree. So I expect a similar acknowledgment a few years from now.

ABSTRACT

This investigation considers a round, turbulent buoyant jet in an ambient crossflow that is either of uniform density or with a linear density stratification. The primary emphasis is the development of a fundamental understanding of the jet properties that are of interest in engineering design problems. These include jet trajectories, characteristic dilutions, and in the case of a stratified crossflow, the maximum and equilibrium heights of rise.

Most previous studies of similar buoyant jet flows have used the integral method to solve for the jet characteristics. This approach requires an assumed relation for the rate of entrainment of ambient fluid by the jet, and also depends upon experimental evidence to estimate values for the coefficients in the assumed relation. Most previous experimental studies have been directed toward evaluating entrainment coefficients and have not considered a systematic investigation of the effects of the various jet and ambient flow parameters.

A major objective of this investigation is to provide a basis for the interpretation and extension of the results from previous theoretical and experimental investigations. A systematic dimensional analysis is performed to define the basic problem and to provide approximate solutions without using the integral equations. The analysis indicates the types of experiments necessary to adequately describe general buoyant jet behavior and also provides a framework for the presentation of experimental data.

The approximate solutions for the jet characteristics were derived from the dimensional analysis by considering asymptotic descriptions of a general buoyant jet as different effects become predominant in determining the flow behavior. The limiting cases considered are for the jet behavior controlled by either its initial momentum or by its buoyancy for situations where the ambient velocity either is relatively large or approaches zero. Combinations of these four asymptotic descriptions can be used to approximately describe a general buoyant jet. Several different types of flow behavior can be expected, depending upon the relative magnitudes of various characteristic length scales associated with these buoyant jet flows. These different types of flow can be compared to the theoretical solutions proposed by other researchers, providing a basis for better understanding previous research.

Experiments were performed to confirm the asymptotic relations developed in the analysis, to evaluate the coefficients in the relations, and to determine the limits of their applicability. The experimental configuration was a salt water jet discharged downward into a tank of less dense fluid with either uniform density or linear density stratification. The Boussinesq approximation implies that these results will be comparable to a buoyant jet rising in a less dense ambient fluid. The crossflow was simulated by towing the jet source along the water surface in the tank.

Jet trajectories and dilutions were measured for the experiments with an unstratified crossflow. For the experiments performed with

the tank stratified, maximum and equilibrium heights of rise, a few trajectories, and jet dilutions were measured. The results of these various experimental measurements are presented in a unified manner to facilitate the application to design problems.

The experimental evidence indicated that the coefficients in the asymptotic relations were somewhat dependent upon the initial jet volume flux, an observation that has not been previously noted by other researchers. This variation can be expected from the dimensional analysis and is shown to be significant in some instances.

TABLE OF CONTENTS

TABLE OF CONTENTS (Continued)

TABLE OF CONTENTS (Continued)

LIST OF FIGURES

LIST OF FIGURES (Continued)

LIST OF FIGURES (Continued)

LIST OF FIGURES (Continued)

LIST OF FIGURES (Continued)

LIST OF FIGURES (Continued)

LIST OF TABLES

NOTATIONS

b	buoyant impulse of a buoyant thermal; $b = B/U_A$ in analogy to jet flow
B	kinematic buoyancy flux; $B = g_o' Q$
c	time-averaged tracer concentration at a point in the flow field
C	characteristic time-averaged tracer concentration at a jet cross-section, $C = C_m$ for the purposes of this study
C_a	ambient tracer concentration
C_d	drag coefficient
C_m	time-averaged maximum tracer concentration measured at a jet cross-section in the vertical plane of jet symmetry
C_{max}	instantaneous maximum tracer concentration at a point in the flow field
C_o	tracer concentration in jet discharge
C_i	(i = 1,16) various experimental constants defined in Chapter 3
D	diameter of jet at source
E	entrainment function
F	source Froude number $F = V_j/\sqrt{g_o' D}$
F_d	drag force
F_ℓ	local characteristic Froude number $F_\ell = U_s/\sqrt{GR}$
g	gravitational constant
G	characteristic value of g' at a jet cross-section
g'	local apparent gravity $g' = g(\rho_a - \rho)/\rho_o$
g_o'	value of g' at jet source $g_o' = g(\rho_{a_o} - \rho_j)/\rho_o$
I	intermittency function
ℓ_a	length scale describing wavelength of oscillations in a stratified crossflow $\ell_a = U_A/\varepsilon^{1/2}$

NOTATIONS (Continued)

ℓ_b	buoyancy length scale $\ell_b = B/U_A^3$
ℓ_b'	length scale describing height of rise of a plume in a stagnant, stratified fluid $\ell_b' = (B/\varepsilon^{3/2})^{1/4}$
ℓ_m	momentum length scale $\ell_m = M/U_A^{1/2}$
ℓ_m'	length scale describing height of rise of a nonbuoyant jet in a stagnant, stratified fluid $\ell_m' = (M/\varepsilon)^{1/4}$
ℓ_M	length scale at which momentum generated by buoyancy becomes comparable to initial momentum $\ell_M = M^{3/4}/B^{1/2}$
ℓ_Q	length scale over which effect of initial volume flux is lost $\ell_Q = Q/M^{1/2}$
m	momentum impulse of a momentum puff; $m = M/U_A$ in analogy to jet flow
M	kinematic momentum flux $M = V_j Q$
Q	volume discharge or kinematic mass flux $Q = \frac{\pi}{4} D^2 V_j$
R	characteristic jet radius at a cross-section
R_e	jet source Reynolds number $R_e = V_j D/\nu$
s	coordinate tangential to jet axis
S	tracer dilution ($S = C_o/c$) at a point in the flow field
S_e	characteristic tracer dilution at equilibrium position of jet in a stratified flow
S_m	characteristic tracer dilution at maximum height of jet rise in a stratified flow $S_m = C_o/C_m$
S_o	characteristic tracer dilution at a jet section $S_o = C_o/C_m$
T	time-averaged temperature at a point in the flow field
T_a	temperature of ambient fluid
U_A	ambient crossflow velocity
u_r	radial jet velocity
u_s	axial jet velocity

NOTATIONS (Continued)

U_s	characteristic axial jet velocity
V	characteristic vertical jet velocity (in z direction)
V_e	entrainment velocity $V_e = E/R$
V_j	jet source velocity
V_{max}	maximum jet velocity at a jet cross-section
x	horizontal coordinate; distance downstream from jet source
x_m	horizontal distance between jet source and maximum height of rise
z	vertical coordinate; vertical distance from jet source
Z_e	equilibrium height of jet rise in a stratified fluid
Z_m	maximum height of jet rise in a stratified fluid
$\alpha, \alpha_1, \alpha_2$	entrainment coefficient
ε	stratification parameter $\varepsilon = \frac{-g}{\rho_o} \frac{d\rho_a}{dz}$
λ	characteristic volume per unit length of a thermal or puff; $\lambda = \mu/U_A$ in analogy to jet flow
λ_m	characteristic value of λ at maximum height of rise $\lambda_m = \mu_m/U_A$
μ	characteristic volume flux at a jet cross-section
μ_m	characteristic volume flux at maximum height of rise
ϕ	a term representing a general dependent variable such as R, μ, V_{max}, etc.
ϕ^*	dimensionless form of ϕ
θ	angle between jet axis and horizontal
τ	time scale associated with stratification; $\tau = \varepsilon^{-1/2}$
ρ	fluid density at a point in the flow field
ρ_a	ambient fluid density
ρ_{a_o}	ambient fluid density at elevation of jet discharge
ρ_j	fluid density in jet discharge

NOTATIONS (Continued)

ρ_o reference density; $\rho_o = \rho_{a_o}$ for the purposes of this study

$\Delta\rho$ density difference; $\Delta\rho = \rho_a - \rho$

superscripts:

$\overline{}$ time-averaged mean value

$'$ fluctuating component

CHAPTER 1

INTRODUCTION

Pollutants are often introduced into the environment as trace species in a fluid medium. Examples of this include the release of bacteria in a sewage discharge, heat in the cooling water from a power plant, and sulfur dioxide in the exhaust gases from industrial combustion processes. One method of dealing with these contaminants is to release them in such a manner that the discharge mixes sufficiently with the ambient fluid so that contaminant concentrations are reduced to relatively small values. A major means of accomplishing this objective is to discharge the fluid containing the contaminant as a turbulent buoyant jet. The initial jet mixing is expected to provide sufficient dilution so that pollutant concentrations are lowered below undesirable or toxic levels. Examples of buoyant jet discharges include smoke plumes from industrial chimneys and sewage wastewater through an ocean outfall diffuser.

Pollution control standards often specify a maximum allowable concentration of a given pollutant at some distance from the source. For example, California thermal standards require that any heated discharge produce a temperature rise not greater than four degrees F beyond 1000 feet from the diffusion structure for more than 50% of any day.[1] Design of a jet discharge structure to meet this or similar requirements thus

---

[1] State Water Resources Control Board, Sacramento, California, "Water Quality Control Plan for Control of Temperature in Coastal and Interstate Waters and Enclosed Bays and Estuaries of California," 8 pp., May 18, 1972.

requires a satisfactory understanding of the jet mixing process in order to ensure compliance with existing regulations.

Buoyant jets in a stagnant ambient fluid are reasonably well understood. Predictive models of the type given by Fan and Brooks (1969), Abraham (1965), and others, can be used to obtain adequate estimates of mean jet behavior such as rate of spread, dilution, etc. However, when the ambient fluid itself is in motion, the problem becomes more complicated. Typically, most receiving fluids such as the atmosphere or ocean exhibit wind or current patterns and also often possess nonuniform density structure. Failure to include these effects may result in substantial error in the analysis of buoyant jet behavior. The presence of ambient currents or density stratification may be significant in some instances in meeting design objectives. For example, the presence of density stratification in the ocean can prevent a sewage discharge from rising to the surface and an ambient current will remove the submerged sewage field from the vicinity of the diffuser preventing the buildup of pollutant concentrations. In contrast to this situation, a density gradient in the atmosphere can prevent smoke from an industrial source from rising a significant distance and may result in relatively high ground level concentrations of contaminants. The design of adequate pollutant discharge structures thus requires an adequate understanding of the complex interaction of a buoyant jet discharge with the ambient fluid.

The present investigation was directed toward obtaining a more thorough understanding of the behavior of a general buoyant jet in an

ambient crossflow with either a uniform density or a linear density stratification. The specific problem considered was the discharge of a vertical, turbulent buoyant jet into a horizontally flowing ambient fluid. This flow is similar to smoke plumes in the atmosphere and other point source discharges.

The major objective of this study was to develop a straightforward method of applying experimental results to design purposes. The jet characteristics of interest in many applications include jet trajectories, dilutions, and in the case of a stratified flow, the maximum or equilibrium heights of rise. Many previous theoretical and experimental investigations have been conducted to study buoyant jet trajectories in an unstratified crossflow, but the results are inconclusive since no systematic examinations of these buoyant jet flows have been performed. One of the study objectives was to make a comprehensive evaluation of buoyant jet trajectories to provide a basis for interpreting these previous experimental and theoretical studies. Another objective was a detailed examination of characteristic dilutions along the jet trajectory. An additional objective was to examine general buoyant jet behavior in a stratified crossflow as there have been essentially no experimental studies of this type.

Chapter 2 presents a review of previous theoretical and experimental investigations that are related to the present study. These include the study of buoyant jets in a stagnant ambient fluid with a linear density stratification and jets in an unstratified crossflow. The various methods of analysis and the resulting solutions are

described in this chapter.

The general problem is analyzed in Chapter 3. A systematic dimensional analysis is performed to define the problem and to provide approximate solutions describing the jet characteristics. These approximate solutions are only valid for limiting cases where certain effects control the flow behavior. These various asymptotic solutions can be combined to provide approximate descriptions of general jet behavior. The correct combination of solutions depends upon the relative magnitudes of several length scales associated with jet flows. The overall flow description is used to interpret the predictions from previous theoretical studies.

Chapter 4 is a description of the experimental apparatus and procedure. Several different types of measurements were made in this investigation and these are discussed in detail in this chapter. The experimental study included a detailed examination of buoyant jet trajectories, dilutions, and heights of rise. A limited examination of the turbulent mixing process within a buoyant jet was also conducted.

The results from the experimental investigation are presented and discussed in Chapter 5. This includes an evaluation of the coefficients in the asymptotic relations developed in Chapter 3. This evaluation provides a method for the unified presentation of the experimental results and a straightforward application to design problems.

Chapter 6 is a general discussion of the results of this investigation. This includes a comparison of the experimental results to previous studies, suggestions for future research, and a presentation

of figures intended to be used as design curves. These figures were developed from the asymptotic solutions presented in Chapter 3 and the coefficients determined from the experimental investigation.

CHAPTER 2

REVIEW OF PREVIOUS STUDIES

Previous investigations of buoyant jets have generally considered cases of ambient density stratification without a crossflow or of a crossflow in a uniform density ambient fluid. They have been primarily concerned with predicting jet trajectories for the case of an ambient crossflow and heights of rise for jets in a nonflowing stratified fluid. Experimental studies have also concentrated on the measurement of these quantities.

2.1 Methods of Solution

There are basically three approaches to the solution of buoyant jet problems. Early attempts at solving simple jet problems consisted of specifying constitutive relations for the turbulent transport terms in the equations for the conservation of mass, momentum, energy, and tracer. Examples of this approach may be seen in Schlichting (1968), but this method has not been generally considered for the solution of more complex problems involving ambient currents and density stratification. Another approach has been to derive relations for mean flow properties from dimensional analysis of the given problem. This method has also been restricted to fairly simple problems which have only a few independent variables characterizing the flow. The other procedure has been to consider the integrated conservation equations mentioned above. This approach consists of integrating the equations across a section normal to the jet trajectory and assuming that all turbulent transport terms

vanish at the jet boundary. This so-called "integral method" was proposed by Morton, Taylor, and Turner (1956) and has become the accepted method of solution in recent years.

Several variations of the general equations have been given depending upon the flow geometry and the ambient conditions. A thorough discussion of the development of the general equations for a buoyant jet in a density-stratified crossflow is given by Hirst (1971a). The equations are typically written with a coordinate system that is oriented tangential to the jet axis as indicated schematically in Fig. 2.1. The flow is assumed to be axisymmetric about the tangential s-axis with a radial coordinate r. This coordinate system is related to the (x,z) coordinate system by the geometrical relations:

$$\frac{dx}{ds} = \cos\theta \tag{2.1}$$

$$\frac{dz}{ds} = \sin\theta \tag{2.2}$$

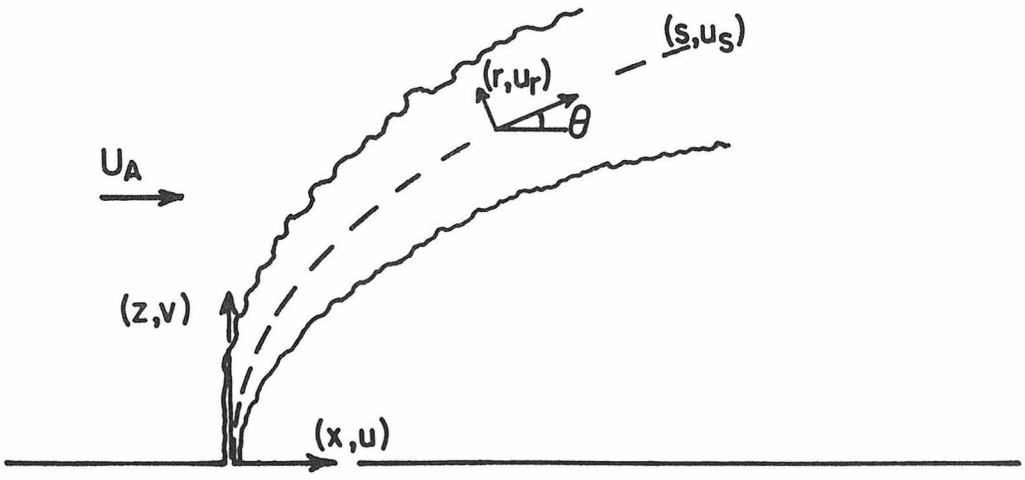

Fig. 2.1 Definition sketch of (s,r) and (x,z) coordinate system.

The coordinate x is in the direction of the ambient current and z is the vertical coordinate in the same direction as the buoyancy forces.

Several assumptions are generally employed in the description of the general problem. The flow is assumed to be steady and axisymmetric and it is further assumed to be completely turbulent such that molecular transports can be neglected with respect to turbulent transports. The fluid is assumed to be incompressible and the Boussinesq approximation is made, i.e., the difference between the fluid density at any point in the flow field and a reference density (e.g., the density of the ambient fluid at the level of the jet source) is important only as a buoyancy force. It is also generally assumed that the curvature of the jet is small and that the effects of the curvature can be neglected. The pressure variation in the flow field is assumed to be hydrostatic and boundary layer approximations are made; i.e., gradients in the tangential (s) direction are much smaller than those in the radial (r) direction. This approximation also implies that the tangential velocity u_s is much greater than the radial velocity u_r. The Reynolds type of equations are used in the analysis; all terms are written in terms of mean and fluctuating values. It is generally assumed that the turbulent tracer transport $\overline{u_s'c'}$ and heat transport $\overline{u_s'T'}$ are negligible with respect to the mean transports, $\overline{u_s c}$ and $\overline{u_s T}$ respectively, of the same quantities. Here the primes indicate fluctuating quantities, the unprimed terms represent mean quantities, c denotes concentration of a tracer, and T is the temperature. Finally, it is assumed that the turbulent momentum transport $\overline{u_s'^2}$ is much less than the mean velocity transport $\overline{u_s^2}$. Given the above approximations, the conservation

equations can be written as follows:

Mass

$$\frac{\partial u_s}{\partial s} + \frac{1}{r}\frac{\partial}{\partial r}(ru_r) = 0 \tag{2.3}$$

Vertical Momentum

$$\left(u_s \frac{\partial u_s}{\partial s} + u_r \frac{\partial u_s}{\partial r}\right) \sin\theta = g \frac{\rho_a - \rho}{\rho_o} - \frac{1}{r}\frac{\partial}{\partial r}(r\overline{u_s' u_r'})\sin\theta \tag{2.4}$$

Horizontal Momentum

$$\left(u_s \frac{\partial u_s}{\partial s} + u_r \frac{\partial u_s}{\partial r}\right) \cos\theta = -\frac{1}{r}\frac{\partial}{\partial r}(r\overline{u_s' u_r'})\cos\theta \tag{2.5}$$

Heat

$$u_s \frac{\partial T}{\partial s} + u_r \frac{\partial T}{\partial r} = -\frac{1}{r}\frac{\partial}{\partial r}(r\overline{u_r' T'}) \tag{2.6}$$

Tracer

$$u_s \frac{\partial c}{\partial s} + u_r \frac{\partial c}{\partial r} = -\frac{1}{r}\frac{\partial}{\partial r}(r\overline{u_r' c'}) \tag{2.7}$$

Equations of state are also required to relate temperature and tracer concentration to fluid density if it is assumed that either effect causes significant variations in fluid density. The typical assumption is to assume a linear relationship between density and either temperature or tracer concentration:

$$\frac{\rho-\rho_a}{\rho_o} = k_1(c-c_a) + k_2(T-T_a) \tag{2.8}$$

The subscript a refers to properties in the ambient fluid, and ρ_o is some reference density such as the density of the ambient fluid at the level of the jet source. This relation can be combined with Eqs. 2.6 and 2.7 to yield an equation for the conservation of buoyancy or density deficiency:

$$u_s \frac{\partial}{\partial s}\left[\frac{g(\rho-\rho_a)}{\rho_o}\right] + u_r \frac{\partial}{\partial r}\left[\frac{g(\rho-\rho_a)}{\rho_o}\right] = -\frac{1}{r}\frac{\partial}{\partial r}\left[\frac{gr}{\rho_o}\overline{u_r'(\rho-\rho_a)'}\right] \tag{2.9}$$

This expression is valid for the above equations of state whether the density variations are caused by temperature differences or by salt or other tracer variations.

The solution of the above equations requires the specification of several terms since there are too many unknown quantities for the number of equations. The typical approach to the solution of these types of equations is to specify constitutive equations relating the turbulent transport terms $\overline{u_s'u_r'}$, $\overline{u_r'T'}$, and $\overline{u_r'c'}$ to mean flow variables. This approach has not been generally accepted for the solution of buoyant jet problems due to the difficulty of defining appropriate constitutive relations.

The more common procedure is to consider the integrated conservation equations. The form of Eqs. 2.3, 2.4, 2.5, 2.7, and 2.9 after integrating across a section normal to the jet boundary is:

Mass*

$$\frac{d}{ds}\left[\int_0^R u_s r dr\right] = -\lim_{r\to R}[ru_r] = E \tag{2.10}$$

Vertical Momentum

$$\frac{d}{ds}\left[\int_0^R u_s^2 r dr\right]\sin\theta = \int_0^R \frac{g(\rho_a-\rho)}{\rho_o} r dr - \lim_{r\to R}(\overline{ru_s' u_r'})\sin\theta \tag{2.11}$$

Horizontal Momentum

$$\frac{d}{ds}\left[\int_0^R u_s^2 r dr\right]\cos\theta = EU_A - \lim_{r\to R}(\overline{ru_s' u_r'})\cos\theta \tag{2.12}$$

Tracer

$$\frac{d}{ds}\left[\int_0^R u_s(c-c_a) r dr\right] = \frac{-dc_a}{ds}\int_0^R u_s r dr - \lim_{r\to R}[\overline{ru_r' c_a'}] \tag{2.13}$$

Buoyancy

$$\frac{d}{ds}\left[\int_0^R u_s g\left(\frac{\rho-\rho_a}{\rho_o}\right) r dr\right] = \frac{-g}{\rho_o}\frac{d\rho_a}{ds}\int_0^R u_s r dr - \lim_{r\to R}\left[\frac{gr}{\rho_o}\overline{u_r'(\rho-\rho_a)'}\right] \tag{2.14}$$

The term R in the above equations refers to some appropriately defined radius of the jet which is a function of distance along the jet trajectory. This term must have a finite value or some of the integrals containing u_s terms will be divergent. Generally, the radius R is arbitrarily defined as the distance from the jet axis to the point where the

*See note, end of chapter (p. 32).

mean concentration of a passive tracer is one-half the maximum value (see Fig. 2.2) or some similar definition. The tracer conservation equation is retained to describe the dilution of a passive tracer (one which does not affect fluid density).

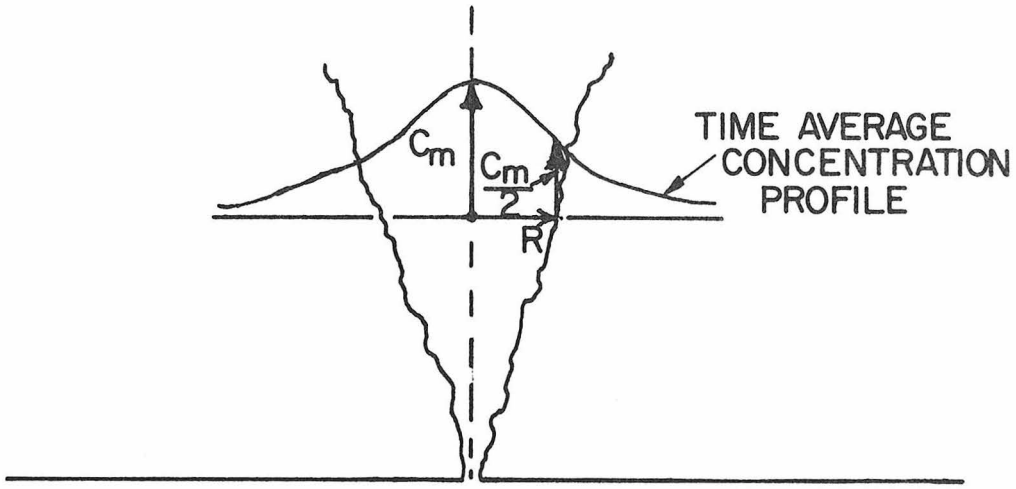

Fig. 2.2 Definition sketch of characteristic jet radius.

The turbulent transport terms are assumed to vanish at the jet boundary R in the above equations. The term on the right-hand side of Eq. 2.10 represents the inflow of ambient fluid across the jet boundary and a relation for this term must be assumed in order to obtain a solution of the above equations. The assumed relation E is referred to as the entrainment function. Assumptions are also required for the shape of the concentration, density, and velocity profiles. Technically, it only need be assumed that the profiles are similar at any jet cross-section since different forms of the assumed profiles only introduce different constant values into the equations. The profiles are generally assumed to be Gaussian in form expressed as excess values above ambient

levels or are considered to be top hat; that is, the velocity, concentration, etc. are assumed to be ambient values for radial distances greater than R and represented by a single value across the jet cross-section. If the tracer equation is assumed to describe a tracer present only in the jet discharge ($c_a = 0$), Eqs. 2.10-2.14 can be written with a top hat representation as:

$$\frac{d}{ds}[U_s R^2] = E \tag{2.15}$$

$$\frac{d}{ds}[U_s^2 R^2]\sin\theta = R^2 G \tag{2.16}$$

$$\frac{d}{ds}[U_s^2 R^2]\cos\theta = U_A E \tag{2.17}$$

$$\frac{d}{ds}[U_s C R^2] = 0 \tag{2.18}$$

$$\frac{d}{ds}[U_s G R^2] = -\varepsilon U_s R^2 \sin\theta \tag{2.19}$$

Here U_s, $G = g\frac{\rho_a - \rho}{\rho_o}$, and C are the top hat values and $\varepsilon = \frac{-g}{\rho_o}\frac{d\rho_a}{dz}$. This set of equations can be solved if the entrainment relation is specified and constitutes the general form of the integral equations used in the analysis of buoyant jets.

The other method of analyzing buoyant jet problems is to use dimensional analysis to deduce the basic characteristics of jets and plumes. This approach can be used only for fairly simple flows which are characterized by two independent variables. The analysis of Batchelor (1954) provides a good example of the dimensional analysis

approach. He considered the case of a pure plume (source of kinematic buoyancy flux B only) in a stagnant ambient fluid. The kinematic buoyancy flux is defined as the integral $\int_0^R u_s g\Delta\rho/\rho_o r dr$ in Eq. 2.14. A general dependent variable such as the velocity on the plume axis V can only be a function of B and the vertical position z, therefore

$$V \propto (B/z)^{1/3} \tag{2.20}$$

This approach can also be used to describe the rate of change of volume flux, momentum flux, or other dependent variables. Similar analyses can be performed for a pure momentum jet in a stagnant ambient fluid and other similar problems.

2.2 Buoyant Jets in a Stagnant, Density-Stratified Ambient Fluid

Investigations of buoyant jets in a stagnant, density-stratified ambient fluid have been performed by several researchers. Theoretical investigations such as those by Morton, Taylor, and Turner (1956), Fan (1967), Abraham and Eysink (1969), Fox (1970), and others have analyzed the problem by means of the integral method. The flow configuration for the following discussion is given schematically in Fig. 2.3 for an axisymmetric jet flow.

Morton, Taylor, and Turner (1956) solved the integrated equations by assuming that the entrainment relation is proportional to the local width and velocity scales of the jet flow. They further assumed that the velocity and density deficiency at a given jet section was self-similar with Gaussian profiles:

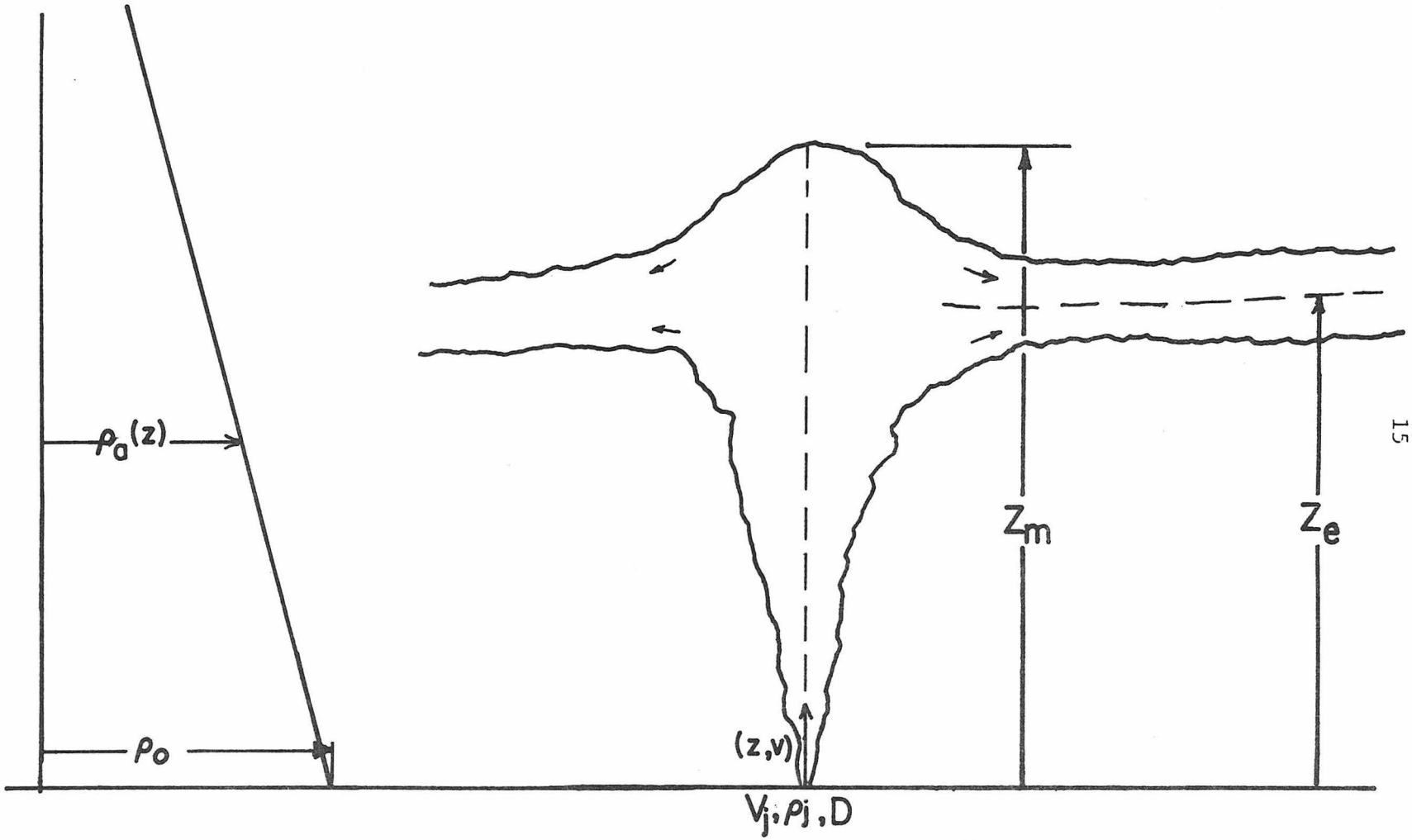

Fig. 2.3 Schematic of a buoyant jet in a stagnant, density-stratified fluid.

$$v(z,r) = V(z)\exp(-r^2/R^2),\ g' = g\left[\frac{\rho_a(z)-\rho(z,r)}{\rho_o}\right] = G(z)\exp(-r^2/R^2), \quad (2.21)$$

where R is a characteristic width of the jet profile. These descriptions of the profiles were substituted into the integrated equations, and relations similar to Eqs. 2.15, 2.16, and 2.19 can be written:

$$\frac{d}{dz}(R^2V) = 2\alpha RV \quad (2.22)$$

$$\frac{d}{dz}(R^2V^2) = 2R^2G \quad (2.23)$$

$$\frac{d}{dz}(R^2VG) = 2R^2V\varepsilon \quad (2.24)$$

The constant α is an undetermined constant in the entrainment relation and must be measured experimentally. The above equations were integrated in non-dimensional form until the vertical velocity vanished. The vertical position at which this occurred was taken as the maximum height of rise for a buoyant jet. Morton, Taylor, and Turner obtained a closed form solution for the limiting case of a buoyant plume (initial buoyancy flux only) in a stratified fluid. Their prediction and experimental measurements indicated that the maximum height of rise Z_m is given by the relation

$$Z_m = 3.79\ B^{1/4}\varepsilon^{-3/8} \quad (2.25)$$

where the kinematic buoyancy flux $B = \frac{g(\rho_a-\rho_j)}{\rho_o}\frac{\pi}{4}V_jD^2$ and $\varepsilon = \frac{-g}{\rho_o}\frac{d\rho_a}{dz}$ as defined previously. Morton (1959) applied the same analysis with top

hat profiles and obtained solutions for various cases of initial jet mass, momentum, and buoyancy. For the case of zero initial mass and buoyancy flux, he obtained a solution:

$$Z_m \propto M^{1/4}\varepsilon^{-1/4} \quad . \tag{2.26}$$

Here M is the kinematic momentum flux; $M = \frac{\pi}{4} D^2 V_j^2$. Numerical solutions were obtained for the more general case of a jet with initial fluxes of mass, momentum, and buoyancy.

Another similar approach was proposed by Priestley and Ball (1955). Their method involved the use of the integrated mechanical energy conservation equation along with the momentum and buoyancy equations. Fox (1970) showed that combining the integrated continuity equation with these three equations and requiring that the four equations in three unknowns be internally consistent indicated that the entrainment function E must follow the relation

$$E = RV(\alpha_1 + \alpha_2/F_\ell^2) \tag{2.27}$$

where F_ℓ is the local Froude number ($F_\ell^2 = V^2/GR$), and α_1 and α_2 are different constants. For a pure plume, the local Froude number is a constant (see Rouse, et al. (1952)), indicating a constant entrainment coefficient which is different than that for a nonbuoyant jet ($F_\ell = \infty$). This result has also been noted by Abraham (1965) and List and Imberger (1973) who showed that the assumption of the same entrainment coefficient for nonbuoyant jets and plumes was not valid.

There are several fundamental difficulties in the theoretical

treatment of a buoyant jet at the maximum height of rise by the integral method. The nonuniform density profile over the jet cross-section implies that different portions of the jet will be neutrally buoyant at different vertical rises. This results in the deceleration of the outer edges of the jet while the central portion of the jet still retains positive buoyancy. One assumption used in the derivation of the general form of the integral equations is that the velocities normal to the major flow direction are small with respect to those in the direction of flow. This assumption is invalid near the maximum height of rise as the flow begins to decelerate and spread radially outward. Another assumption used in most analyses is that of a constant vertical flux of a passive tracer present in the jet discharge. This assumption implies an infinite jet radius where the vertical velocity vanishes.

Abraham and Eysink (1969) proposed a solution which attempted to avoid some of these difficulties by suggesting a region of negative entrainment near the point of maximum jet rise. The fluid within the jet flows outward and becomes part of the ambient fluid in this model. This solution is not necessarily more valid than the others by Fox or Morton since it is the integrated equations as derived that are incorrect and not the particular entrainment relation. The fundamental difference between the solution proposed by Abraham and Eysink and the others is thus one of definition because the radially spreading jet fluid is defined by Morton as remaining part of the jet flow, while the Abraham and Eysink model proposes that this fluid is outflow from the jet. The different models proposed predict nearly the same maximum heights of rise in spite of the different entrainment relations. This is due in

part to the fact that one or more constants in the entrainment relation must be determined from the experimental data. Thus, while a given model may be reasonably good at predicting experimental results, there is no assurance that the physical model is valid. The use of the integral method for stratified flows has inherent difficulties which cannot be resolved on the basis of the comparison of experimental data with predicted results.

Other theoretical work of the same nature has been proposed to consider variable angles of initial jet discharge. Fan (1967) proposed a model similar to that given by Morton, while Hirst (1971b) suggested one similar to that given by Fox. These analyses can be regarded as refinements to the theory of a vertically discharged jet.

There has been relatively little experimental work done for buoyant jets in a density-stratified ambient fluid. Most of the investigations have been directed at measuring maximum heights of rise and most of these studies have been for buoyancy-driven jets. Morton, Taylor, and Turner (1956) and Fox (1970) have presented measurements obtained from photographs of buoyancy-driven jets in a stratified fluid. Crawford and Leonard (1962) also performed experiments of the same type. Abraham and Eysink (1969) discharged fresh water jets into an ambient fluid that had been stratified with salt. They made conductivity measurements to determine the location of the jet ceiling level. This was defined as the vertical position where the conductivity measurements indicated that the salt concentration was that of the jet one-half of the time and that of the ambient fluid the rest of the time.

Fan (1967) also performed experiments in which buoyant jets were released at various angles from the vertical. He determined jet trajectories and maximum heights of rise from photographs of the flow. He also performed experiments to measure the height of rise for three vertical momentum-driven jets.

2.3 Buoyant Jets in an Unstratified Crossflow

The basic flow configuration for the following discussion is given schematically in Fig. 2.4.

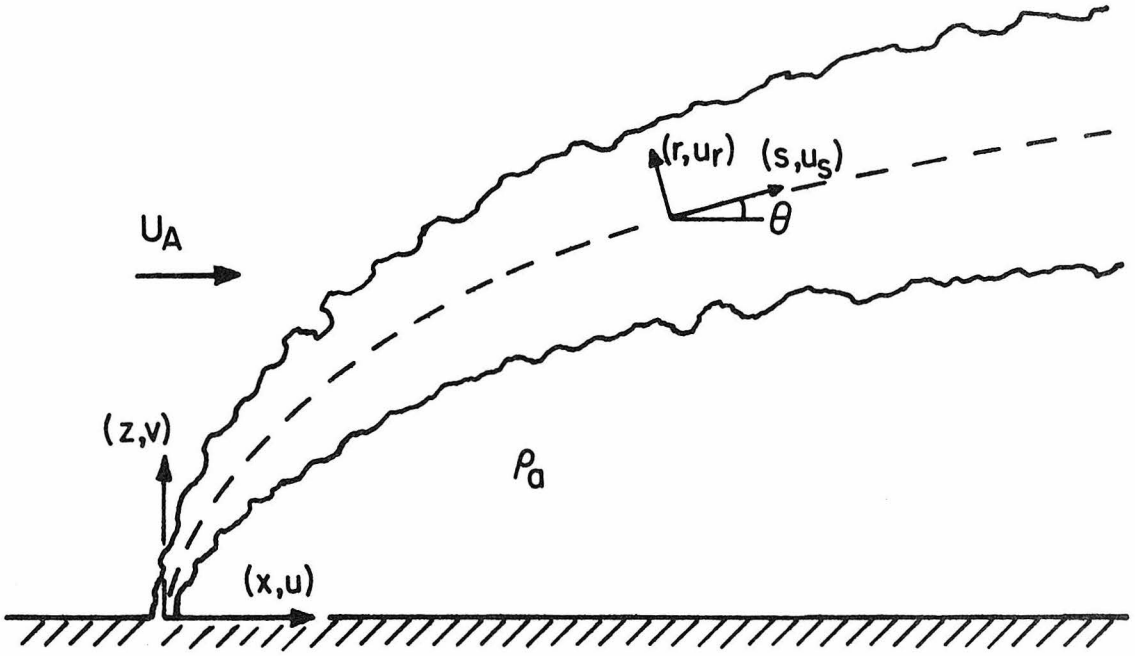

Fig. 2.4 Schematic of a buoyant jet in an unstratified crossflow.

Some of the earliest analyses of buoyant jets in a crossflow were made by fairly simple reasonings about the effect of the crossflow on jet behavior. Priestley (1956) analyzed the problem of a buoyancy-driven plume in a crossflow. He assumed that the effect of the crossflow was to deflect the plume horizontally such that the angle with the horizontal was given by the relation

$$\tan\theta = V/U_A \tag{2.28}$$

He further assumed that the variation of the vertical plume velocity V with vertical rise was similar to what it would be in the absence of a crossflow. The resulting trajectory relation predicted for a plume in a crossflow is

$$z \propto \frac{B^{1/4} x^{3/4}}{U_A^{3/4}} \tag{2.29}$$

Scorer (1959) developed trajectory relations for the cases of a buoyant plume and a nonbuoyant jet in a crossflow by combining dimensional analysis with a simplified description of the flow behavior. He concluded that a jet bent over by the crossflow and moving horizontally at the crossflow velocity would develop a flow structure similar to that of a cylindrical momentum puff for a nonbuoyant jet or a cylindrical thermal for a plume. These analogies resulted in a trajectory relation of $z \sim x^{2/3}$ for a buoyancy-driven flow and $z \sim x^{1/3}$ for a momentum jet in a crossflow.

Later attempts at analyzing the behavior of a buoyant jet in a crossflow generally made use of the integral approach. The representation of the jet velocity in the integral equations is somewhat more difficult, but the general approach is to represent the tangential velocity U_s as the sum of the component of the ambient velocity in the tangential direction and a top hat component:

$$U_s(s,r) = U_A\cos\theta + u_s(s) \tag{2.30}$$

Some investigators such as Fan (1967) and Abraham (1971) include a term representing the drag force on the buoyant jet due to relative motion between the jet and the ambient fluid.* If U_s is defined as $U_A\cos\theta + u_s$ the general form of the integral equations given in Eqs. 2.15-2.19 is

Mass

$$\frac{d}{ds}\left[U_s R^2\right] = E \tag{2.31}$$

Vertical Momentum

$$\frac{d}{ds}\left[U_s^2 R^2\right]\sin\theta = R^2 G - \frac{F_d}{\pi}\cos\theta \tag{2.32}$$

Horizontal Momentum

$$\frac{d}{ds}\left[U_s^2 R^2\right]\cos\theta = U_A E + \frac{F_d \sin\theta}{\pi} \tag{2.33}$$

Tracer

$$\frac{d}{ds}\left[U_s C R^2\right] = 0 \tag{2.34}$$

Buoyancy

$$\frac{d}{ds}\left[U_s G R^2\right] = 0 \tag{2.35}$$

Here, F_d is the drag force per unit length divided by the reference density and is assumed to be due to a variation in the pressure field around the jet due to an interaction between the jet and the free stream similar to flow around a rigid body. The term containing $U_A E$ represents the

*This assumes that the pressure distribution is not hydrostatic as previously assumed.

entrainment of horizontal momentum from the ambient flow. The solution of the above set of equations requires the specification of relations for the entrainment and the pressure drag. The form of the solution thus depends upon the particular assumptions employed in the specification of these terms.

There have been numerous theoretical studies which have considered the integral method to analyze buoyant jets in a crossflow. The most common approach has been to neglect the pressure drag effects and to specify an entrainment relation which is valid for a buoyant jet in a crossflow. Other researchers have considered the pressure drag, but have ignored the entrainment of horizontal momentum. A few studies have included both effects simultaneously, but this has not been a common approach. Closed form solutions can be obtained in some instances for relatively simple entrainment functions, but generally it is necessary to integrate the equations numerically. Table 2.1 is a summary of the principal types of solutions including a list of the entrainment functions, drag relations, the types of jets for which the results are applicable, and the nature of the solutions. The term nonbuoyant jet in this table refers to a jet with zero initial buoyancy, buoyant plumes refer to a plume with negligible initial momentum; and a buoyant jet is considered to possess both buoyancy and initial momentum. The terms V and U refer to the vertical and horizontal components of the jet velocity relative to the ambient flow and the constants k_i in the trajectory relations are generally related to the α's in the entrainment relation.

Table 2.1 Summary of the principal solutions for buoyant jets in a crossflow.

Investigation	Type of Jet	Entrainment Relation $V_e = E/R$	Drag Relation F_d	Remarks
Abraham (1971)	buoyant jet	$\alpha_1 U_s + \alpha_2 U_A \sin\theta\cos\theta$	$C_d U_A^2 \sin^2\theta R$	Solution obtained by numerical integration
Abramovich (1963)	buoyant jet	--	$C_d U_A^2 \sin^2\theta R$	Closed form solution $\frac{z}{\ell_m} = \frac{\rho_j}{C_d \rho_a} \log\left[1 + 1\frac{x}{D}\left(1 + \sqrt{1 + \frac{k_1 D}{x}}\right)\right]$
Chan and Kennedy (1972)	nonbuoyant jet	$\alpha_1 V + \alpha_2 (U_A - U)$	--	Closed form solutions, 3 limiting cases near-field zone, curvilinear zone, and far-field zone far-field result: $z/\ell_m = k_1 (x/\ell_m)^{1/3}$
Chan, et al. (1976)	nonbuoyant jet	$\alpha_1 V + \alpha_2 (U_A - U)$	$C_d U_A^2 R$	Closed form solutions Similar results to Chan and Kennedy except drag force is included in near field zone
Chu and Goldberg (1974)	buoyant jet	αV	--	Closed form solutions $\frac{z}{\ell_b} = k_1\left[\frac{1}{2}\left(\frac{x}{\ell_b}\right)^2 + \left(\frac{\ell_m}{\ell_b}\right)^2\left(\frac{x}{\ell_b}\right)\right]^{1/3}$
Fan (1967)	buoyant jet	$\alpha(U^2+V^2)^{1/2}$	$C_d U_A^2 \sin^2\theta R$	Solution obtained by numerical integration

Table 2.1 (Continued)

Investigation	Type of Jet	Entrainment Relation $V_e = E/R$	Drag Relation F_d	Remarks
Hewett, et al. (1971)	buoyant jet	$\alpha_1(U_s - U_A\cos\theta) + \alpha_2 U_A \sin\theta$	--	Closed form solutions - two limiting cases $\frac{z}{\ell_m} = \left(\frac{V_j/U_A}{\alpha_2 + \alpha_1 V_j/U_A}\right)^{1/2}\left(\frac{x}{\ell_m}\right)^{1/2}$ momentum jets $\frac{z}{\ell_b} = k_1\left(\frac{x}{\ell_b}\right)^{2/3}$ buoyant plumes
Hoult and Weil (1972) Fay, et al. (1970) Hoult, et al. (1969)	buoyant jet	$\alpha_1(U_s - U_A\cos\theta) + \alpha_2 U_A \sin\theta$	--	Closed form solutions Same as Hewett's, et al. plus additional solution for non-buoyant jets $\frac{z}{\ell_m} = k_2\left(\frac{x}{\ell_m}\right)^{1/3}$
Hirst (1971a)	buoyant jet	$\left[\alpha_1 + \frac{\alpha_2 \sin\theta}{F_\ell^2}\right](U_s - U_A\cos\theta) + \alpha_3 U_A(1-\sin\theta)$	--	Solution obtained by numerical integration
Keffer (1969)	nonbuoyant jet	$\alpha_1(U_s - U_A\cos\theta) + \alpha_2 U_A(1-\sin\theta)$	--	Solution obtained by numerical integration

Table 2.1 (Continued)

Investigation	Type of Jet	Entrainment Relation $V_e = E/R$	Drag Relation F_d	Remarks
Keffer and Baines (1963)	nonbuoyant jet	$\alpha_1(U_s-U_A)$	--	Solution obtained by numerical integration
Lin (1971)	nonbuoyant jet	$\alpha_1 U_s \sin\theta+\alpha_2 U_A$	--	Closed form solution $\frac{x}{D} = \left(1+k_1\frac{V_j}{U_A}\right)\left[\exp\ k_2\frac{z}{\ell_m} - k_1\frac{V_j}{U_A}\left(\frac{z}{\ell_m}\right)\right]$
Moore (1974)	buoyant plume	$\alpha V U_A^{1/3}$	--	Closed form solution $z = k_1\frac{B^{1/4}x^{3/4}}{U}$
Shwartz and Tulin (1972)	buoyant plume	αV	--	Used mechanical energy equation instead of momentum equation. Closed form solution $\frac{z}{\ell_b} = k_1\left(\frac{x}{\ell_b}\right)^{2/3}$
Slawson and Csanady (1967)	buoyant plume	αV	--	Closed form solution $\frac{z}{\ell_b} = k_1\left(\frac{x}{\ell_b}\right)^{2/3}$
Vizel and Mostinskii (1965)	buoyant jet	--	$\frac{C_d}{2} U_A^2 \frac{z}{2}(4.5D+.22x)$	Closed form solution $\left(\frac{z}{\ell_m}\right)^2 = \frac{k_1\rho_j}{C_d\rho_a}\log\left(1+k_1\frac{x}{D}\right)$

There have also been numerous experimental studies for buoyant jets in a crossflow. These are primarily concerned with the measurement of jet trajectories, although other measurements have been made in some instances. Major experimental studies are summarized in Table 2.2. Several field studies have measured the rise of smoke plumes from industrial chimneys. Moore (1974), Slawson and Csanady (1967), Bringfelt (1968), and the TVA (1968), present a description of many of these studies. Briggs (1969) has also presented a good summary of measurements on plume rise.

2.4 Buoyant Jets in a Stratified Crossflow

Several theoretical investigations of buoyant jets in a crossflow have included the additional effect of ambient density stratification. It is assumed that the entrainment or drag relations are not altered by the presence of density stratification in all of these studies. The only change necessary in the integral equations in Eqs. 2.31 - 2.35 is to add a term to the right-hand side of Eq. 2.35:

$$\frac{d}{ds}\left[U_s G R^2\right] = -U_s R^2 \varepsilon \sin\theta \qquad (2.36)$$

Numerical integration of the equations can be performed until the vertical jet velocity vanishes when the jet is at its maximum height of rise Z_m which is indicated schematically in Fig. 2.5. Slawson and Csanady (1971) derive a relation for maximum height of rise in a stratified crossflow which is valid for buoyant plumes only:

$$Z_m \sim (B/U_A \varepsilon)^{1/3} \qquad (2.37)$$

Table 2.2 Summary of laboratory investigations of buoyant jets in a crossflow.

Investigation	Type of jet	Measurements	Method
Barilla (1968)	buoyant jet (dyed salt solutions in fresh water, towed experiments)	trajectories	photographs
Chan, et al. (1976)	nonbuoyant jet (air jet in wind tunnel)	jet velocities, pressure distributions, entrainment, trajectories	hot-wire anemometer, pitot-Prandtl tube, trajectories from velocity profiles
Chu and Goldberg (1974)	buoyant jet (dyed salt solution in fresh water)	trajectories	photographs
Fan (1967)	buoyant jet (dyed salt solution in fresh water, some towed experiments)	concentrations, distribution, trajectories	conductivity probe, trajectories from concentration profiles and photographs
Gordier (1959)	nonbuoyant jet (dyed fresh water jet in fresh water)	velocity distribution, trajectories	pitot tube, trajectories from velocity profiles and photographs
Hewett, et al. (1971)	buoyant jet (heated air plumes, plume with helium-air mixture in wind tunnel)	temperature distribution, trajectories	thermocouple, trajectories from temperature profiles

Table 2.2 (Continued)

Investigation	Type of jet	Measurements	Method
Keffer and Baines (1963)	nonbuoyant jet (oil aerosol-nitrogen mixture in wind tunnel)	velocity distributions, trajectories	hot wire anemometer, trajectories from velocity profiles
Pratte and Baines (1967)	nonbuoyant jet (oil aerosol jets in wind tunnel)	trajectories	photographs
Vadot (1965) from (Hoult and Weil (1972))	buoyant jet (salt solution in fresh water, towed experiments)	trajectories	photographs
Weil (1968)	buoyant jet (salt solution in fresh water, towed experiments)	trajectories	photographs

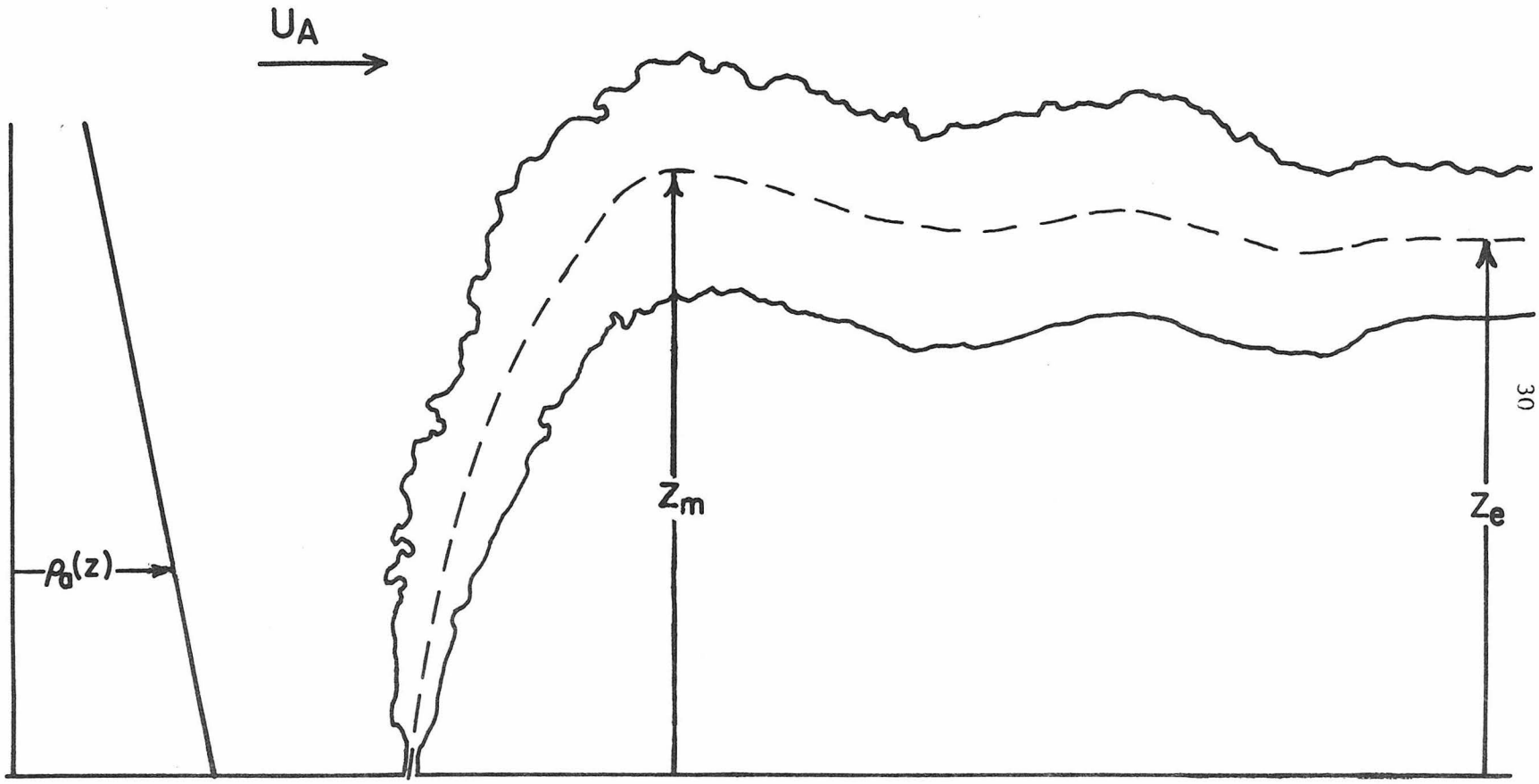

Fig. 2.5 Definition sketch of a buoyant jet in a stratified crossflow.

This result has also been derived in other analyses, including those by Fay, et al. (1970) and Shwartz and Tulin (1972). Briggs (1969) proposed a similar relation for nonbuoyant jets:

$$Z_m \sim (M/U_A \varepsilon^{1/2})^{1/3} \tag{2.38}$$

Results of laboratory experiments are presented by Hewett, et al. (1971) and results from field measurements have been given by various researchers including Bringfelt (1968), Briggs (1969) and others. The field measurements typically consist of maximum heights of rise and jet trajectories.

2.5 Summary of Previous Investigations

The most common procedure for the solution of general buoyant jet problems involves the use of the integral approach. The equations generally used are those for the conservation of mass, momentum, and buoyancy, although in some cases, the integrated mechanical energy equation has been used. The choice of equations is not fundamental to the determination of a solution, as for example, the solutions of Slawson and Csanady (1967) and Shwartz and Tulin (1972) are identical for buoyant plumes in a crossflow even though the Slawson and Csanady analysis considered the integrated momentum equation and Shwartz and Tulin used the energy equation in place of the momentum equation. Since the rate of entrainment of ambient fluid is generally specified for closure of a given set of equations, the nature of the solution depends more directly on the entrainment relation assumed. It can

readily be seen from Table 2.1 that there is no general consensus as to the form of this relation in the presence of a crossflow. Thus, there are several different predictions for buoyant jet behavior in a crossflow. Many of the entrainment functions specified involve two or more arbitrary constants, the values of which are determined by fitting the solutions to the available data. It should not be surprising, therefore, that most of the models appear in good agreement with experimental data even though many of them do not agree qualitatively.

The use of dimensional analysis to solve problems relating to buoyant jets in a crossflow has not generally been attempted because of the large number of independent variables involved in the specification of the flow. The investigation by Scorer (1959) is a notable exception as he derived relations for jet trajectories and dilutions without solving the integral equations. Scorer's analysis did not require the specification of an entrainment relation which avoids the difficulty of assuming a relation for a quantity that is not particularly intuitive. However, his results do agree with the predictions of several models that were derived by the integral approach including those of Slawson and Csanady (1967), Chu and Goldberg (1974), and others, which can be taken as a partial verification of their entrainment relations.

Note: A recent communication with Schatzmann (1977) has indicated that the use of a finite radius R (variable with axial distance) in the integration adds addition terms to the above equations (from the Leibnitz rule). This difficulty arises if the velocity does not vanish at the edge of the jet ($U_A \neq 0$) and has generally not been considered by other investigators.

CHAPTER 3

ANALYSIS

3.1 Dimensional Analysis

3.1.1 Basic Assumptions

Several assumptions are made to limit the number of independent variables to be considered. The analysis in this chapter considers round buoyant jets discharged vertically to a horizontal crossflow with either a uniform density or a linear stratification. The jet flow is assumed to be fully turbulent such that effects of fluid viscosity on mean flow characteristics can be neglected. In addition, the Boussinesq approximation is made; density differences between the jet and ambient fluids are small and important only in causing buoyant forces. Finally, any effects of ambient turbulence on the jet flow are not considered.

3.1.2 Jet and Ambient Flow Variables

A round turbulent buoyant jet can be represented by three independent variables with the above limitations. Past studies have typically considered the jet diameter D, the exit velocity V_j, and a term relating to the initial density difference between the jet and ambient fluids $g_o' = g(\rho_{a_o}-\rho_j)/\rho_o$ where ρ_o is some reference density (generally the ambient density at the level of the jet source ρ_{a_o}). However, List and Imberger (1973) and others have demonstrated the advantage of considering the kinematic fluxes of mass $Q=\frac{\pi}{4} D^2V_j$, momentum

$M = V_j Q$, and buoyancy $B = g_o' Q$ as the variables characterizing a buoyant jet. Since the flux variables are independent combinations of the first group of variables, either set is equally representative of a given buoyant jet. The advantage of considering the flux variables is that the volume flux can generally be neglected or accounted for by using a virtual origin correction which extrapolates the jet to a point source of momentum and buoyancy. A reduction in the number of independent variables that are important can thus be achieved.

An ambient crossflow with a linear density stratification can be characterized by two variables; the crossflow velocity U_A which is assumed constant over the flow depth, and the parameter $\varepsilon = \frac{-g}{\rho_o} \frac{d\rho_a}{dz}$. A general dependent variable ϕ (such as maximum velocity, jet width, or minimum dilution) that is a characteristic of a buoyant jet at a given cross-section in the flow field must then be a function of these independent variables and the position:

$$\phi = f(Q, M, B, U_A, \varepsilon, z) \quad . \tag{3.1}$$

These independent variables have units as follows:

Q	L^3T^{-1}	U_A	LT^{-1}
M	L^4T^{-2}	ε	T^{-2}
B	L^4T^{-3}	z	L

Since the variables have units of lengths and time only, the Buckingham Π-theorem indicates that there will be five dimensionless groups of the seven variables.

3.1.3 Length Scales Associated with the Independent Variables

The jet and ambient flow variables can be combined into length scales, each of which characterizes a particular aspect of the general problem. These length scales have direct physical significance and should be considered in the formulation of the entire problem. Dimensionless groups can be conveniently formed as ratios of the various characteristic lengths.

According to List and Imberger (1973), a general buoyant jet in a stagnant, unstratified ambient fluid exhibits three regions where the jet behavior is determined by different effects. The jet discharge is important near the source, while further away the flow is determined by the kinematic momentum and buoyancy fluxes. The appropriate length scale for the flow behavior near the source is $\ell_Q = Q/M^{1/2}$, which is proportional to the jet diameter ($\ell_Q = \sqrt{\pi/4}\, D$). In the region where z/ℓ_Q is small (on the order of 10 or less), the source geometry will have a direct influence on the flow characteristics, but for $z/\ell_Q \gg 1$ the effect of the initial jet diameter becomes unimportant and only the jet momentum and buoyancy are important. As a momentum-driven jet continues along its trajectory, the buoyancy will generate additional momentum which will ultimately be of the same order of magnitude as the initial jet momentum. This will occur at a distance from the source approximately equal to $\ell_M = M^{3/4}/B^{1/2}$; for $z/\ell_M \ll 1$ the initial momentum effect will dominate over the buoyancy effect, but for $z/\ell_M \gg 1$, the flow behavior will be controlled by the buoyancy. Thus, a general buoyant jet with both initial momentum and buoyancy can be considered to be in

transition from jet-like ($B \approx 0$) to plume-like ($M \approx 0$) flow with increasing distance from the jet source. For the special case of $\ell_M < \ell_Q$, there will be no momentum-dominated flow region and the flow will be plume-like except near the source where the effect of the initial volume flux is important. This phenomenon is dependent upon the ratio ℓ_M/ℓ_Q which is proportional to the densimetric source Froude number, F:

$$\frac{\ell_M}{\ell_Q} = \left(\frac{\pi}{4}\right)^{-1/4} F \quad , \quad F = \frac{V_j}{\sqrt{g_o' D}} \quad .$$

When the ambient velocity is considered as an additional variable, several other length scales can be defined. If the mass flux can generally be disregarded as a minor influence except near the source, the more relevant length scales are $\ell_m = M^{1/2}/U_A$ and $\ell_b = B/U_A^3$. The length scale ℓ_m relates to the interaction of a momentum-dominated jet with a crossflow while the length scale ℓ_b is important for buoyancy-dominated flow. These length scales are proportional to the vertical distance over which a jet travels before its vertical velocity decays approximately to that of the ambient crossflow velocity. For example, for $z/\ell_m \ll 1$ a nonbuoyant jet will be nearly rising vertically since the jet velocity will be much greater than the crossflow velocity. When z/ℓ_m is on the order of 1, the jet and ambient velocities will be approximately equal and the jet will be deflected by the crossflow at an angle of approximately 45 degrees from the vertical. When $z/\ell_m \gg 1$, the jet will be bent over by the crossflow and moving nearly horizontally. The same arguments apply for buoyancy-dominated flow depending upon the

relative value of z/ℓ_b. That is, for $z/\ell_b \ll 1$, the plume will be nearly vertically rising and for $z/\ell_b \gg 1$, it will be significantly bent over by the crossflow.

Length scales can also be formed with the jet variables and the stratification parameter in a similar manner. The appropriate length scales in this instance are $\ell_m' = (M/\varepsilon)^{1/4}$ and $\ell_b' = (B/\varepsilon^{3/2})^{1/4}$. The length ℓ_m' relates to the maximum height of rise of a nonbuoyant jet in a stagnant, density-stratified ambient fluid. Similarly, the length ℓ_b' is proportional to the distance that a plume will rise in a stratified fluid. These length scales can also be viewed as the distance required for the density stratification to remove momentum (or buoyancy, depending upon the length scale) from the jet flow in an amount equal to the initial value. A third length scale relating to the ambient density stratification can be formed with the crossflow velocity, $\ell_a = U_A/\varepsilon^{1/2}$. A list of the various length scales and their definitions is presented in Table 3.1. Note that there are only four independent length scales (e.g., ℓ_Q, ℓ_m, ℓ_b, and ℓ_a) and the other length scales can be formed from combinations of these lengths.

Table 3.1 Definitions of length scales associated with buoyant jets in a stratified crossflow.

jet length scales	crossflow length scales	stratification length scales
$\ell_Q = Q/M^{1/2}$	$\ell_m = M^{1/2}/U_A$	$\ell_m' = M^{1/4}/\varepsilon^{1/4}$
$\ell_M = M^{3/4}/B^{1/2}$	$\ell_b = B/U_A^3$	$\ell_b' = B^{1/4}/\varepsilon^{3/8}$
	$\ell_a = U_A/\varepsilon^{1/2}$	

If the functional relationship in Eq. 3.1 is expressed in non-dimensional parameters formed from the various length scales, one possible result is

$$\phi^* = f\left(\frac{z}{\ell_b}, \frac{\ell_Q}{\ell_b}, \frac{\ell_m}{\ell_b}, \frac{\ell_b'}{\ell_b}\right) \tag{3.2}$$

where ϕ^* is a dimensionless form of ϕ. The choice of ratios is such that the initial buoyancy flux and the crossflow are involved in all terms (through ℓ_b), while the second term (ℓ_Q/ℓ_b) is the only one involving the initial volume flux Q, the term ℓ_m/ℓ_b is the only one involving the jet momentum flux, and the last term includes the stratification parameter. This arrangement facilitates consideration of limiting cases. For instance, the second term is of minor importance except near the origin, the third is negligible for buoyancy-dominated flow, and the last can be ignored for a very weak density stratification. This approach clearly points out the significance of the various length scales.

An interesting point has been made by List (1976) with respect to the more common approach to dimensional analysis of a buoyant jet in an unstratified crossflow. His point is that most analyses have considered the relevant non-dimensional parameters to be the velocity ratio V_j/U_A, the densimetric Froude number F, and the distance normalized by the jet diameter (z/D). These parameters can be expressed in terms of the various length scales as

$$\phi^* = f\left(\frac{z}{D} \propto \frac{z}{\ell_Q}, \frac{V_j}{U_A} = \frac{\ell_m}{\ell_Q}, \frac{V_j}{\sqrt{g_o' D}} \propto \frac{\ell_m^{3/2}}{\ell_Q \ell_b^{1/2}}\right) \tag{3.3}$$

Note that the length scale ℓ_Q appears in each term even though it is of relatively minor importance in defining jet behavior. Clearly, the use of the parameters in Eq. 3.3 obscures the study of buoyant jet behavior and the more instructive approach is to consider the parameters in Eq. 3.2.

3.2 Approximations Used in the Analysis

3.2.1 General Approach

Dimensional analysis alone is insufficient to provide approximate solutions because of the number of independent variables that must be considered. It can, however, be applied to simplified descriptions of the flow behavior to yield approximate solutions. For instance, an obvious reduction in the number of independent variables can be achieved by considering the effects of the jet momentum and the buoyancy separately. A solution obtained for a nonbuoyant jet in a stratified crossflow can then be applied as an approximate solution to that portion of the total jet flow where the jet momentum dominates the flow behavior. The results derived for a buoyant plume can be applied in a similar manner to regions of buoyancy-dominated flow.

The effects of the ambient flow can also be examined separately. That is, the density stratification can be assumed to have a relatively minor influence on the jet characteristics until the jet travels a sufficiently large distance from the source that it begins to approach its maximum height of rise. The stratification effect can be neglected relatively near the source and the problem is analyzed as that of a buoyant jet in a uniform density crossflow. This general approach will

not yield exact solutions, but the results can be considered as first order approximations to the correct solutions.

3.2.2 Near-Field Flows

Near-field flows consist of the regions where $z/\ell_m \ll 1$ for momentum-dominated flows and where $z/\ell_b \ll 1$ for buoyancy-dominated flows. The distinction between the near-field and the far-field to be discussed in the next section is indicated schematically in Fig. 3.1. It is also assumed that $z \gg \ell_Q$ so that effects of the initial volume flux can be neglected. The jet has not been significantly deflected by the crossflow in the near-field and is still nearly vertically rising. The assumption made in this instance is that the effect of the crossflow is relatively unimportant and serves primarily to advect the jet horizontally at the ambient velocity. This assumption is not entirely valid since the jet enters the ambient flow field with zero horizontal velocity and must be first accelerated to the crossflow velocity. This acceleration comes from the pressure force on the jet and from the entrainment of horizontal momentum from the crossflow due to turbulent shear from the unequal horizontal velocities. It is assumed, however, that this acceleration region is only on the order of a few initial jet diameters from the source and thus occurs in that region (z/ℓ_Q small) where the analysis that is developed in this study is not valid in any case. This argument has been advanced by Hirst (1971a), Chu and Goldberg (1974), and others as a justification for ignoring drag forces in the analysis of a buoyant jet. Several buoyant jets that Priestley (1956) observed experimentally were advected horizontally at the crossflow velocity very near the source which justifies neglecting the acceleration region. Therefore, while the acceleration effects may influence the shape of

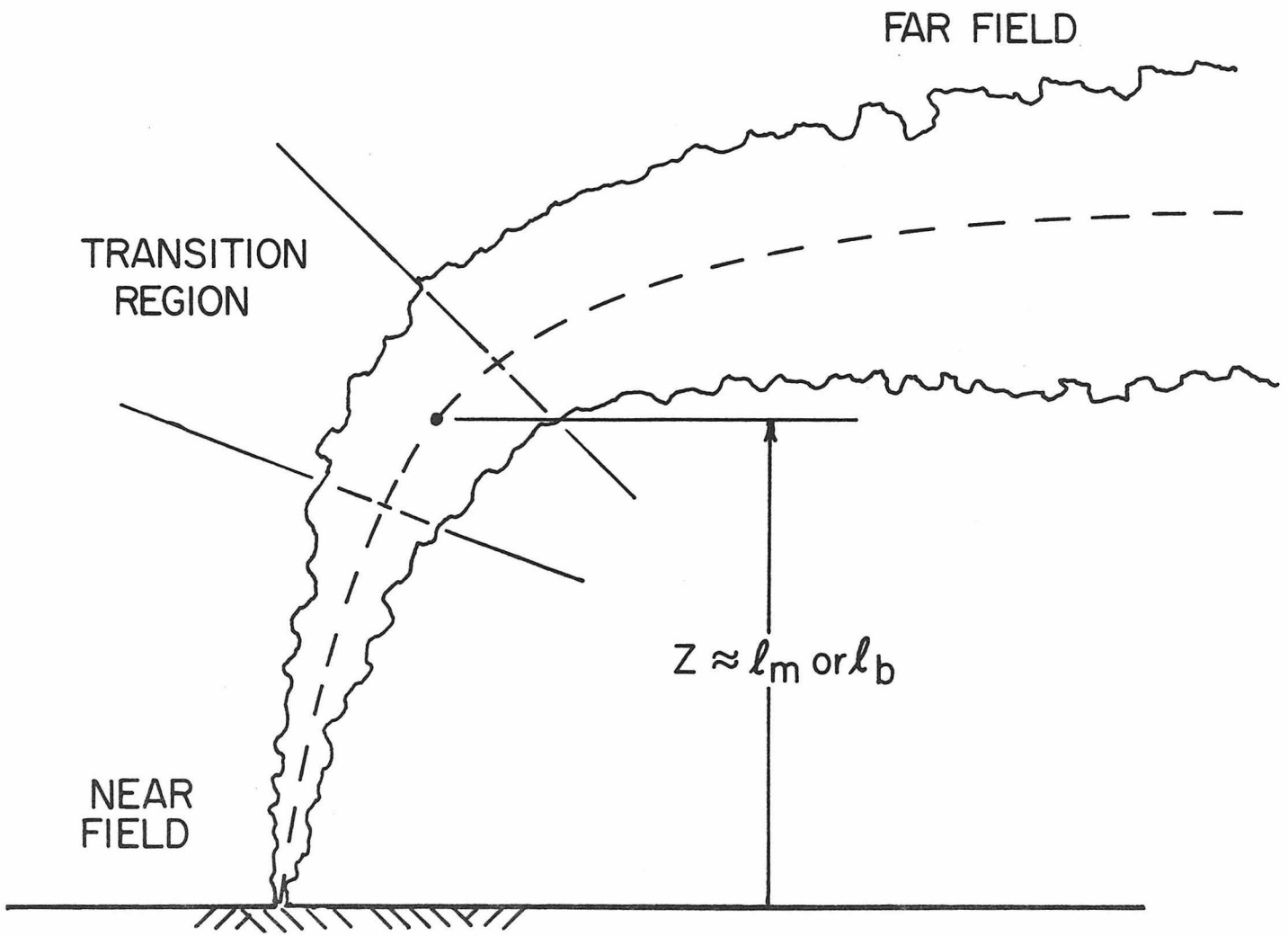

Fig. 3.1 Definition sketch of distinction between near-field and far-field flows.

the velocity and concentration profiles at a jet cross-section, it will not significantly alter the qualitative relations that describe characteristic velocities or concentrations. The characteristic vertical velocity should thus follow the same general relation for a jet in a stagnant ambient fluid, as should the characteristic jet width and the dilution of a passive tracer. The near-field is thus that region greater than a few jet diameters from the source, but where the buoyant jet is still rising nearly vertically.

3.2.3 Far-Field Flows

A somewhat different approach is considered in the far-field regions ($z/\ell_m \gg 1$ for a momentum-driven jet or $z/\ell_b \gg 1$ for a buoyancy-driven flow). The vertical jet velocity has decayed to a value less than that of the crossflow in the far-field and the ambient flow will have significantly deflected the jet. The behavior of the bent-over jet at a given vertical position is assumed to be approximately equivalent to that of a cylindrical momentum puff or buoyant thermal at the same vertical rise. This assumption is based on the concept that a vertical cross-section of a nearly horizontal jet is similar to a section of an analogous cylindrical puff or thermal. The flow similarity between a buoyant thermal and a plume in a crossflow depicted in Fig. 3.2 has been suggested previously by Scorer (1959) and others. A momentum puff is an instantaneous release of nonbuoyant fluid along a horizontal line source, while a buoyant thermal is a similar release of buoyant fluid. As the fluid rises above the source, the flow pattern is that of a pair of counter-rotating vortices, a phenomenon also noted for

buoyant jets in a strong crossflow. To complete the analogy to a jet in a crossflow, the release of the fluid must be such that the discharge begins at one end and progresses along the line source at velocity U_A. The resulting flow pattern would be a continuous source of momentum or buoyancy moving at velocity U_A through a stagnant ambient fluid. Superimposing a crossflow on the system will complete the analogy with a stationary jet bent over by the ambient current. The independent variables characterizing these flows are the vertical rise z and the momentum impulse m or the buoyant impulse b per unit length. These quantities are related to the continuous releases per unit time for a fixed source in a crossflow by the relations; $m = M/U_A$ and $b = B/U_A$.

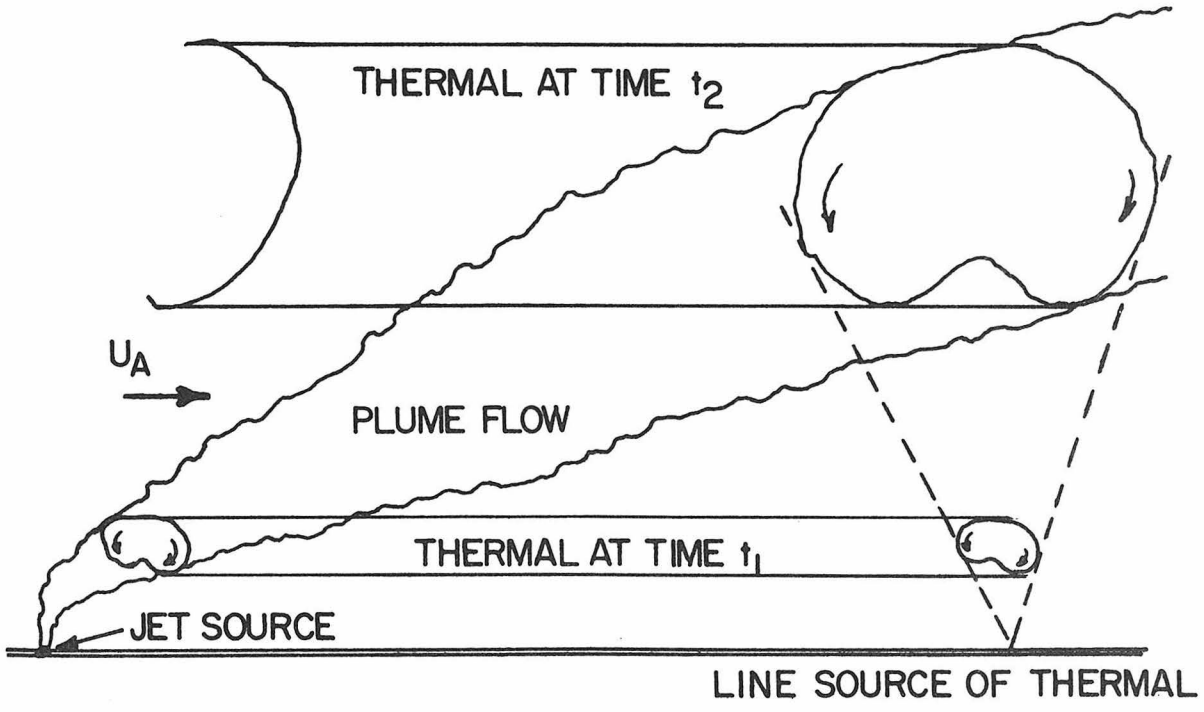

Fig. 3.2 Schematic indicating similarity between a far-field flow and a buoyant thermal.

3.3 Buoyant Jets in an Unstratified Crossflow

Approximate solutions can be obtained for the prediction of mean flow properties such as velocities, jet widths, dilutions, etc., by using the flow descriptions presented in the previous section. Analyses will be presented for four cases: near-field and far-field results for both momentum- and buoyancy-dominated flows.

3.3.1 Momentum-Dominated Jets

The behavior of a nonbuoyant jet in a crossflow depends upon the relative importance of the jet momentum compared to the ambient velocity as discussed previously. For a relatively weak crossflow, the resulting flow pattern should be similar to that of a jet in a stagnant ambient fluid except that the jet is advected with the ambient velocity. The vertical velocity variation of a nonbuoyant jet in a stagnant ambient fluid can be shown by dimensional analysis to follow the relation

$$\frac{Vz}{M^{1/2}} = \text{constant} \tag{3.4}$$

This relation is confirmed by the experimental evidence of Albertson, et al. (1950) except for that region near the source (z/ℓ_Q less than about 6) where the mass flux must be considered. The kinematic relation for a jet moving horizontally at the crossflow velocity is

$$\frac{dx}{U_A} = \frac{dz}{V} \tag{3.5}$$

Substituting for the vertical velocity and integrating the above expression yields the following relation for the momentum-dominated

near-field (mdnf):

$$\frac{z}{\ell_m} = C_1 \left(\frac{x}{\ell_m} + C_I \right)^{1/2} \tag{3.6}$$

which should be valid for $z/\ell_m \ll 1$ and z/ℓ_Q greater than about 10. The integration constant can be considered as a virtual origin correction which is ignored for the purpose of this analysis by assuming that $z = 0$ at $x = 0$.

For relatively larger values of z/ℓ_m, the ambient flow will have a more direct effect on the flow pattern, and the behavior of the bent-over jet can be likened to that of a cylindrical momentum puff. The characteristic vertical velocity of a puff must depend only upon the momentum impulse m (instantaneous input of kinematic momentum flux per unit length) and vertical rise. Dimensional considerations imply that

$$\frac{Vz^2}{m} = \text{constant} \tag{3.7}$$

The analogy between the momentum puff and a nonbuoyant jet in a cross-flow is completed by replacing m by M/U_A in the above expression. The trajectory relation for the momentum-dominated far-field is obtained by substituting this expression into the kinematic relation and integrating which yields

$$\frac{z}{\ell_m} = C_2 \left(\frac{x}{\ell_m} + C_I \right)^{1/3} \tag{3.8}$$

The constant of integration is evaluated from the values of z/ℓ_m and

and x/ℓ_m at the transition between the near and far-field flows and is assumed to be negligible. This assumption can be verified only by experimental determination of the constants C_1 and C_2.

Relationships for characteristic dilutions within a nonbuoyant jet can be determined by similar methods. The definition of a characteristic jet dilution at a cross-section implicitly assumes similarity of concentration profiles, but no assumptions as to the actual shape of the profiles are required. An appropriate dilution might be the minimum value in the vertical plane of symmetry of the jet. Fan (1967) measured some concentration profiles and found absolute minimum dilutions occur to either side of the plane of symmetry. These might also be conveniently defined as characteristic dilutions. The exact definition is not important so long as it is consistent for different jets.

The analysis for the dilution of a buoyant jet can be performed by considering that the flux of a passive tracer is conserved along the jet trajectory. The expression for the conservation of a tracer of concentration c is given by

$$\text{Flux} = \int cu_s dA = \text{constant} = C_o Q \tag{3.9}$$

where C_o is the tracer concentration at the jet source. The assumption of similarity implies that the integral can be represented by characteristic quantities at a jet cross-section:

$$\int cu_s dA \propto CU_s R^2 \tag{3.10}$$

A characteristic dilution S_o of the tracer can be defined as $S_o = C_o/C$ and is given by

$$S_o \propto \frac{U_s R^2}{Q} \tag{3.11}$$

The dilution of a tracer can thus be determined from dimensional analysis by considering the characteristic volume flux $\mu = U_s R^2$ as the appropriate dependent variable.

It is assumed that the crossflow does not affect the relation for the characteristic dilutions for near-field flows. Thus, the dilution should be the same as for a nonbuoyant jet in a stagnant ambient fluid. Dimensional considerations imply that

$$\frac{\mu}{zM^{1/2}} = \text{constant} \tag{3.12}$$

or in terms of the dilution $S_o \propto \mu/Q$

$$\frac{S_o Q}{U_A \ell_m^{\,2}} = C_3 \left(\frac{z}{\ell_m} \right) \tag{3.13}$$

Dilutions for the far-field are obtained by considering the momentum puff analogy. The dependent variable to consider is the characteristic volume per unit length λ. This variable is related to the volume flux parameter by $\lambda = \mu/U_A$ if the analogy between the bent-over jet and the momentum puff is considered. The relevant dimensionless relation is

$$\frac{\lambda}{z^2} = \text{constant} \tag{3.14}$$

which upon substitution for λ and rearrangement gives

$$\frac{S_o Q}{U_A \ell_m^2} = C_4 \left(\frac{z}{\ell_m}\right)^2 \tag{3.15}$$

Relations for the characteristic jet radius R can also be determined by dimensional analysis. A characteristic jet radius at a jet section can be defined as the transverse distance between the location of maximum tracer concentration and the position where the concentration is one-half that value as depicted in Fig. 3.3.

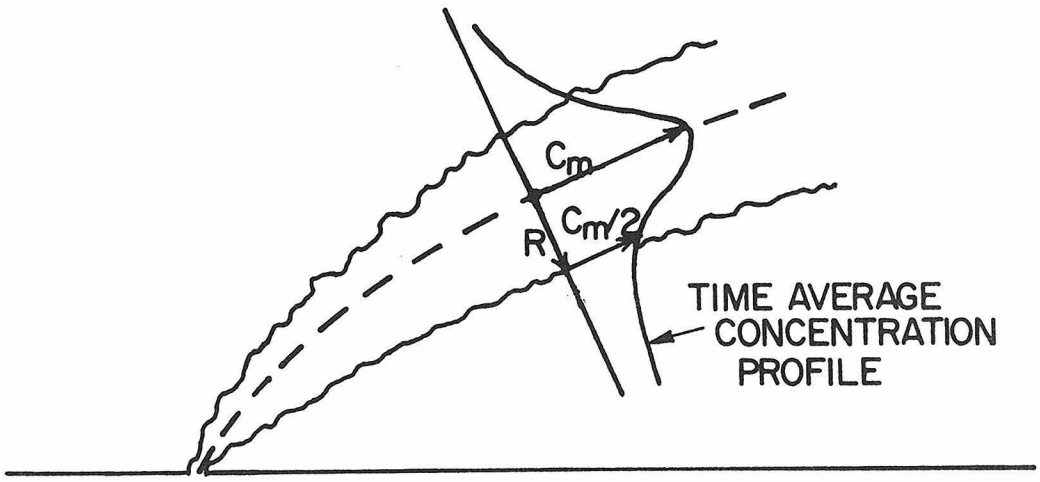

Fig. 3.3 Definition sketch of characteristic jet radius.

The jet radius can be determined by dimensional reasoning to be proportional to the appropriate local length scale. The only length scale associated with the two asymptotic cases of a nonbuoyant jet in a stagnant ambient fluid and a cylindrical momentum puff is the vertical rise z. This implies that

$$\frac{dR}{dz} = \text{constant} \tag{3.16}$$

is approximately valid for both the near- and far-field flows. The jet spread is thus linear with vertical rise but with different constants of proportionality for the mdnf and the mdff.

3.3.2 Buoyancy-Dominated Jets

The analysis for a buoyant plume in a crossflow proceeds in a similar manner to that of a nonbuoyant jet. For $z/\ell_b \ll 1$, the flow will be similar to a plume in a stagnant fluid, but advected with the crossflow. The velocity variation of a plume in a stagnant ambient fluid obtained by dimensional analysis and confirmed by the experimental data of Rouse, et al. (1952) is

$$\frac{V_z^{1/3}}{B^{1/3}} = \text{constant} \tag{3.17}$$

Substituting the vertical velocity variation into the kinematic relation and integrating gives the result for the buoyancy-dominated near-field (bdnf):

$$\frac{z}{\ell_b} = C_5 \left(\frac{x}{\ell_b}\right)^{3/4} \tag{3.18}$$

For $z/\ell_b \gg 1$, the plume should behave similarly to a buoyant thermal. The relation between the buoyant impulse b, vertical velocity, and vertical rise for a thermal as given by dimensional reasoning is

$$\frac{V_z^{1/2}}{b^{1/2}} = \text{constant} \tag{3.19}$$

If b is replaced by B/U_A, the analogy to a buoyant plume in a crossflow can be made. Substituting the above expression into the kinematic relation gives the result for the buoyancy-dominated far-field (bdff):

$$\frac{z}{\ell_b} = C_6 \left(\frac{x}{\ell_b} \right)^{2/3} \tag{3.20}$$

The integration constants are neglected in the above relations (cf. p. 45).

Dilutions can be analyzed for buoyancy-dominated flow by again considering the characteristic volume flux μ as the relevant dependent variable. The variation of μ for the bdnf should be that for a plume in a stagnant ambient fluid which is

$$\frac{\mu z^{5/3}}{B^{1/3}} = \text{constant} \tag{3.21}$$

or in terms of the dilution $S_o = \mu/Q$ and the length scale ℓ_b:

$$\frac{S_o Q}{U_A \ell_b^{\,2}} = C_7 \left(\frac{z}{\ell_b} \right)^{5/3} \tag{3.22}$$

In the far-field, dimensional considerations for a buoyant thermal imply that

$$\frac{\lambda}{z^2} = \text{constant} \tag{3.23}$$

where λ is the characteristic thermal volume equal to μ/U_A by the appropriate analogy. The result for the bdff in terms of S_o and ℓ_b is

$$\frac{S_o Q}{U_A \ell_b^2} = C_8 \left(\frac{z}{\ell_b} \right)^2 \tag{3.24}$$

Analysis can also be performed to determine the variation of the width of a buoyancy-driven jet in a crossflow. For the limiting cases of a plume in a stagnant fluid and a buoyant thermal, dimensional reasoning implies that a characteristic jet width must scale as the vertical rise since there are no other length scales associated with the asymptotic flow descriptions. This again implies that the relation

$$\frac{dR}{dz} = \text{constant} \tag{3.25}$$

will be valid in both the near- and far-fields. The fact that all four cases analyzed indicate a linear increase in jet width with elevation does not imply that the constant of proportionality should be the same for any of the cases. There is a different phenomenon controlling the turbulent diffusion in each situation, so it would be unlikely that the spreading rate would be the same. Thus although a buoyant jet would exhibit a linear spread with vertical rise in each of the flow regimes, nonlinear variations in jet width would be expected at the transition regions between flow regimes.

3.3.3 Summary of Results for Buoyant Jets in an Unstratified Crossflow

The relations developed in the preceding sections are the asymptotic solutions for the trajectories and dilutions of a buoyant jet in a uniform-density crossflow. The analysis does not consider the initial volume flux and is therefore not valid for vertical rises

less than a few jet diameters above the source. It is unlikely that a general solution for the jet behavior in that region can be developed since the jet exit conditions vary depending on the release structure and these must be considered. The regions of interest for most application are generally at greater distances from the source and one of the flow descriptions presented in the preceding sections can be used to describe approximately the jet trajectory and dilution. The application of the general model will be discussed in more detail in Section 3.5. The various trajectory and dilution relations are summarized in Table 3.2.

Table 3.2 Trajectory and dilution relations.

Flow regime	Trajectory relation	Dilution relation
Momentum-dominated near field	$\frac{z}{\ell_m} = C_1 \left(\frac{x}{\ell_m}\right)^{1/2}$	$\frac{S_o Q}{U_A \ell_m^2} = C_3 \frac{z}{\ell_m}$
Momentum-dominated far field	$\frac{z}{\ell_m} = C_2 \left(\frac{x}{\ell_m}\right)^{1/3}$	$\frac{S_o Q}{U_A \ell_m^2} = C_4 \left(\frac{z}{\ell_m}\right)^2$
Buoyancy-dominated near field	$\frac{z}{\ell_b} = C_5 \left(\frac{x}{\ell_b}\right)^{3/4}$	$\frac{S_o Q}{U_A \ell_b^2} = C_7 \left(\frac{z}{\ell_b}\right)^{5/3}$
Buoyancy-dominated far field	$\frac{z}{\ell_b} = C_6 \left(\frac{x}{\ell_b}\right)^{2/3}$	$\frac{S_o Q}{U_A \ell_b^2} = C_8 \left(\frac{z}{\ell_b}\right)^2$

3.4 Buoyant Jets in a Stratified Crossflow

3.4.1 General Discussion

When the additional effect of density stratification is considered in the analysis, the addition of another independent variable makes the general problem intractable by the methods that have been presented. However, if only the maximum height of rise and associated dilution are desired, the vertical position is removed as an independent variable and the total number of variables is still the same as in the preceding section. Then dimensional analysis can be applied to the simplified flow descriptions to obtain approximate solutions. The following analysis thus predicts the maximum height of rise and the dilution for momentum- and buoyancy-dominated jets in a linearly stratified crossflow.

Buoyant jet behavior will again be considered to be dominated either by the jet momentum or by the buoyancy. There will be essentially two limiting possibilities in either case; the jet is still in the near-field when it reaches its maximum height of rise or else it will be significantly bent over and in the far-field before the stratification causes it to stop rising. The results corresponding to these two situations will be referred to in the following discussion as near-field and far-field results. This refers to the flow regime that a buoyant jet is in when it reaches its maximum height of rise.

3.4.2 Momentum-Dominated Flow

For a momentum-dominated jet, the magnitude of the ratio ℓ_m'/ℓ_m (where these length scales were previously defined as

$\ell_m' = M^{1/4}/\varepsilon^{1/4}$ and $\ell_m = M^{1/2}/U_A$) will indicate whether it will be in the near-field or in the far-field when it reaches the maximum height of rise. If $\ell_m'/\ell_m \ll 1$ a nonbuoyant jet will reach its maximum rise Z_m before it is significantly bent over by the crossflow. Dimensional considerations imply that

$$\frac{Z_m}{\ell_m'} = f\left(\frac{\ell_m'}{\ell_m}\right) \tag{3.26}$$

where $f(\ell_m'/\ell_m)$ indicates some unknown functional relation. As the ratio $\ell_m'/\ell_m \to 0$ or as the crossflow velocity becomes relatively small, the result should be the same as for a nonbuoyant jet in a stratified, stagnant ambient fluid. In that case, the relation

$$\frac{Z_m}{\ell_m'} = \text{constant} \tag{3.27}$$

is the correct relation for the maximum height of rise. It follows that the height Z_e at which the jet reaches its equilibrium position should also be proportional to ℓ_m' since there are no other lengths to scale this phenomenon. Z_m and Z_e should therefore be proportional to each other.

The dilution of a jet at its maximum and equilibrium heights of rise should also approximately follow the relation for a nonflowing ambient fluid. Dimensional analysis with the characteristic volume flux μ_m can be used to obtain a description of the dilution of a tracer. The characteristic volume flux at the maximum height of rise must scale with the stratification parameter ε and the initial kinematic

momentum flux M. The appropriate non-dimensional relation is

$$\frac{\mu_m \varepsilon^{1/4}}{M^{3/4}} = \text{constant} \tag{3.28}$$

or in terms of the dilution $S_m = \mu_m/Q$:

$$\frac{S_m Q}{U_A \ell_m^2} \propto \frac{\ell_m'}{\ell_m} \tag{3.29}$$

If $\ell_m'/\ell_m \gg 1$, a nonbuoyant jet will already be in the far-field when it reaches the elevation at which it would stop rising in a stagnant fluid. The length scale ℓ_m' is no longer an accurate measure of the height of rise in this case. A more appropriate length scale is the height to which a cylindrical momentum puff (with $m = M/U_A$) would rise in a linearly stratified ambient fluid. This distance can be obtained from the non-dimensional relation

$$\frac{Z_m \varepsilon^{1/6}}{m^{1/3}} = \text{constant} \tag{3.30}$$

Thus for $\ell_m'/\ell_m \gg 1$, the appropriate relation for maximum and equilibrium heights of rise is

$$Z_m,\ Z_e \sim \left(\frac{M}{U_A \varepsilon^{1/2}}\right)^{1/3} \tag{3.31}$$

or

$$\frac{Z_m}{\ell_m'},\ \frac{Z_e}{\ell_m'} \sim \left(\frac{\ell_m'}{\ell_m}\right)^{-1/3} \tag{3.32}$$

The effect of a strong crossflow can be seen from Eq. 3.31 or 3.32 to decrease the maximum height of rise compared to a relatively weaker crossflow for the same jet and stratification conditions.

The characteristic volume per unit length for a momentum puff at its maximum height of rising ($\lambda_m = \mu_m/U_A$ by the corresponding analogy) can be used to estimate the dilution of a bent-over jet. Dimensional arguments imply that

$$\frac{\lambda_m \varepsilon^{1/3}}{m^{2/3}} = \text{constant} \tag{3.33}$$

which indicates that the characteristic dilution S_m is given by

$$\frac{S_m Q}{U_A \ell_m^{\,2}} = \left(\frac{\ell_m'}{\ell_m} \right)^{4/3} \tag{3.34}$$

3.4.3 Buoyancy-Dominated Flow

The same type of arguments can be applied to derive similar results for buoyancy-dominated flow. For plume-like flow, the relevant parameter to consider is the ratio of the length scales $\ell_b' = B^{1/4}/\varepsilon^{3/8}$ and $\ell_b = B/U_A^{\,3}$. If $\ell_b'/\ell_b \ll 1$, the general behavior should be the same as for a buoyant plume in a nonflowing stratified fluid. The maximum and equilibrium heights of rise should thus be directly proportional to the length scale ℓ_b':

$$\frac{Z_e}{\ell_b'}, \frac{Z_m}{\ell_b'} = \text{constants} \tag{3.35}$$

The dilution for a plume in a stratified fluid at its maximum height of rise is determined by the non-dimensional relation for the volume flux μ_m:

$$\frac{\mu_m \varepsilon^{5/8}}{B^{3/4}} = \text{constant} \tag{3.36}$$

The dilution $S_m = \mu_m/Q$ of a passive tracer for buoyancy-dominated near-field flows is given by

$$\frac{S_m Q}{U_A \ell_b^2} \propto \left(\frac{\ell_b'}{\ell_b} \right)^{5/3} \tag{3.37}$$

A buoyant thermal in a stratified fluid will rise according to the dimensionless relation:

$$\frac{Z_m \varepsilon^{1/3}}{b^{1/3}} = \text{constant} \tag{3.38}$$

where $b = B/U_A$ by the analogy between a thermal and a bent-over plume. Thus, for $\ell_b'/\ell_b \gg 1$, the maximum and equilibrium heights of rise for a buoyant plume in a stratified crossflow are given by the relation:

$$\frac{Z_e}{\ell_b'}, \frac{Z_m}{\ell_b'} \sim \left(\frac{\ell_b'}{\ell_b} \right)^{-1/9} \tag{3.39}$$

The dilution of a buoyant thermal can be obtained from the relation

$$\frac{\lambda_m \varepsilon^{2/3}}{b^{2/3}} = \text{constant} \tag{3.40}$$

where λ_m has been defined previously. Expressed in terms of the dilution S_m of a tracer, Eq. 3.40 becomes

$$\frac{S_m Q}{U_A \ell_b^2} \propto \left(\frac{\ell_b'}{\ell_b} \right)^{16/9} \tag{3.41}$$

3.4.4 Other Flow Properties in a Stratified Crossflow

There are several other characteristics of the jet behavior that can be deduced from simple physical arguments. For example, the jet widths must scale according to the proper length characterizing the given limiting case. A nonbuoyant jet with $\ell_m'/\ell_m \gg 1$ (one which reaches Z_m in the mdff) must scale according to the length

$$\ell = \left(\frac{M}{U_A \varepsilon^{1/2}} \right)^{1/3} = \left(\ell_m'^2 \ell_m \right)^{1/3} \tag{3.42}$$

which is also proportional to the maximum height of rise. It can therefore be concluded that the jet widths are proportional to the maximum height of rise in each asymptotic case.

A buoyant jet will possess negative buoyancy after it reaches its maximum height of rise due to the fact that the jet possesses a nonzero vertical momentum when it first reaches its neutrally buoyant position which causes it to rise above this level. The flow will oscillate with a decreasing amplitude until it finally comes to rest at some equilibrium level. The time scale associated with these oscillations which are a result of the stratification must be $\tau = \varepsilon^{-1/2}$. The period of

oscillation must be proportional to τ and the wavelength of an oscillation should be proportional to the length scale $\ell_a = U_A/\varepsilon^{1/2}$.

3.4.5 Summary of Analysis for Stratified Flows

The relations developed for the maximum height of rise and associated dilutions can be summarized in a more straightforward manner if they are presented in terms of the length scale $\ell_a = U_A/\varepsilon^{1/2}$. The preceding discussion has considered the four length scales ℓ_m, ℓ_b, ℓ_m', and ℓ_b' in the development of the various relations. However, the number of independent variables indicates that only three length scales are necessary to characterize the general problem. The relations will therefore be developed in terms of the length scales ℓ_m, ℓ_b, and ℓ_a. The length scales ℓ_m' and ℓ_b' can be expressed as combinations of these three lengths:

$$\ell_m' = \ell_m^{1/2} \ell_a^{1/2} \tag{3.43}$$

$$\ell_b' = \ell_b^{1/4} \ell_a^{3/4} \tag{3.44}$$

The various height of rise and dilution relations are presented in Table 3.3 in terms of these definitions. The dilution relations are also expressed in terms of Z_m to facilitate comparison with the results for the unstratified case. Note that the exponents on the various relations correspond directly to the equivalent trajectory or dilution relations for an unstratified crossflow.

The equilibrium rise Z_e will be proportional to Z_m for all cases so these relations are also valid at the equilibrium height of rise with

different constants of proportionality.

Table 3.3 Maximum height of rise and associated dilution relations for buoyant jets in a stratified crossflow.

Flow regime where Z_m is reached	Height of Rise Relation	Dilution Relation
Momentum-dominated near-field	$\frac{Z_m}{\ell_m} = C_9\left(\frac{\ell_a}{\ell_m}\right)^{1/2}$	$\frac{S_m Q}{U_A \ell_m^2} = C_{13}\frac{Z_m}{\ell_m}$
Momentum-dominated far-field	$\frac{Z_m}{\ell_m} = C_{10}\left(\frac{\ell_a}{\ell_m}\right)^{1/3}$	$\frac{S_m Q}{U_A \ell_m^2} = C_{14}\left(\frac{Z_m}{\ell_m}\right)^2$
Buoyancy-dominated near-field	$\frac{Z_m}{\ell_b} = C_{11}\left(\frac{\ell_a}{\ell_b}\right)^{3/4}$	$\frac{S_m Q}{U_A \ell_b^2} = C_{15}\left(\frac{Z_m}{\ell_b}\right)^{5/3}$
Buoyancy-dominated far-field	$\frac{Z_m}{\ell_b} = C_{12}\left(\frac{\ell_a}{\ell_b}\right)^{2/3}$	$\frac{S_m Q}{U_A \ell_b^2} = C_{16}\left(\frac{Z_m}{\ell_b}\right)^2$

3.5 Discussion of Analysis

3.5.1 Application of the Model

The results in Section 3.3 must be interpreted in order to apply the solution that is valid for a general buoyant jet in an unstratified crossflow. This is accomplished by examining the relative magnitude of various length scales, primarily ℓ_m and ℓ_b if it is assumed that the analysis is to be applied for distances somewhat greater than ℓ_Q from the source. A given buoyant jet flow will generally be controlled by the initial momentum as discussed previously and will ultimately be influenced primarily by the buoyancy.

Thus, most buoyant jet flows will originate in the momentum-dominated near-field and will ultimately reach the buoyancy-dominated far-field. The intermediate behavior depends upon the magnitude of the ratio ℓ_m/ℓ_b which is a type of Froude number:

$$\frac{\ell_m}{\ell_b} = \frac{U_A^2}{g_o' D\sqrt{\pi/4}}$$

The field of solutions is depicted schematically in Fig. 3.4 which assumes values of unity for the various constants. This figure is intended only to indicate the nature of the model and the same type of figure with experimental values of the constants will be presented in Chapter 6.

If $\ell_m/\ell_b \ll 1$, the jet momentum is relatively weak compared to the buoyancy and the jet will not be bent over significantly by the cross-flow when the buoyancy begins to control the jet behavior. The flow will pass from the mdnf to the bdnf and then as z/ℓ_b becomes large, will go to the bdff. However, if $\ell_m/\ell_b \gg 1$, the buoyancy effect is relatively weaker and the momentum-dominated flow will pass from the near-field to the far-field before the buoyancy effect begins to dominate. Thus there are essentially two trajectory sequences with increasing x: the flow sequence will be mdnf-bdnf-bdff (1/2,3/4,2/3 trajectory relations) when $\ell_m/\ell_b \ll 1$ and if $\ell_m/\ell_b \gg 1$, the sequence is mdnf-mdff-bdff (1/2,1/3,2/3 trajectories). Fig. 3.4 clearly indicates these two possibilities and also indicates that when ℓ_m/ℓ_b is on the order of 1, the trajectory will go from the mdnf directly to the

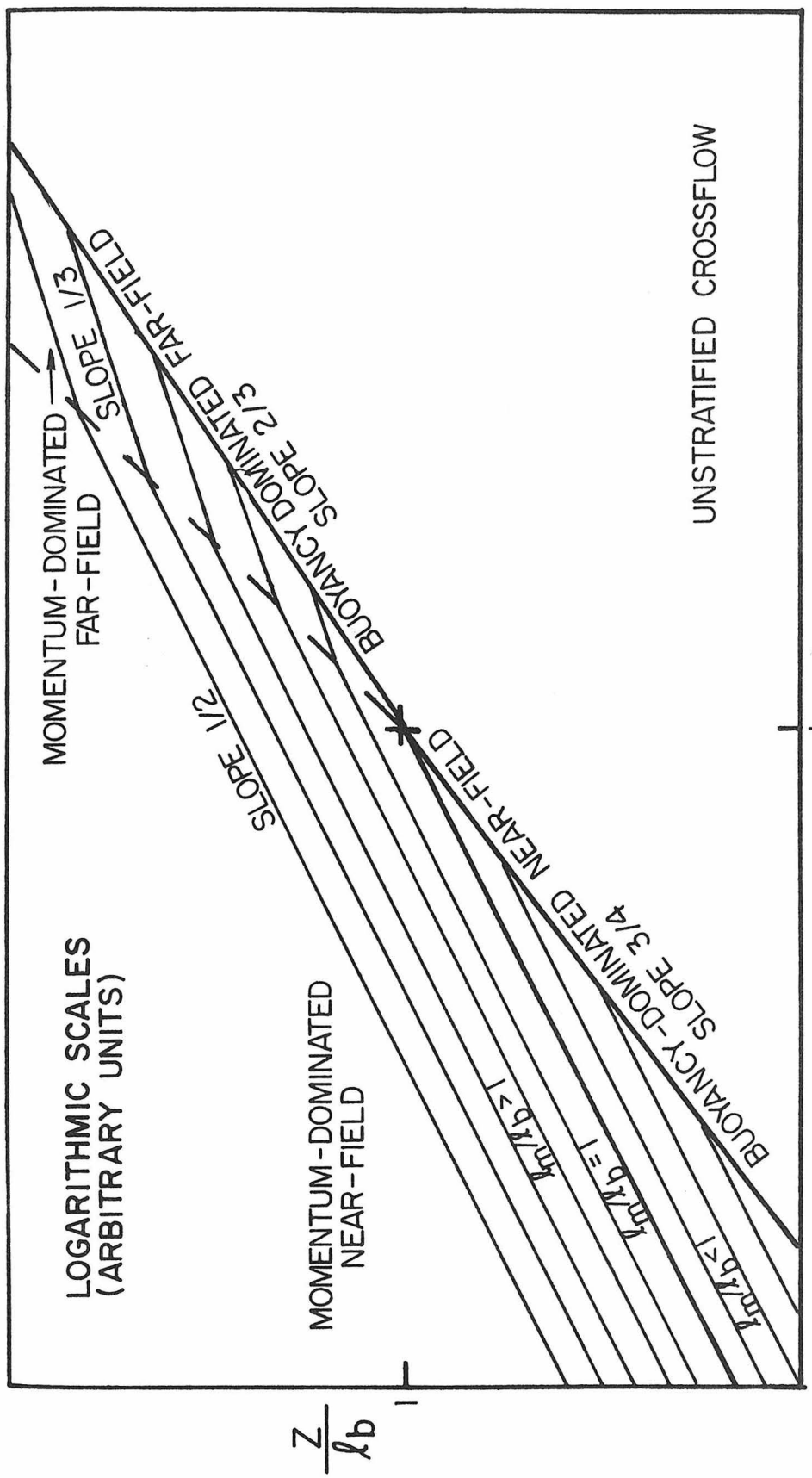

Fig. 3.4 Schematic of trajectories for buoyant jets in an unstratified crossflow.

bdff (1/2,2/3 variations). It is not possible for the flow to go from the bdnf to the mdff as Fig. 3.4 clearly indicates. This is to be expected since once the flow becomes buoyancy-dominated, there is no mechanism for it to become controlled by the initial momentum again. Thus, there will be no 3/4,1/3,2/3 trajectory sequences. If the additional effect of the initial volume flux is considered, there are several variations of the trajectories mentioned above. If $\ell_m/\ell_Q \ll 1$ then it is not possible to consider a momentum-dominated near-field flow regime since if $z/\ell_m \ll 1$, then z/ℓ_Q will be much less than one and the effect of the initial volume flux cannot be ignored. Fig. 3.5 is a schematic of the various possible flow sequences with the different power law relations indicated (i.e., 1/2 refers to the mdnf, 1/3 to the mdff, etc.). Again, this figure is only intended to describe the qualitative nature of the flow, and values for the various constants were assumed to be unity. The use of actual experimental values would change the figure somewhat but the general idea will be the same.

The dilution of a buoyant jet depends upon the flow regimes it passes through. It is possible to use Fig. 3.4 to determine the appropriate flow regime for a specified horizontal or vertical location and to apply the dilution relation which is valid for that flow regime. It is also possible to develop a figure such as that given schematically in Fig. 3.6 from which the dilution can be obtained directly given the vertical rise and the jet and ambient conditions. The reason that the mdff and bdff collapse to a single curve in this figure is that a value of unity was used for the various constants. Since these constants

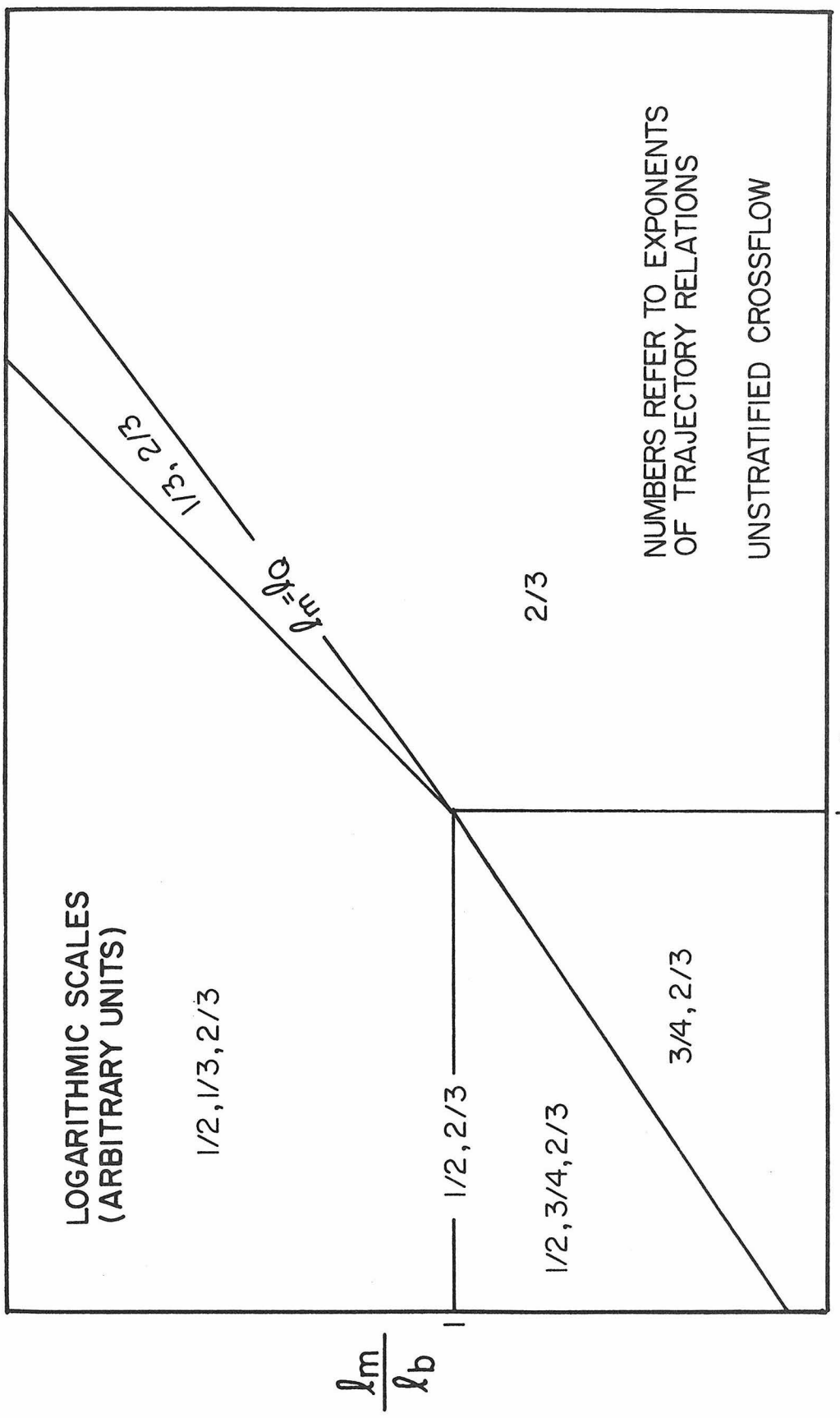

Fig. 3.5 Schematic of trajectory sequences indicated by the unstratified flow model.

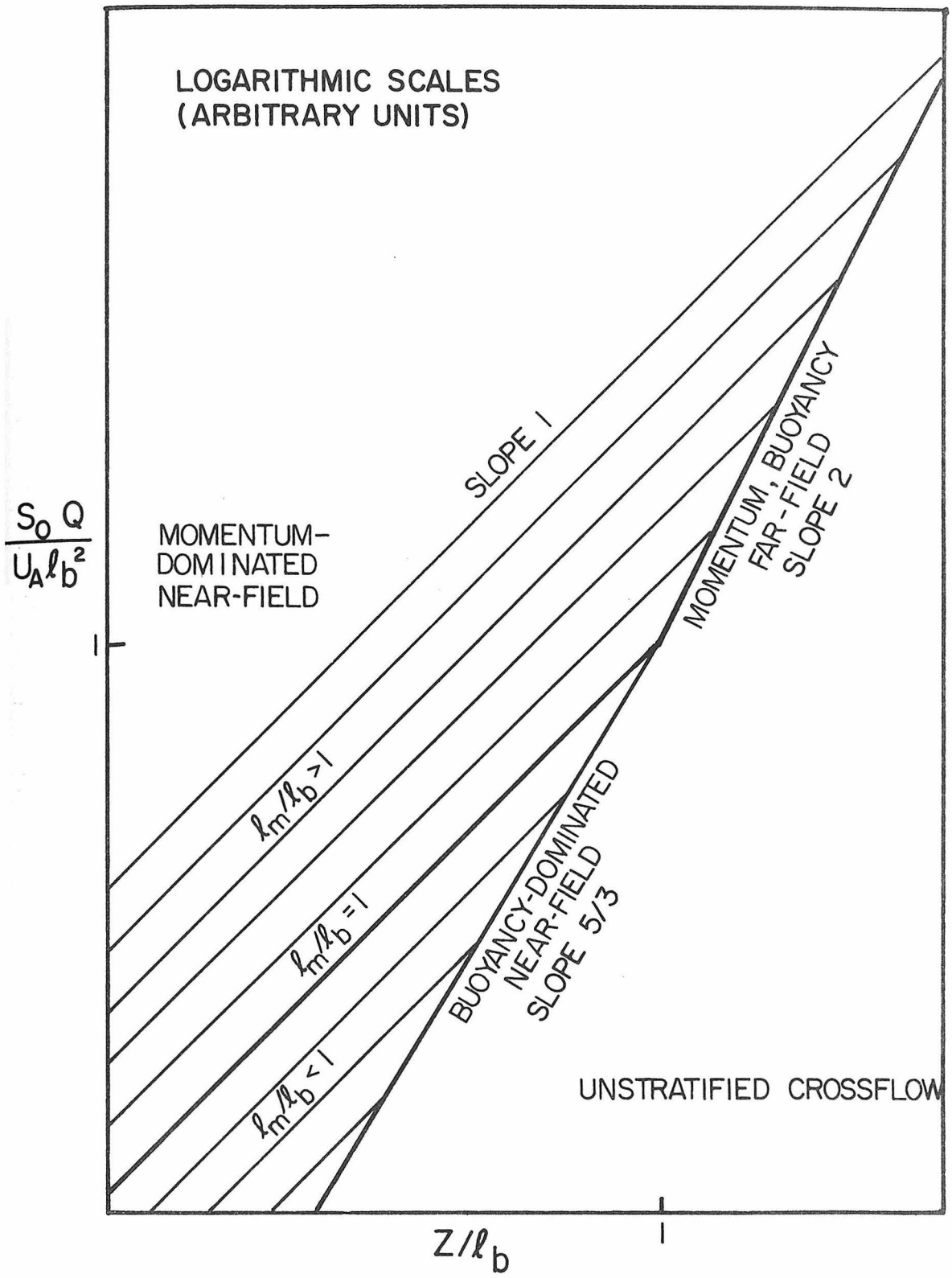

Fig. 3.6 Schematic of dilutions for buoyant jets in an unstratified crossflow.

would not generally be equal, the result would be that the two far-field regimes would be indicated by parallel lines on the figure with transition curves where the flow passes from the mdff to the bdff.

Jet trajectories in a density-stratified crossflow can be estimated up to the maximum height of rise by considering the above results for a uniform density flow. This can be justified, for example, if the distance ℓ_m' is regarded as the distance required for the density stratification to extract the momentum flux from a nonbuoyant jet. It seems reasonable that if $z/\ell_m' \ll 1$, the density structure will not have removed significant momentum from the jet and the jet trajectory will be essentially the same as for an unstratified crossflow. The same argument should apply for a buoyant plume with respect to ℓ_b'. A reasonable first approximation would then be to extend the jet trajectory and other characteristics to the maximum height of rise after which the unstratified results are no longer valid. A further justification can be demonstrated by comparison of the dilution relations in Tables 3.2 and 3.3. The relations for any flow regime agree to within a constant, indicating that the dilution variation with vertical distance for a buoyant jet in a uniform density crossflow is approximately valid except downstream from the location of the maximum height of rise.

The trajectory and dilution of a buoyant jet in a stratified crossflow can thus be approximately obtained up to the maximum height of rise by using the uniform density results. It is necessary to determine which flow regime a jet will be in when it reaches its maximum rise in order to determine the appropriate height of rise relation. This

depends upon the relative magnitude of the three length scales, ℓ_m, ℓ_b, and ℓ_a. Fig. 3.7 presents a schematic of the maximum height of rise as a function of these variables, again assigning a value of 1.0 to all constants. A figure similar to this with actual experimental values for the constants could be used with figures similar to Figs. 3.4 and 3.6 to determine the trajectories and dilutions of a buoyant jet up to the maximum height of rise.

3.5.2 Comparison of Predictions from Previous Investigations

The general model thus predicts several types of flow behavior which are consistent with other models. The prediction from this study for the mdnf ($z/\ell_m \sim (x/\ell_m)^{1/2}$) agrees somewhat with the models presented by Hewett, et al. (1971), Hoult and Weil (1972), and others, for the jet behavior near the source. Their predictions differ from the mdnf model only in that their models indicate a dependence of the trajectory coefficient C_1 on the velocity ratio V_j/U_A. However, their relation for C_1 approaches a constant for large values of the velocity ratio, or equivalently ℓ_m/ℓ_Q, and only varies significantly for values of ℓ_m/ℓ_Q on the order of 1 or less. For ℓ_m/ℓ_Q small, the effect of the jet geometry is important, and neither model can be assumed to be valid. Thus the models are essentially equivalent for the domain where they can be applied.

The buoyancy-dominated near-field result from this study agrees with that given by Priestley (1956) which is to be expected since they were derived from the same assumptions. The model proposed by Moore (1974) does not agree with the present model even though the $z \sim x^{3/4}$

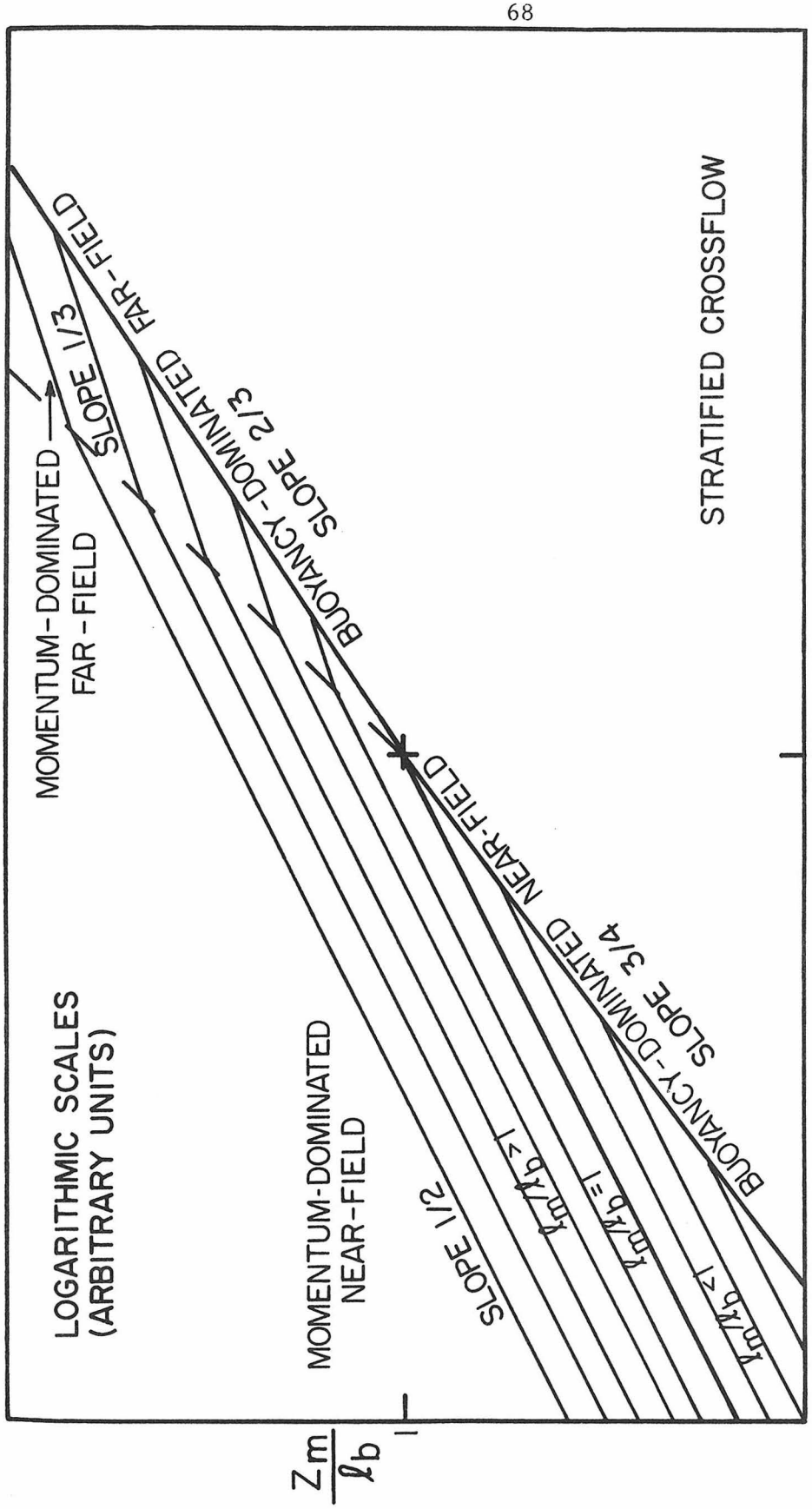

Fig. 3.7 Schematic of maximum height of rise as a function of the flow variables.

relation is similar. His trajectory relation is not dimensionally homogeneous and is therefore questionable. Finally, the far-field relations agree with the models presented by Scorer (1959) again because they were derived by the same methods. Other models presenting the same result for the momentum-dominated far-field have been presented by Chan and Kennedy (1972) and Hoult and Weil (1972). The two-thirds trajectory relation in the buoyancy-dominated far-field has also been proposed by numerous researchers including Slawson and Csanady (1967), Shwartz and Tulin (1972), and Hewett, et al. (1971).

The combined model predicts various types of flow behavior which are consistent with the models presented by other researchers. For example, if ℓ_m/ℓ_Q is very small and $\ell_m/\ell_b \gg 1$, the mdnf will be negligible and the model proposed by Chu and Goldberg (1974) (1/3 and 2/3 powers for trajectory relations) will agree with the present formulation. For $\ell_m/\ell_b \approx 1$, the prediction by Hewett, et al. (1971) (1/2,2/3 powers) agrees with the present model. The general relation of Hoult and Weil (1972) and others (1/2,1/3,2/3 power law relations) is equivalent to the results of the present analysis if $\ell_m/\ell_b \gg 1$. The information in Fig. 3.5 is repeated in Fig. 3.8 with the domains where the predictions by other researchers agree with the present model. Significantly, the case for $\ell_m/\ell_b \ll 1$ (1/2,3/4,2/3 trajectories) has not been proposed by other researchers. Results of many previous studies can thus be regarded as special cases of the general model, given certain restrictions on ℓ_Q, ℓ_m, and ℓ_b.

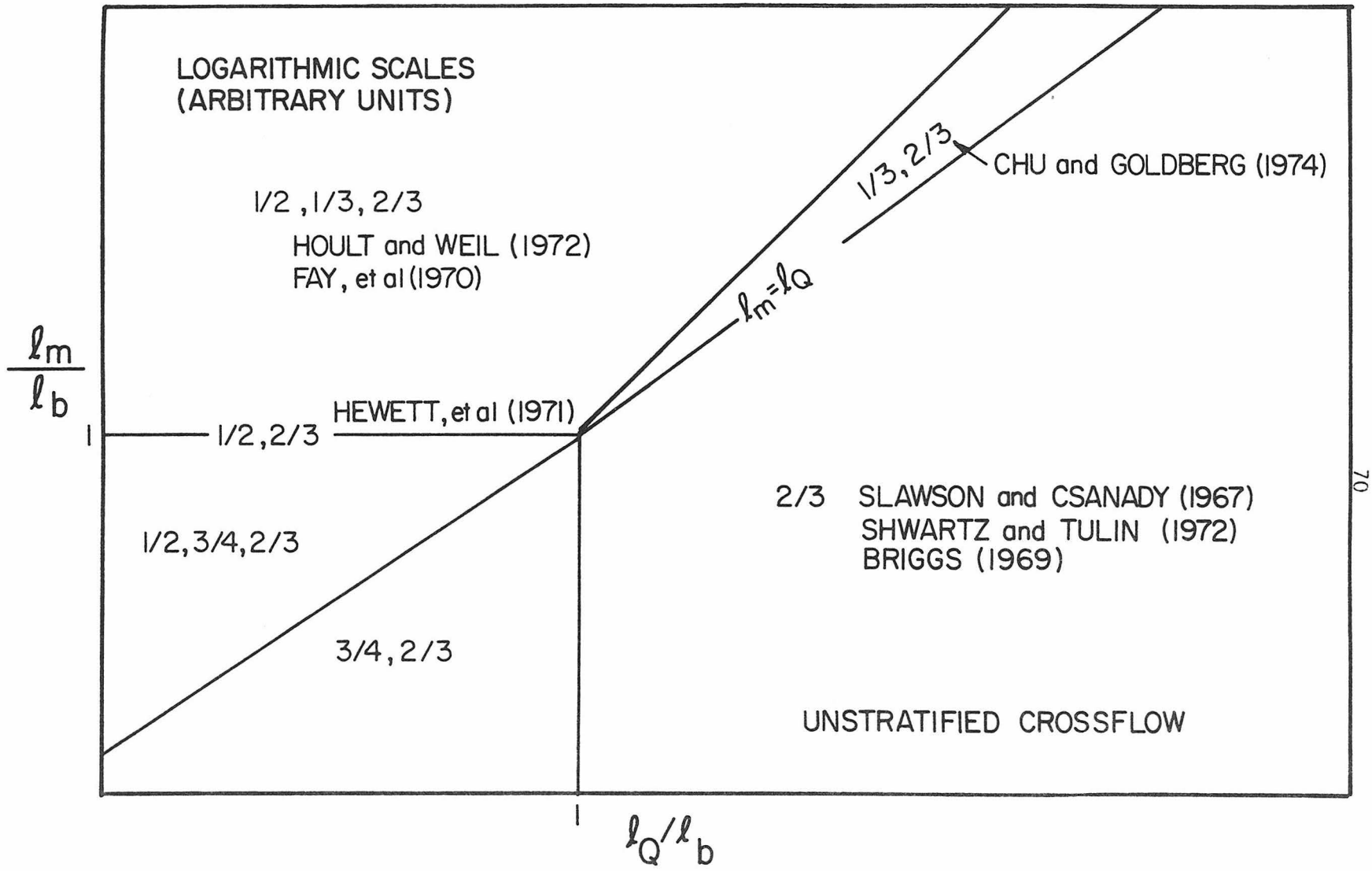

Fig. 3.8 Comparison of previous theoretical investigations with the unstratified crossflow model.

Predictions for the maximum height of rise in a stratified crossflow presented by Shwartz and Tulin (1972), Fay, et al. (1970) and others agree with the result predicted for the buoyancy-dominated far-field by the present model. The result for the mdff also agrees with that presented by Briggs (1969) for a nonbuoyant jet in a stratified crossflow. There have been no theoretical analyses which derive the results for the maximum height of rise for the near-field flows, although these results correspond to analyses for stagnant ambient fluids by Morton (1959) and others.

CHAPTER 4

EXPERIMENTAL INVESTIGATION

4.1 Experimental Objectives

The primary objective of the experimental investigation was to study the behavior of a round buoyant jet over a wide range of jet and ambient conditions. Initial experiments were performed in an unstratified crossflow with the objective of verifying the validity of the trajectory and dilution relations that were presented in the preceding chapter. Various parameters were varied including the crossflow velocity, jet discharge, and initial density difference. These variables were adjusted such that the jet behavior could be examined for each of the regions of interest: near- and far-field regimes for both momentum- and buoyancy-dominated flows. The experiments were performed to supplement previous measurements of the same type performed by Fan (1967).

The second phase of the experimental investigation involved the additional effect of density stratification. These experiments were performed to measure heights of rise and associated dilutions. Experiments were conducted to verify each of the relations presented in the analysis. The jet and ambient conditions were varied to cover as wide a range of experimental conditions as possible within the constraints of the apparatus.

4.2 Description of Apparatus

4.2.1 Towing Tank and Jet Discharge

All experiments were performed in a towing tank 61 cm square in cross-section and 8.7 m in length. The effect of a crossflow was simulated by towing a jet source the length of the tank at a constant velocity. This avoided the necessity of producing a density-stratified crossflow of uniform velocity. This arrangement also avoided any difficulties due to nonuniformities in ambient velocity over the jet cross-section or any effects caused by the presence of ambient turbulence.

The jet fluid was released downward from the water surface with the density difference created by adding sodium chloride to the jet solution. This arrangement resulted in a negative buoyant force and downward initial momentum, which is analogous to an upward buoyant jet. This can be justified if the Boussinesq approximation is valid, since the only important density effects are the buoyancy of the jet with respect to the ambient fluid. The jet discharge box was mounted so that it was just touching the water surface so that there was no significant wake as the jet was towed along the tank. Another advantage of this arrangement (saltwater jet into freshwater) was that the amount of salt required to produce density differences was much less than it would have been for a freshwater jet discharged into a saltwater tank.

The density differences for the jet discharge and for the ambient fluid stratification were produced by using aqueous solutions of sodium chloride. Temperatures for all fluids in the experiments were generally

in the range of 23° ± 2°C and density variations caused by temperature differences were negligible with respect to the variation caused by salt concentration. The fluid densities were measured with a Troemer Model S-100 specific gravity chain balance which was capable of measuring to the nearest 0.0001 g/mℓ. Specific gravities were measured at the ambient temperature of the fluid, which directly considered any variations in density due to temperature differences between different fluids.

The experiments were performed with the jets discharging into the towing tank which was filled to a depth of approximately 55 cm. The jet discharge structure consisted of a lucite box approximately 8 cm on a side with an orifice plate mounted to the bottom. A photograph and schematic of the box and orifice plate is presented in Fig. 4.1. The discharge box was filled with a fibrous material to ensure uniformity of flow from the sharp-edged orifice. The jet exit diameter was taken as 0.8 of the actual orifice diameter to allow for jet contraction. No direct measurements of the jet contraction were made. Different orifice plates with diameters of 0.25, 0.50, 1.00, and 1.25 cm were used in the experimental investigation, yielding jet diameters of 0.2, 0.4, 0.8, and 1.0 cm, respectively. The discharge box was positioned so that the bottom of the orifice plate just touched the water surface in the towing tank.

The discharge through the box was provided from a supply reservoir to a constant head tank, as shown schematically in Fig. 4.2. The flow was metered through a Fischer-Porter precision bore flow meter (tube no.

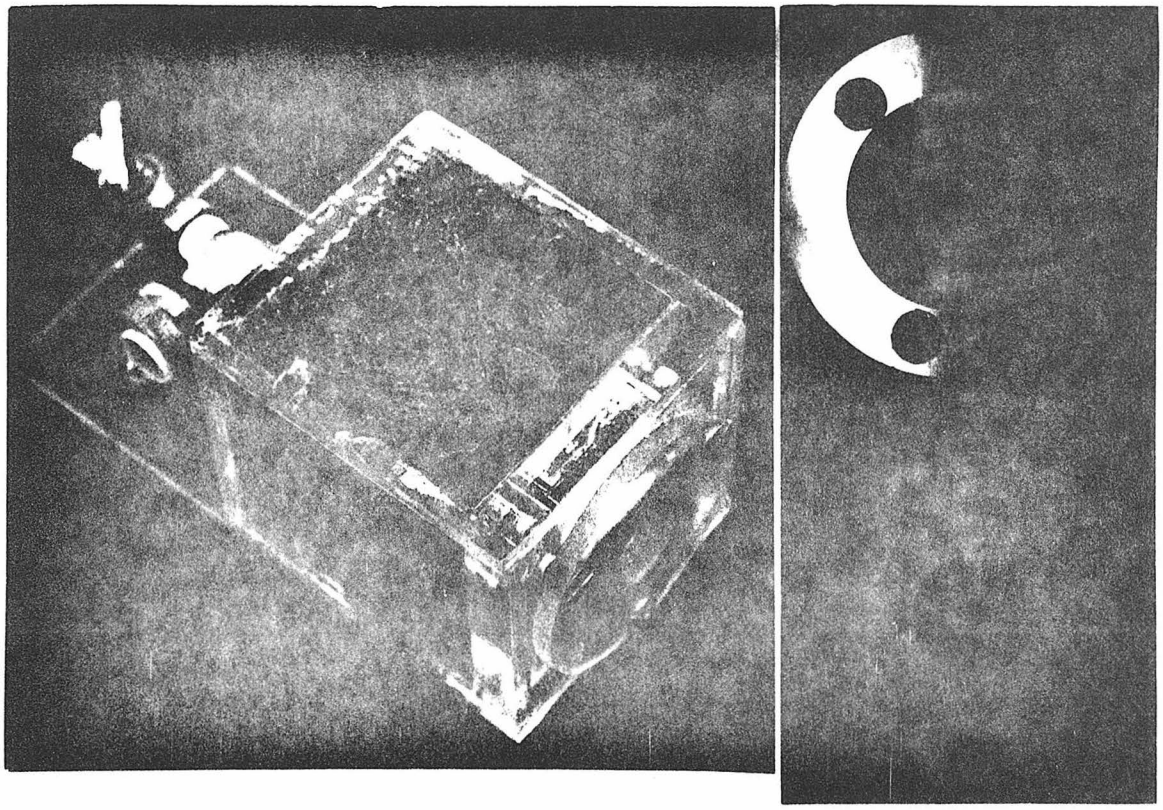

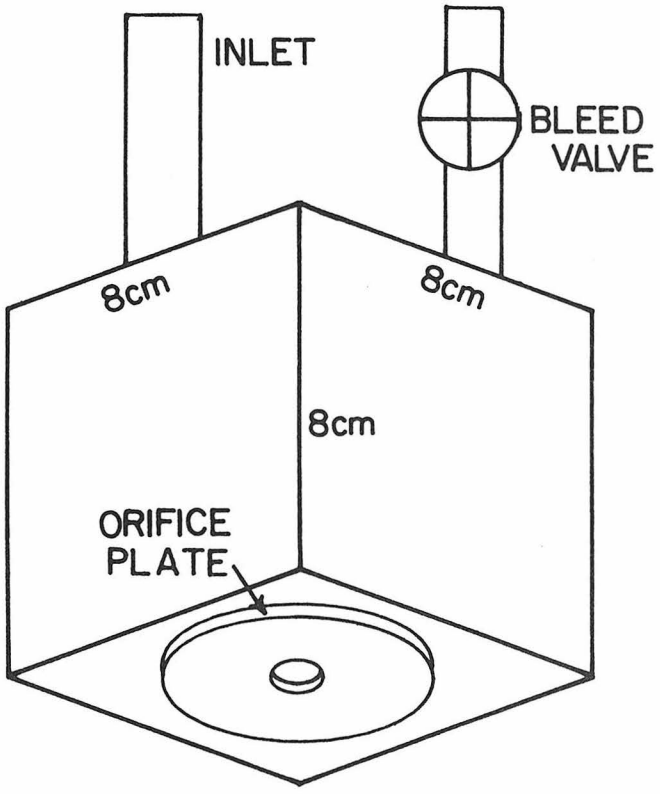

Fig. 4.1 Photograph and schematic of jet discharge box.

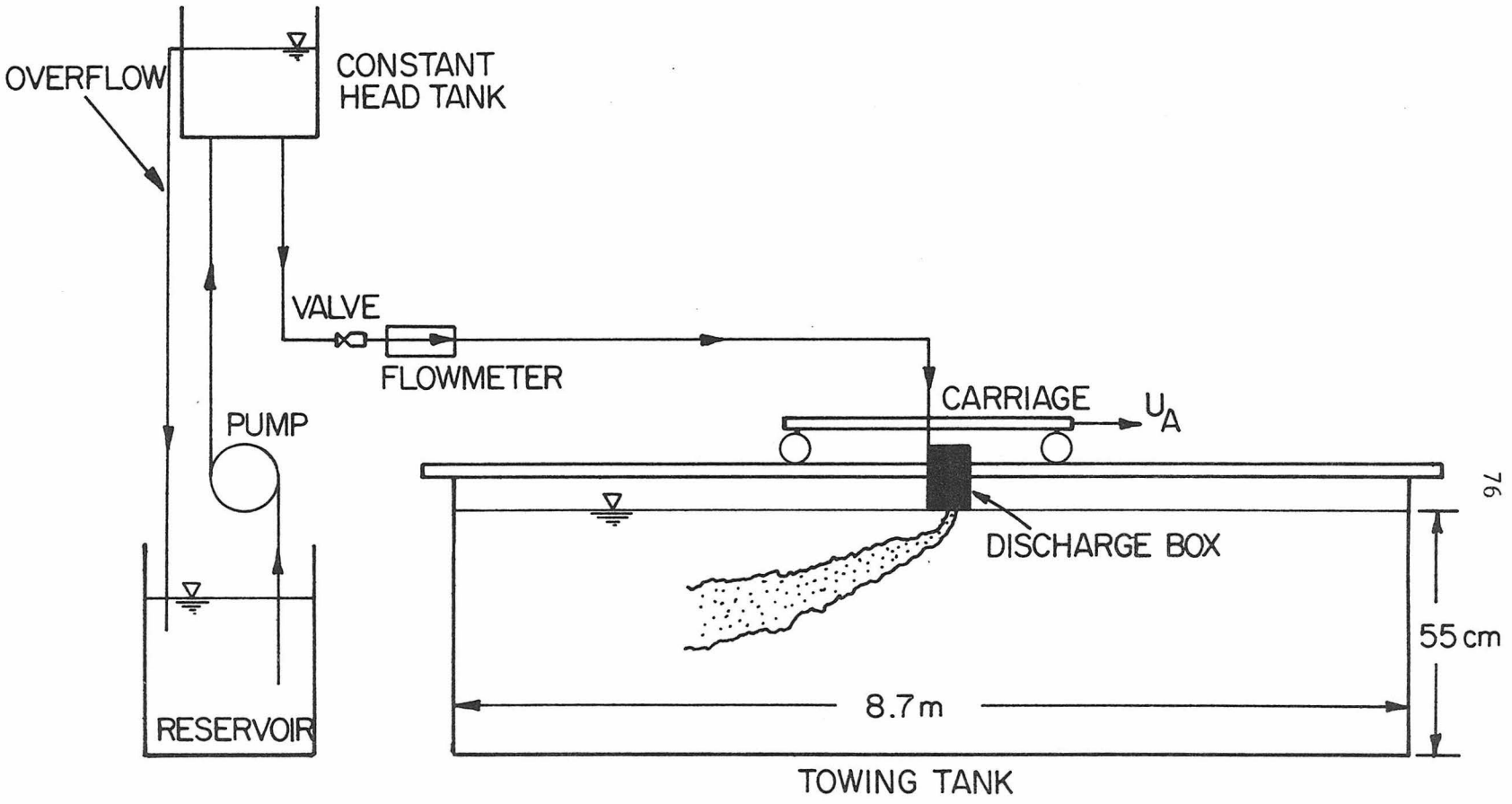

Fig. 4.2 Schematic of jet discharge system.

FP-$\frac{1}{2}$-27-G-10/77) with a discharge range of approximately 4-55 mℓ/sec.

The jet Reynolds numbers ($R_e = V_j D/\nu$) were in the range of 500 to 13,600 for the experimental investigation. These jets were observed to be turbulent from the jet exit in all cases. Some flow visualization experiments were performed with Reynolds numbers as low as 240 and the jets at the lowest Reynolds numbers were still turbulent. Hewett, et al. (1971) measured jet trajectories for buoyant jets with Reynolds numbers in the range of 156 - 573 and noticed no variations in the trajectories for the different jets. Since the lowest Reynolds number considered in this study (500) was substantially higher than Hewett's lowest value of 156, it was assumed that any effects due to Reynolds number effects could be neglected.

The jet box was attached to a carriage which was towed along the flume at a constant velocity. The carriage was designed such that the horizontal position of the jet source could be varied with respect to a fixed measurement system. A schematic of the towing apparatus is given in Fig. 4.3. The carriage was propelled by a cable which was driven by a pulley on a DC motor. The towing velocity was regulated by a Minarik speed control and could be varied over a range of 0.75 - 35 cm/sec. The carriage speed was determined by measuring the time of travel over a distance of 3.38 m along the tank. The timer was actuated by two microswitches and gave times to the nearest 0.1 seconds (approximately 1% of the least time). The towing velocities for successive operations at the same speed setting were reproducible to within approximately 1 - 2% for most experiments with a maximum variation of

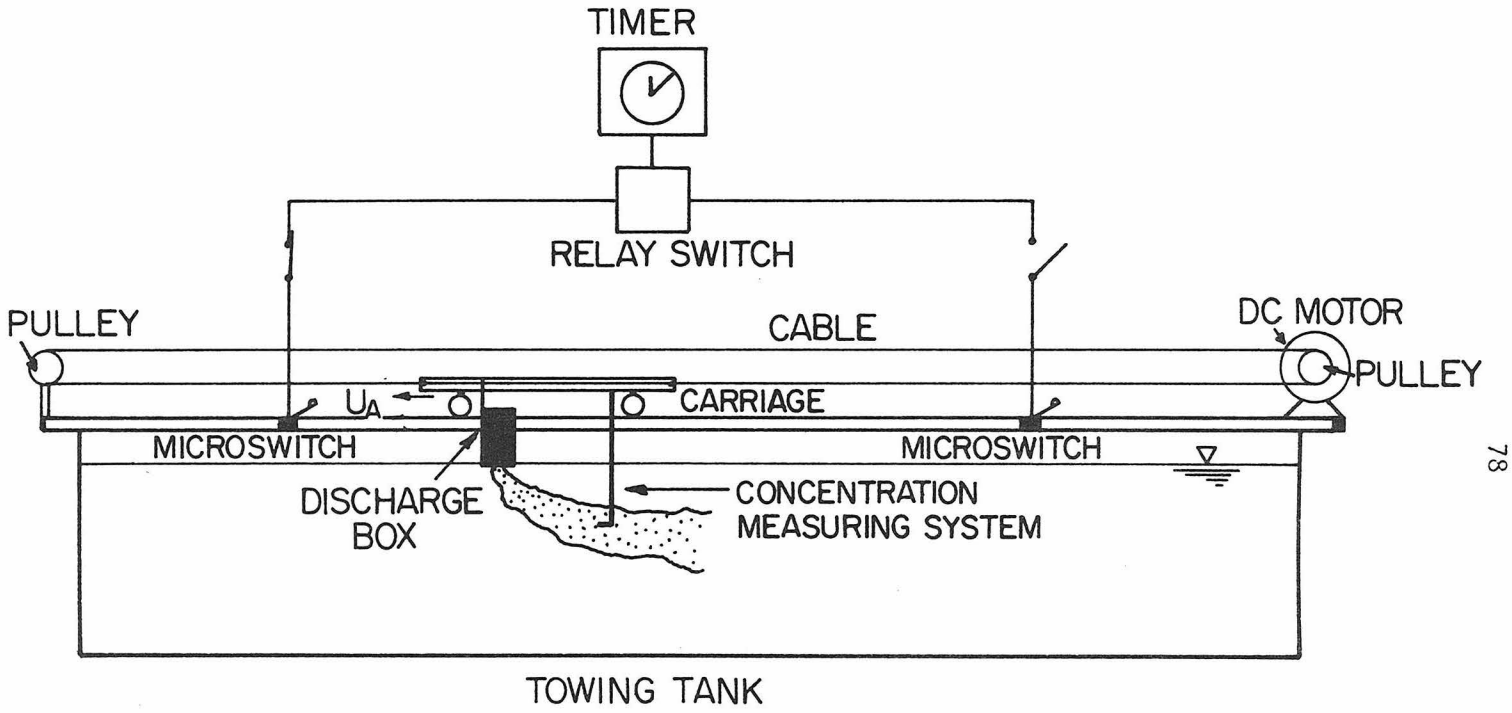

Fig. 4.3 Schematic of towing apparatus.

approximately 5%.

4.2.2 Density Stratification

Linear density stratifications were produced with sodium chloride to avoid any possible double diffusion effects which might have occurred with a saltwater jet in a thermally stratified tank. An additional advantage is that the molecular diffusion of salt is much slower than for heat, which gives a longer time to conduct experiments before the stratification decays. The stratifications were created with a continuous filling procedure. A large mixing tank with a capacity of about one-half of the towing tank volume (3000 liters) was filled with tap water and mixed with enough sodium chloride to provide a density equal to the value required for the ambient fluid at the bottom of the towing tank. A schematic of the stratification system is given in Fig. 4.4. The fluid in the mixing tank was kept well-mixed by means of an air jet discharged at the bottom of the tank. Linear stratifications were created by pumping water from the mixing tank to the towing tank at an arbitrary discharge Q and adding tap water at a rate of Q/2 to the mixing tank. The result of this procedure is the fluid density discharged from the mixing tank will decrease linearly with time. The fluid was pumped to the towing tank through a manifold onto three floating surface spreaders 35 cm in diameter. The purpose of the spreaders was to provide horizontal flow of the incoming fluid along the surface, thereby preventing significant mixing with the heavier fluid previously discharged. Any mixing that occurred at the surface was quickly damped out and molecular diffusion tended to smooth out any

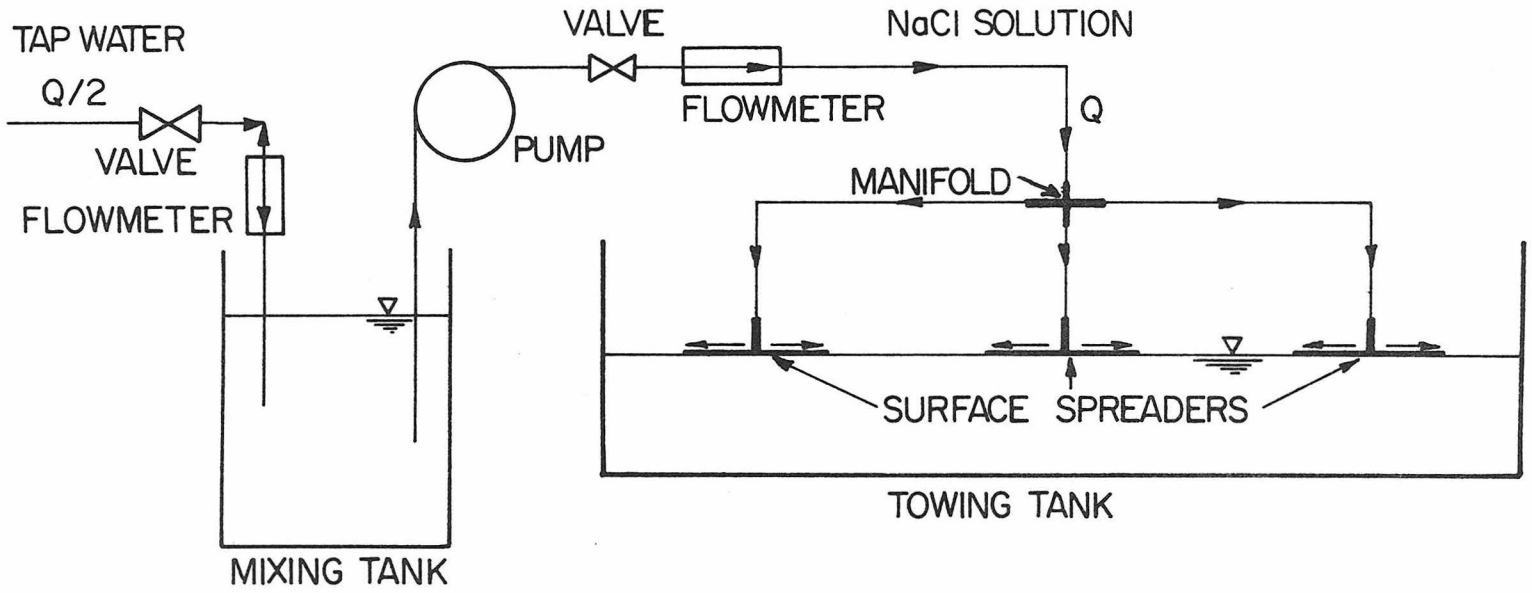

Fig. 4.4 Schematic of stratification system.

local nonuniformities in the density profile.

The density profile for each stratification produced was determined from salt concentration measurements made by a conductivity probe of the type described by Cannon (1974). Fig. 4.5 is a photograph and schematic of the probe used. This probe was constructed in the W. M. Keck Hydraulics Laboratory shop and is 60 cm long, allowing it to traverse the entire depth of the towing tank. A single channel Sanborn Model 151NK recorder with a 1100AS Carrier Preamplifier was used to measure the conductivity of the solution. The bridge circuit used in conjunction with the Sanborn recorder is given schematically in Fig. 4.6. The recorder output from the conductivity probe was recorded on a strip chart.

A sample of the salt solution in the mixing tank was taken before the beginning of each experiment. This was mixed with tap water to produce reference samples which were 0, 25, 50, 75, and 100 percent by volume of the salt water. The sample densities were measured on the Troemer specific gravity balance described previously, and the samples were used for the calibration of the conductivity probe. A typical calibration is given in Fig. 4.7. The calibration curve is nonlinear due to the fact that the electrical conductivity is not linear with salt concentration. Calibrations were taken before each measurement and were checked for instrument drift after the completion of the profile measurement.

The probe was mounted on a point gage to adjust its vertical position to the nearest 0.1 mm. Conductivity measurements were taken at 2.0 or 4.0 cm vertical intervals, depending upon the resolution desired.

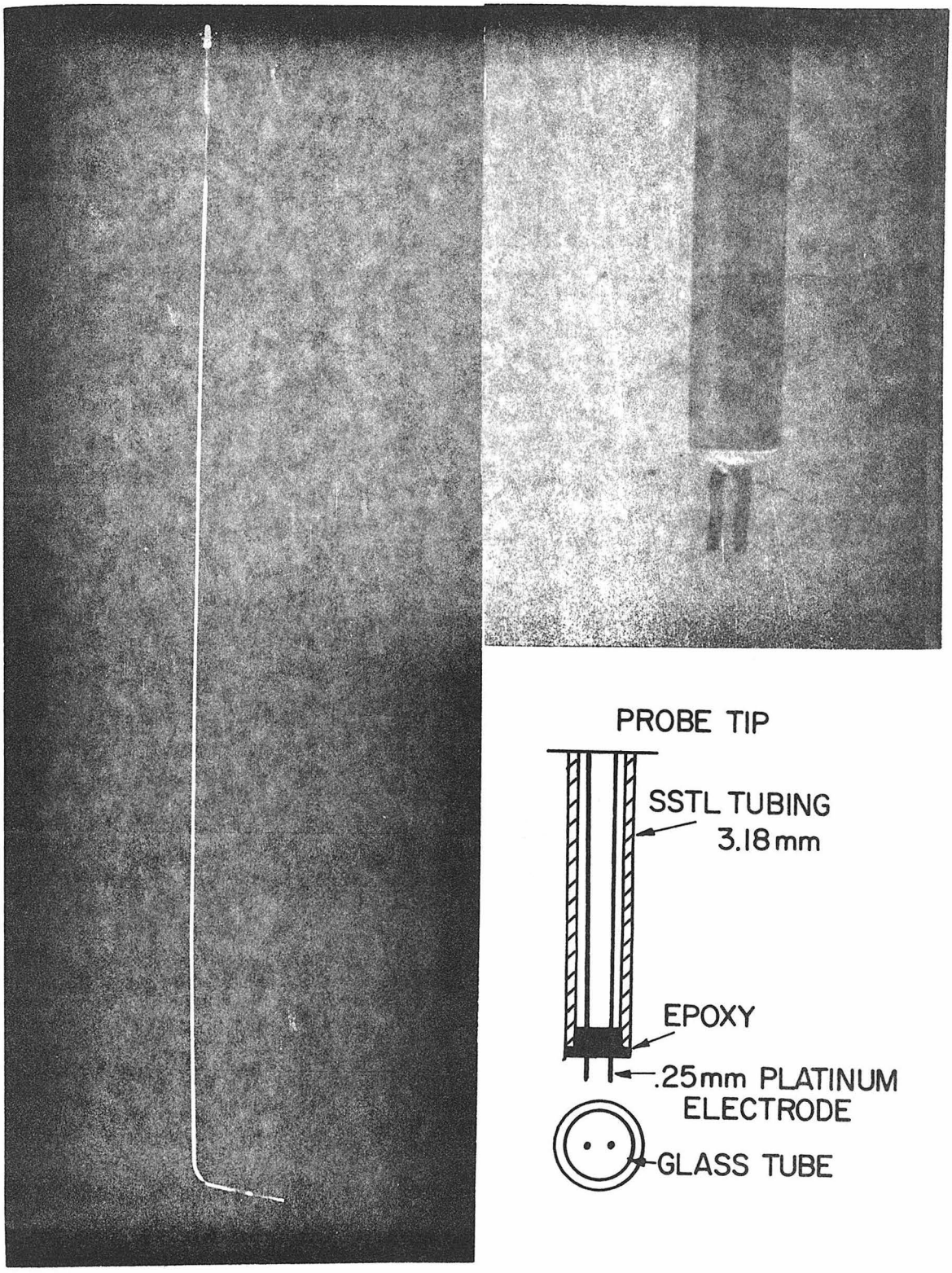

Fig. 4.5 Photograph and schematic of conductivity probe used to measure density profiles.

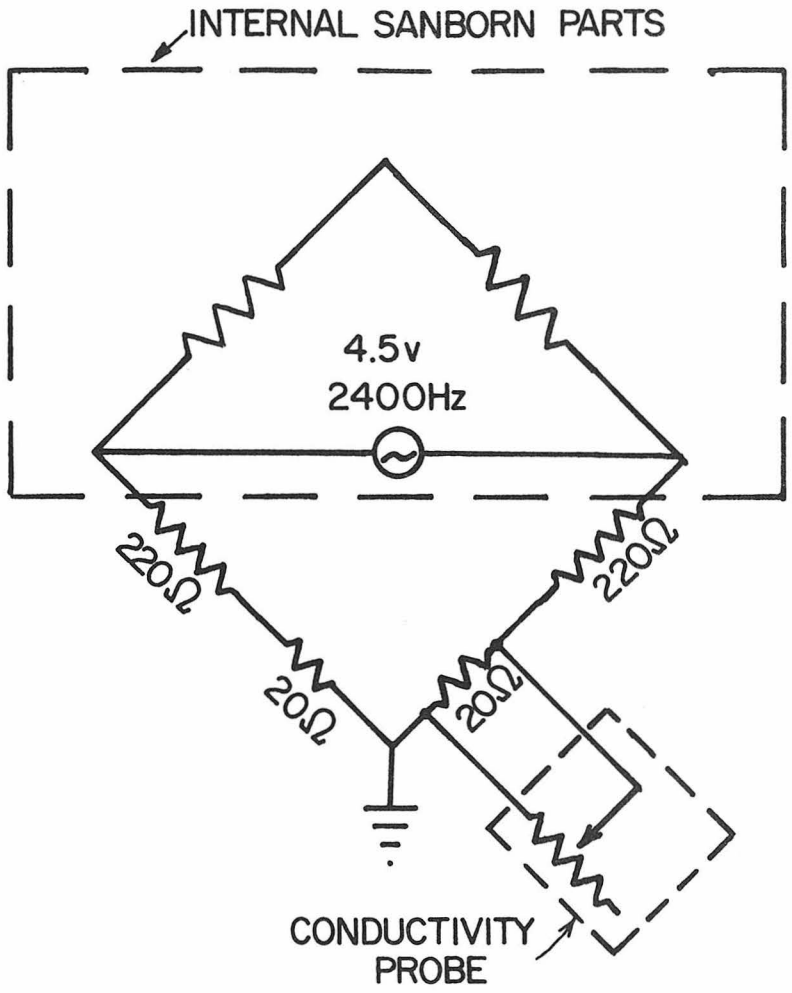

Fig. 4.6 Bridge circuit used with conductivity probe.

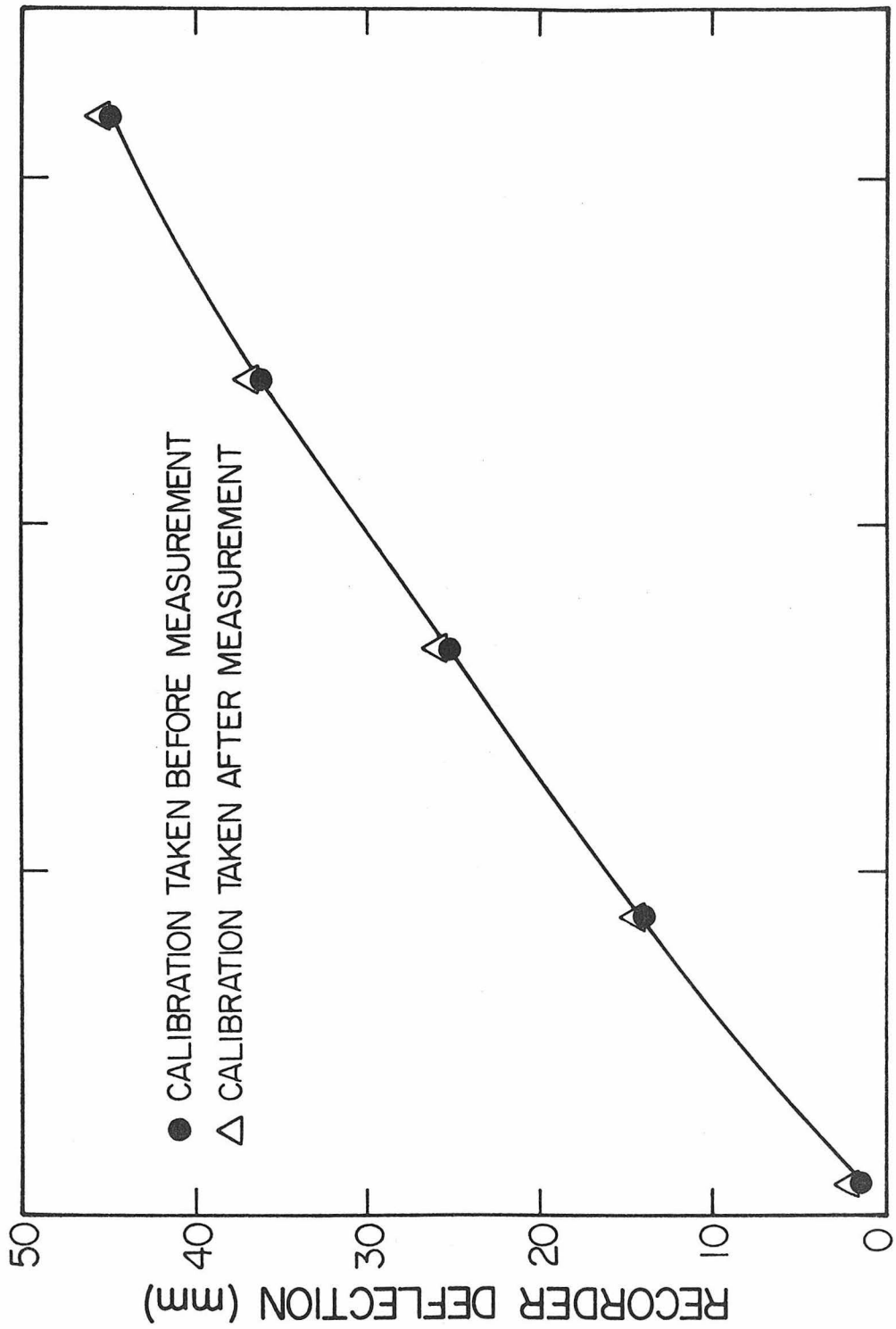

Fig. 4.7 Typical calibration of conductivity probe.

Most density profiles were measured about one-half hour after filling of the towing tank was completed, a time judged sufficient for fluid motions in the tank to damp out and for molecular diffusion to produce a nearly linear density profile. A thin layer at the water surface was relatively well-mixed because of a convection cell set up at the free surface. The thickness of this layer increased with time as shown in Fig. 4.8 for density profiles taken one-half and six hours after filling of the tank for a typical density stratification. The thickness of the mixed layer was typically in the range of 1 - 5 cm.

Some temperature profiles were measured along with the conductivity measurements to observe any temperature effects on the density structure. Temperatures were determined with a Victory Engineering Company Model No. 32A1 thermistor. The thermistor was calibrated by immersing in water baths of known temperatures and observing the thermistor resistance on a Hewlett-Packard Model 34702A digital multimeter. The thermistor was mounted on the point gage with the conductivity probe and the resistance at each vertical position was noted. Corrections to the density profiles were made assuming that the thermal expansion coefficient was the same as that of fresh water. A typical temperature-corrected density profile is compared to the corresponding uncorrected profile in Fig. 4.9 and indicates that the only major difference is that a slightly thicker well-mixed layer exists than indicated by conductivity measurements alone.

Tests were also performed to observe the effect of the jet discharge on the stratification. This was done since it was desirable to perform

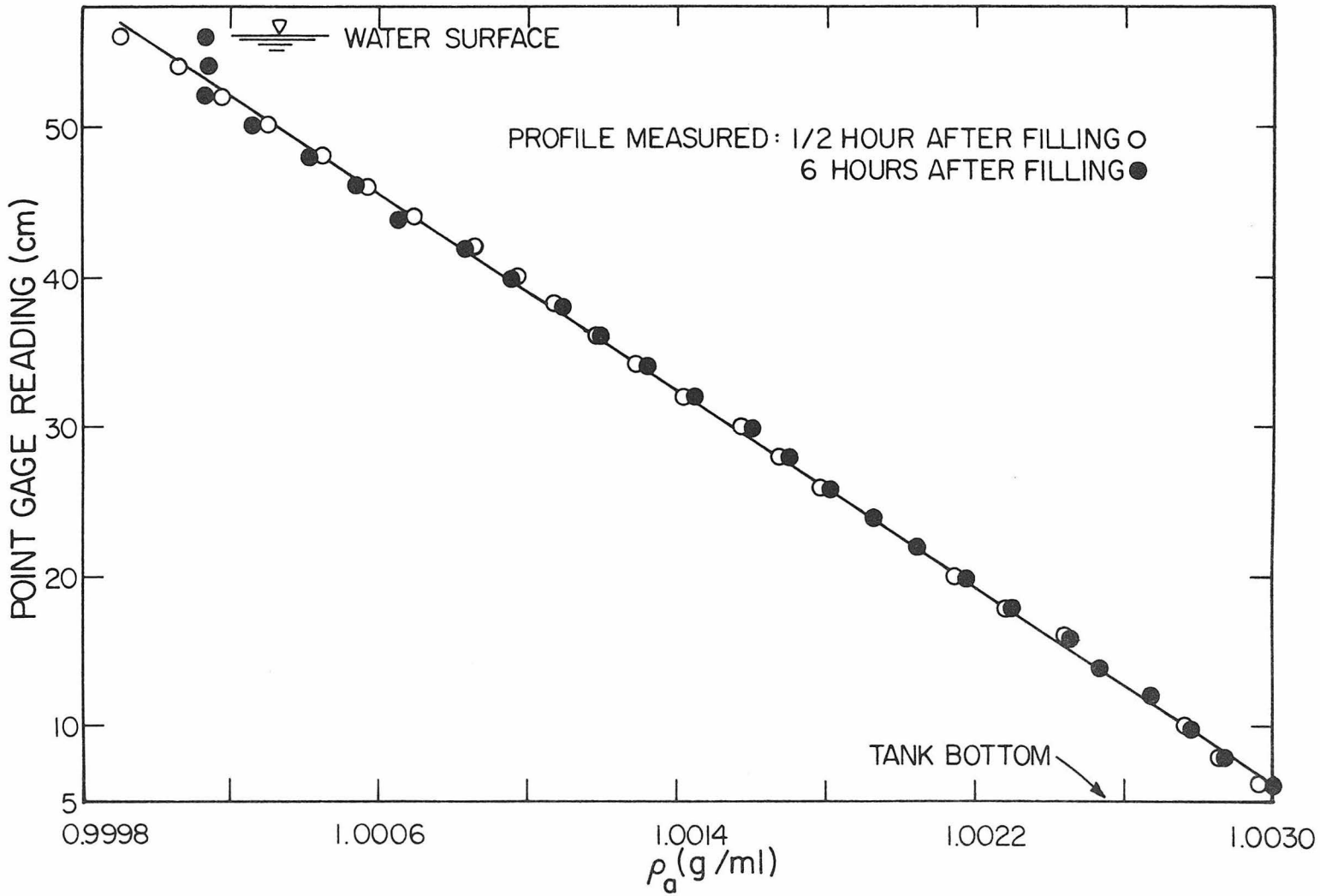

Fig. 4.8 Density profiles to demonstrate the increase in thickness of the surface mixed-layer with time.

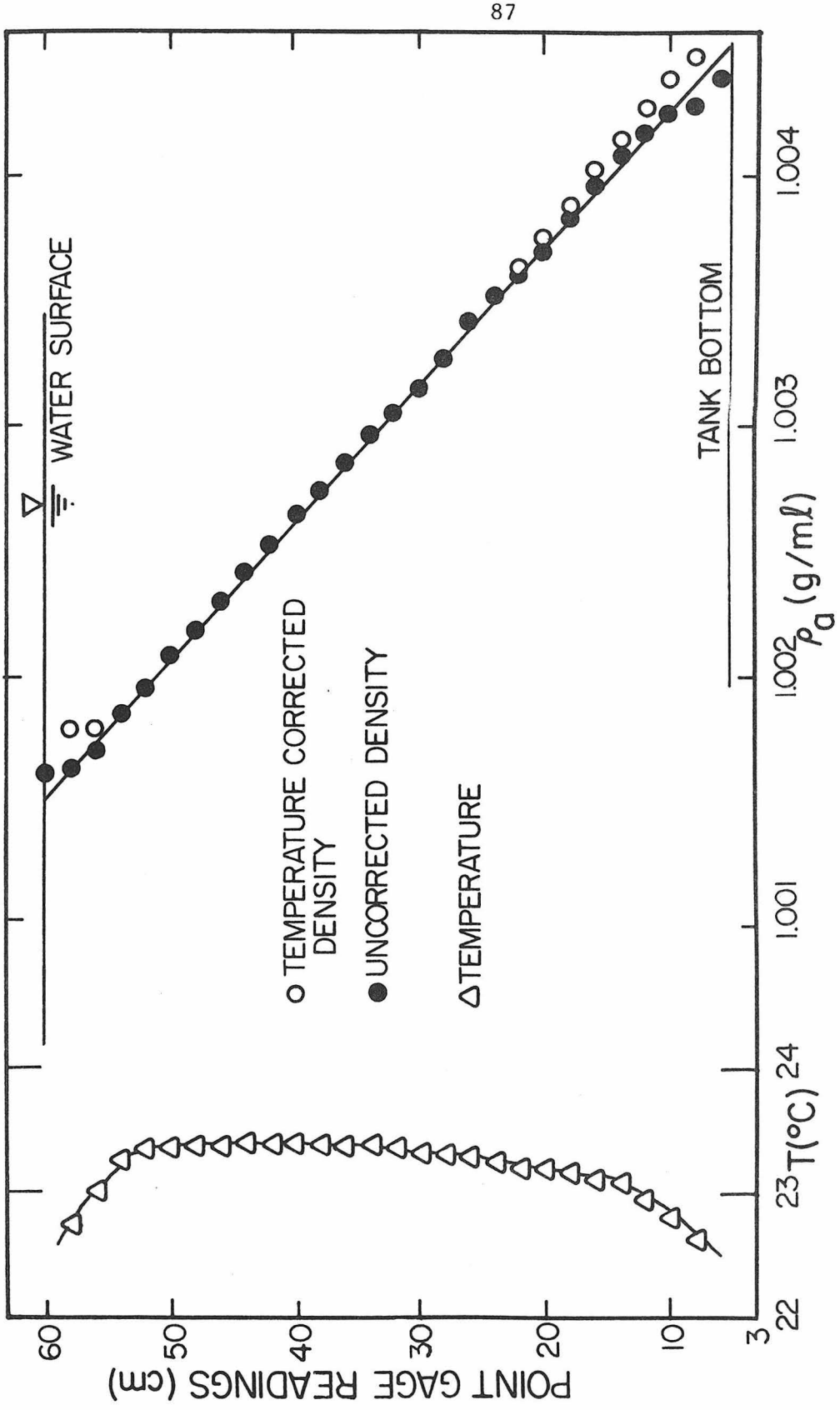

Fig. 4.9 Temperature-corrected density profile.

more than one experiment per stratification due to the time involved in setting up the stratification (generally four to five hours). Buoyant jets with an initial density difference of approximately 0.03 g/mℓ were discharged at approximately 10 mℓ/sec while being towed at a speed of 2 cm/sec. Density profiles were measured prior to any jet discharges and again after several runs were completed. Fig. 4.10 indicates that for a fairly strong stratification ($\varepsilon = 0.22$ sec^{-2}), the density structure was relatively undisturbed even after thirty discharges were made. Fig. 4.11 indicates, however, that for a relatively weaker stratification ($\varepsilon = 0.04$ sec^{-2}) the density profile was affected by four runs, and was significantly altered from a linear profile by four more. The change in the density structure is apparently due to the salt added by the buoyant jet and is not due to the jet turbulence. These experiments were performed in fairly rapid succession and there was insufficient time for molecular diffusion to smooth out the nonuniformity in the density profile. Thus, it was judged that a sufficient length of time should elapse between experiments and that only a few experiments could be performed for relatively weaker stratifications.

4.2.3 Photographic Equipment and Technique

Flow visualization and preliminary estimates of buoyant jet behavior were obtained by analyzing photographs taken as the jet was towed past a stationary camera. The photographs were taken at a given section of the towing tank with fiduciary marks taped on the glass walls as indicators of various horizontal and vertical positions. Photographs were taken with a 35 mm single-lens-reflex camera using either Kodak

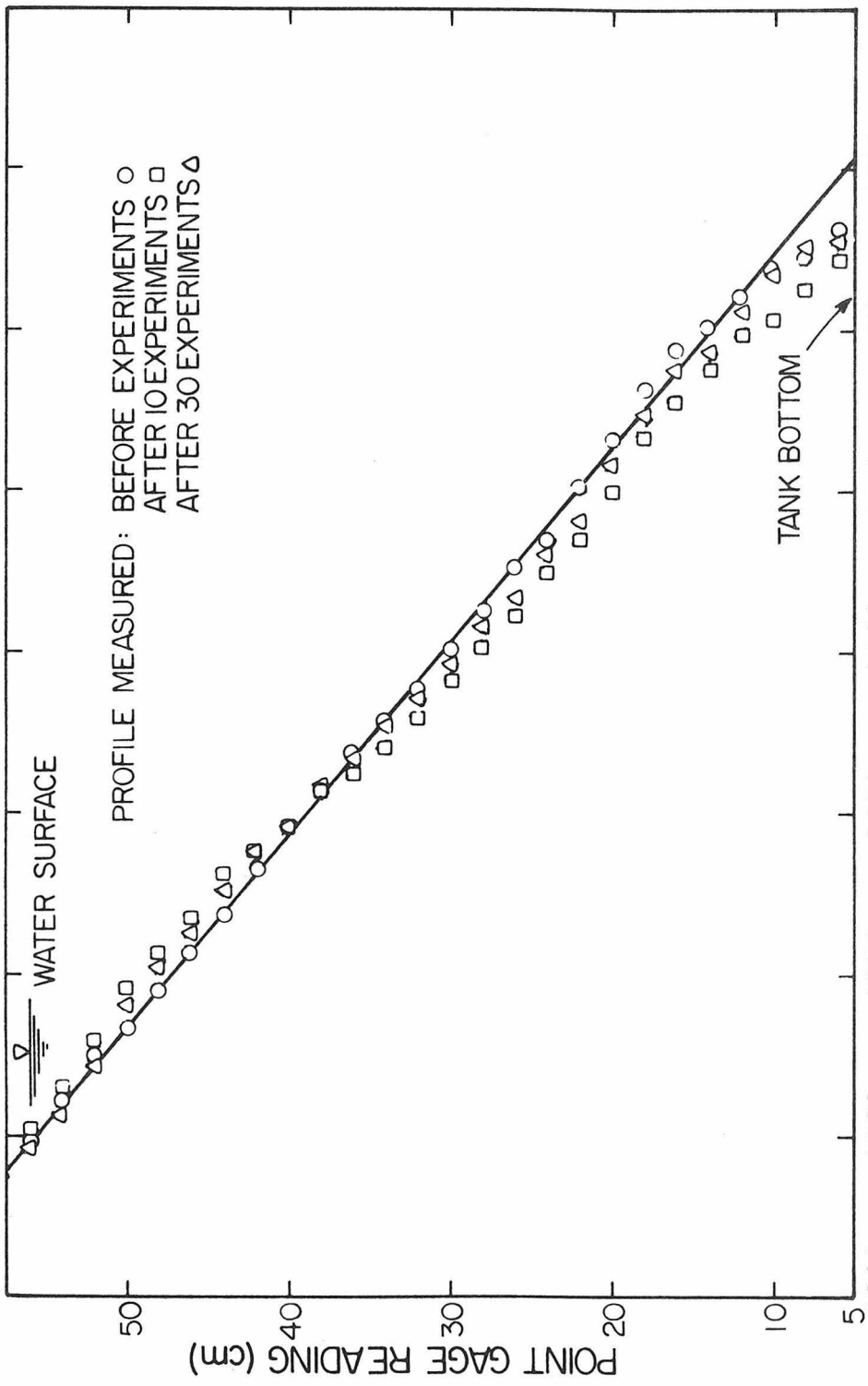

Fig. 4.10 Effect of jet discharge on density structure for a relatively strong stratification.

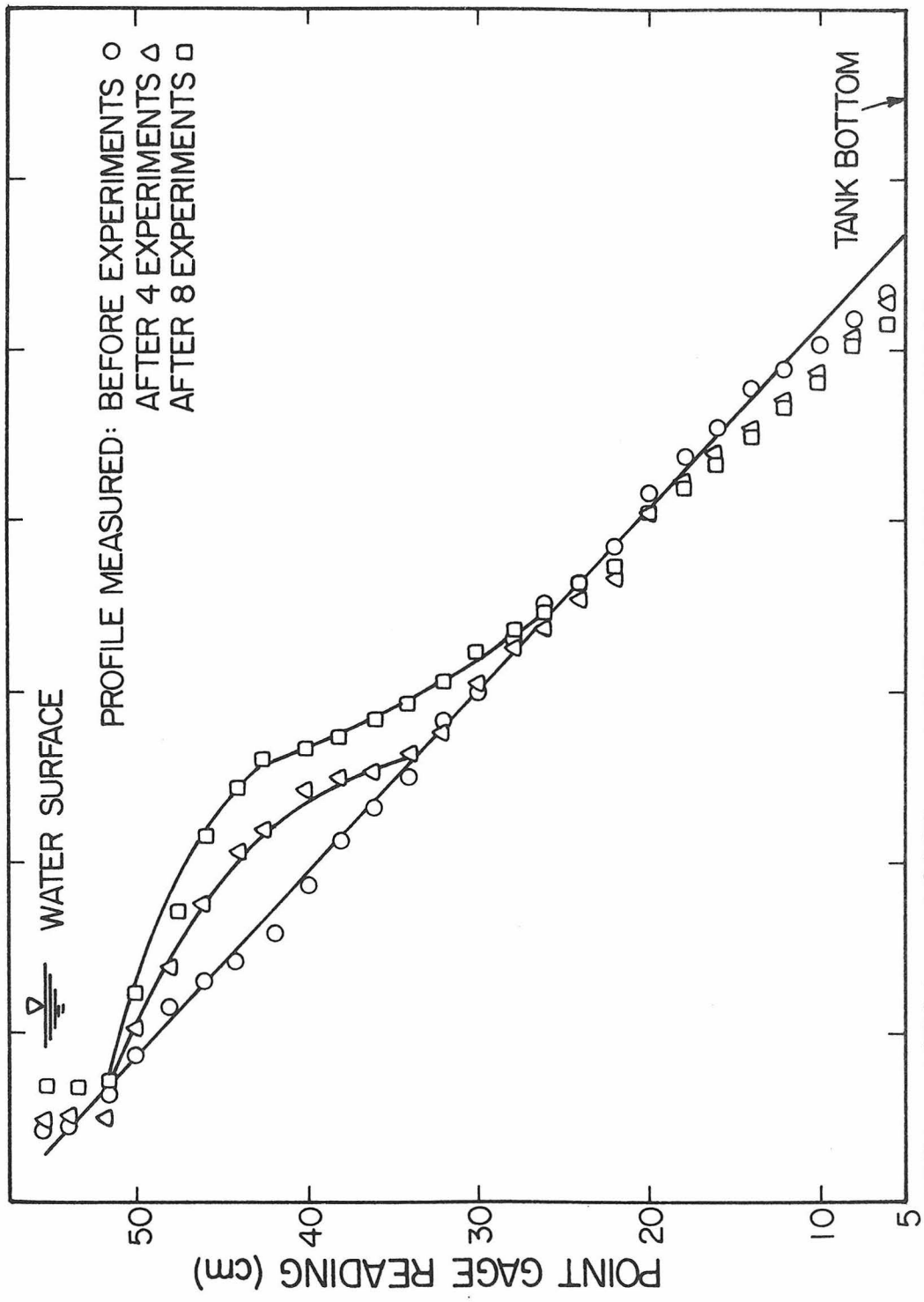

Fig. 4.11 Effect of jet discharge on density structure for a relatively weak stratification.

High-Contrast Copy or Kodak Photomicrography Monochrome film. The jet properties were measured from enlargements made from the negatives. The marks on the flume walls appearing in the enlargements were used to scale the dimensions for a coordinate system with its origin at the jet source. The length scale for the coordinate system was determined by considering the reference locations to be halfway between the corresponding marks on the front and back of the tank, as indicated in Fig. 4.12a. The outline of the jet was sketched on tracing paper as in Fig. 4.12b and the jet trajectory was taken as the smooth curve visually drawn halfway between the jet boundaries. Equilibrium heights of rise of jets in a stratified fluid were determined in a similar manner with the height of rise defined as the midpoint of the dye layer.

4.2.4 Fluorometer and Associated Apparatus

The concentration measurements for the examination of jet trajectories and dilutions in an unstratified crossflow were made using fluorescent dye, Rhodamine B Extra, as a tracer in the jet fluid. The general procedure was to withdraw samples of the fluid in the tank at fixed locations with respect to the jet source and to determine the relative concentration of jet fluid at those points by fluorometric analysis. Fluid samples were obtained with a suction-type sampling system similar to that used by Prych (1970). This system consisted of a rake of seven probes, a pressure box with test tubes for collection of the samples, a vacuum pump, and a control valve. Fig. 4.13 is a schematic of the sampling system.

The sampling rake consisted of seven L-shaped tubes and a bracket

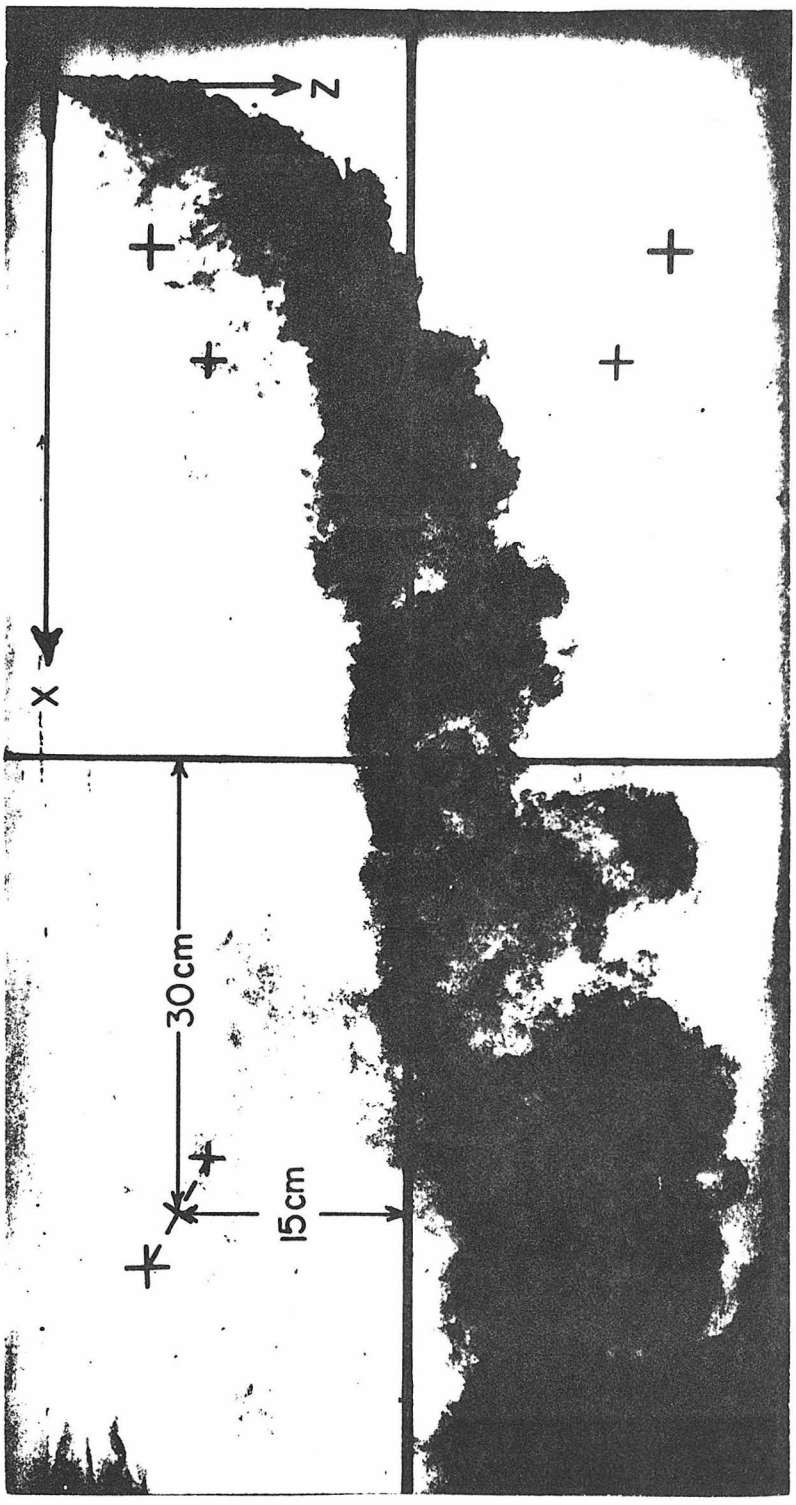

Fig. 4.12a Typical photograph used to determine jet trajectory.

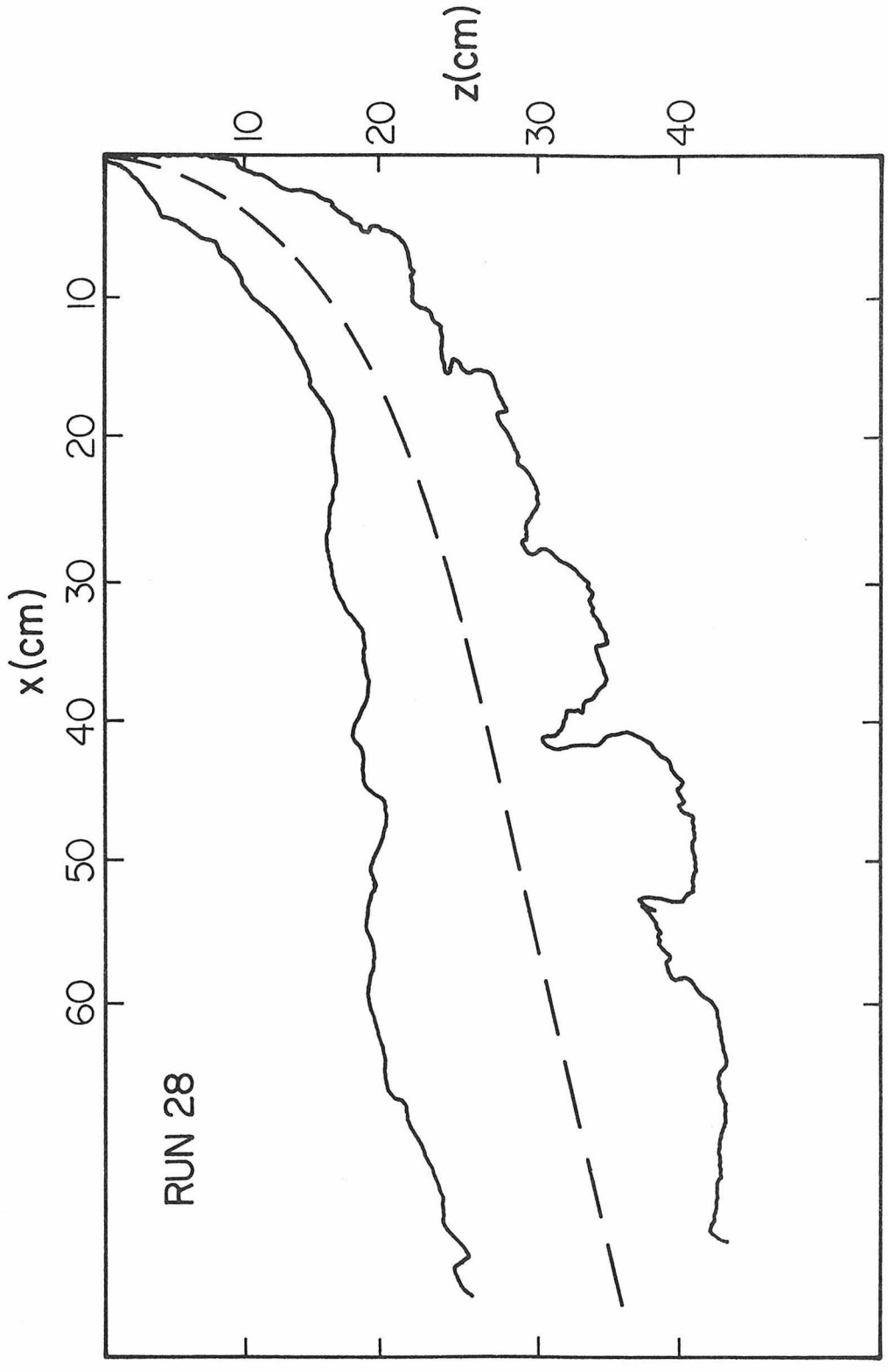

Fig. 4.12b Tracing from photograph.

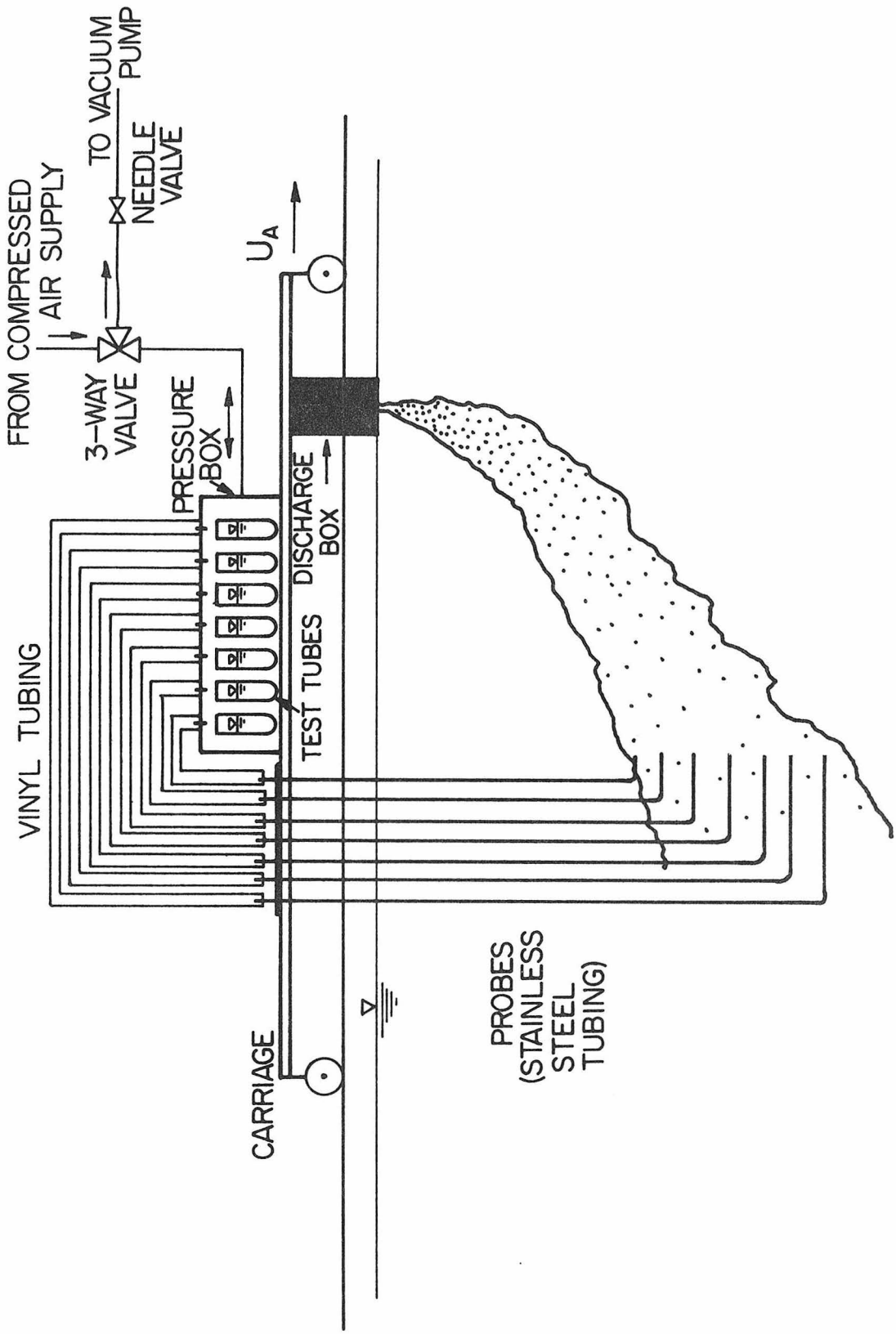

Fig. 4.13 Schematic of suction sampling system.

as shown in the photograph in Fig. 4.14. The stainless steel tubes had a 3.18 mm outside diameter and a 1.78 mm inside diameter. This diameter of tubing was selected so that a 15 mℓ sample could be withdrawn in a length of 6 m if the sampling velocity was equal to the towing velocity. The bracket was clamped to a horizontal bar which could be adjusted for any vertical placement of the probes. The vertical spacing between probes in the bracket was adjustable.

Samples were collected in 35 mℓ test tubes in the lucite pressure box. The test tubes were filled through nipples of stainless steel tubing in the top of the box which were connected to the probes with vinyl tubing. The pressure in the box could be made positive or negative from either a compressed air source or a vacuum source by adjustment of a three-way valve. The vacuum source consisted of a 20 liter reservoir evacuated by a vacuum pump. A needle valve was used to control the intake rate such that the inflow velocity into the tubes was nearly the same as the towing velocity. Since the length of tubing in all of the probes was not equal, the inside diameters of the nipples in the top of the pressure box were varied until test tubes filled in the same amount of time.

The sample procedure consisted of first switching on the compressed air source and purging the lines of any residual fluid. When the carriage was moving forward and the jet source was discharging the vacuum was applied and fluid was drawn up into the test tubes. At the end of the experiment, the compressed air source was again applied and the lines purged of fluid.

There was some initial difficulty with residual chlorine in the

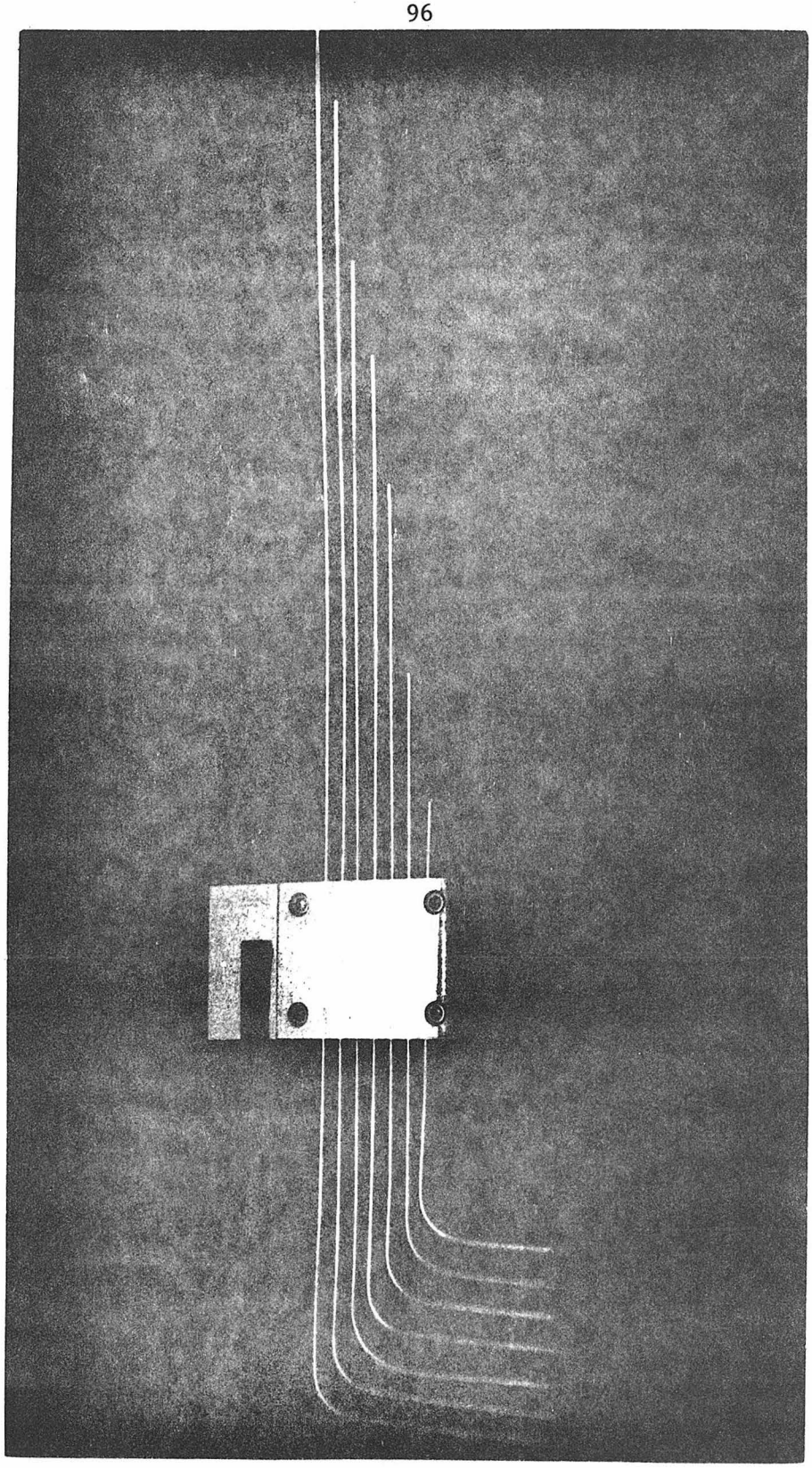

Fig. 4.14 Photograph of sampling rake.

towing tank water oxidizing the organic dye resulting in erroneous concentration measurements. This problem was corrected by adding a reducing agent, sodium sulfite (Na_2SO_3), to the tank water to react with the chlorine or other oxidizing agents that were present.

The fluid samples were analyzed in a G. K. Turner Associates Model 111 fluorometer to determine the relative concentrations of fluorescent dye in the samples. Filters that were provided with the instrument to improve the measurements of fluorescence from Rhodamine dye were used. The output from the fluorometer was read from a rotating dial with a scale from 0 to 100. The dial was adjusted to give a zero reading when a sample of the ambient water from the towing tank was placed in the fluorometer. The fluorometer output is essentially linear for the low dye concentrations considered (10^{-6} g/mℓ or less) and only one reference sample needed to be considered. This was obtained by taking a sample of the jet fluid and diluting it with ambient water from the towing tank. The dilution was made such that the dye concentration in the reference sample was approximately the same as the highest concentration of the samples to be analyzed, and generally involved a dilution S_s between 20 and 100 to 1. The output R_f of the reference sample was then noted and the dilution of each fluid sample was determined by noting its respective reading R_s and computing the ratio

$$S = \frac{C_o}{c} = \frac{R_f S_s}{R_s}$$

where c is the dye concentration measured at any point.

4.2.5 Light Probe and Associated Apparatus

A new in-situ measurement system was developed to make concentration measurements for the portion of the investigation involving density stratification. The basic measurement system was based on the attenuation of light by dye present in the jet fluid. The probe consisted of a device to pass light across a small gap on the order of 3 mm within the jet and a photodetector to determine the amount of light passing from a light source through the sample volume. By relating the light attenuation to the amount of dye in the sample volume, instantaneous in-situ measurements of jet dilution could be obtained.

The light source was a Spectra Physics Model 162-2 argon ion laser with an adjustable power output and a stabilized power output to within ± 0.5%. This capability was desirable since other alternating current light sources tested did not give uniform light output with time. The laser was operated at a wavelength of 514.5 nm. Light from the laser beam was passed through a 0.76 mm optical fiber, across a gap of approximately 3 mm to another similar optical fiber which led to a photodetector as shown schematically in Fig. 4.15. The fibers were enclosed in a probe constructed of stainless steel tubing which is shown in the photograph in Fig. 4.16. Precise alignment of the fiber tips was not required since the laser beam was no longer coherent after passing through the optical fiber. The effect of any tip misalignment was automatically accounted for in the probe calibration. The photodetector was an EG&G PV-100A photovoltaic photodiode with an operational-amplifier circuit as shown in Fig. 4.17.

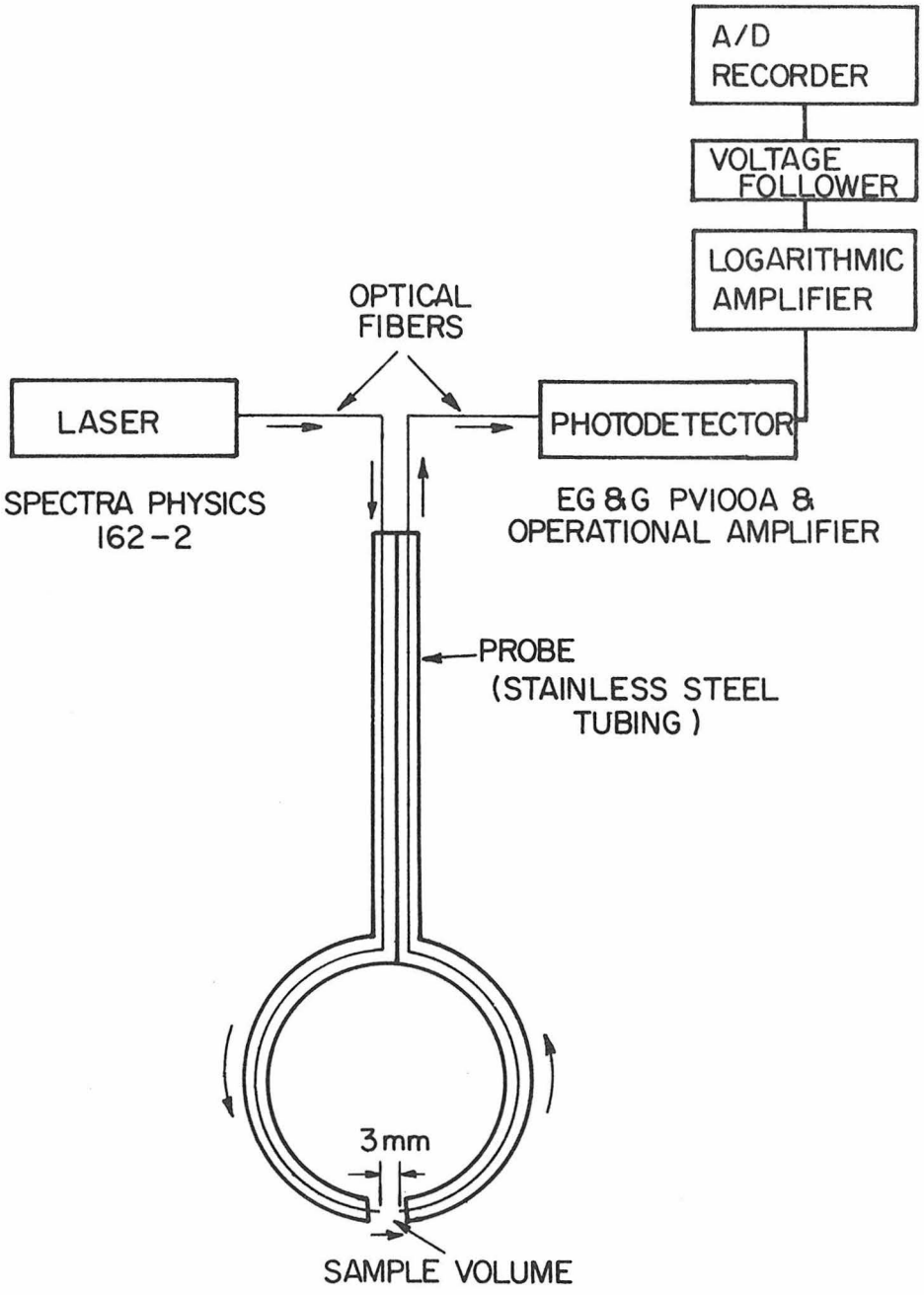

Fig. 4.15 Schematic of light probe.

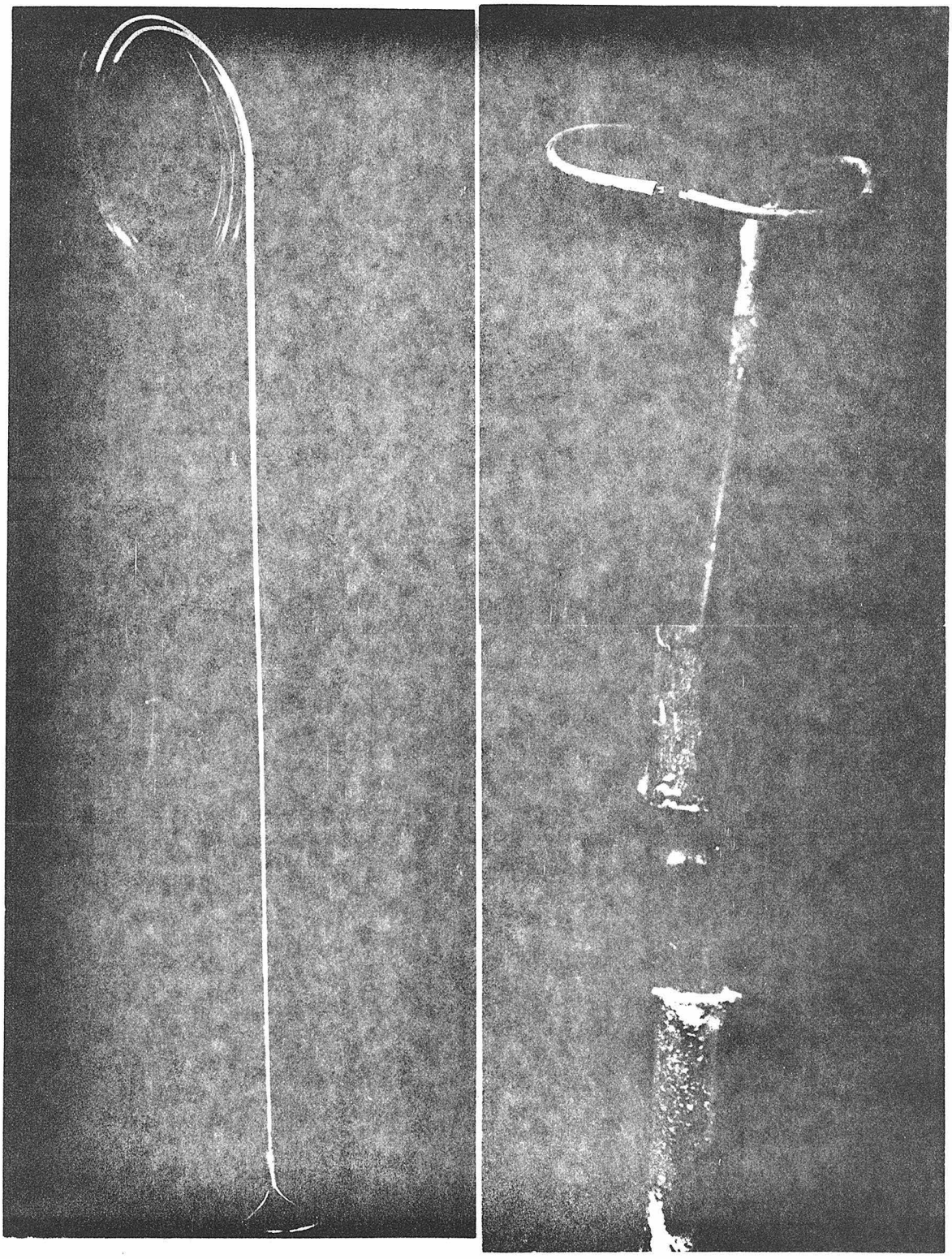

Fig. 4.16 Photograph of light probe.

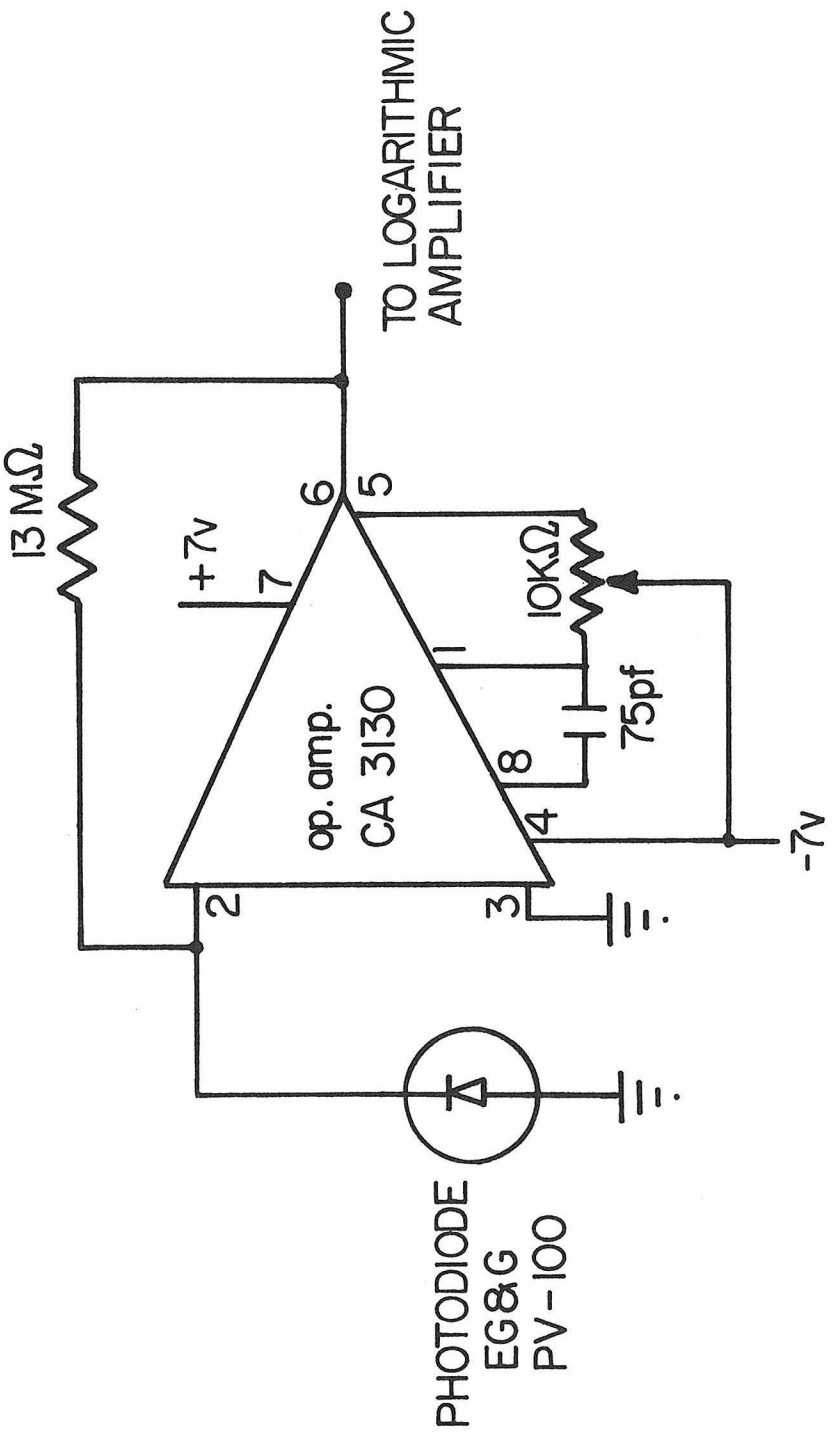

Fig. 4.17 Operational amplifier circuit used with the photodiode.

An additional amplifier, constructed to obtain the logarithm of the voltage signal from the photodiode-operational-amplifier unit was designed and constructed by the Electrical Engineering Department at California Institute of Technology; a circuit diagram of the amplifier is given in Fig. 4.18. This amplifier was constructed in an attempt to linearize the relation between the dye concentration and output voltage since the attenuation of light in a fluid medium follows Beer's law (see Wood (1934)) to a first approximation:

$$I = I_o e^{-\alpha c} \quad \text{or} \quad c = -\frac{1}{\alpha} \log_e \frac{I}{I_o}$$

Here I is light intensity, I_o is the original light intensity, α is an attenuation constant, and c is the concentration of dye or other light adsorbing material. Since the photodiode output was not linear with light intensity over the entire range, the logarithmic amplifier only partially linearized the output.

The output from the logarithmic amplifier was recorded by an analog-to-digital recorder (Digital Data Systems, series 1103) which is described in more detail by Roberts (1977). In order to reduce the output impedance of the logarithmic-amplifier to a level compatible with the input impedance required by the A/D recorder, the voltage follower circuit shown in Fig. 4.19 was used between the amplifier and the recorder. The output from the A/D recorder was stored on magnetic tape in a format compatible with the IBM 370/158 computer. The recorded information was later retrieved by the computer with the use of pre-existing subroutines.

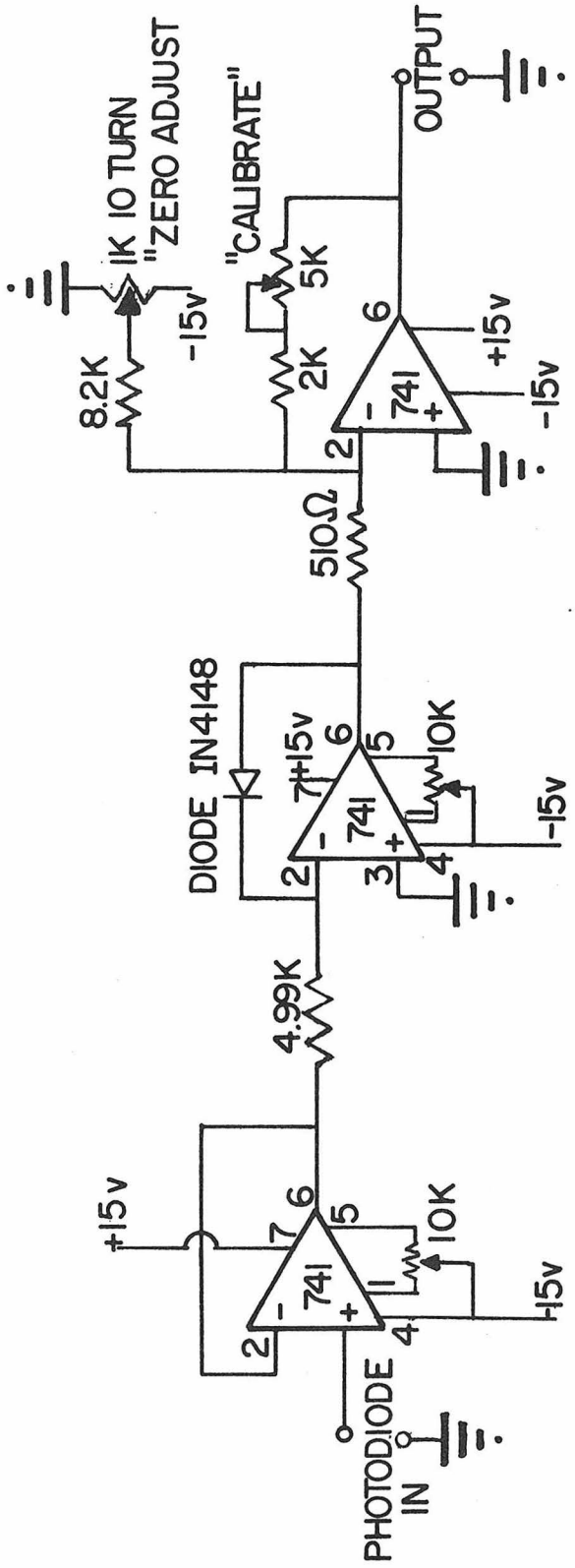

Fig. 4.18 Circuit diagram of logarithmic amplifier.

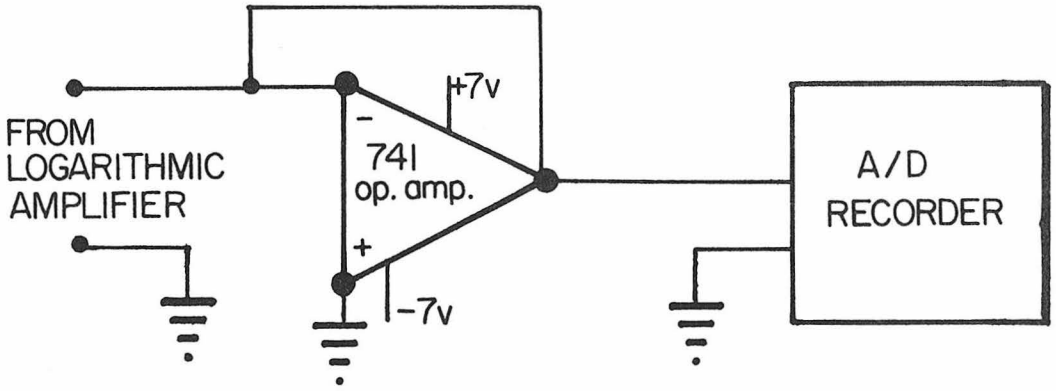

Fig. 4.19 Voltage follower circuit to reduce the output impedance of the logarithmic amplifier.

Two different types of dye were used during the course of the experiments. It was necessary to select a dye that absorbed light at the wavelength generated by the laser and an additional consideration related to the possibility of performing more than one experiment for each density stratification. Approximately one liter of liquid swimming pool chlorine (10% sodium hypochlorite solution) was added to the mixing tank while the towing tank was being stratified. This served to oxidize the dye added to the towing tank from a jet discharge which allowed several experiments to be performed without residual dye from previous experiments affecting the results. It was desirable that the chlorine oxidize the dye over a time of approximately one-half hour but not substantially less because the concentration measurements might be influenced if the dye deteriorated too rapidly. Red Extra Concentrate Powder A-3-G-7 produced by the 7-K Color Corporation was initially used but it appeared that the dye was oxidized too rapidly and also left a brown residue in the flume. Later experiments were performed with Rhodamine B Extra dye which gave better results for the intended use.

The probe was calibrated by obtaining a sample of the jet fluid which had been previously mixed with dye to some arbitrary concentration. The sample was diluted with tap water to produce several reference samples with relative dye concentrations in the range of 0.1 to 0.0001. Sodium sulfite was added to prevent oxidation of the dye. Calibrations were obtained by immersing the light probe into each of the reference samples and obtaining a 20 second record of the photodiode output on the A/D recorder. The relative concentration of the reference sample

was recorded as header information on the data tape recorder. The calibration curve for each set of experiments was then calculated by the IBM 370/158 computer. Seven or eight reference samples were used for each calibration and a curve was fitted to the negative logarithm of the sample concentrations and the output from the logarithmic amplifier. Curves from linear to fifth order were fitted to one set of samples in a least-squares manner to examine accuracy of fit. The resulting curves are indicated in Fig. 4.20 with the 4th and 5th order curves not plotted since they essentially correspond to the 3rd order curve. A 3rd order polynomial was selected as adequate for future calibrations on the basis of these results.

An additional test was performed to observe changes in the probe calibration with time. Table 4.1 presents the results of this observation for the range of relative dye concentrations measured in any jet in this investigation. Here c/C_o is the concentration of the reference sample relative to the value in the jet discharge. There was some instrument drift at very high relative concentrations (on the order of 0.3 to 1.0) but this was not considered since it was outside the range of relative concentrations measured in this study. Since it was difficult to calibrate the probe during a set of experiments, it was concluded that the change in the calibration was within acceptable limits and only one calibration need be performed at the beginning of a day's experiments.

A device on the principle of a cam was constructed to raise and lower the probe through the jet at a fixed horizontal position relative to the jet discharge orifice (i.e., the probe was also towed through the

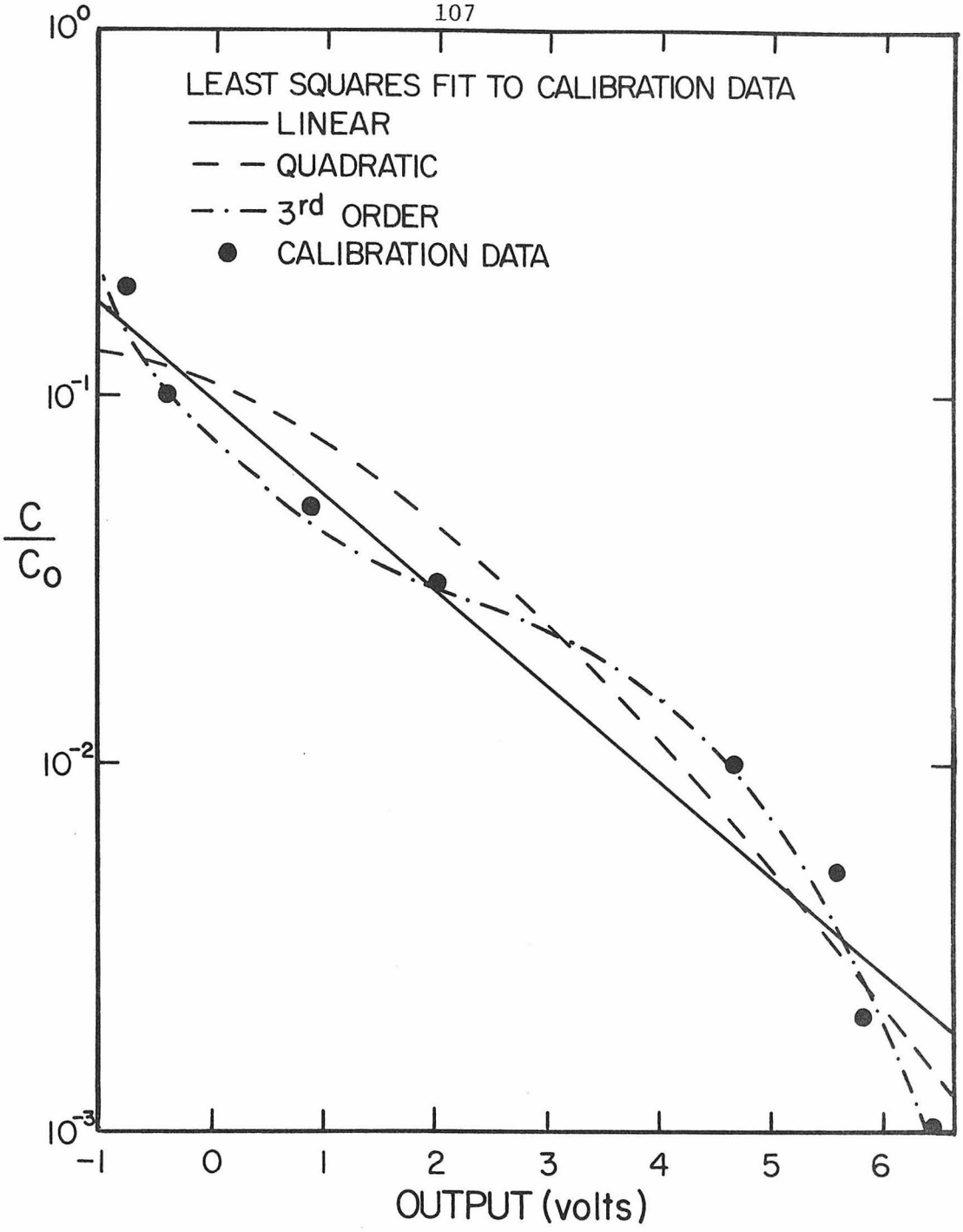

Fig. 4.20 Calibration curves for light probe.

Table 4.1 Results of observations of drift of light probe calibration with time.

c/C_o \ Output (volts)	Hour				
	1	2	3	4	5
0	5.49	5.49	5.48	5.48	5.48
0.00083	5.49	5.48	5.47	--	5.47
0.0028	5.46	5.45	5.43	5.42	5.42
0.0083	5.32	5.31	5.31	5.31	5.31
0.0333	4.61	4.61	4.61	4.61	4.61
0.10	2.94	2.93	2.93	2.93	2.92
the following relative concentrations were outside of the range of experimental measurements					
0.333	1.78	1.55	1.50	1.55	1.58
1.0	1.58	1.51	1.50	1.41	1.41

tank). This device connected the probe movement to the towing mechanism such that the probe performed the same number of passes through the jet for an experiment regardless of towing velocity. The probe movement is indicated schematically in Fig. 4.21. The probe made one complete cycle for every 61 cm of carriage travel or approximately 28 passes were made through every vertical position for each experiment. The horizontal and

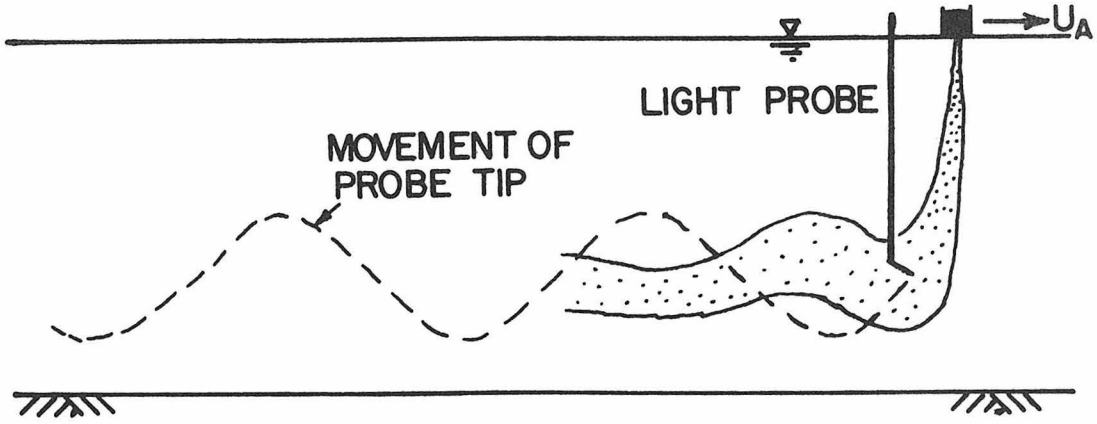

Fig. 4.21 Schematic of probe movement for an experiment.

vertical positions of the probe relative to the jet exit were adjustable and the length of the vertical sweep could be varied between 10 and 30 cm. The vertical position of the probe was monitored by means of a resistance potentiometer which was connected to the probe such that the resistance varied with vertical probe position. A 7.5 volt battery was connected to the potentiometer and the signal was recorded on the A/D recorder simultaneously with the output from the probe. A calibration was made for the probe position as a function of resistance across the potentiometer by setting the probe at several known vertical positions, the values of which were recorded as header data, and recording the corresponding voltage outputs on the A/D recorder. A calibration curve such as that given in Fig. 4.22 was generated by the computer fitting of a least squares straight line to the calibration points. A typical magnetic tape record thus consisted of: (1) an initial calibration of the light probe; (2) a calibration for the position sensor, and (3) a run in which the outputs of the position sensor and the light probe were recorded simultaneously. The second two sets of data were recorded for each additional experiment.

Several tests were performed to observe the characteristics of the light probe. The response time of the probe was determined by plunging the probe into a solution of dyed water while recording the instrument response on the A/D recorder at a rate of 1000 samples/sec. The output from these tests indicated that the voltage dropped from its original level to its final value within the time for two samples to be recorded indicating a response time on the order of 0.001 seconds or less.

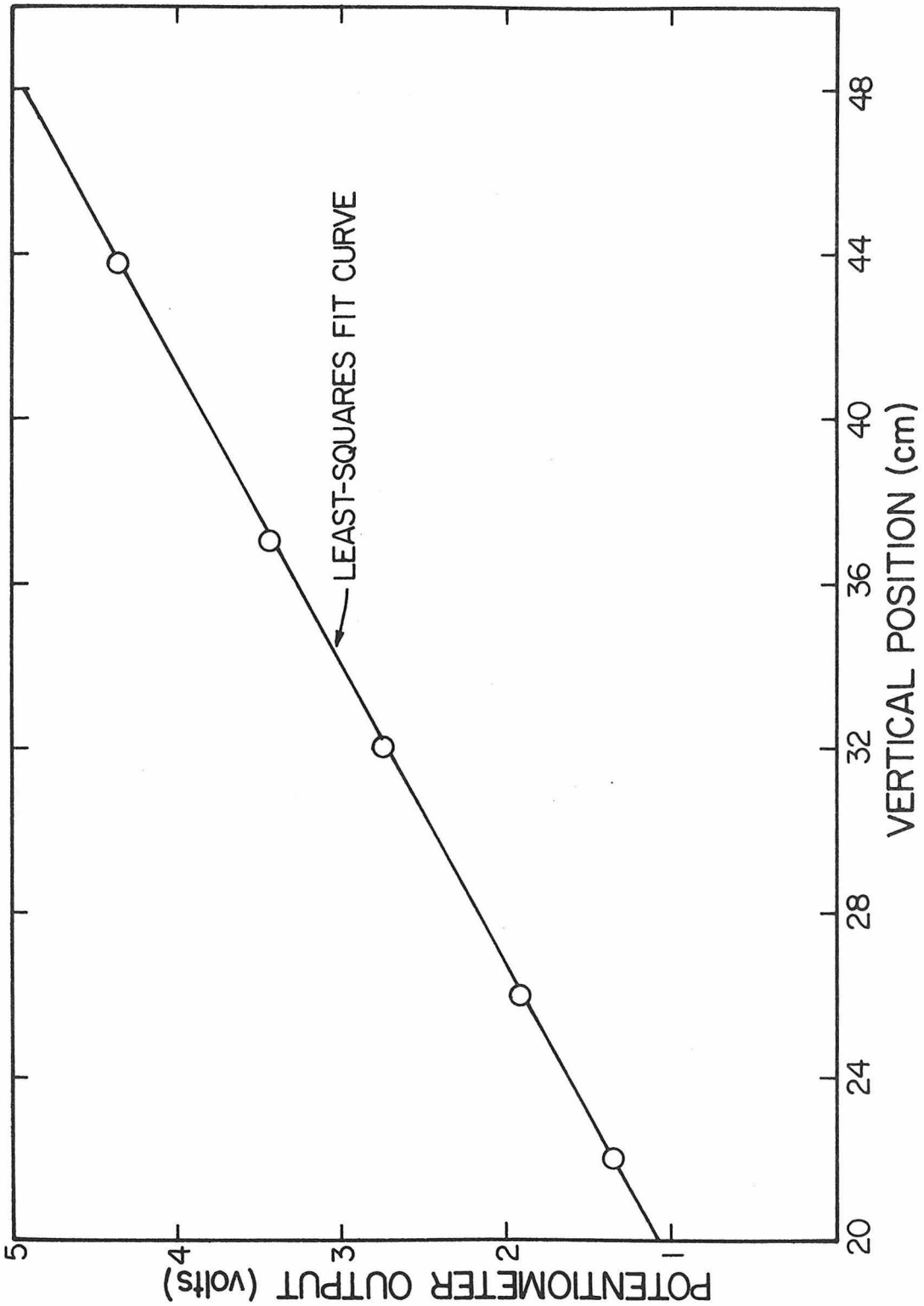

Fig. 4.22 Calibration curve for position sensor.

Another measurement was made to observe any effect due to the motion of the apparatus. One seven minute sample was obtained with the entire apparatus stationary and was compared to a similar sample obtained with the system in operation. The average stationary voltage was 2.684 volts with a standard deviation of 0.074 volts compared to values of 2.680 and 0.080 volts when the system was in motion. It was concluded that the motion had a relatively minor effect on the operation of the light probe.

An estimate of the sample rate required to observe the turbulent fluctuations was determined by connecting the probe output to a Hewlett-Packard Model 3580A spectrum analyzer and obtaining a frequency spectrum of the signal fluctuations at an arbitrary location within a jet flow. The output of the spectrum analyzer was displayed on an X-Y plotter and a sample output is given in Fig. 4.23. It was estimated from this that a sample rate of 20 samples/sec was sufficient to observe the major components of the motion.

An estimate of the minimum length of sample record necessary to determine an adequate sample mean was obtained by following the procedure discussed by Kotsovinos (1975). An experiment was performed with the light probe at a fixed position with respect to the jet source and a 400 sec sample was recorded at a rate of 20 samples/sec. This record was subdivided into samples of a given interval such as 5 sec. The average voltage of each of these subsets was computed and the standard deviation of all of the sample averages was calculated. This information is presented in Fig. 4.24 for several time intervals between 5

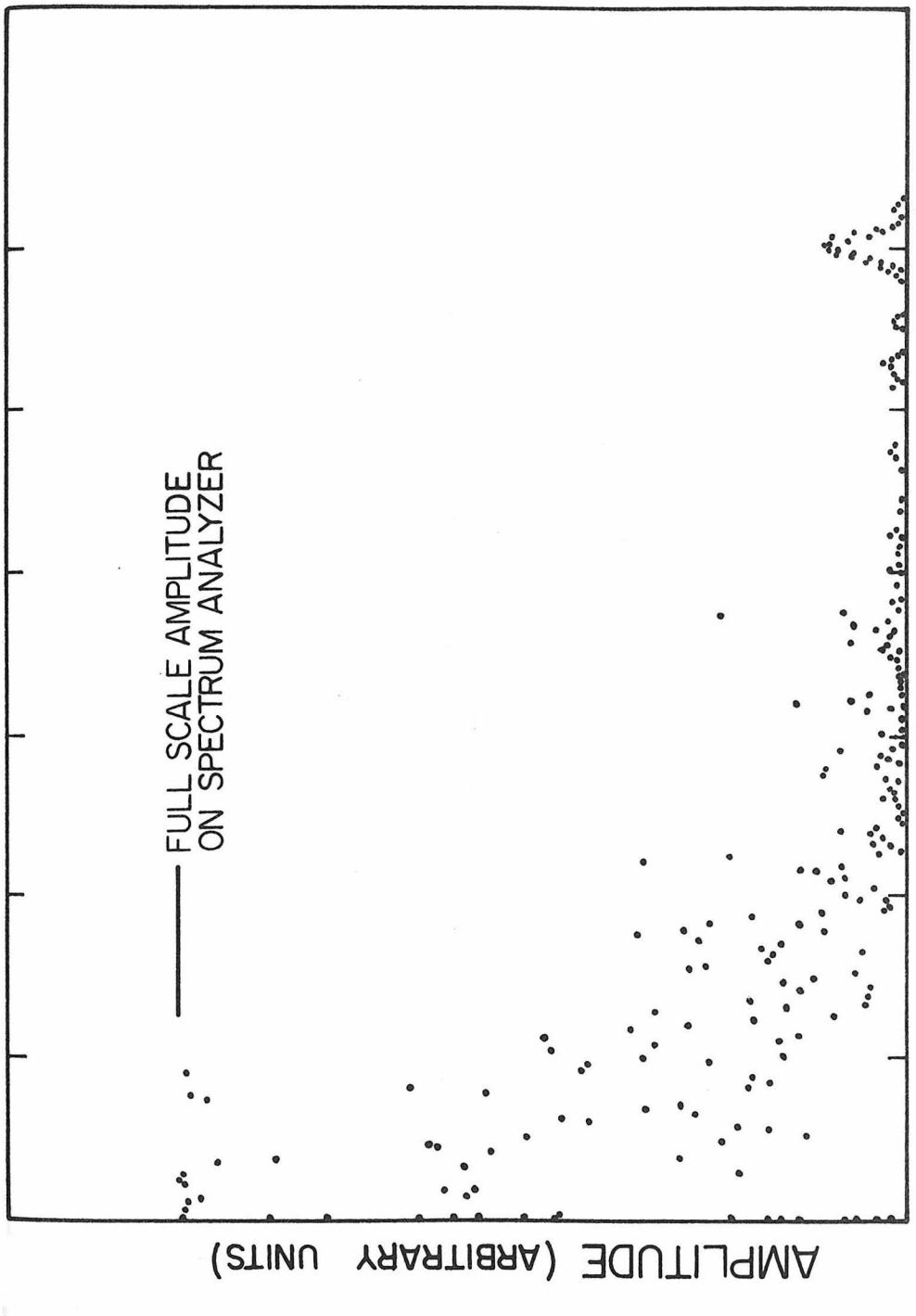

Fig. 4.23 Frequency spectrum of output from light probe at a point within a jet flow.

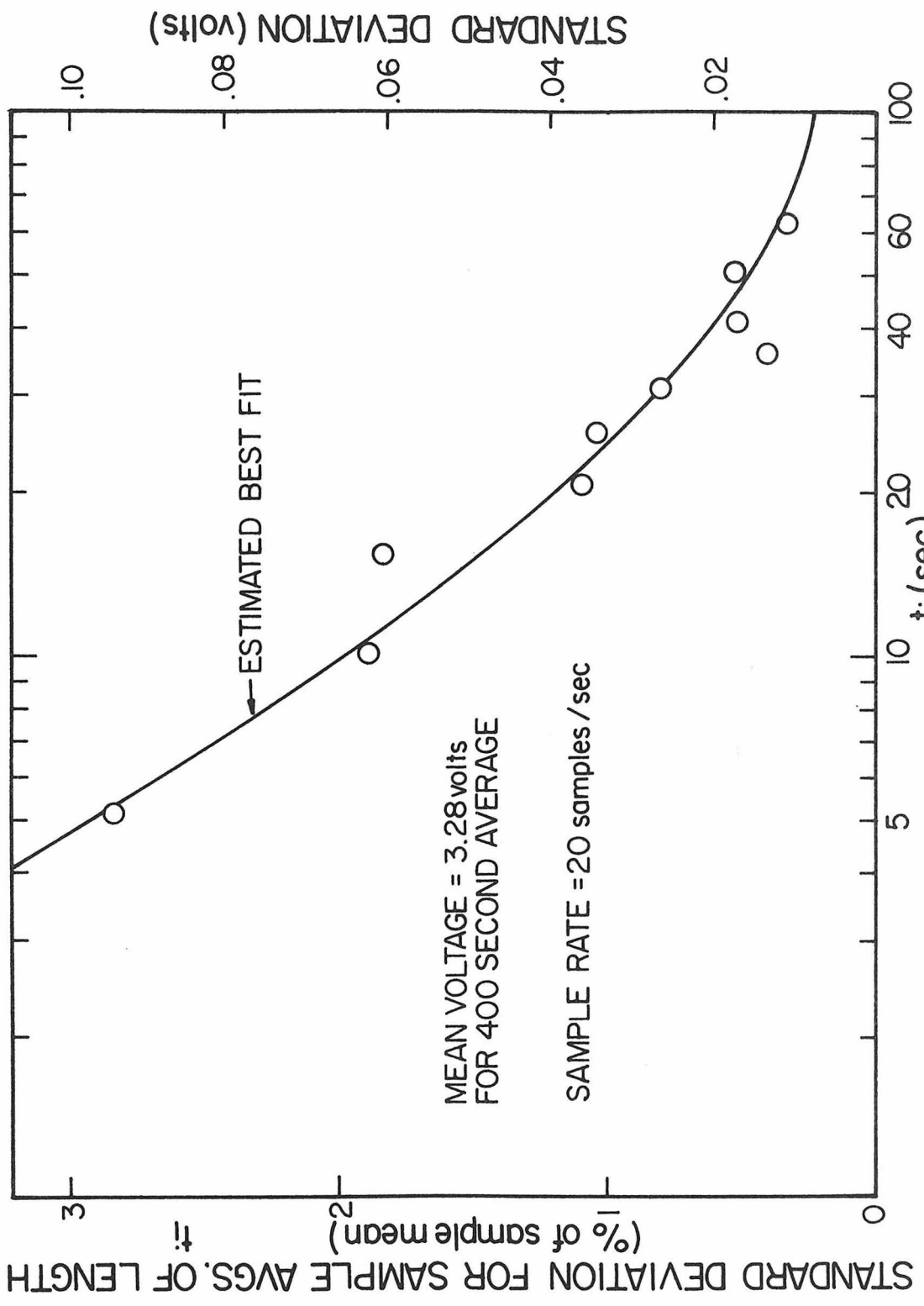

Fig. 4.24 Standard deviations of sample mean for various lengths of record.

and 60 sec. No calibration was taken to correlate the output voltage with dye concentration but the calibration in Fig. 4.20 was used to estimate the sample error for the same output voltage. For example, a 10 sec sample with a 0.065 volt standard deviation would have on the order of a 5% standard deviation for the relative concentration corresponding to an output of 3.28 volts. It was decided that a 10 sec sample was fairly adequate to obtain an estimate of the average concentration at a point.

The total sample time for an experiment was limited by the length of the flume and the towing velocity. For example, a typical towing velocity of 2 cm/sec indicates a sample time on the order of 400 sec for the 8 m of sampling distance in the tank. It was decided to divide the vertical distance covered by the probe into 25 cells of equal thickness and to designate all signals generated within a particular cell as belonging to one vertical position. For a total sample time of 400 seconds, this provided a sample time of approximately 16 seconds for each cell. This would indicate an error in determining the sample mean of less than 5% if the results above are valid.

One experiment was made to test the system by repeating an experiment which had been performed previously for a buoyant jet in an unstratified crossflow. The earlier results had been obtained by the fluorometric method described previously. A comparison of the profiles measured by the two methods is given in Fig. 4.25 and indicates good agreement between the two measurements.

The system was then used to measure maximum heights of rise and

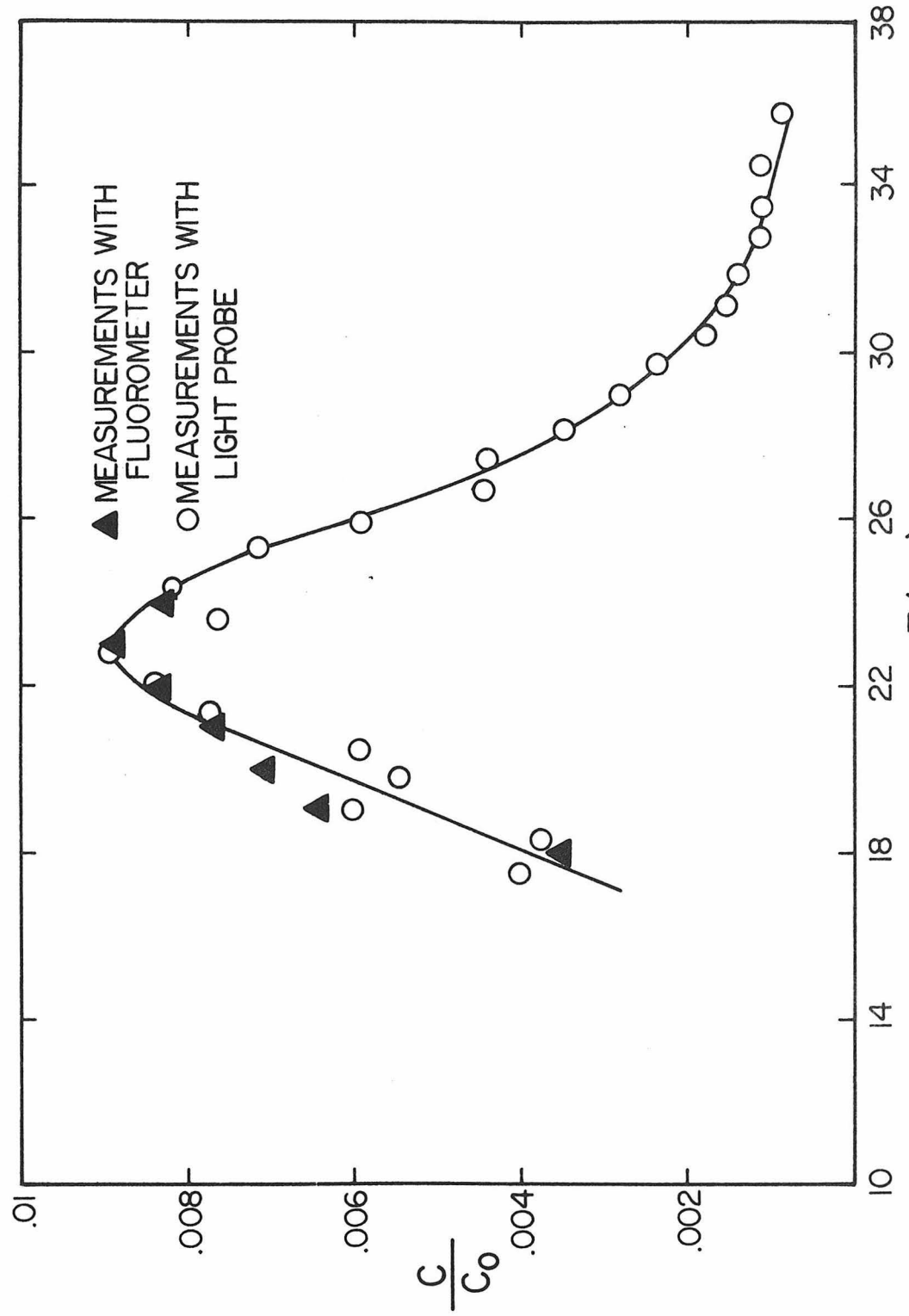

Fig. 4.25 Comparison of measurements made with the light probe and the suction sampling system.

associated dilutions for stratified flows. Before an experiment was made, the approximate vertical position and the horizontal location of the maximum height of rise needed to be determined. This was accomplished by placing the probe at some arbitrary position with respect to the source to establish a camera reference and beginning the experiment with the conditions to be modeled. A Polaroid photograph was taken of the resulting flow pattern which indicated the relative position of the probe with respect to the location of the maximum height of rise. This was used to adjust the probe to the correct horizontal and vertical positions. The length of the vertical sweep was also adjusted to the approximate width of the jet. Then the actual experiment was performed and the data collected.

4.3 Discussion of Experimental Error

4.3.1 Errors in Measurement of Flow Variables

There were several sources of error in the experimental investigation due to the large number of experimental variables that were considered. Table 4.2 presents a summary of the precision of the measurements of flow variables and probe coordinates. The table also presents the range of the experimental variables for the entire investigation and the estimated probable error ($\pm.707\sigma$ where σ is the standard deviation) associated with the measurement of these variables. No systematic analysis of the error associated with each measurement was undertaken since these errors are apparently small with respect to the errors associated with the concentration measurements.

Table 4.2 Summary of the precision of the experimental measurements and the estimated probable error.

Measurement	Precision	Typical Experimental Values	Estimated Probable Error (± %)
discharge Q	0.1 mℓ/sec	4-50 mℓ/sec	2-5
density difference		~0 (nonbuoyant jets)	--
$\frac{\Delta\rho}{\rho_o}$	0.0001 g/mℓ	~.015-.110 (buoyancy-driven flows)	2
towing velocity U_A (towing time over 3.38 m)	0.01 sec	10-350 sec	<2
stratification parameter ε $\frac{-g}{\rho_o}\frac{d\rho_a}{dz}$	2×10^{-3} sec^{-2}	0.035-.25 sec^{-2}	1-5
horizontal probe coordinate	0.1 cm	2-45 cm	0.5-10
vertical probe coordinate	0.1 cm	8-40 cm	0.5-2.5

There was an additional error introduced into the measurement of the jet discharge as the flowmeter used to measure the discharge tended to become clogged from impurities in the jet fluid. The flow rate through the meter then became less than indicated by the meter setting, especially at lower discharges. It is possible that errors in flow measurement on the order of 10-15% may have resulted in some instances, but this was not a common occurrence. The error due to this factor

was essentially negligible at discharges greater than approximately 20 mℓ/sec and was only appreciable for flow rates less than about 10 mℓ/sec. Since most of the experiments to measure maximum heights of rise were performed at low jet discharges, these measurements may have been influenced somewhat by this effect. The other types of experiments were generally performed at higher discharges and should not have errors in the measurement of the jet discharge greater than approximately ± 5%.

4.3.2 Error Associated with the Measurement of Concentration

Tracer concentrations for the unstratified experiments were measured with the fluorometer, while the light probe was used for the measurements in the stratified experiments. The errors for each type of measurement will be discussed separately below.

The magnitude of the error associated with the use of the fluorometer to measure concentrations for the nonstratified experiments was evaluated by preparing samples of different dilutions from a quantity of dyed fluid. Several specimens from each of these samples were analyzed in the fluorometer and the average and standard deviation of the specimens for each sample were computed. The standard deviations varied from 2-8% of the average reading for the different samples which indicates probable errors on the order of 5-10% for the determination of relative concentration with the fluorometer.

The major source of error associated with the use of the light probe to measure jet dilutions was due to the limited length of sample time which was controlled by the length of the towing tank and the towing velocity. This does not indicate a fundamental inaccuracy of

the measurement system but is a result of the experimental procedure and the method of data analysis. The magnitude of the instrument error is assumed to be much less than the sampling error for relative concentrations of the magnitude measured in this investigation. For very low relative concentrations (less than approximately 0.001), the instrument error becomes significant but since most average concentrations measured were much greater than this amount, the instrument error is estimated to be less than 5%.

Experiments could only be performed for a limited range of towing velocities. A very small towing velocity would result in a nearly vertical jet and an incorrect measure of the maximum height of rise can occur as indicated schematically in Fig. 4.26. The maximum relative

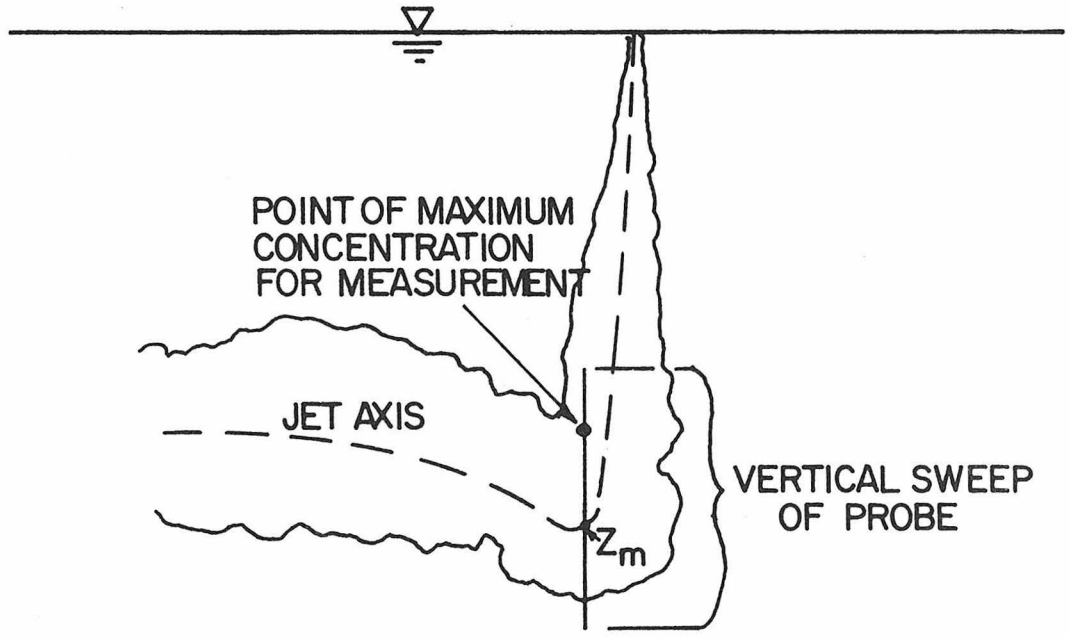

Fig. 4.26 Schematic of possible error involved in measuring the maximum height of rise in a very weak cross current.

concentration measured in this instance does not coincide with the maximum height of rise since the dilution along the jet axis provides for a lower concentration than would occur at some distance from the jet axis for a smaller vertical rise.

For the experiments with larger towing velocities, the mean concentrations were subject to larger sampling errors due to the very short length of record. For example, one experiment with a towing velocity of 3.5 cm/sec had only 59 instantaneous concentration measurements for one vertical location, representing only three seconds of total sampling time. Extrapolation of the results from Fig. 4.24 would indicate a probable error of up to 20% for a sample that short. However, the sampling error associated with a discontinuous sample (since measurements were made at that location for each of the approximately 28 sweeps made with the probe) should be somewhat less than a continuous record of the same total length. Sampling errors of this type are believed to be mainly responsible for the scatter in the concentration profiles measured with the light probe that are presented in the next chapter. The greatest errors are for the far-field flows where the towing velocities are highest and the sample lengths are correspondingly shorter.

There is probably a greater error associated with the concentration measurements than with the determination of the maximum height of rise from these measurements. The indicated height of rise would probably be within one or two vertical positions of the actual height of rise (on the order of 10% error) since the shape of the concentration profile makes it unlikely that the apparent

maximum concentration will be a large distance from the true maximum.

4.3.3 Errors in the Measurement of Trajectories and Heights of Rise

Error may have been introduced into the determination of the jet trajectories from the photographs since a photograph is essentially an instantaneous representation of a turbulent flow. It is necessary to obtain an exposure over a longer period of time to provide a more nearly correct view of the mean trajectory. An instantaneous representation of a typical jet is shown in Fig. 4.27. The outside or longer boundary of the jet was always observed to be much more irregular than the inner boundary. It was assumed that a time exposure photograph of the jet would indicate boundaries as depicted

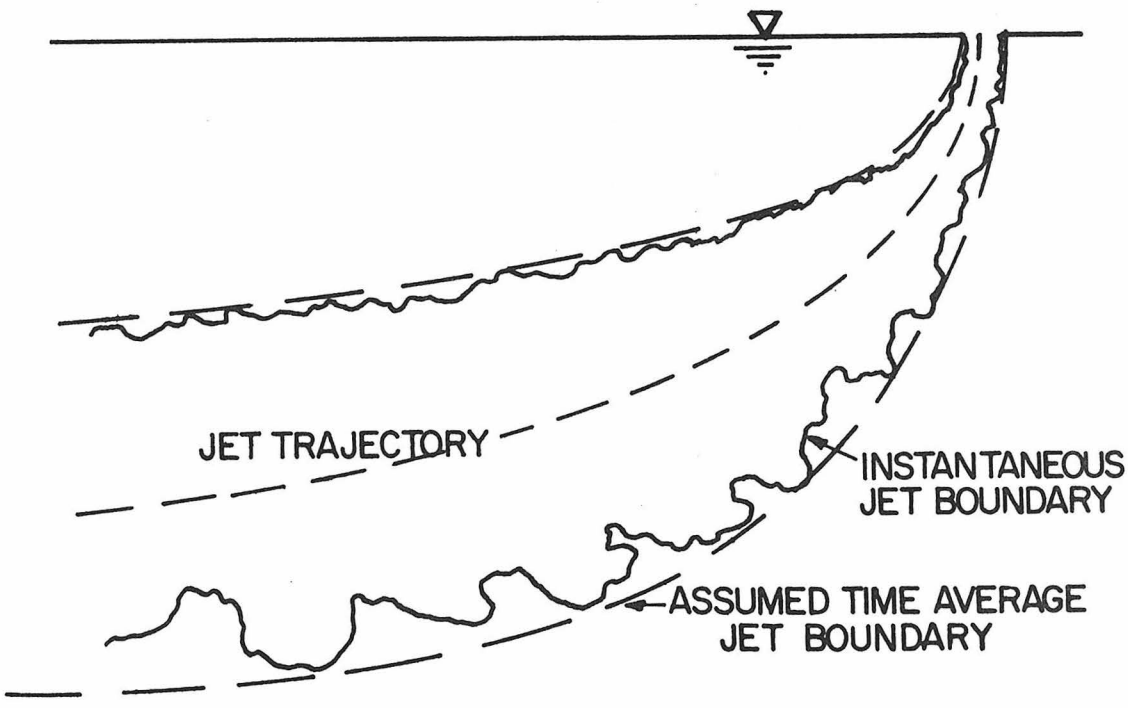

Fig. 4.27 Schematic of instantaneous view of a jet.

in the figure. Since the jet trajectory was taken as a smooth curve, it is felt that this removed a major portion of the uncertainty from the determination of the jet trajectory and that errors associated with the measurement of jet trajectories were small. The major errors were probably for the measurement of very small horizontal and vertical distances where the precision was on the order of 10% of the distances measured.

The accuracy of the vertical position measurements that were made with the suction probe or with the light probe was limited by the instrument resolution. For example, the suction probes were spaced at 1 cm vertical intervals which can only give the vertical jet position to the nearest 0.5 cm. For a 20 cm vertical rise this indicates an uncertainty of 2.5%. The light probe had a somewhat better resolution depending on the vertical sweep. The major errors were probably caused by inaccuracies in the concentration measurements and are estimated to be on the order of 5-10% for most cases.

A source of error in the stratified flow experiments was the presence of the mixed layer at the ambient water surface. It is difficult to assess the effect of this phenomenon quantitatively, but it is possible to make a general observation of the influence on the experimental results. The flow configuration is depicted in Fig. 4.28. The influence of the uniform density layer at the surface will result in the entrainment of relatively more dense fluid than would occur for an idealized linear density profile. This will result in a somewhat greater maximum height of rise than anticipated. For a large maximum

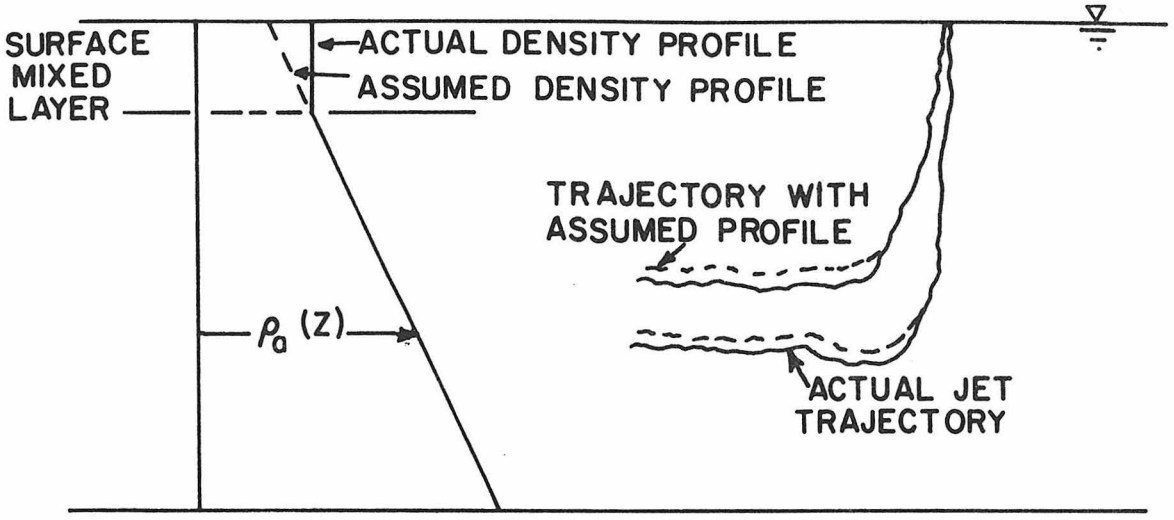

Fig. 4.28 Schematic indicating effect of surface mixed layer on height of rise.

height of rise, this effect should be relatively minor as it occurs over a lesser portion of the total flow. When the maximum height of rise is not significantly greater than the thickness of the surface mixed layer, the effect due to this phenomena should be relatively greater. It is assumed that the effect of this phenomena on the maximum height of rise was small compared to the other sources of error in the height of rise measurements.

4.3.4 Summary of Estimated Experimental Error

The estimated probable errors for each type of measurement are summarized in Table 4.3.

Table 4.3 Estimated probable errors for the measurement of various parameters.

Parameter	Estimated Probable Error
Trajectories (from photographs)	< 5%
Trajectories (from concentration measurements)	5%
Dilutions (with fluorometer)	5-10%
Heights of rise (from concentration measurements)	5-10%
Dilutions (with light probe)	5-20% (depending upon length of sample)
ℓ_b	5-10%
ℓ_m	10%
ℓ_Q	< 5%
ℓ_a	< 5%

CHAPTER 5

PRESENTATION AND DISCUSSION OF EXPERIMENTAL RESULTS

5.1 Experiments in an Unstratified Crossflow

5.1.1 Trajectory Measurements

Two methods were used to obtain estimates of buoyant jet trajectories in an unstratified crossflow. Several photographs were taken of various jets to obtain preliminary estimates of jet behavior. These experiments could be performed quickly, so it was possible to do experiments over a wide range of jet and ambient flow conditions. The other method of measuring jet trajectories was with the concentration measurement system involving the fluorometer. These experiments were intended to supplement experimental measurements made previously by Fan (1967). The combined experimental results were sufficient to observe buoyant jet trajectories for each of the flow regimes described in the analysis of Chapter 3. Experimental conditions for all experiments performed in the present investigation are presented in Appendix A. Information regarding jet trajectories and dilutions are included with the listing of the basic experimental parameters including the jet discharge, the jet diameter, the density difference, and the crossflow velocity.

Photographs of 60 buoyant jet flows were analyzed to provide information on jet trajectories. These experiments were performed for a wide range of jet parameters and crossflow velocities so that sufficient information could be obtained for each flow regime

described in the analysis. The jet trajectories, determined by the method described in Chapter 4, were taken as the smooth curve visually drawn halfway between the upper and lower dye boundaries of the jet. The trajectories were scaled from the fiduciary marks on the photographs and were plotted on logarithmic paper so that the trajectory slope could be easily determined. For example, if the trajectory plot indicated a slope of one-third when plotted on logarithmic paper, the flow was assumed to correspond to the momentum-dominated far-field. The horizontal origin ($x = 0$) was taken at the center of the jet orifice while the vertical origin ($z = 0$) was defined as the upper side of the orifice plate.

A photograph that clearly corresponds to the definition of a near-field flow (a nearly vertically rising jet) is given in Fig. 5.1 along with the corresponding trajectory plot. The slope of three-fourths for the trajectory can be taken as an indication that this particular flow corresponds to the bdnf. A similar photograph and trajectory plot for a jet that is clearly in the far-field for the major portion of the jet trajectory is presented in Fig. 5.2. The trajectory slope of one-third indicates that this jet corresponds to the momentum-dominated far-field regime.

Some of the more interesting trajectory plots and the corresponding photographs are presented in Figs. 5.3 and 5.4. Fig. 5.3 is a case where $\ell_m/\ell_b = .16$ and the jet trajectory clearly goes through the mdnf (1/2 slope), the bdnf (3/4 slope) and the bdff (2/3 slope) over the portion of the jet trajectory covered in the photograph.

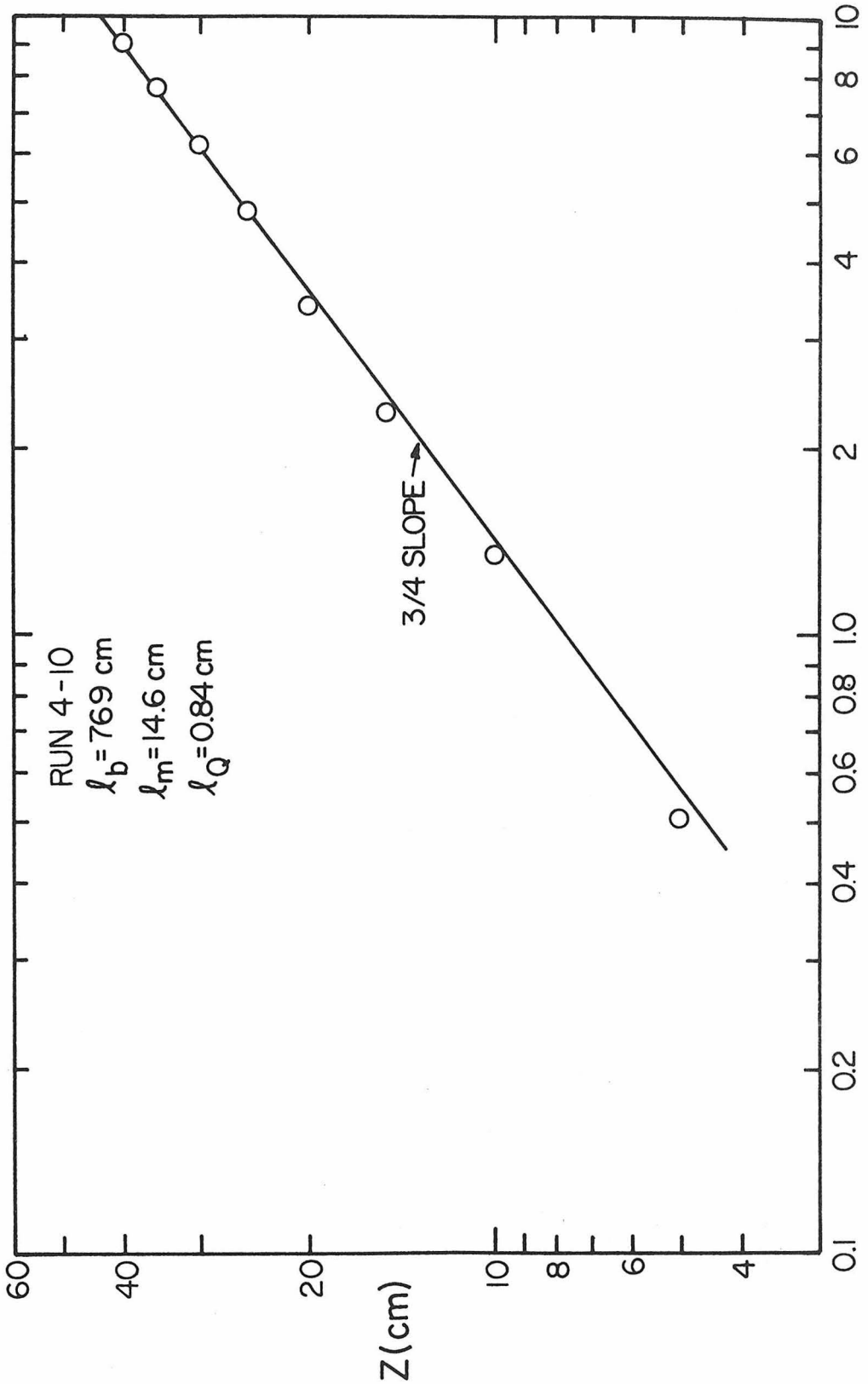

Fig. 5.1a Trajectory plot.

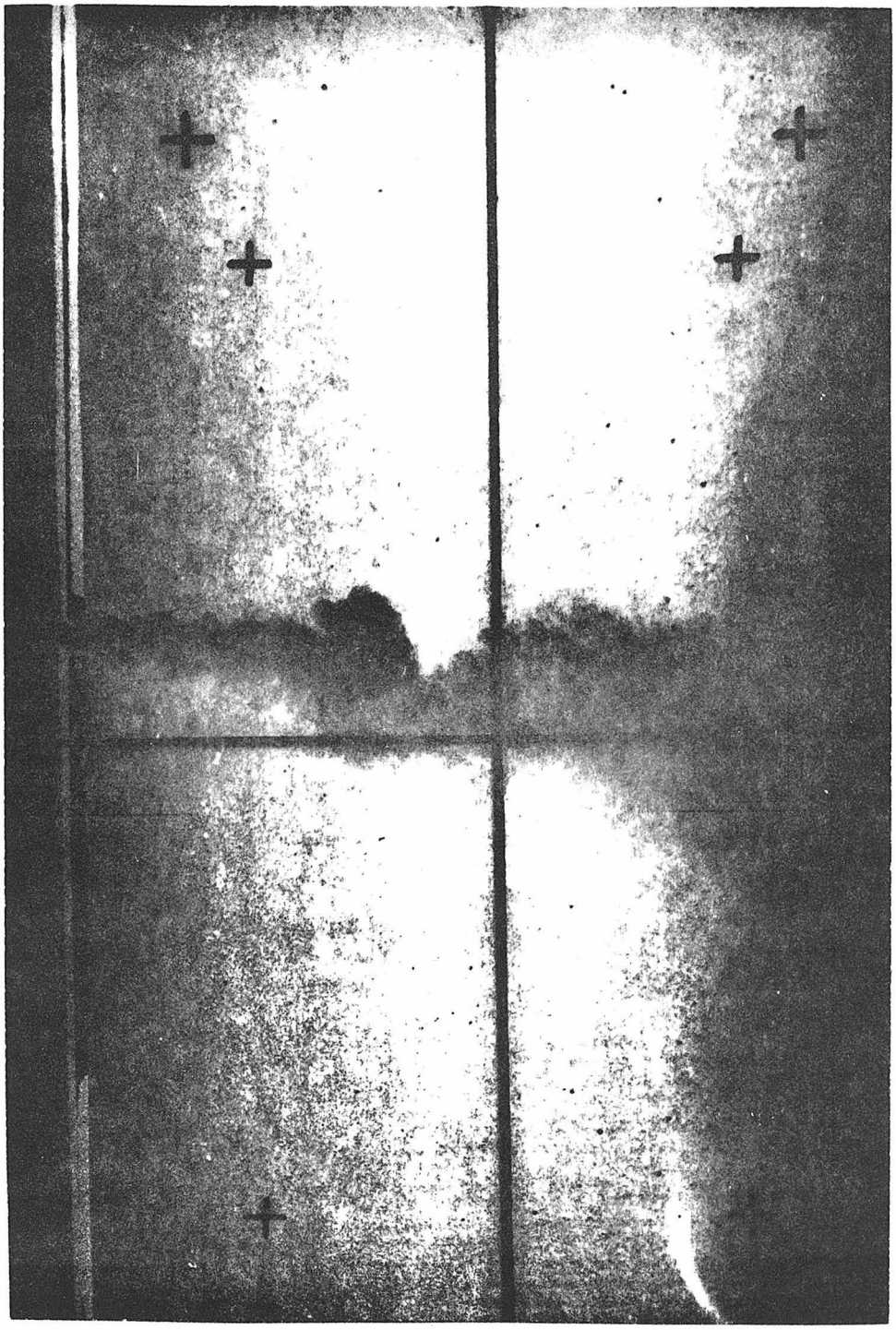

Fig. 5.1b Photograph of a jet in the buoyancy-dominated near-field.

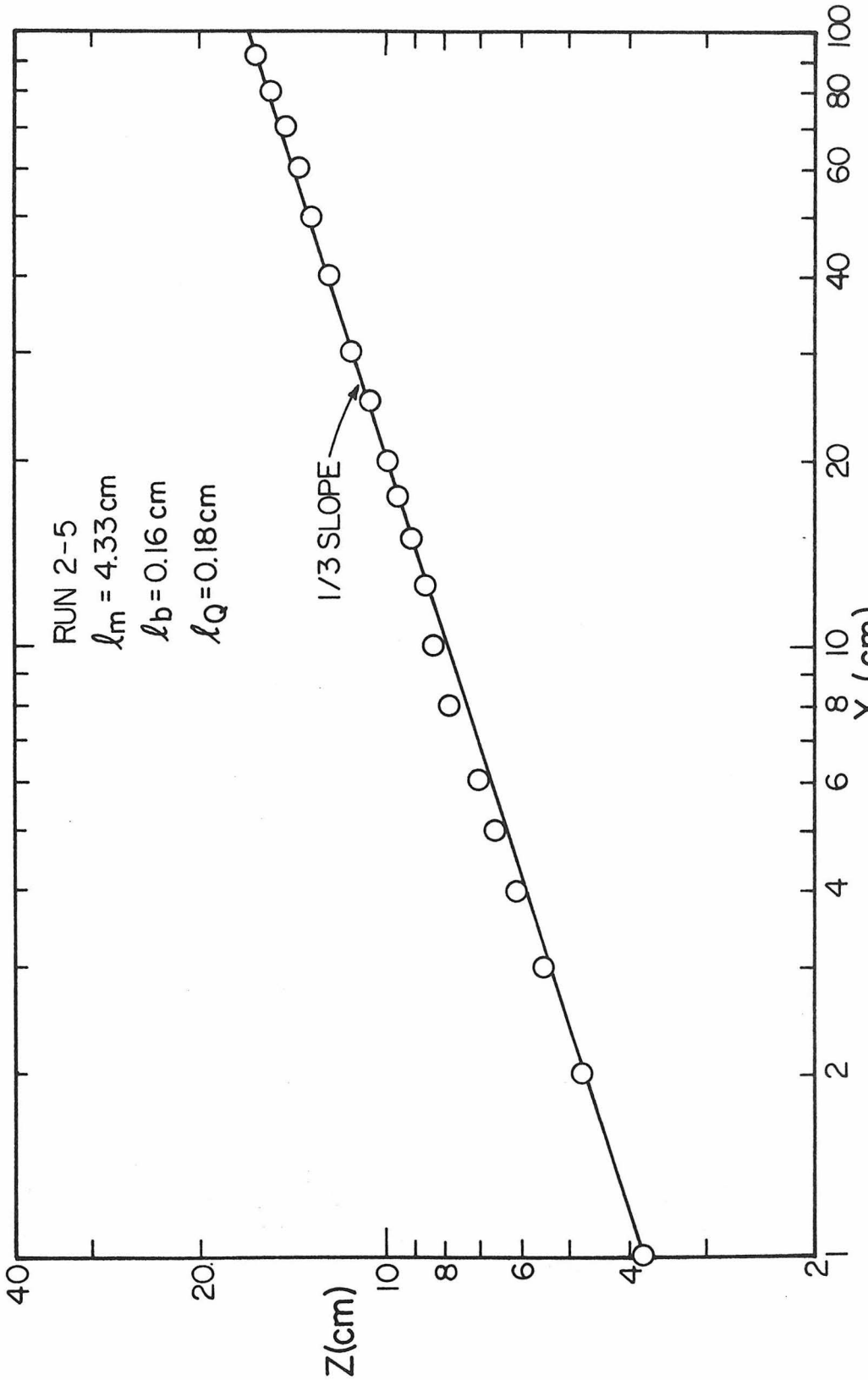

Fig. 5.2a Trajectory plot.

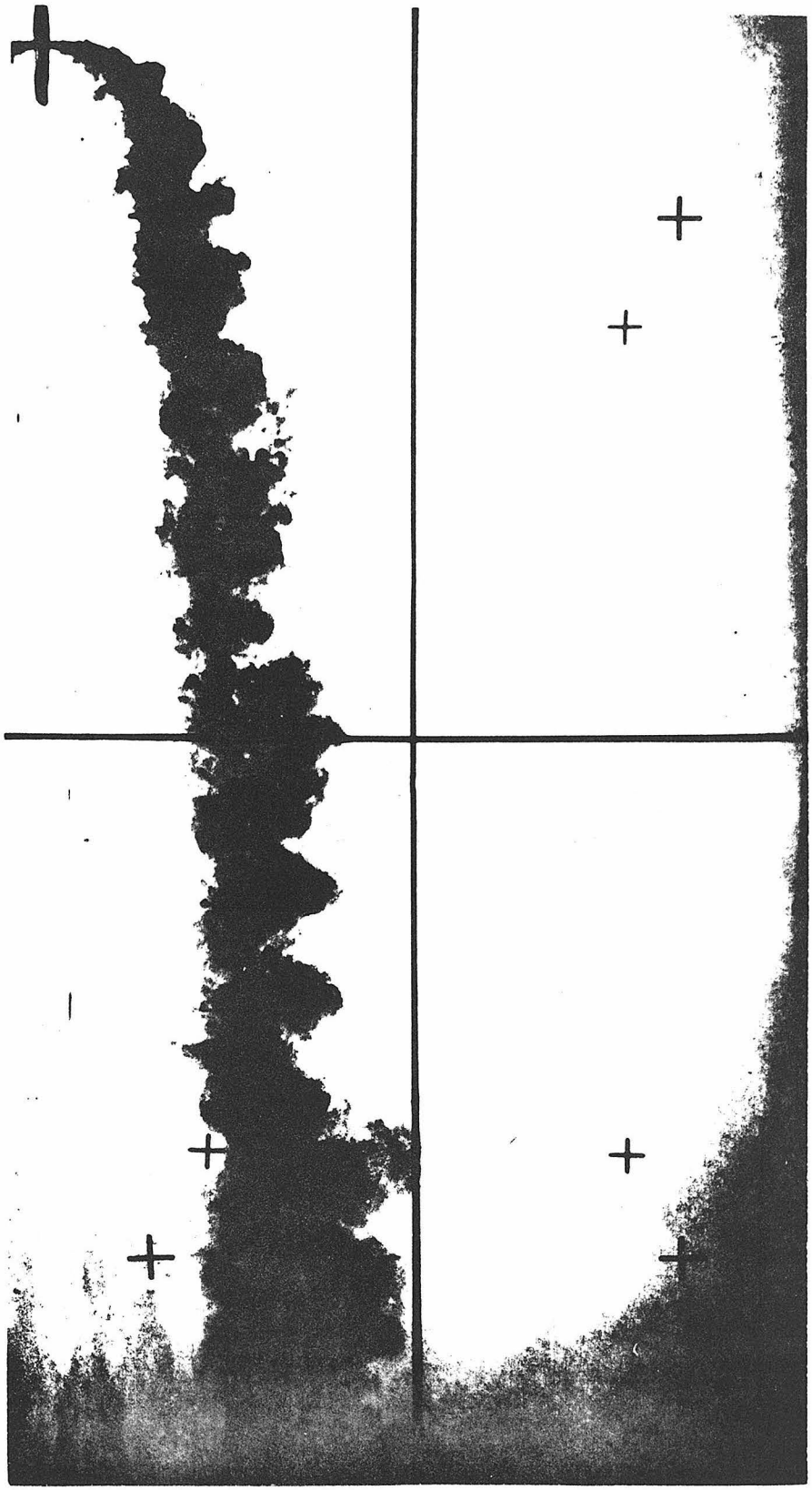

Fig. 5.2b Photograph of a jet in the momentum-dominated far-field.

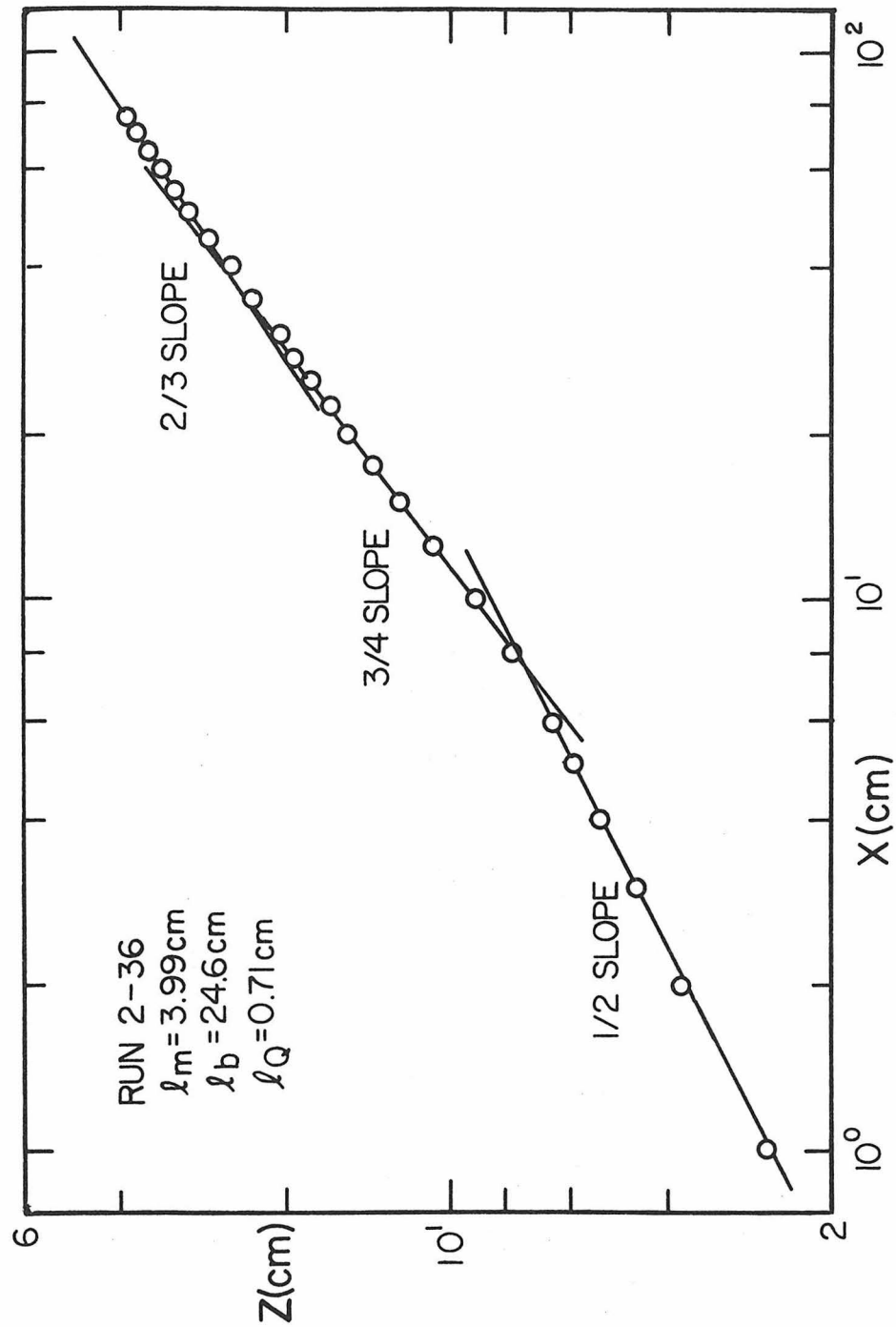

Fig. 5.3a Trajectory of a jet which demonstrates the three trajectory regimes for $\ell_m/\ell_b < 1$.

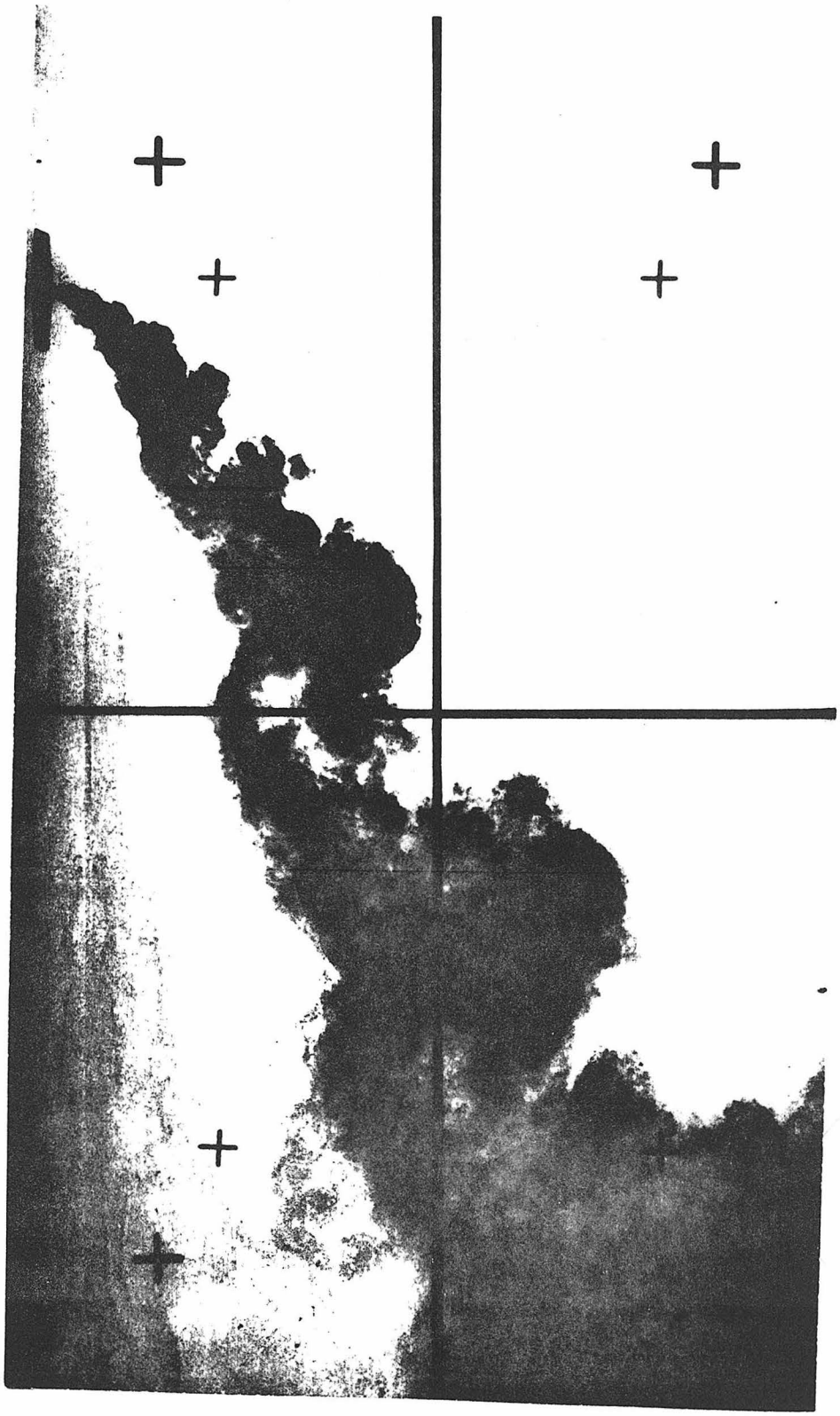

Fig. 5.3b Photograph of buoyant jet (run 2-36).

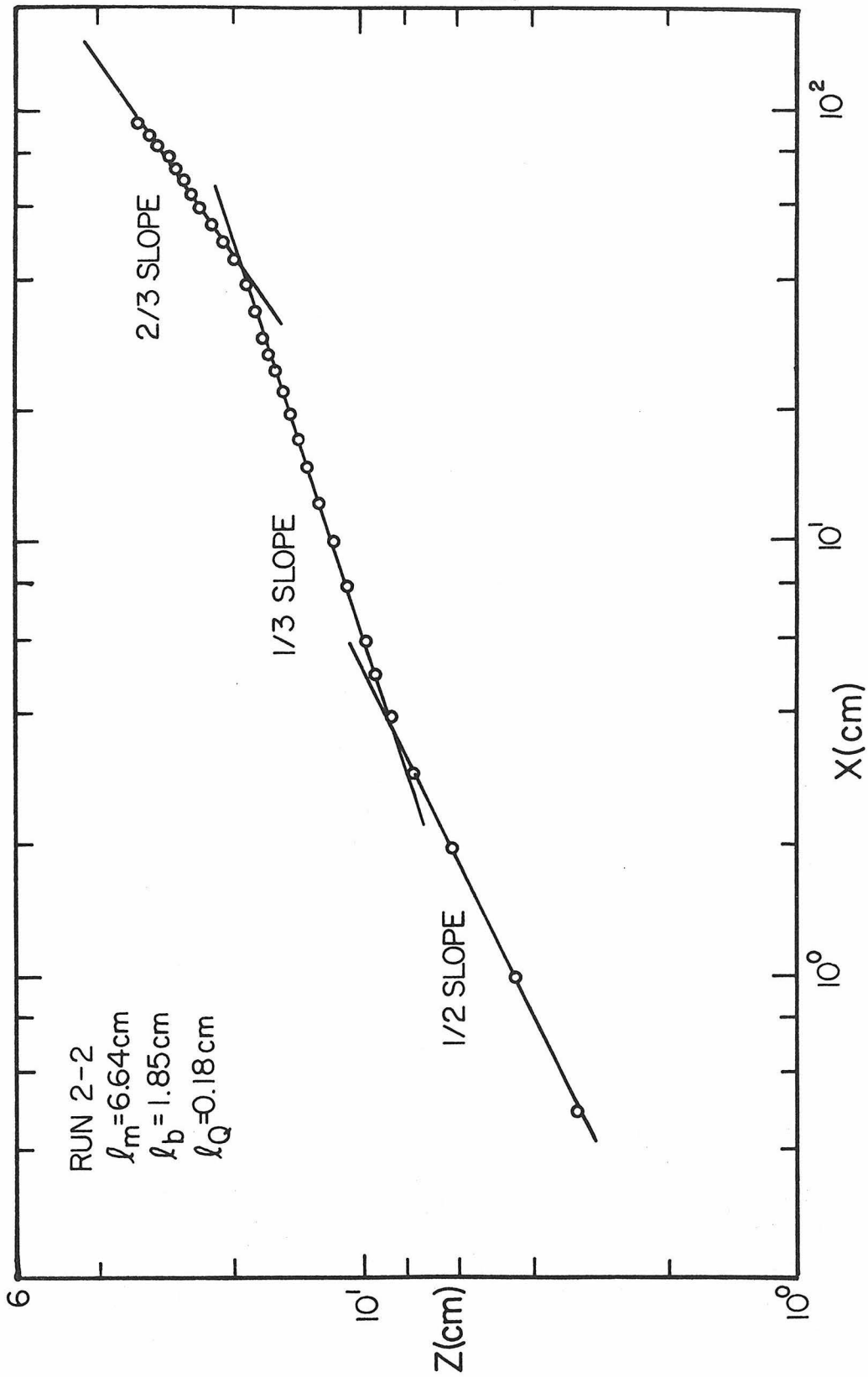

Fig. 5.4a Trajectory of a jet which demonstrates the three trajectory regimes for $\ell_m/\ell_b > 1$.

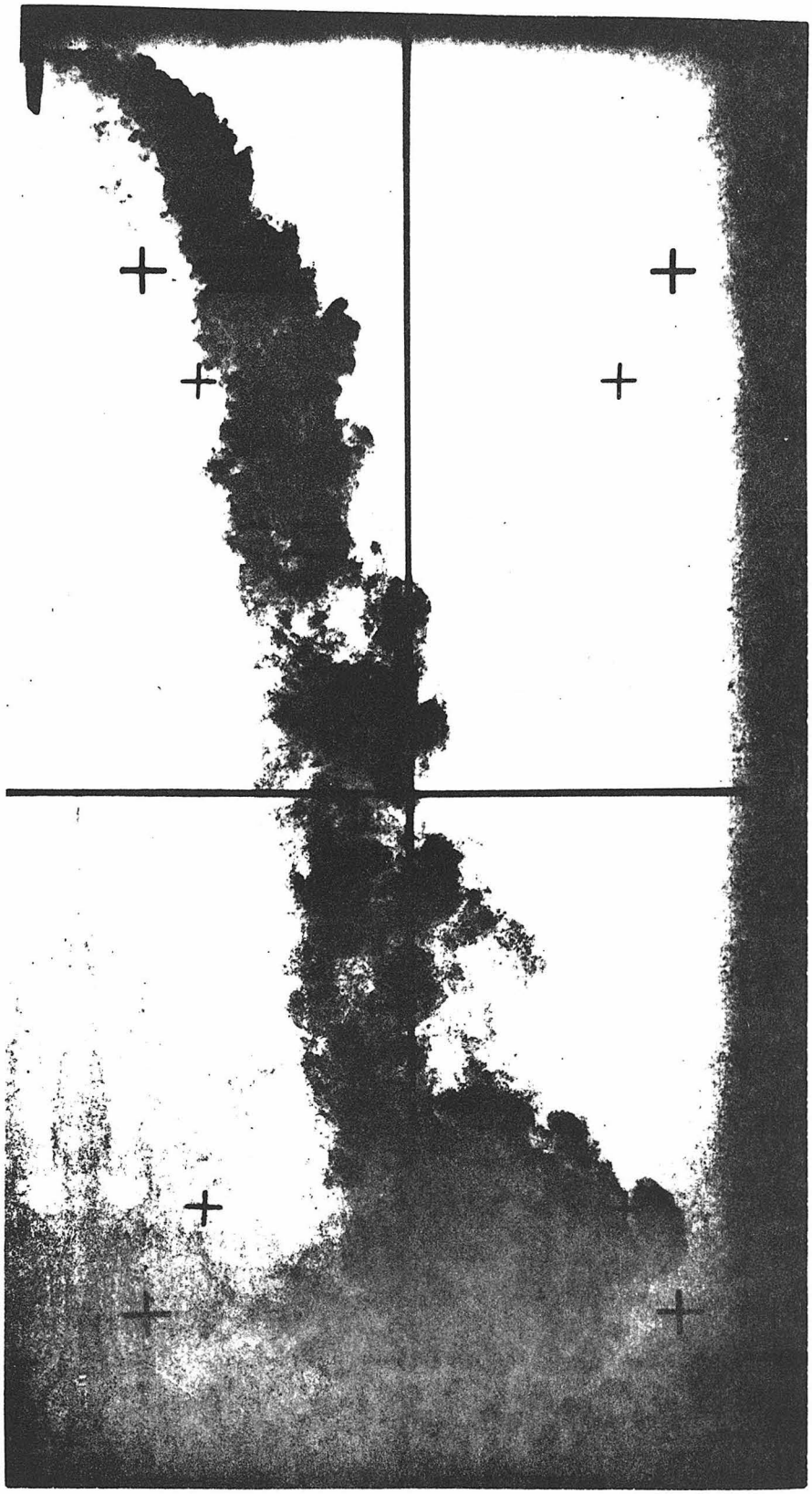

Fig. 5.4b Photograph of buoyant jet (run 2-2).

This trajectory sequence is to be expected for flows with $\ell_m/\ell_b < 1$ and indicates that the asymptotic solutions suggested by the analysis are valid. A further confirmation can be seen from Fig. 5.4 which is a trajectory plot for $\ell_m/\ell_b = 3.6$. The slopes of 1/2,1/3, and 2/3 correspond to the results predicted for the mdnf, the mdff, and the bdff respectively, which would be the expected trajectory sequence for $\ell_m/\ell_b > 1$.

The collective data from all of the experiments were plotted in non-dimensional form according to the various trajectory relations predicted by the analysis. Each individual trajectory plot was examined to observe the apparent slopes for that trajectory. When a portion of the trajectory appeared to be best described by a slope of 1/2, for instance, the results were assumed to correspond to the mdnf. The values of the length scales were also considered in the interpretation of the data. Trajectories for several different buoyant jets are presented in Figs. 5.5-5.7. Fig. 5.5 presents the trajectories for momentum-dominated jets while Figs. 5.6 and 5.7 are the results for the buoyancy-dominated near- and far-fields, respectively. A line with the slope appropriate for the particular flow regime is also indicated in each figure.

A fairly obvious observation from the examination of these figures is that while individual trajectories indicate the correct slopes, the collective data do not collapse onto a single curve which would be expected from the development of the asymptotic models. However, this observation can be expected from dimensional analysis of the entire

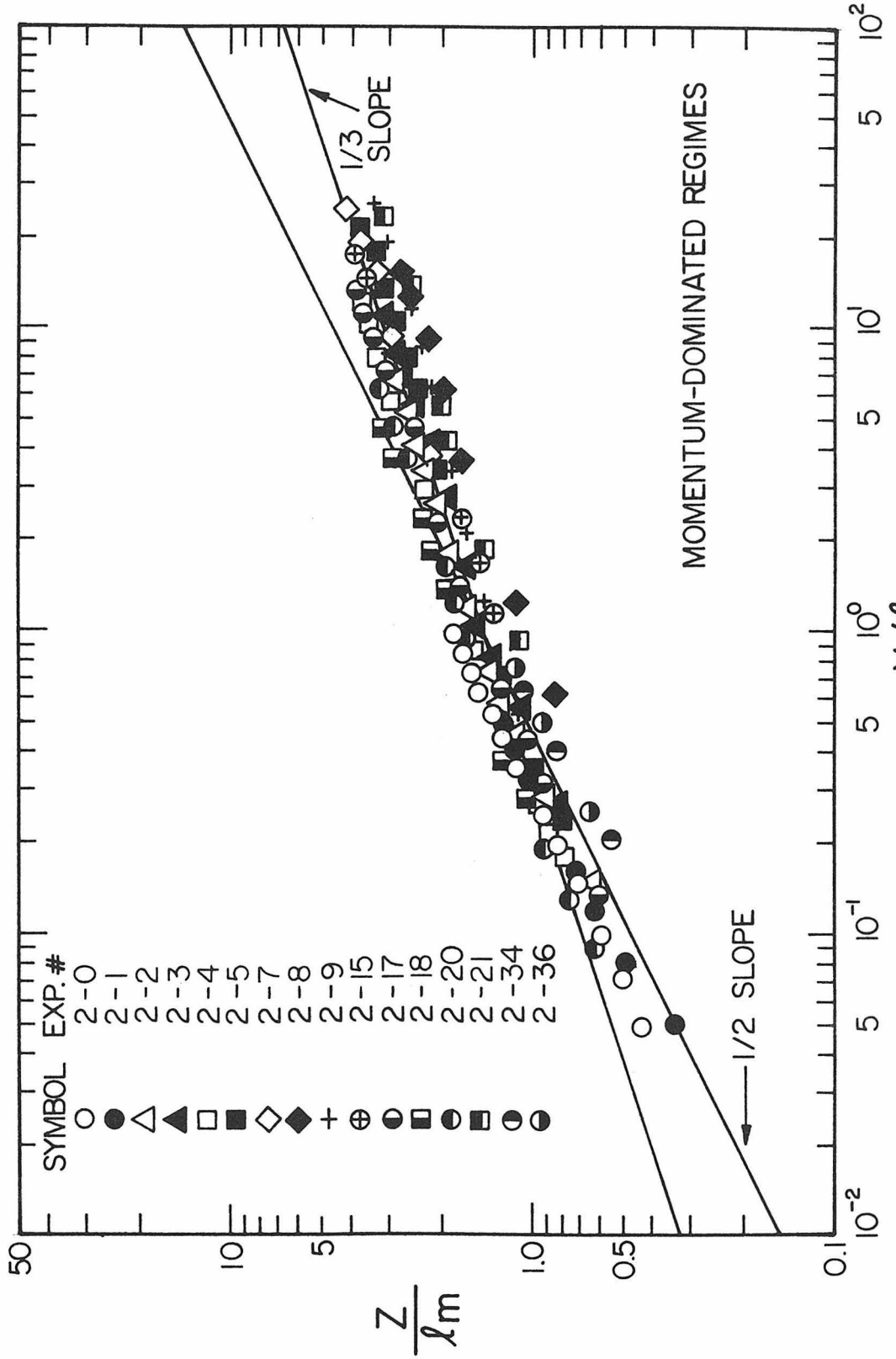

Fig. 5.5 Momentum-dominated trajectories (from photographs).

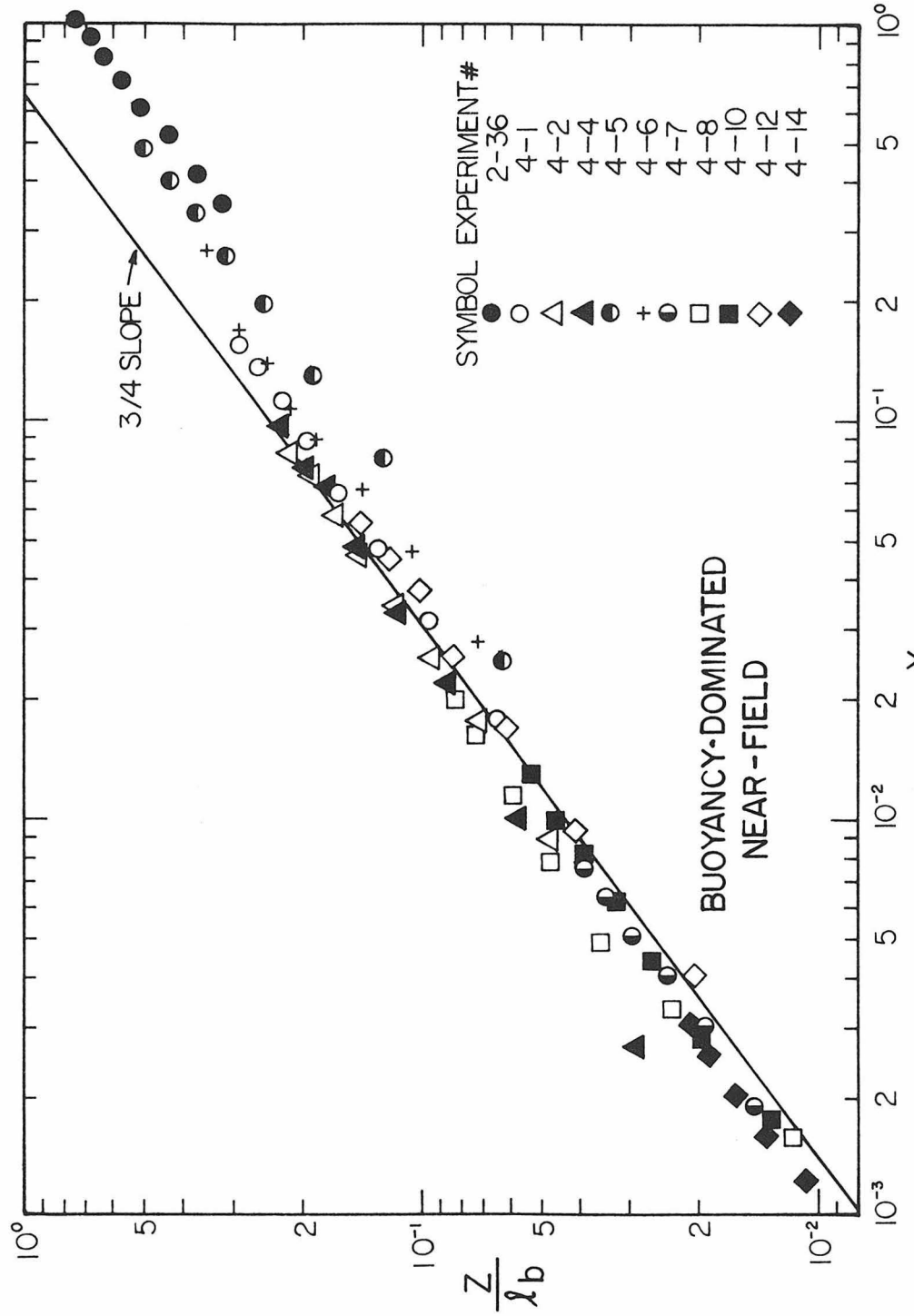

Fig. 5.6 Buoyancy-dominated near-field trajectories (from photographs).

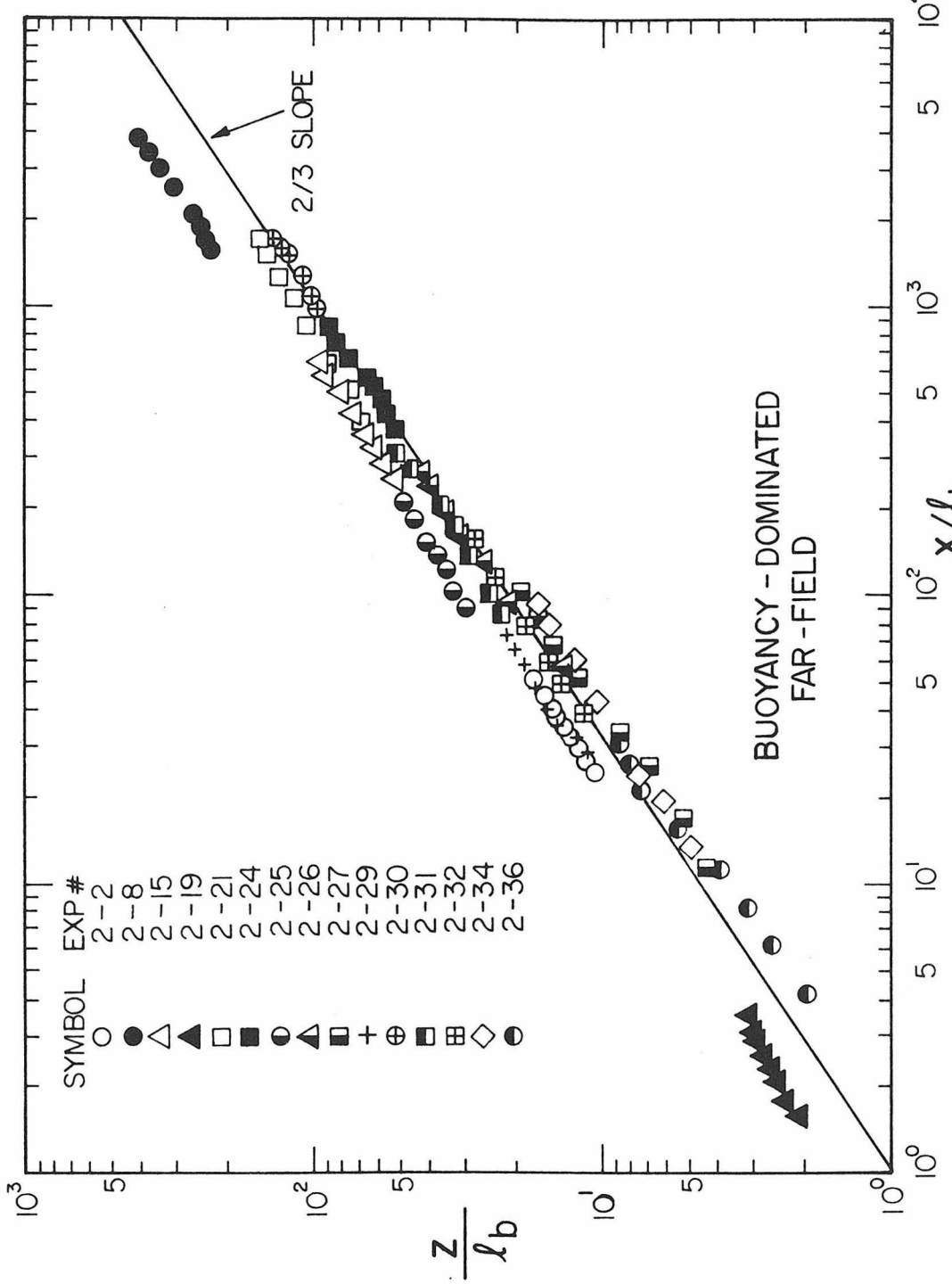

Fig. 5.7 Buoyancy-dominated far-field trajectories (from photographs).

problem. The trajectory relations were predicted for the limiting cases where there was only one jet variable characterizing a particular jet. In fact, there are three independent variables characterizing any jet, even though one variable may have a dominating influence on the flow behavior. Dimensional analysis thus implies that the trajectory for a general buoyant jet can be expressed in the following form:

$$\frac{z}{\ell_b} = f\left(\frac{x}{\ell_b}, \frac{\ell_Q}{\ell_b}, \frac{\ell_m}{\ell_b}\right) \tag{5.1}$$

Even though the trajectory relation corresponding to any one of the asymptotic cases presented in Chapter 3 may be valid, it can be anticipated that the effect of the other jet variables will be observed in the value of the trajectory coefficient. For example, trajectories corresponding to the bdnf will exhibit a 3/4 slope, but the coefficient may depend upon the initial volume and momentum fluxes:

$$\frac{z}{\ell_b} = C_5\left(\frac{x}{\ell_b}\right)^{3/4}, \quad C_5 = f\left(\frac{\ell_Q}{\ell_b}, \frac{\ell_m}{\ell_b}\right) \tag{5.2}$$

When the results for the different trajectory plots are analyzed on the basis of this reasoning, the explanation for the variation in the collective data is apparent. The values for the various trajectory coefficients are given in Figs. 5.8-5.11 as a function of the jet variables for which there appeared to be a correlation. The trajectory coefficients were taken as the values which described a line of the proper slope visually fitted to each experiment (for example, if a trajectory plot indicated that a slope of 2/3 described

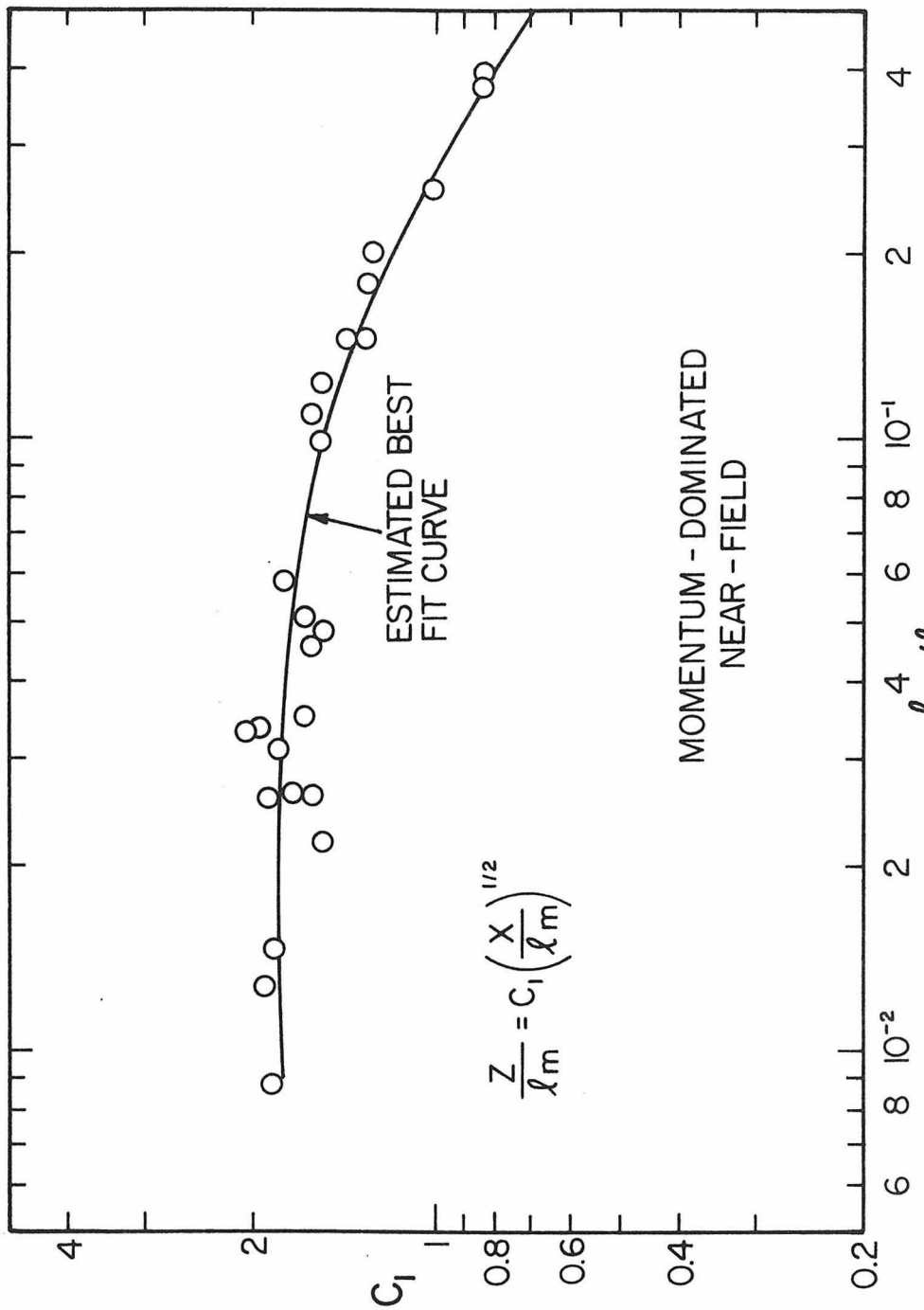

Fig. 5.8 Variation of C_1 with ℓ_Q/ℓ_m (from photographs).

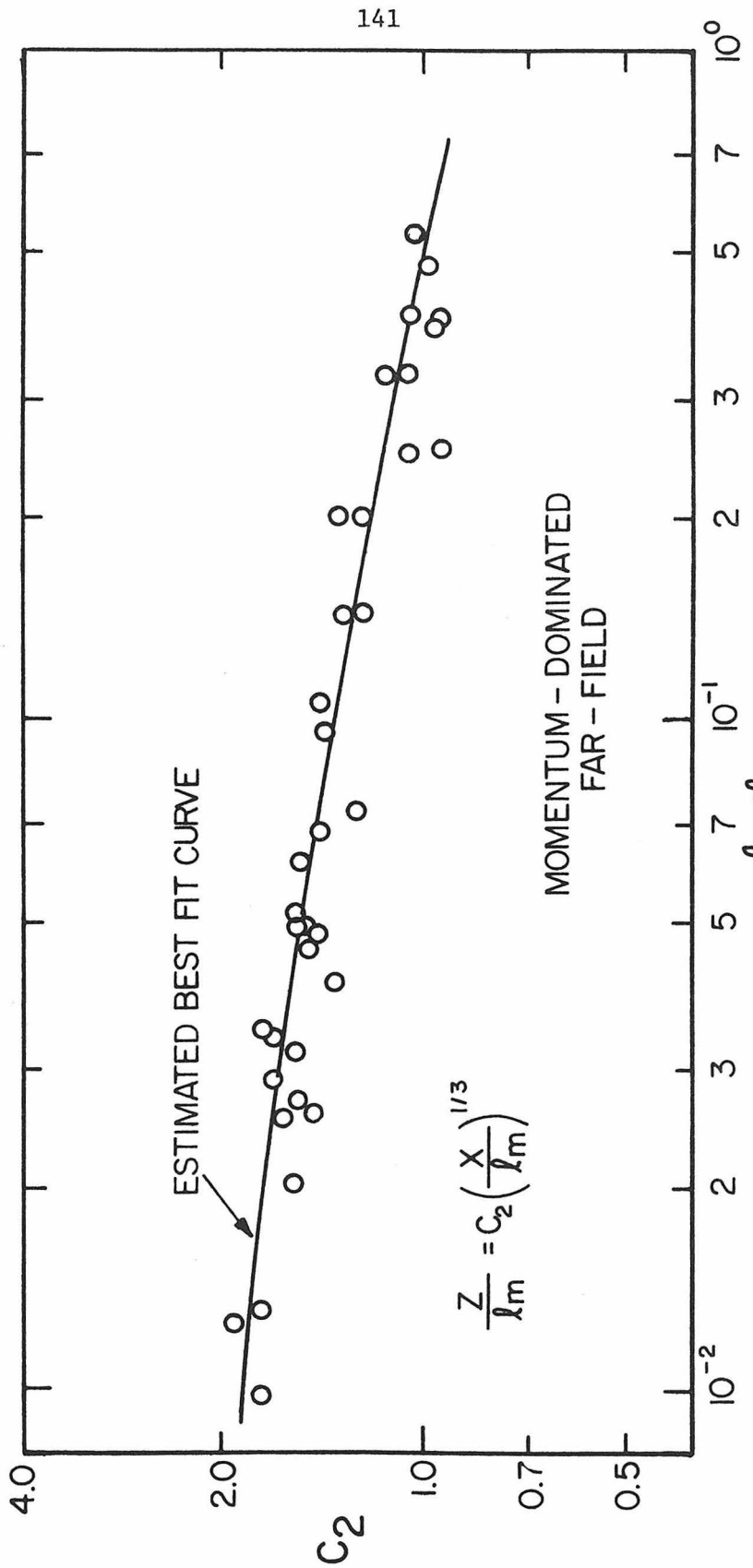

Fig. 5.9 Variation of C_2 with ℓ_Q/ℓ_m (from photographs).

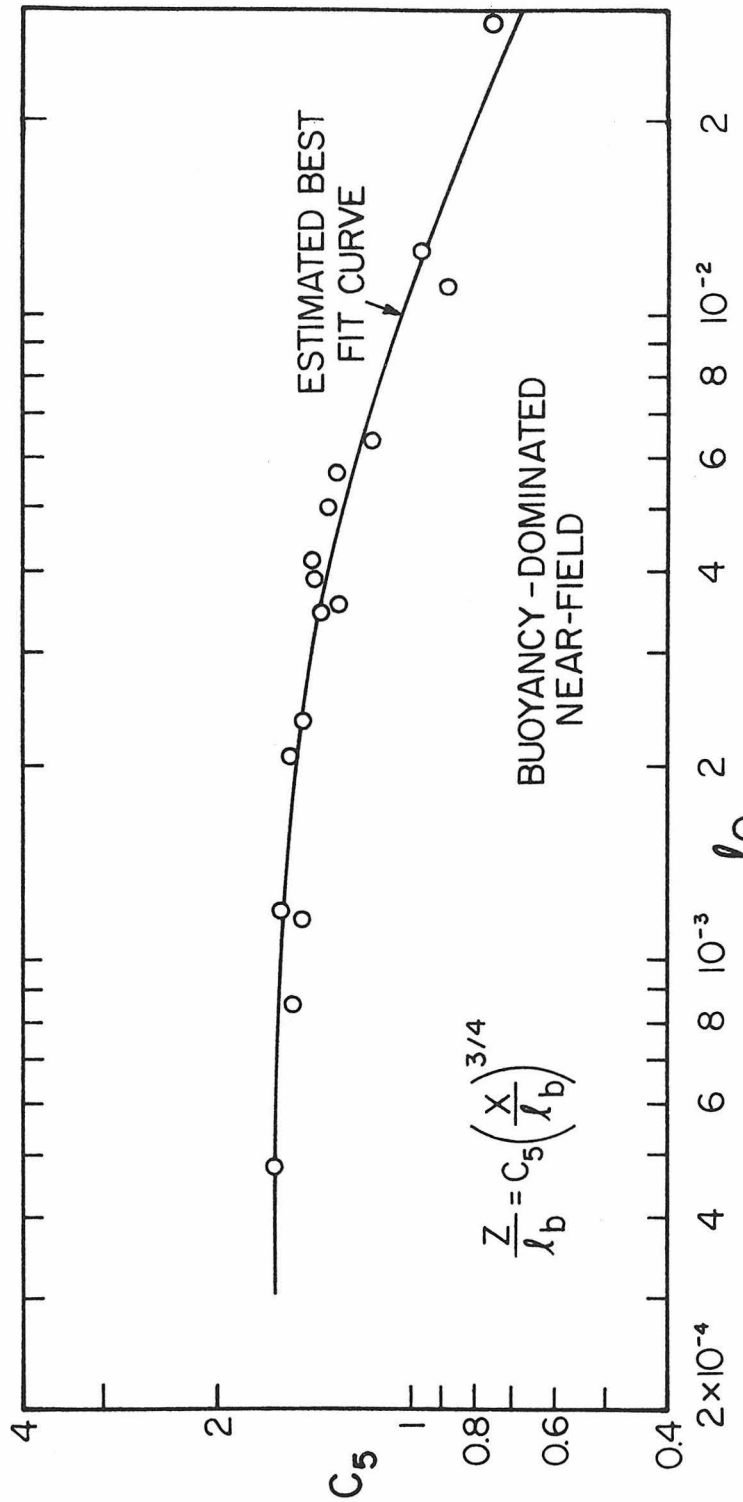

Fig. 5.10 Variation of C_5 with ℓ_Q/ℓ_b (from photographs).

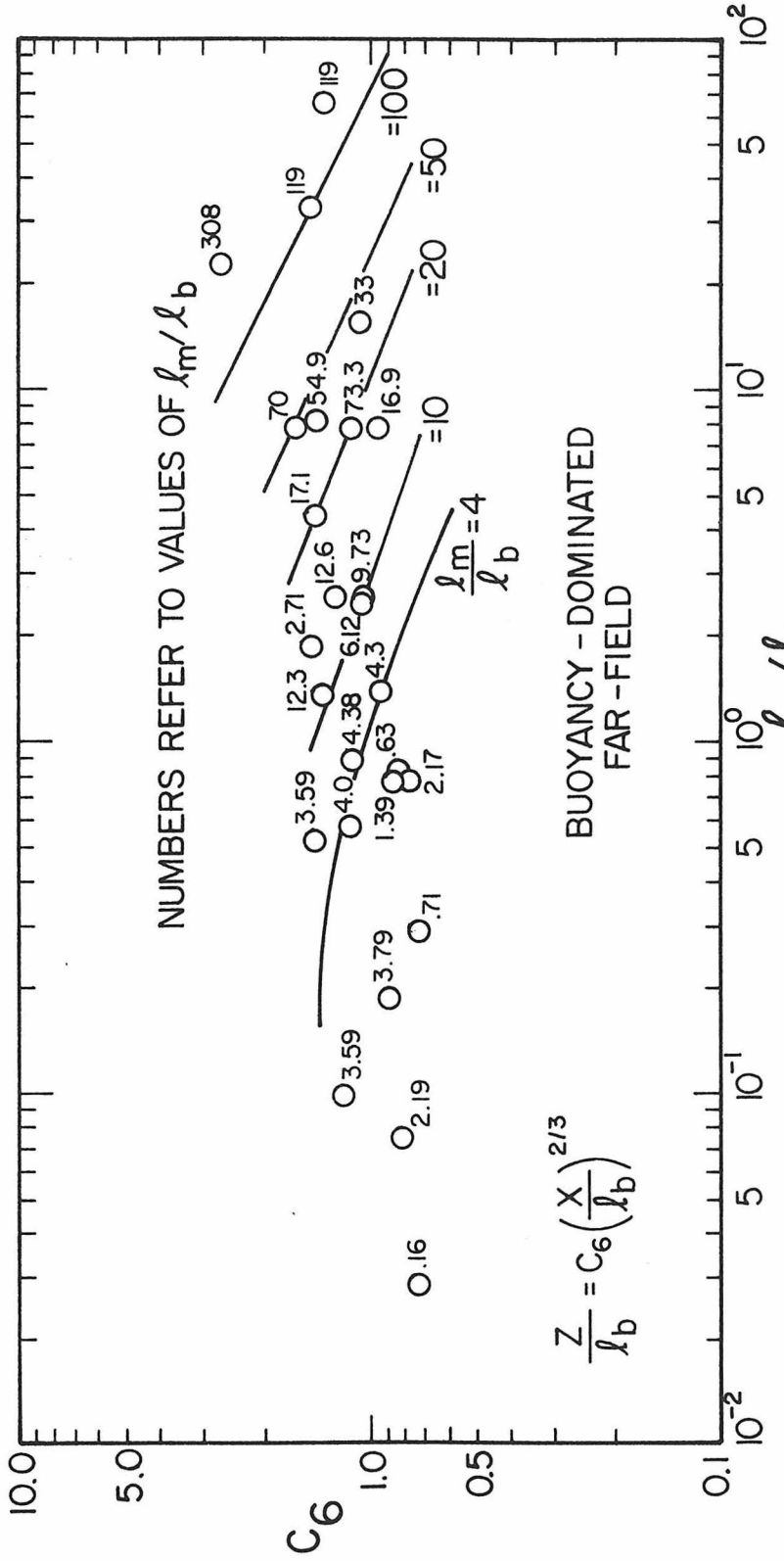

Fig. 5.11 Variation of C_6 with ℓ_Q/ℓ_b and ℓ_m/ℓ_b (from photographs).

the data, the coefficient C_6 was defined as the value for a line with 2/3 slope that appeared to fit the data best).

Each of the flow regimes indicated a dependence of the trajectory coefficient on the initial volume flux in the form of the non-dimensional ratio ℓ_Q/ℓ_m for the momentum-dominated trajectories and ℓ_Q/ℓ_b for the buoyancy-dominated regimes. The general trend is that the value of the coefficient decreases with increasing values of ℓ_Q/ℓ_m or ℓ_Q/ℓ_b. Although the figures indicate that in some instances, the coefficients appear to approach a constant value for small relative values of ℓ_Q, there are insufficient data to verify this observation.

There is an additional variation for the trajectory coefficient C_6 for the buoyancy-dominated far-field with the initial momentum flux in the form of the ratio ℓ_m/ℓ_b. The data in Fig. 5.11 are presented in an alternate manner in Fig. 5.12 which clearly indicates the variation with ℓ_m/ℓ_b. The trend is that the value of the coefficient increases with increasing ℓ_m/ℓ_b for ℓ_Q/ℓ_b constant. The values for C_6 for all experiments ranged from approximately 0.7-2.7. This is a significant variation, as all previous analyses (e.g., Slawson and Csanady (1967), etc.) that correspond to the buoyancy-dominated far-field consider C_6 to be invariant.

Information regarding jet trajectories was also obtained from the concentration measurements made with the fluorometer and associated apparatus. The results obtained from this portion of the experimental investigation cannot be compared directly with the trajectories from

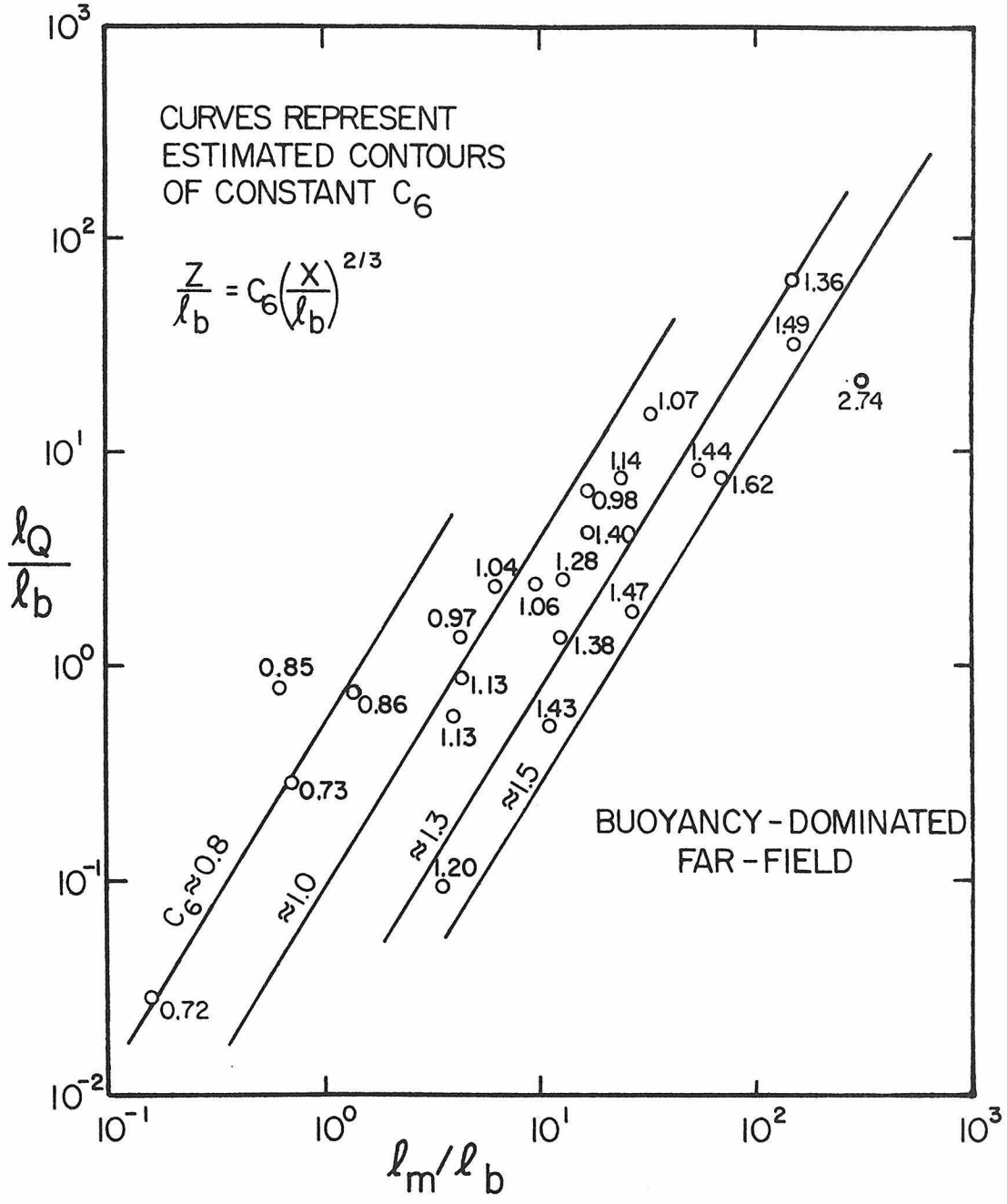

Fig. 5.12 Alternate presentation of variation of C_6.

the photographs since the definition of the vertical rise of the jet is not the same for the two experimental methods. The concentration measurements were primarily intended to supplement the same type of information obtained in an earlier study by Fan (1967). The majority of his data were determined to correspond to the two far-field regimes (mdff and bdff) so most of the measurements made in this portion of the experimental investigation were intended to examine the near-field flow regimes more closely.

The trajectory measurements from this study and the earlier one by Fan are indicated in Figs. 5.13-5.15 for the various flow regimes. Each data point was assigned to a particular flow regime on the basis of the results from the trajectory measurements from the photographs. This was necessary since it was difficult to determine the trajectory slope from the limited amount of data for each set of experimental conditions. The values of the vertical rise z, the horizontal distance x, and the length scales ℓ_Q, ℓ_m, and ℓ_b were compared to the results indicated in Figs. 5.5-5.7 and each data point was assigned to the flow regime to which the values of these variables corresponded. Since the definitions of the trajectories were different for the two types of measurements, some error might result in assigning a data point that was near the transition between flow regimes, but the effect on the overall results should be negligible.

The interpretation of these experimental results is somewhat more difficult since there is greater experimental scatter and the experiments did not cover as wide a range of variables as the experiments for which the trajectories were measured from the photographs. Figs.

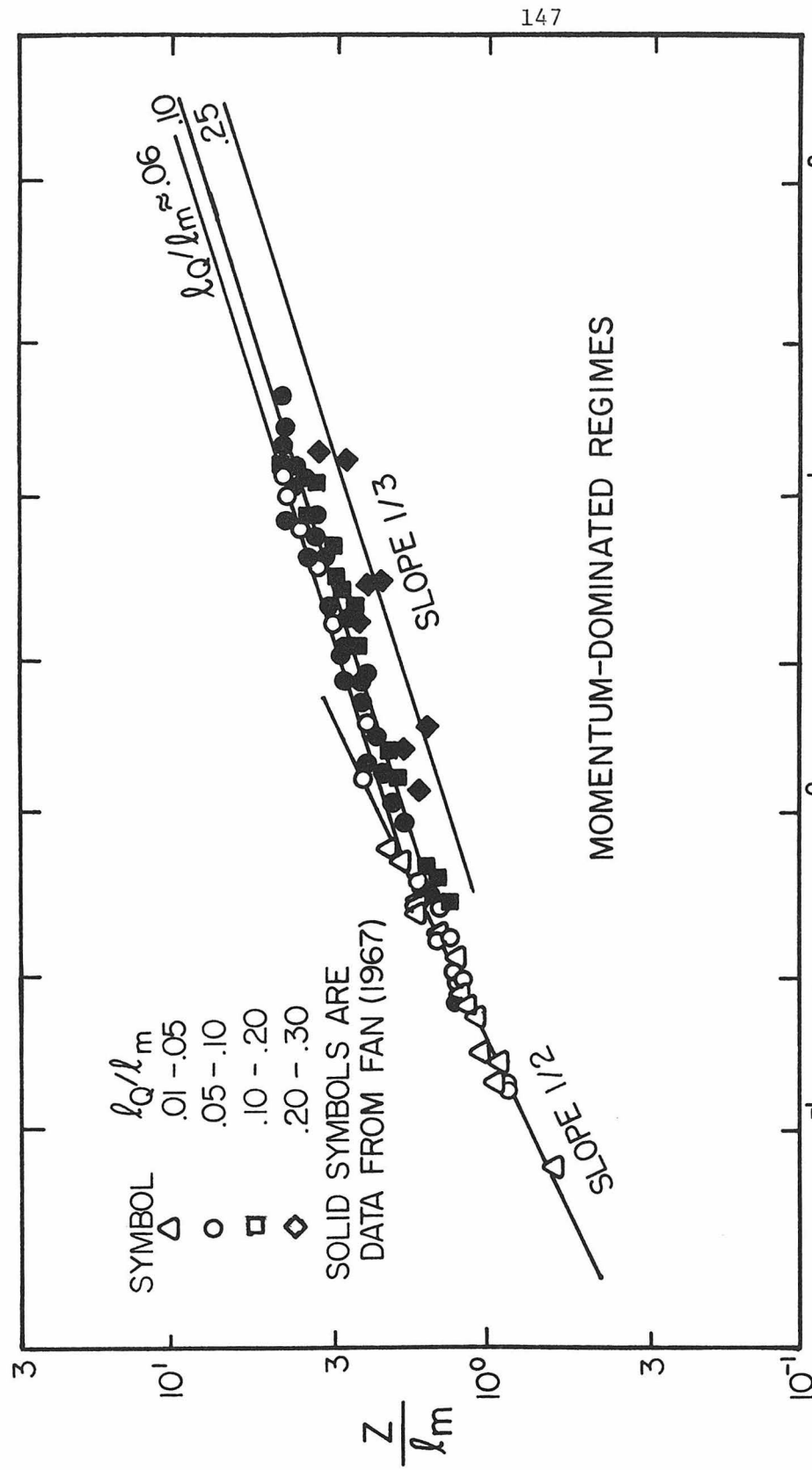

Fig. 5.13 Momentum-dominated trajectories (from concentration measurements).

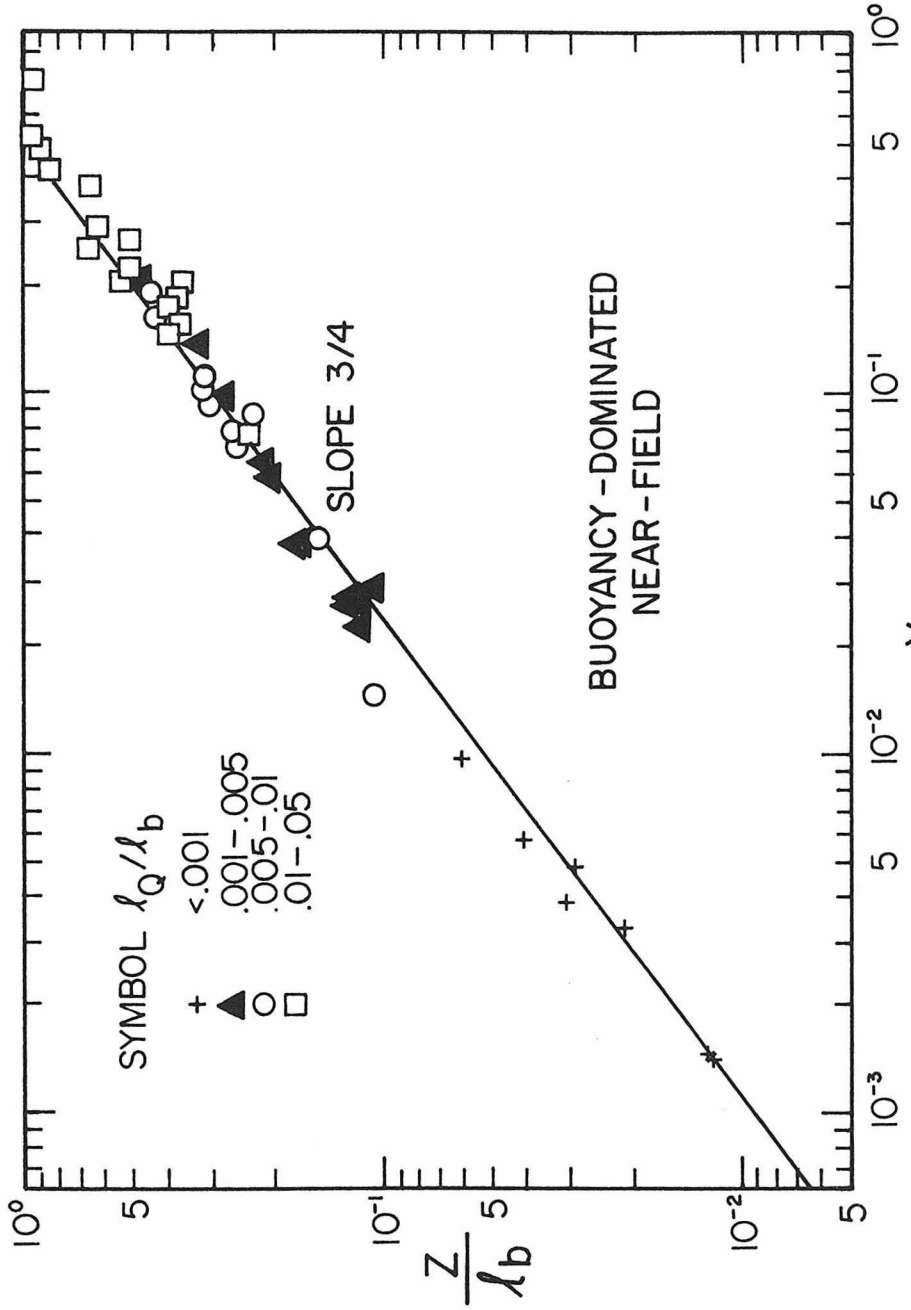

Fig. 5.14 Buoyancy-dominated near-field trajectories (from concentration measurements).

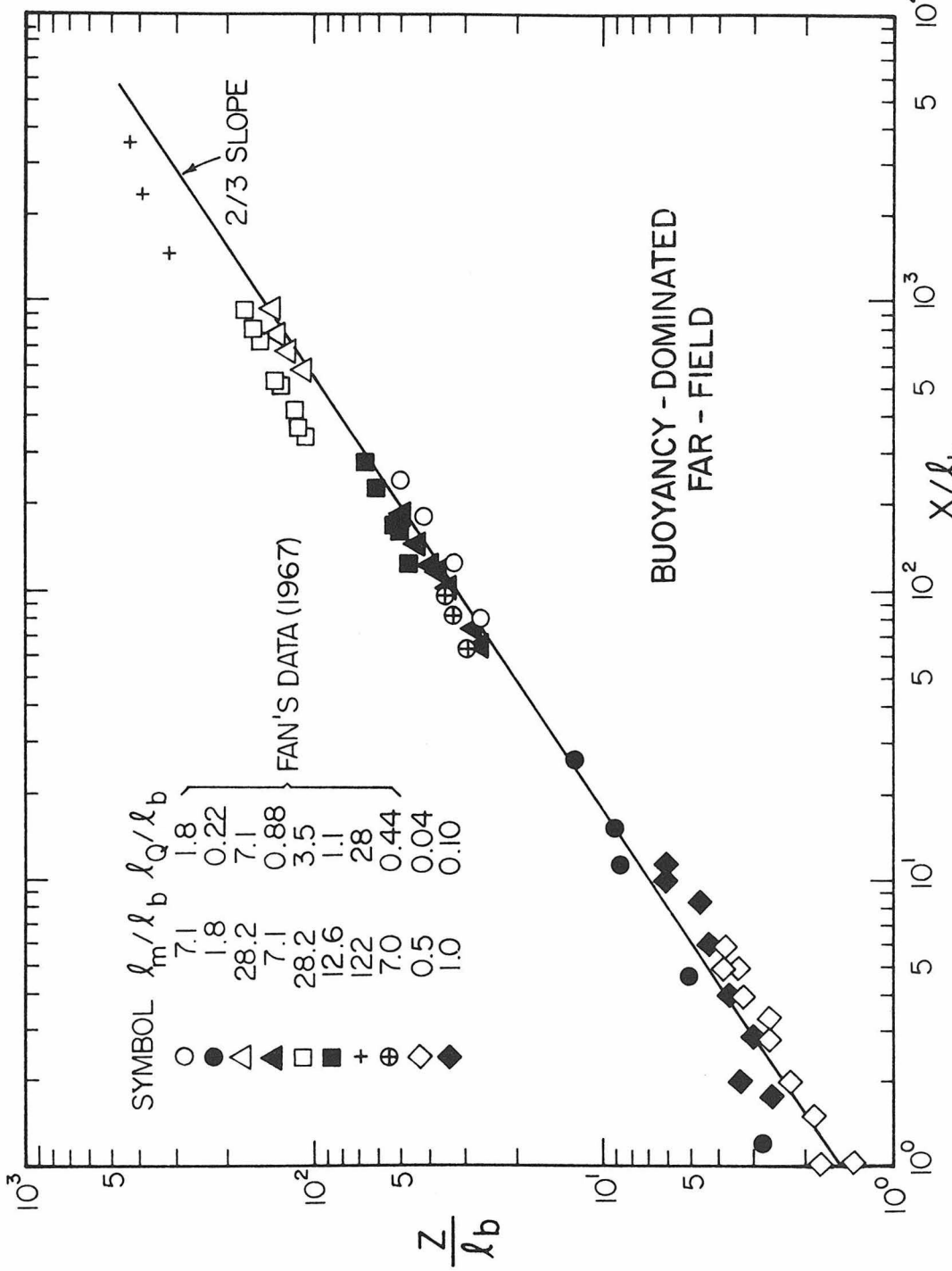

Fig. 5.15 Buoyancy-dominated far-field trajectories (from concentration measurements).

5.16-5.19 present the average values of the different trajectory coefficients as a function of the jet variables. Each data point represents the average value for all the experiments performed for a given set of jet and ambient flow conditions. The curves in these figures represent the shape of the curve for the same coefficient in Figs. 5.8-5.11. These curves appear to fit the data fairly well for the range of variables presented. These values of the trajectory coefficients are approximately 20% greater than the corresponding values measured from the photographs. This is due to the difference in definition of the jet trajectory in the two cases. These latter trajectory coefficients would probably be the ones used in applications of the results since the location of the minimum dilution is likely to be the desired information.

Table 5.1 summarizes the experimental investigations for the measurements of jet trajectories.

5.1.2 Dilution Measurements

The experimental data from the concentration measurements described in the preceding section were also used to determine the dilution within the jet along its trajectory in an unstratified crossflow. The experimental results from the study by Fan (1967) are also included in the presentation of these results. The characteristic dilution is taken as the minimum value (or maximum concentration) in the plane of jet symmetry for a given jet cross-section. Fan made his concentration measurements across a section taken perpendicular to the jet axis, while the measurements in the present investigation were obtained for vertical cross-sections of the jet. This difference would not give substantially different experimental results except for very low crossflow velocities where the jet is very nearly

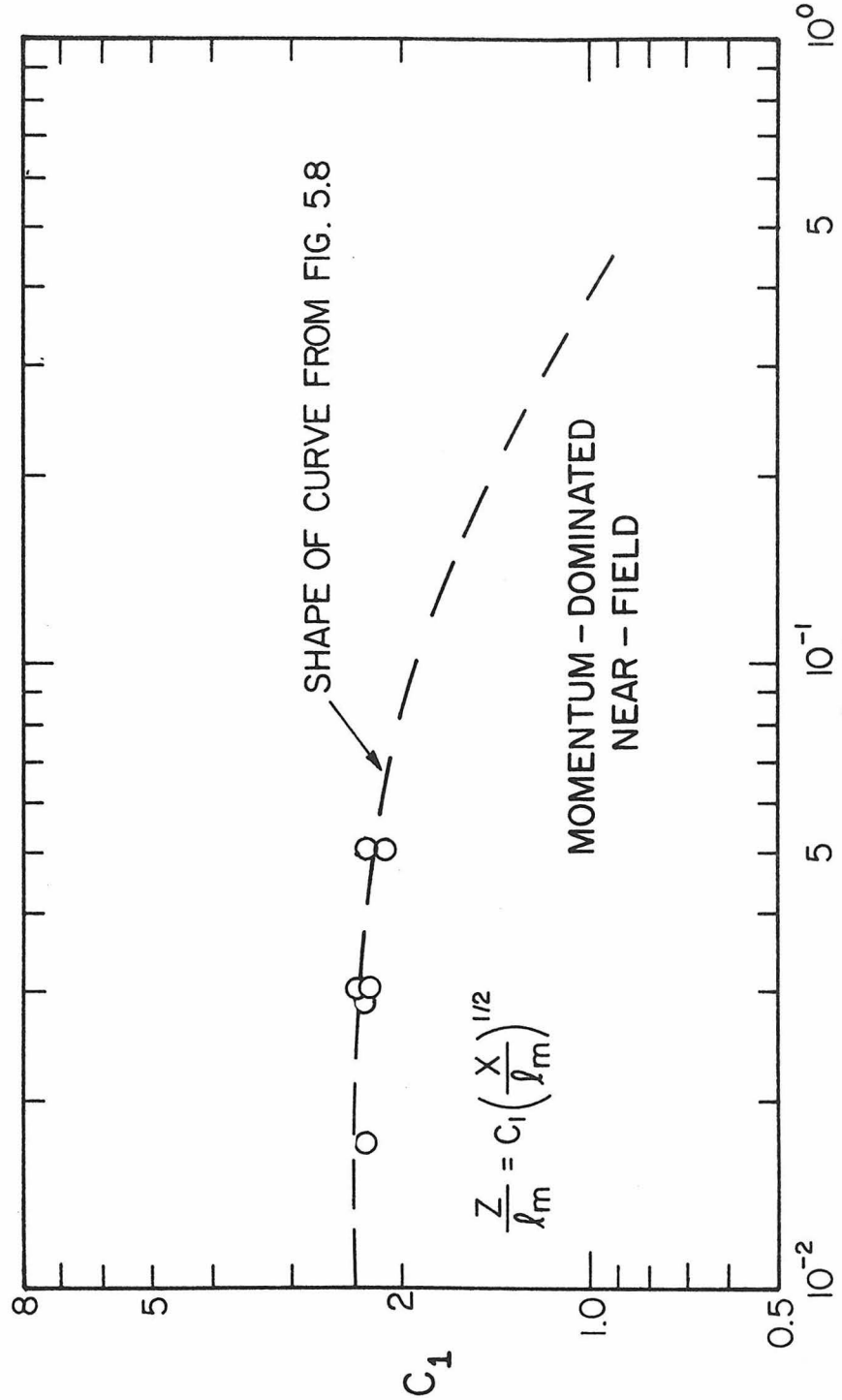

Fig. 5.16 Variation of C_1 with ℓ_Q/ℓ_m (from concentration measurements).

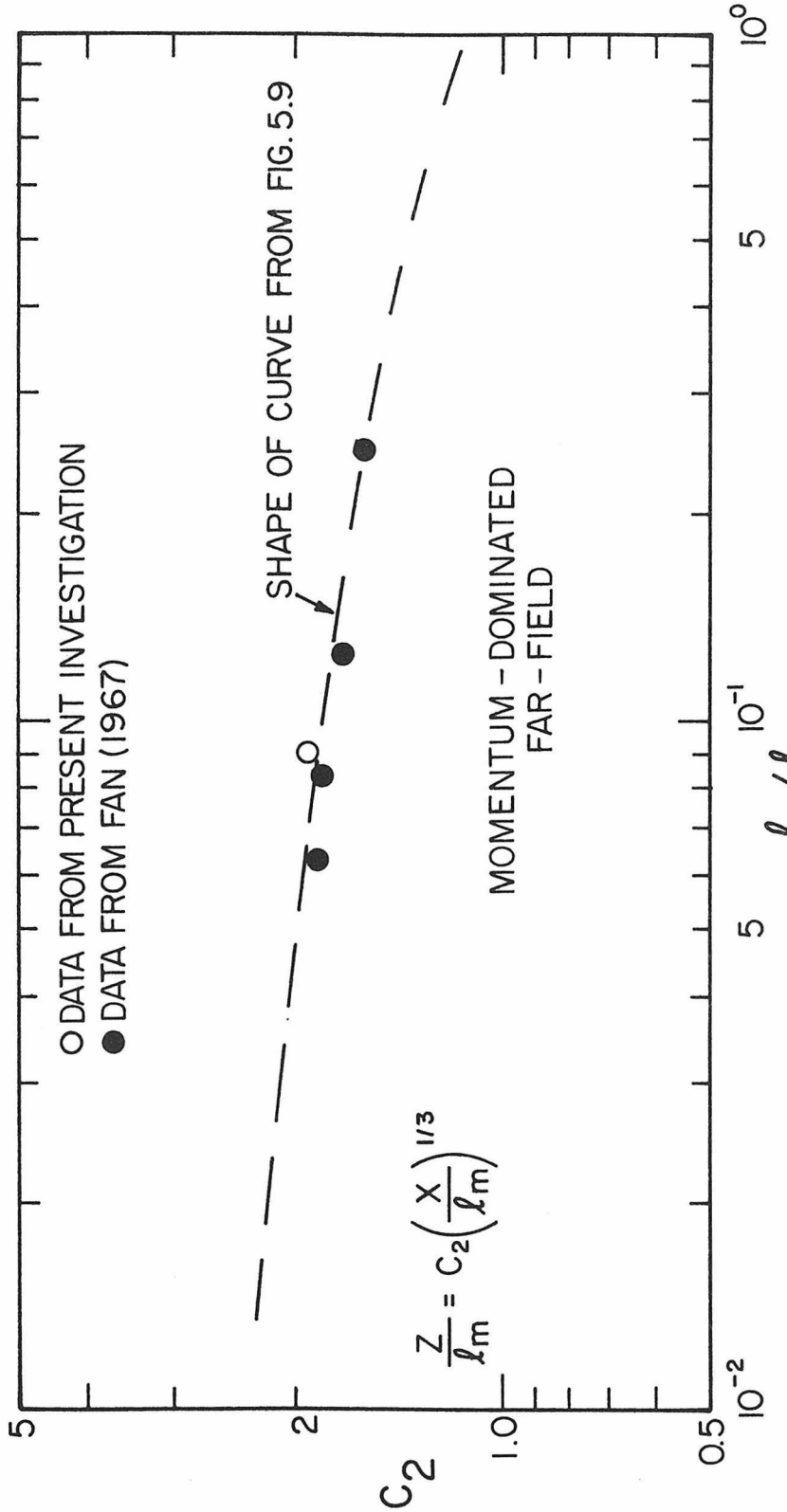

Fig. 5.17 Variation of C_2 with ℓ_Q/ℓ_m (from concentration measurements).

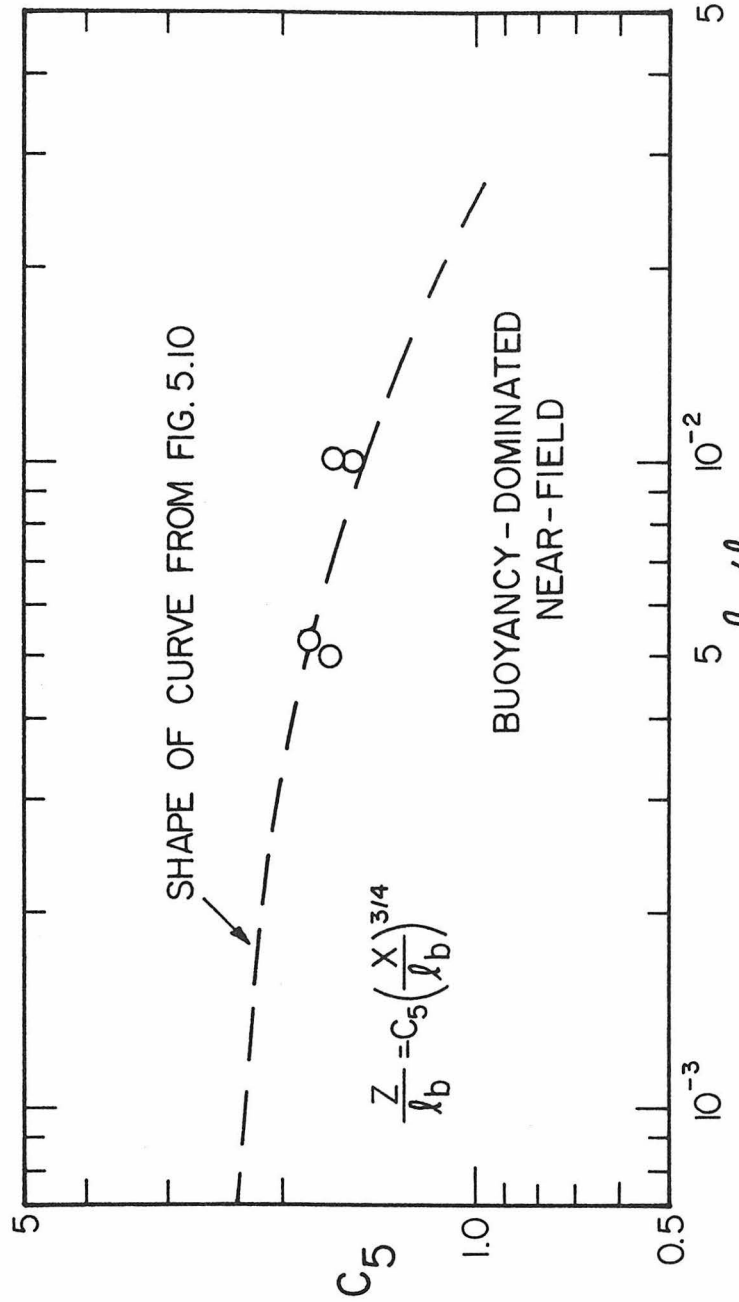

Fig. 5.18 Variation of C_5 with ℓ_Q/ℓ_b (from concentration measurements).

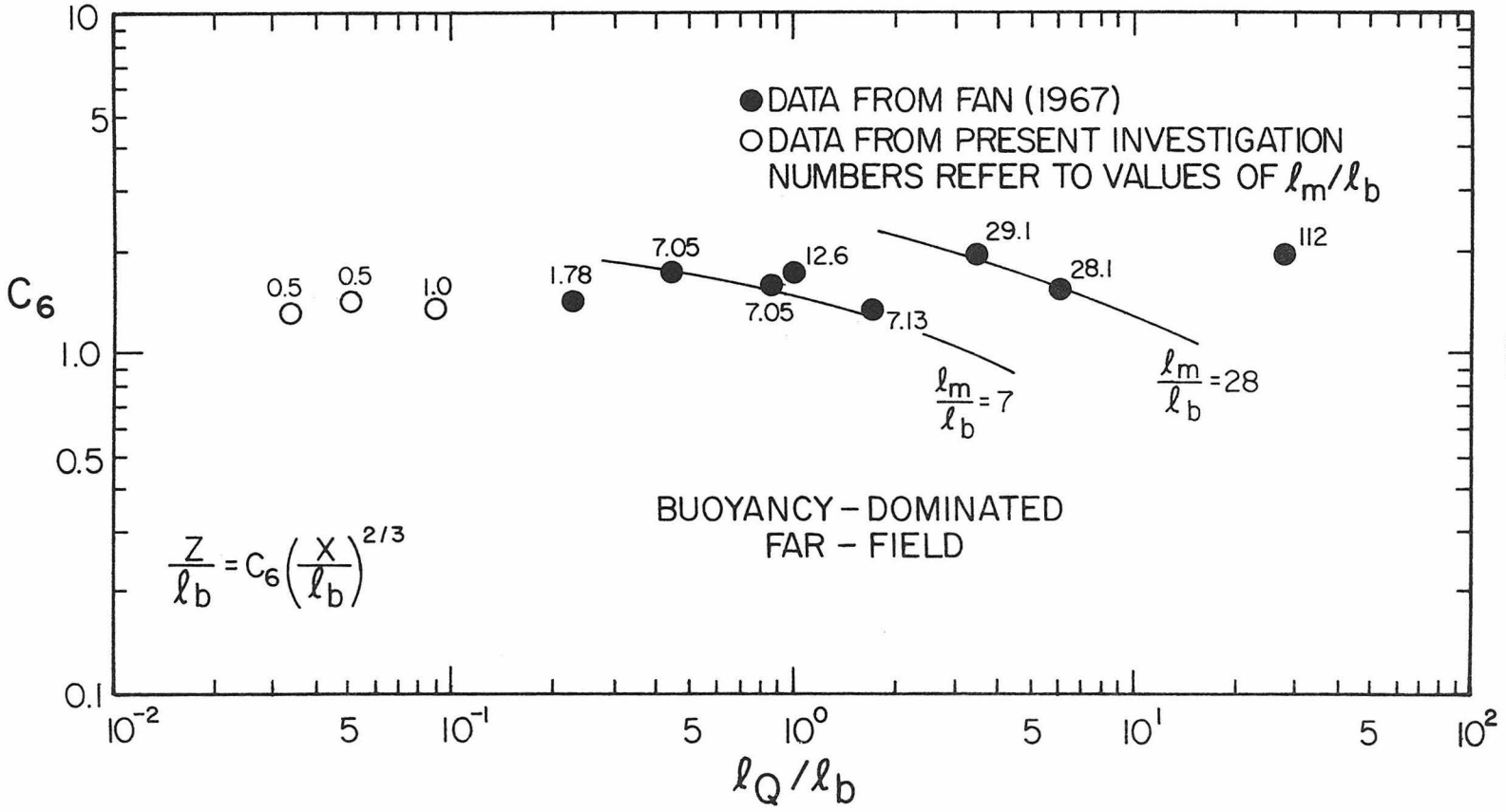

Fig. 5.19 Variation of C_6 with ℓ_Q/ℓ_b and ℓ_m/ℓ_b (from concentration measurements).

Table 5.1 Summary of trajectory measurements for buoyant jets in an unstratified crossflow.

Flow Regime	Trajectory Relation	Data Presented in Figures	Values of Coefficients Given in Figures
Momentum-dominated near-field	$\frac{z}{\ell_m} = C_1\left(\frac{x}{\ell_m}\right)^{1/2}$	5.5 5.13	5.8 5.16
Momentum-dominated far-field	$\frac{z}{\ell_m} = C_2\left(\frac{x}{\ell_m}\right)^{1/3}$	5.5 5.13	5.9 5.17
Buoyancy-dominated near-field	$\frac{z}{\ell_b} = C_5\left(\frac{x}{\ell_b}\right)^{3/4}$	5.6 5.14	5.10 5.18
Buoyancy-dominated far-field	$\frac{z}{\ell_b} = C_6\left(\frac{x}{\ell_b}\right)^{2/3}$	5.7 5.15	5.11 or 5.12 5.19

vertically rising.

The experimental data were assigned to the different flow regimes on the same basis as the trajectory data discussed in the preceding section. That is, it was determined to which flow regime the (x,z) coordinates would correspond for the given values of the jet and ambient flow variables. The results are indicated in Fig. 5.20 for the two momentum-dominated regimes and in Figs. 5.21 and 5.22 for the buoyancy-dominated near- and far-fields, respectively. Lines with the slope indicated by the analysis in Chapter 3 are included in each figure.

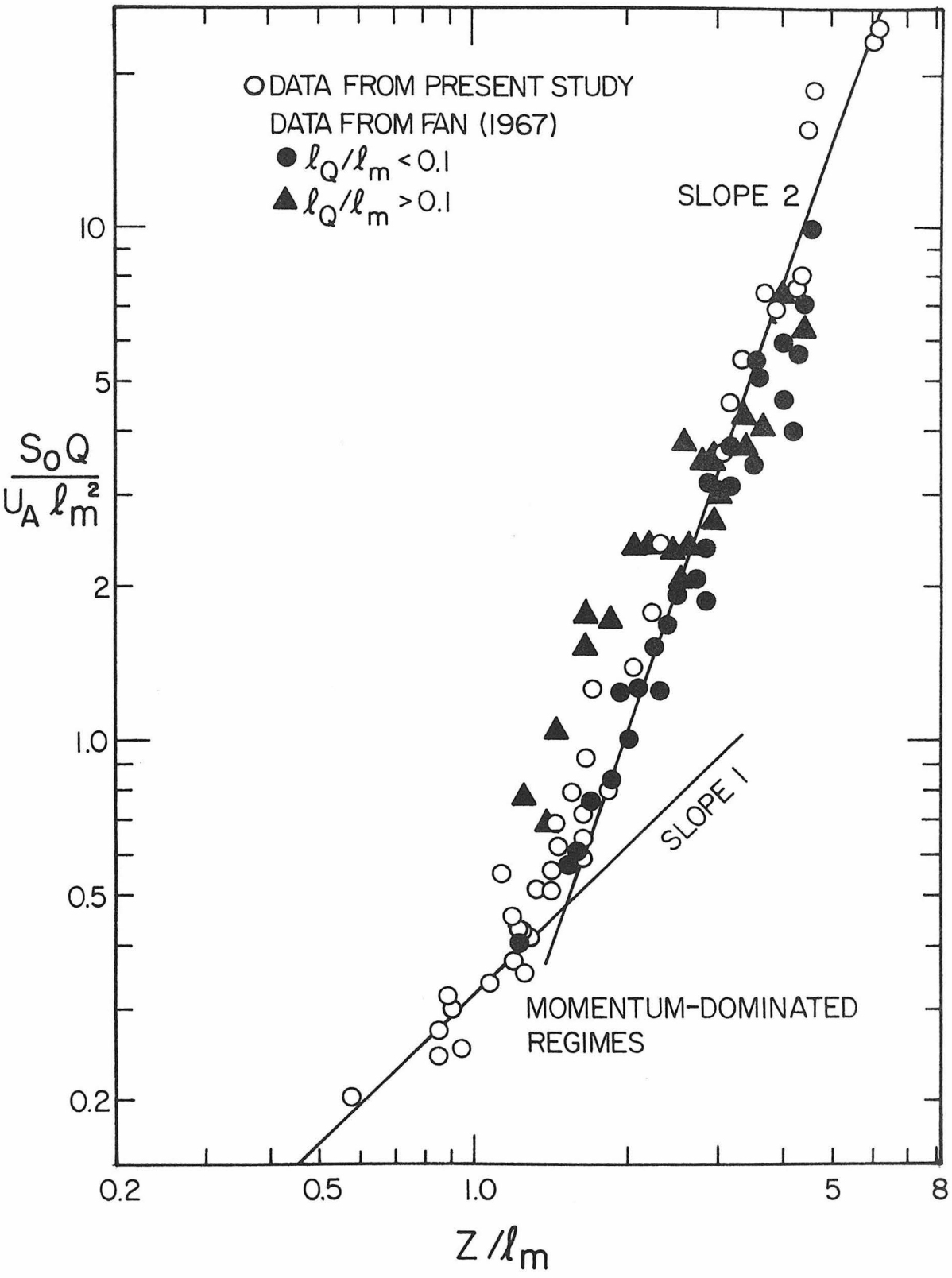

Fig. 5.20 Characteristic dilutions for momentum-dominated flow.

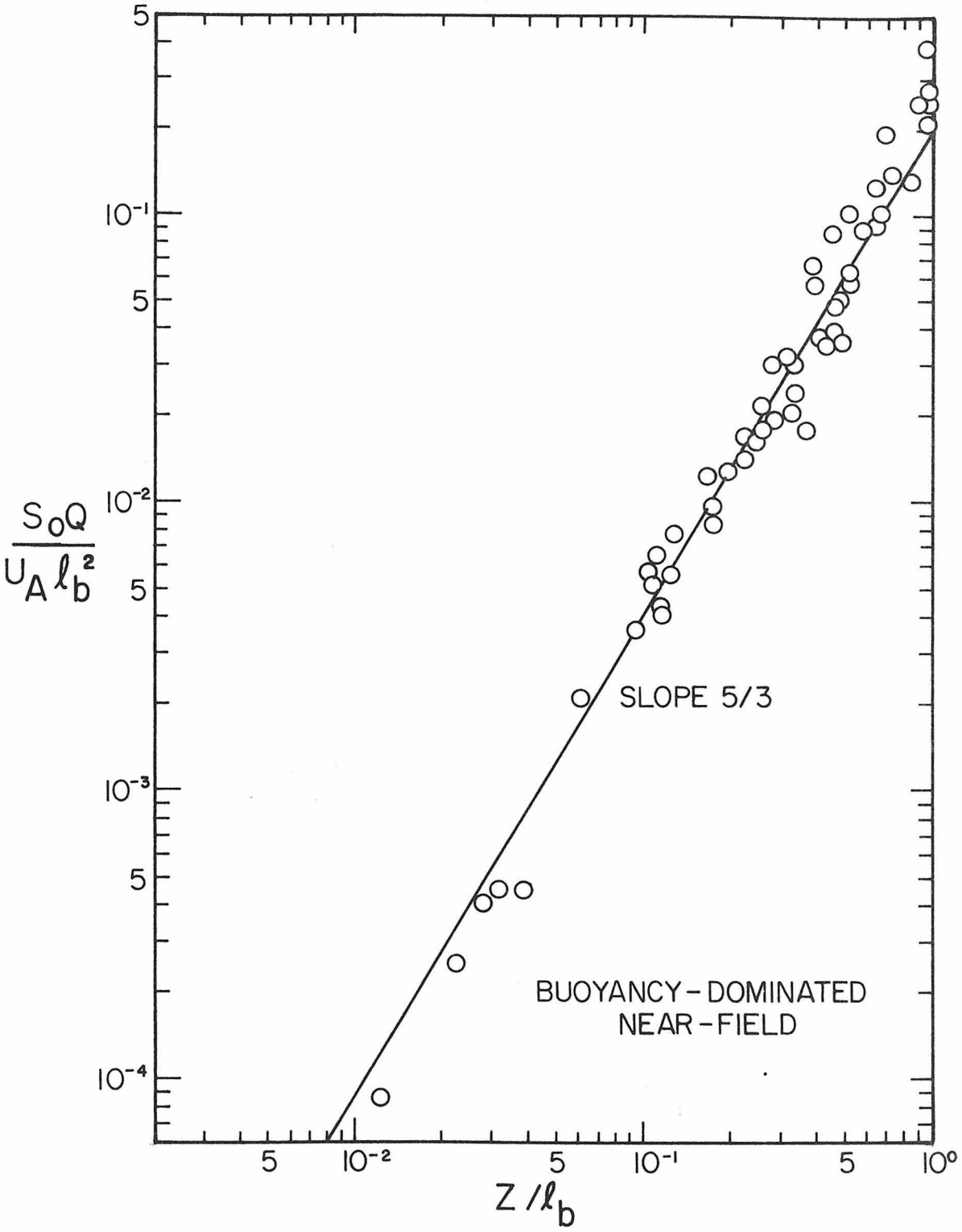

Fig. 5.21 Characteristic dilution for the buoyancy-dominated near-field.

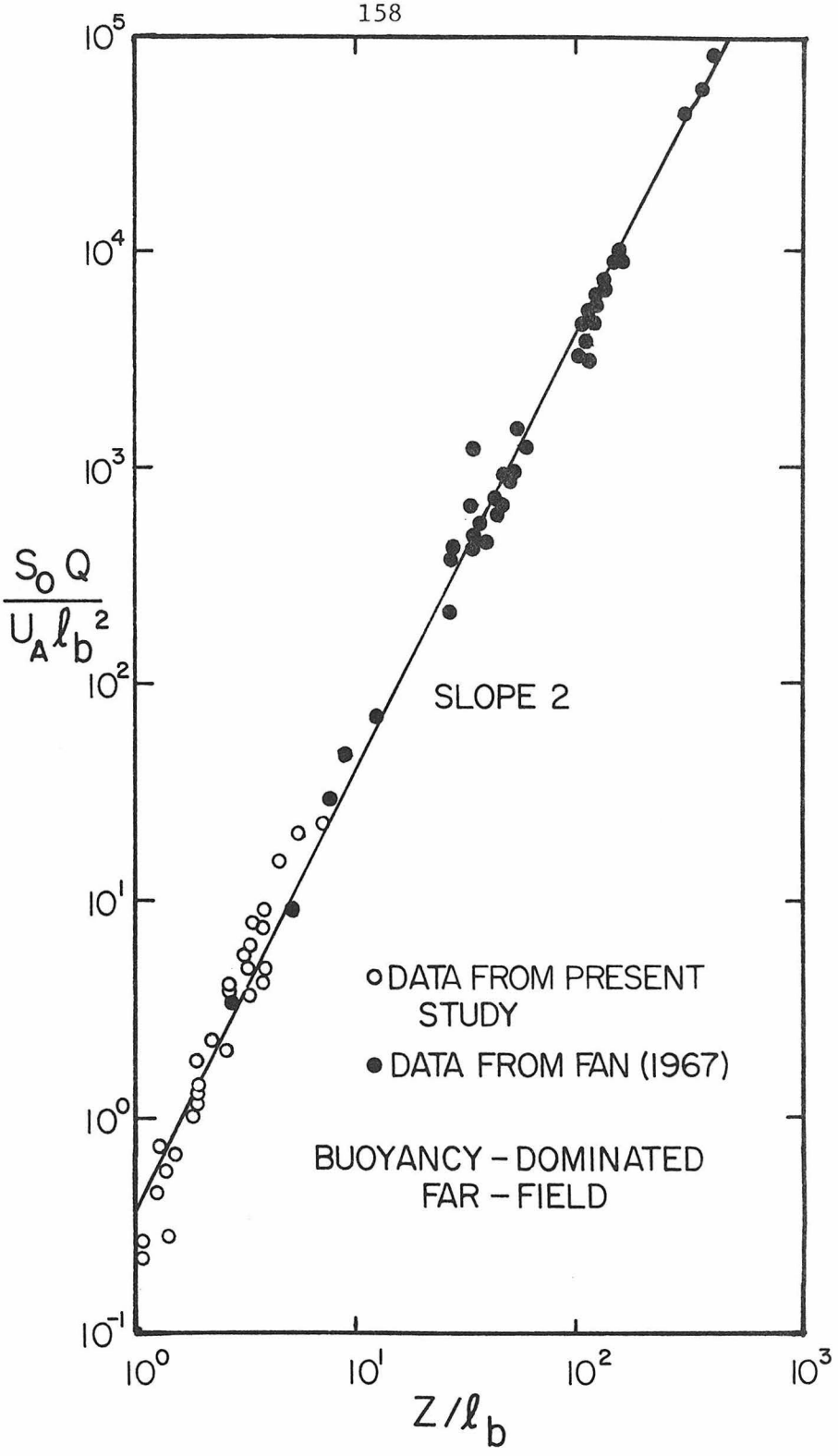

Fig. 5.22 Characteristic dilution for the buoyancy-dominated far-field.

There is little apparent indication that the values for the dilution constants depend upon the initial volume flux when the data are presented in this manner. The data seem to follow a single curve of the correct slope in all of these figures. However, since there is a fair amount of experimental scatter and a wide range of experimental variables was not covered, it is not possible to conclude definitely that the dilution relations are not affected by the initial volume flux. The average value of the dilution constant for each flow regime and the range of jet variables for which it was measured is presented in Table 5.2. Note that the values of the various constants are nearly equal for all flow regimes.

5.2 Experiments in a Stratified Crossflow

5.2.1 Trajectory Measurements

A detailed analysis of jet trajectories in a stratified crossflow was not undertaken because of the large amount of data that would be required to consider the many possible combinations of experimental variables. However, a preliminary investigation of the assumption that the jet trajectory would be relatively unchanged up to the maximum height of rise was undertaken. Photographs of several buoyant jets in a stratified crossflow were taken to observe the effect of the density stratification on the jet trajectories. These photographs were analyzed in a manner similar to that described previously for the unstratified experiments; tracings of the jet outline were obtained from the photographs and the fiduciary marks were used to scale the coordinates of the jet. Photographs and tracings of three of these

Table 5.2 Average values of the dilution constants for the range of experimental variables examined in this investigation.

Flow Regime	Dilution Relation	Average Value of Constant Dilution	Range of Jet Parameters	Refer to Figures
Momentum-dominated near-field	$\frac{S_o Q}{U_A \ell_m^2} = C_3 \frac{z}{\ell_m}$	0.42	$0.027 < \ell_Q/\ell_m < 0.051$	5.20
Momentum-dominated far-field	$\frac{S_o Q}{U_A \ell_m^2} = C_4 \left(\frac{z}{\ell_m}\right)^2$	0.38	$0.027 < \ell_Q/\ell_m < 0.25$	5.20
Buoyancy-dominated near-field	$\frac{S_o Q}{U_A \ell_b^2} = C_7 \left(\frac{z}{\ell_b}\right)^{5/3}$	0.42	$0.003 < \ell_Q/\ell_b < 0.014$	5.21
Buoyancy-dominated far-field	$\frac{S_o Q}{U_A \ell_b^2} = C_8 \left(\frac{z}{\ell_b}\right)^2$	0.41	$0.03 < \ell_Q/\ell_b < 28.0$ $0.5 < \ell_m/\ell_b < 112$	5.22

jets are presented in Figs. 5.23-5.25. The maximum height of rise was defined for this purpose as the deepest projection (greatest vertical rise z) of the dye boundary of the jet in the photograph. The trajectory of a jet in an unstratified crossflow with the same values of ℓ_Q, ℓ_m, and ℓ_b is indicated in each figure. The values of the trajectory coefficients used in developing these plots were obtained from Figs. 5.8-5.11.

Fig. 5.23 is a jet that is in the near-field when it reaches its maximum height of rise. In this particular case, the flow has become buoyancy-dominated before the point of maximum rise and this result would correspond to the analysis for the buoyancy-dominated near-field. Figs. 5.24 and 5.25 are cases where the jets are bent over and in the far-field before they reach their maximum heights of rise. Fig. 5.24 is a momentum-dominated jet while Fig. 5.25 corresponds to the buoyancy-dominated far-field.

Each of these figures clearly indicates that the trajectory of the jet is approximately given by the unstratified trajectory up to the maximum height of rise. The vertical rise predicted by the unstratified trajectory model deviates from the actual trajectory by less than 10% at that point. Thus, the use of the model developed for unstratified flow can be used with reasonable accuracy to predict jet trajectories in a stratified fluid up to the maximum height of rise.

5.2.2 Measurements of Equilibrium Heights of Rise

The equilibrium height of rise Z_e was defined in this investigation as the position of a buoyant jet in the stratified towing tank when all motion had ceased after an experiment was

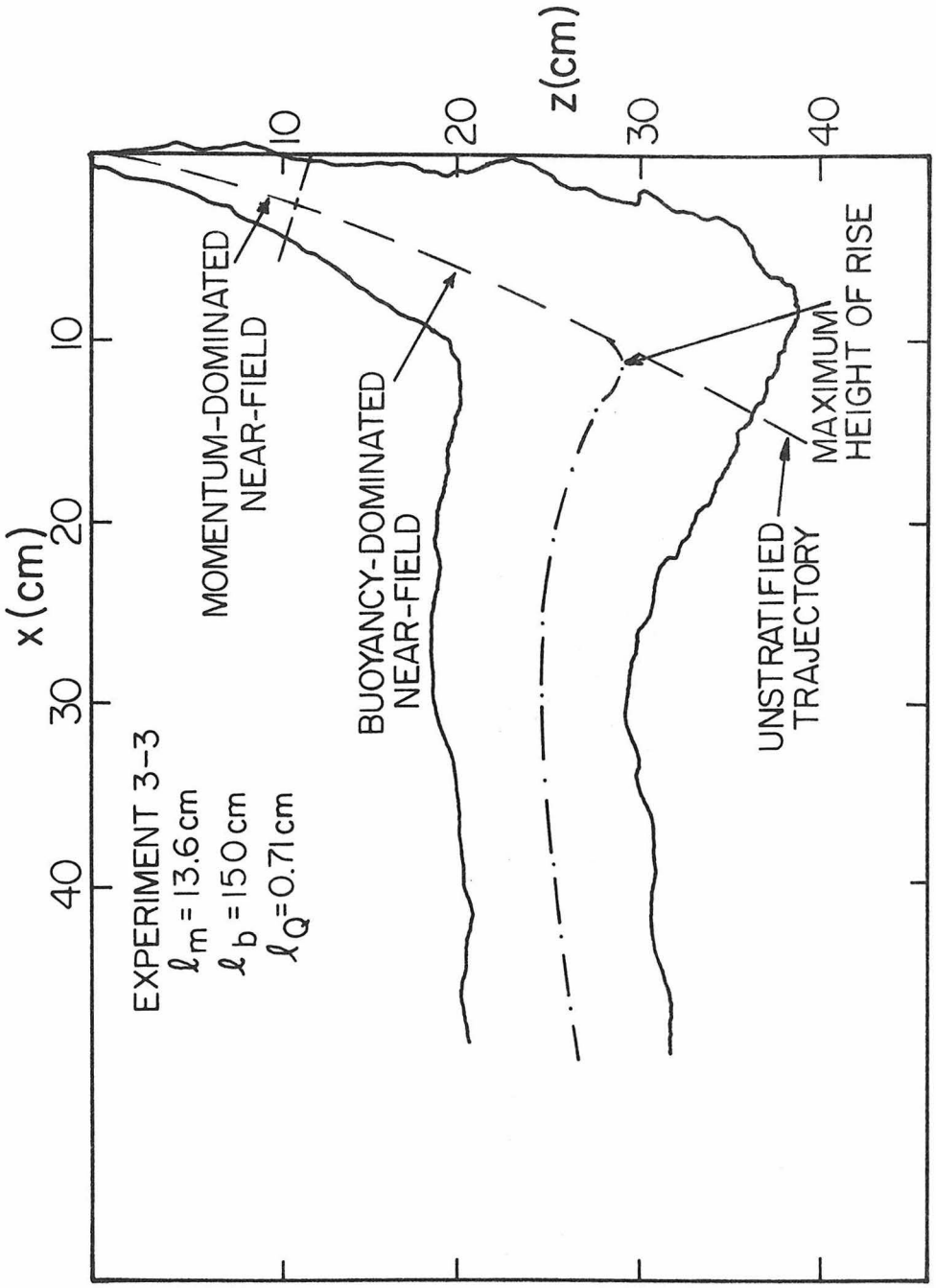

Fig. 5.23a Jet trajectory in a stratified crossflow corresponding to the buoyancy-dominated near-field.

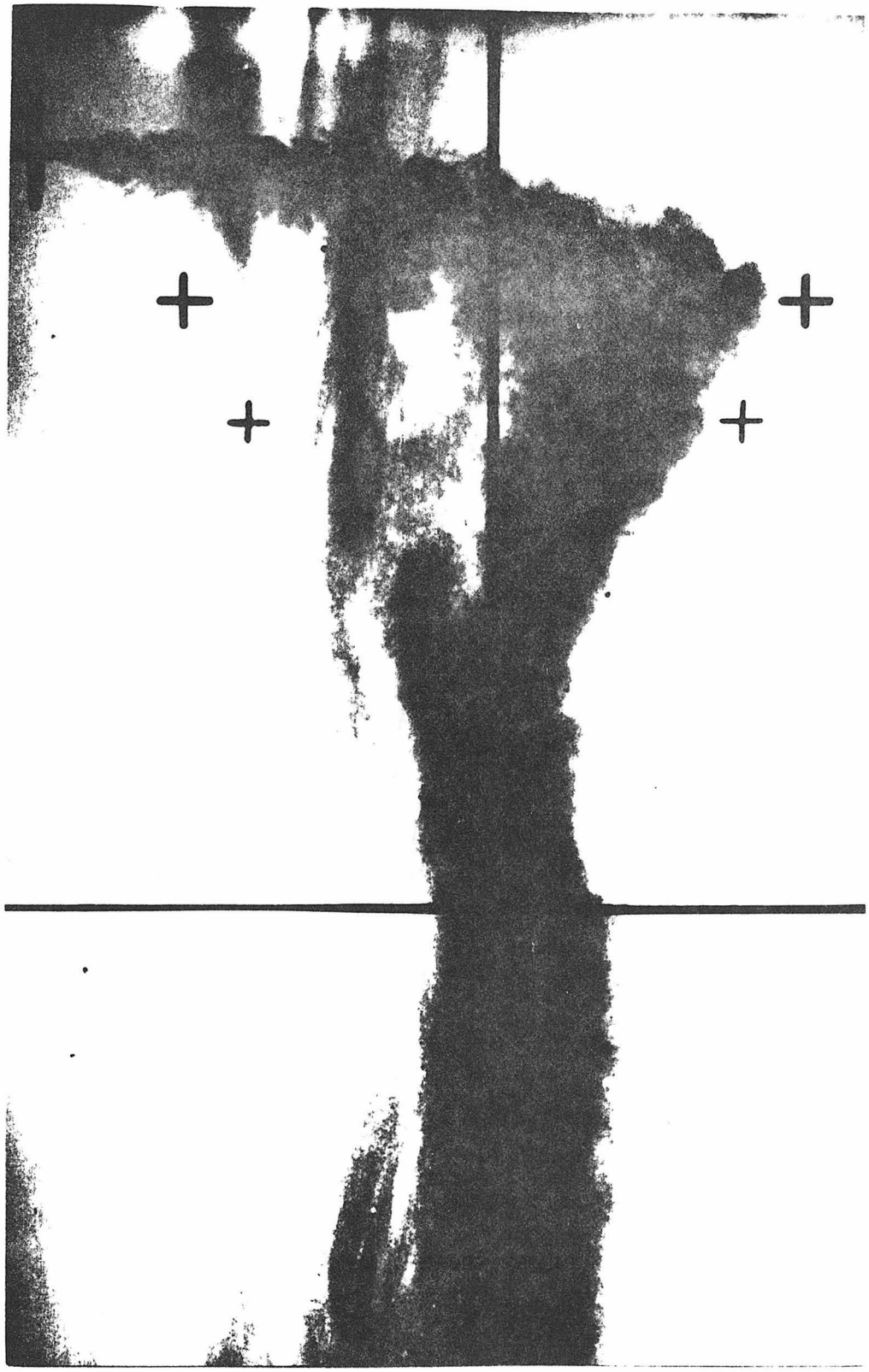

Fig. 5.23b Photograph of buoyant jet (run 3-3)(dye streaks from previous experiments).

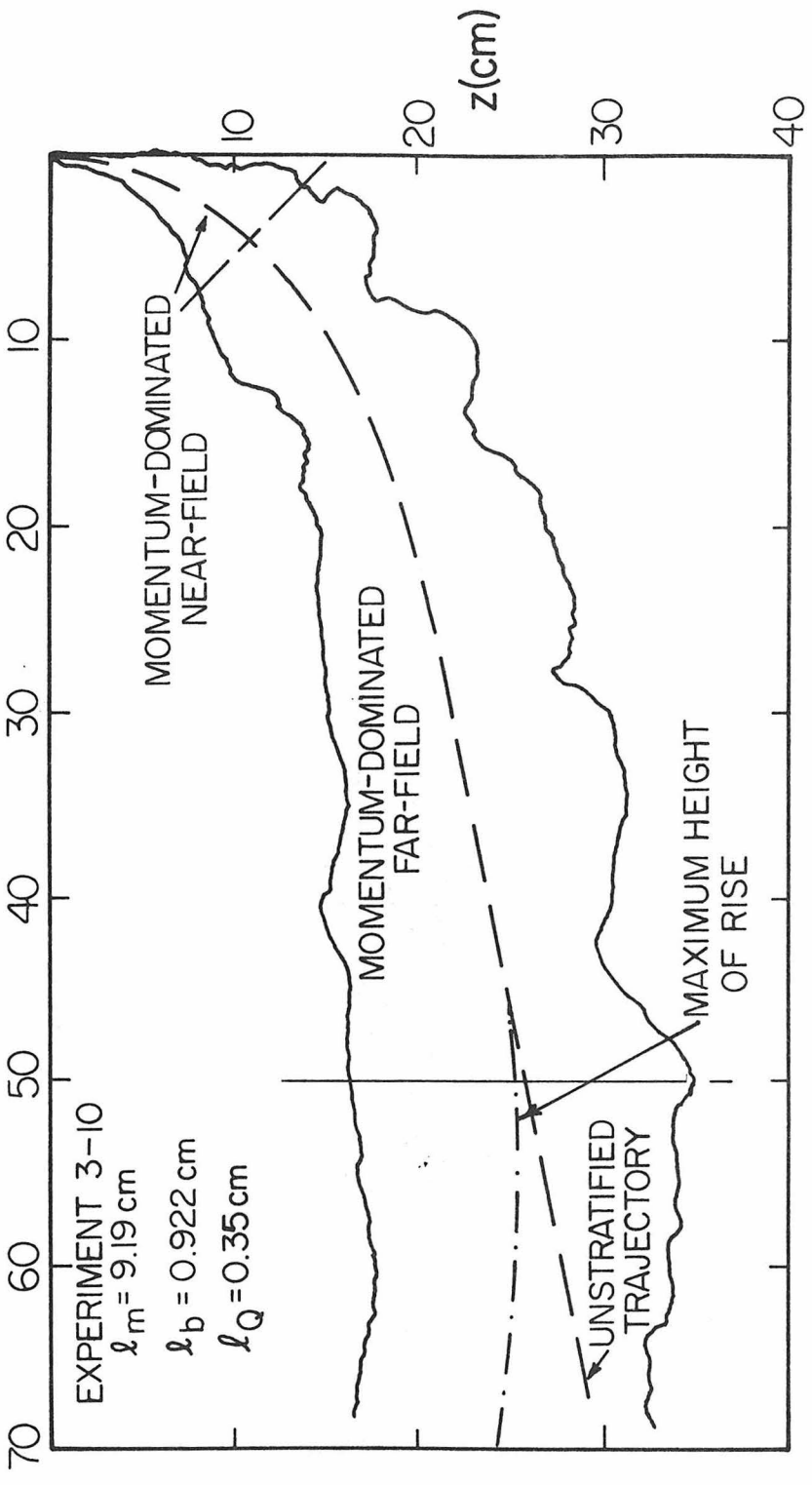

Fig. 5.24a Jet trajectory in a stratified crossflow corresponding to the momentum-dominated far-field.

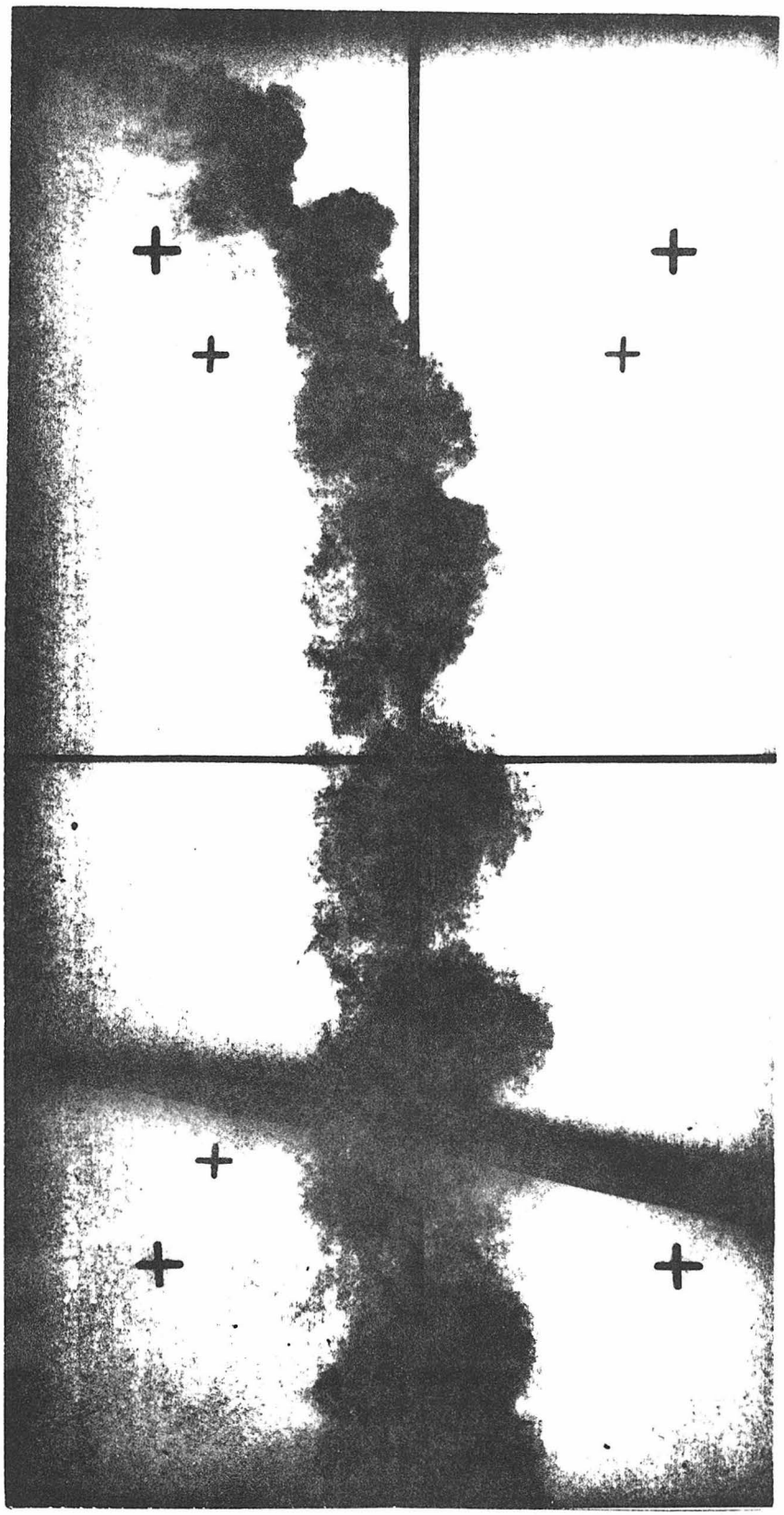

Fig. 5.24b Photograph of buoyant jet (run 3-10).

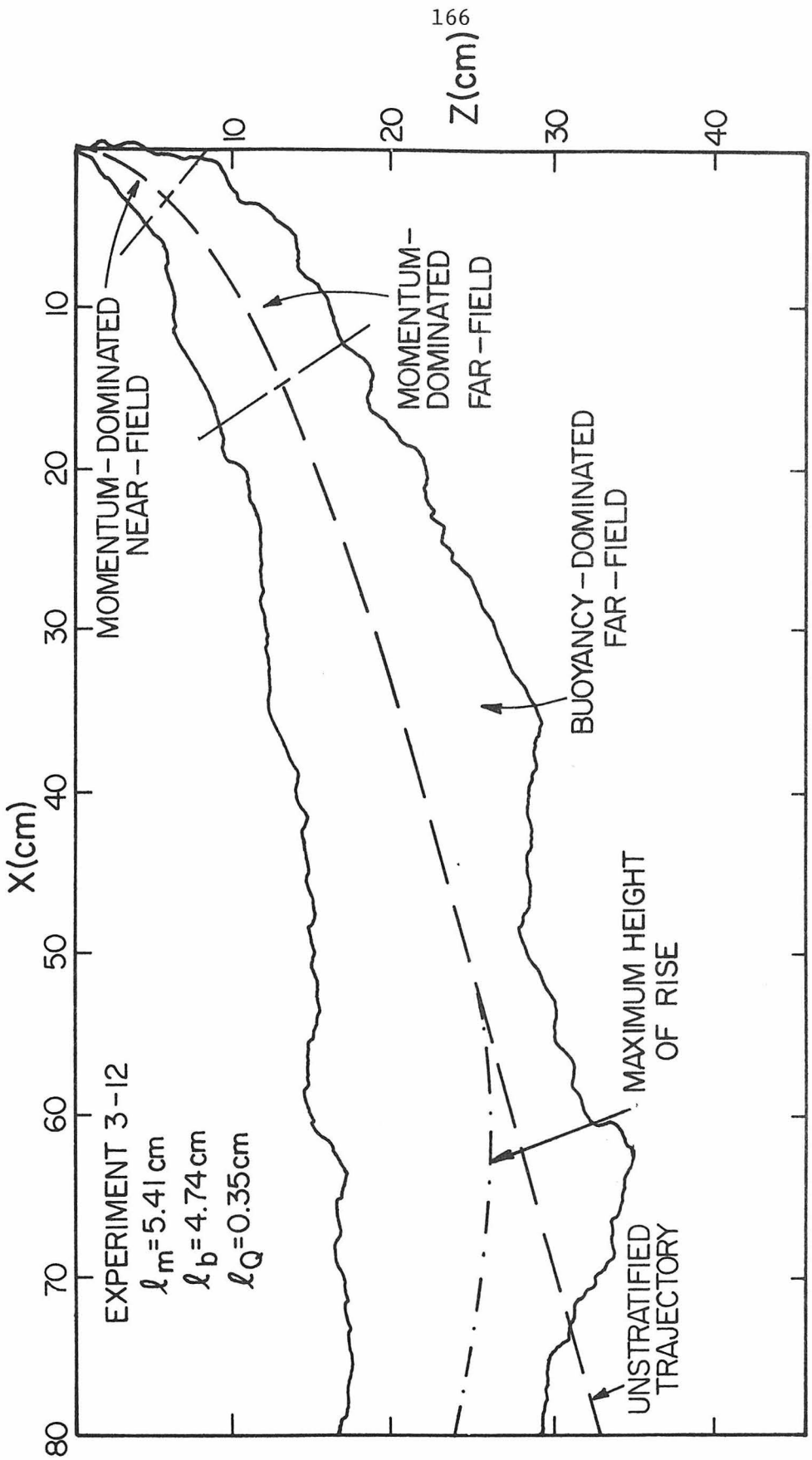

Fig. 5.25a Jet trajectory in a stratified crossflow corresponding to the buoyancy-dominated far field.

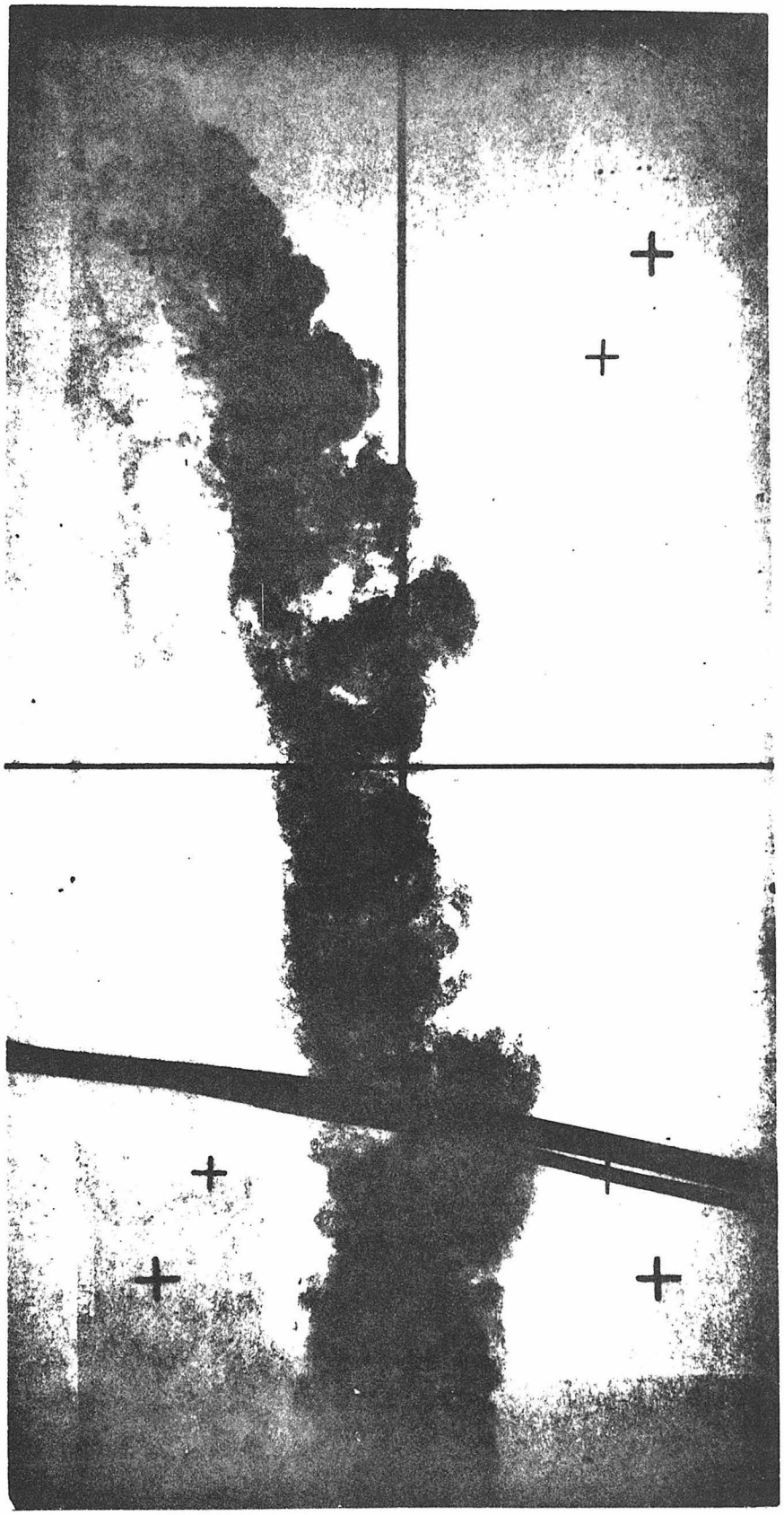

Fig. 5.25b Photograph of buoyant jet (run 3-12).

completed. The equilibrium height of rise is the neutrally buoyant position of the jet after it mixes with the ambient fluid. Measurements of equilibrium heights of rise were obtained from photographs taken of the dyed jet discharge after all motion in the towing tank appeared to have ceased. The equilibrium height of rise was taken as the center of the horizontal dye patch in the tank as indicated in the photograph and schematic in Fig. 5.26.

Several experiments were performed for each stratification. Liquid swimming pool chlorine was mixed with the fluid in the mixing tank before the beginning of each stratification. The chlorine oxidized the organic dye present in the jet discharge so that additional experiments could be performed without the presence of residual dye from previous experiments affecting the measurements.

Dilutions were not measured during this phase of the experimental investigation. After a jet reached its maximum height of rise and began to approach its equilibrium position, it began to spread rapidly in the horizontal direction. The presence of the flume walls generally restricted the horizontal spread and it was assumed that this would have a significant effect on the jet concentration profile at the equilibrium height of rise. It is believed that the location of the equilibrium height of rise was not significantly affected by the wall effects since this would only prevent further horizontal spread and would not significantly influence the mean position of the jet. Thus, the only measurements made at the equilibrium height of rise were the position measurements from the photographs.

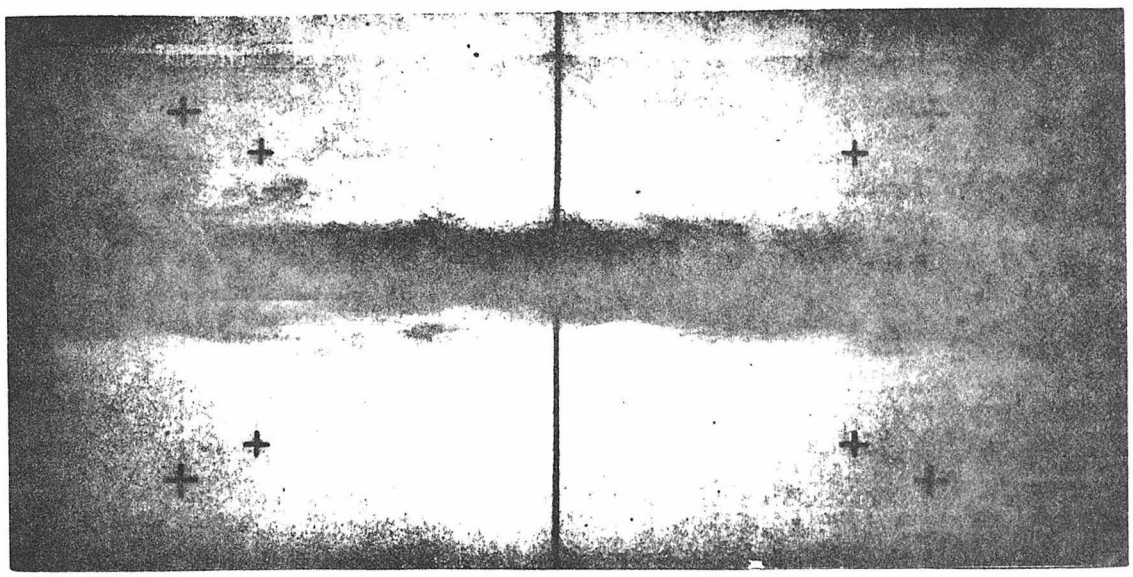

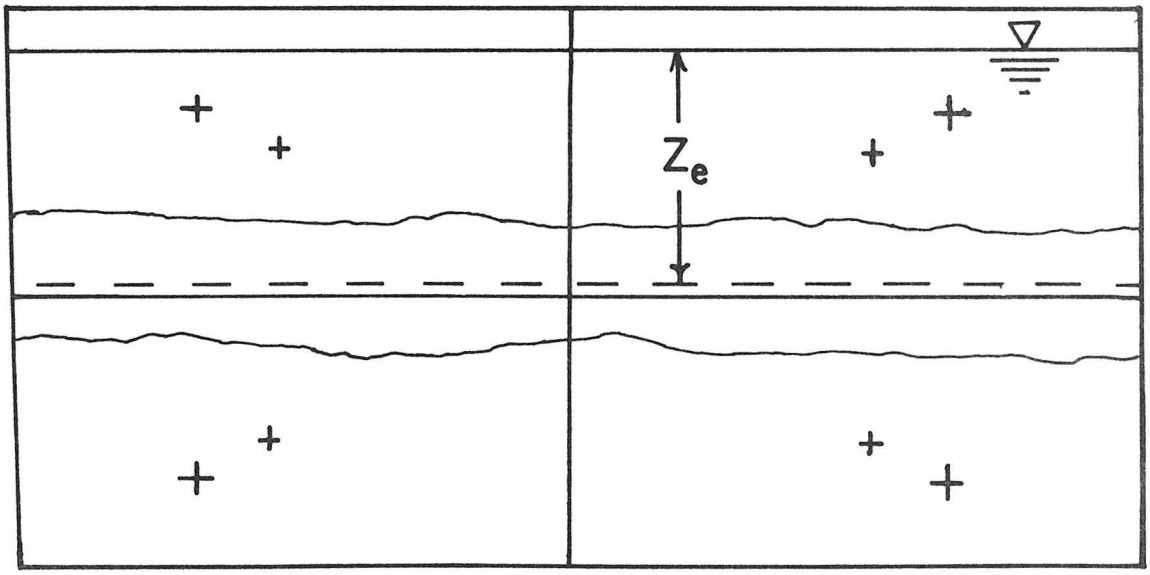

Fig. 5.26 Photograph and definition sketch of equilibrium height of rise.

The results from the measurements of the equilibrium heights of rise are presented in Fig. 5.27 for momentum-dominated flow and in Fig. 5.28 for buoyancy-dominated flow in terms of the relations developed in the analysis. The experimental conditions for each measurement are given in Appendix A. The experimental results were assigned to these two figures on the basis of the unstratified trajectory data in Figs. 5.8-5.11. That is, if the values of the length scales ℓ_Q, ℓ_m, and ℓ_b indicated that a jet in an unstratified flow at the same vertical rise as the equilibrium height of rise would be in a momentum-dominated regime, then that experiment was assigned to the momentum-dominated data in Fig. 5.27. This approach may result in an error in assigning the results from a few experiments where the transition between momentum- and buoyancy-dominated flow occurs at $z \approx Z_e$, but it is not likely to significantly affect the overall results as most experiments clearly corresponded to one flow regime or the other.

A fair amount of scatter is indicated in these figures. If the initial jet volume flux is considered as an additional variable as discussed in Section 5.1.1, it is apparent that much of the scatter can be attributed to this effect. Figs. 5.29-5.32 present the values of the coefficients in the equilibrium height of rise relations as a function of the initial volume flux. The experiments corresponding to the bdff were for a fairly limited range of the ratio ℓ_m/ℓ_b (0.13-2.5), so it is not possible to conclude that this ratio affects the value of the height of rise coefficient. This would be expected on the basis of the experimental results from the jet trajectories in

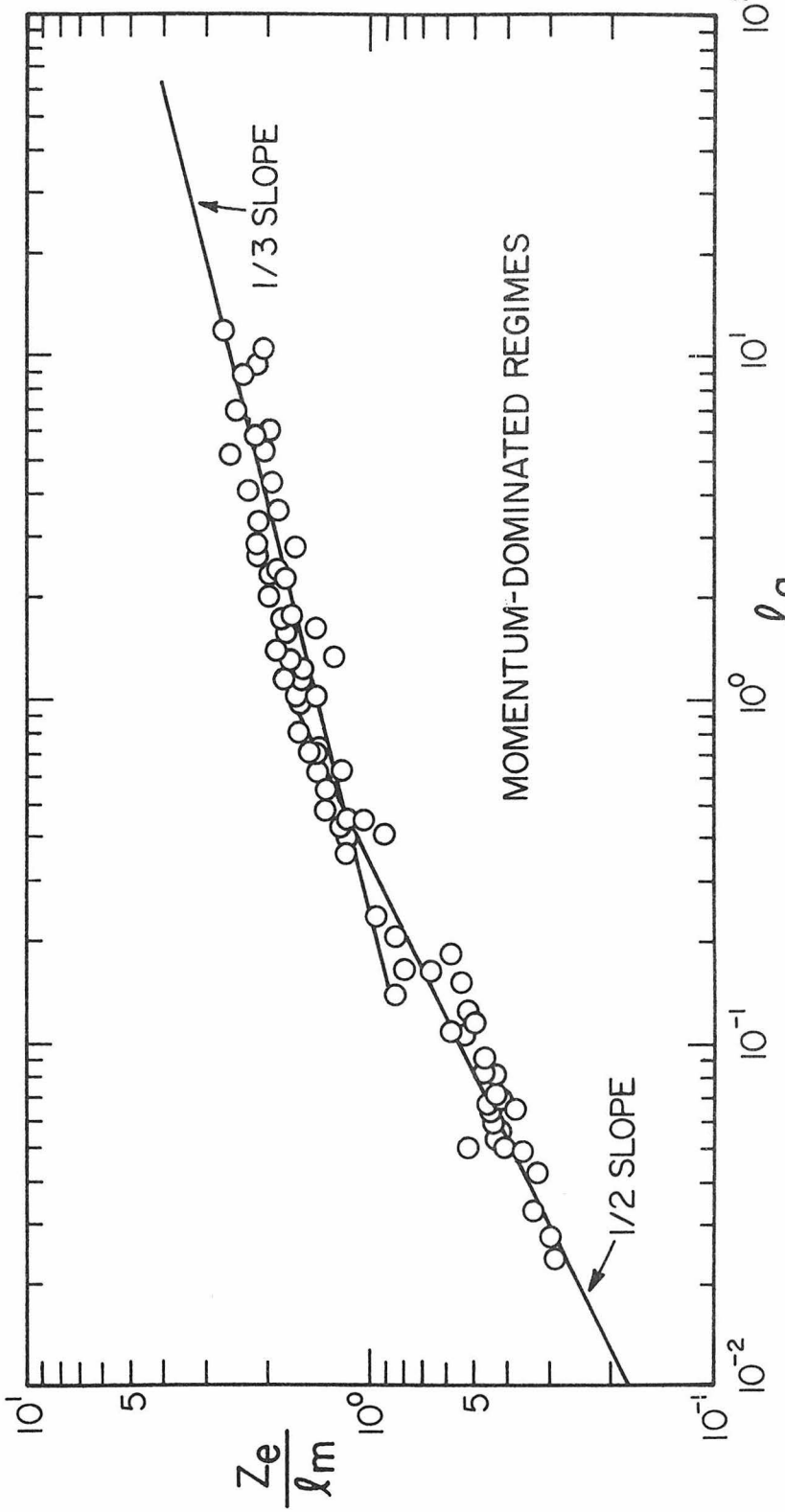

Fig. 5.27 Equilibrium heights of rise for momentum-dominated flow.

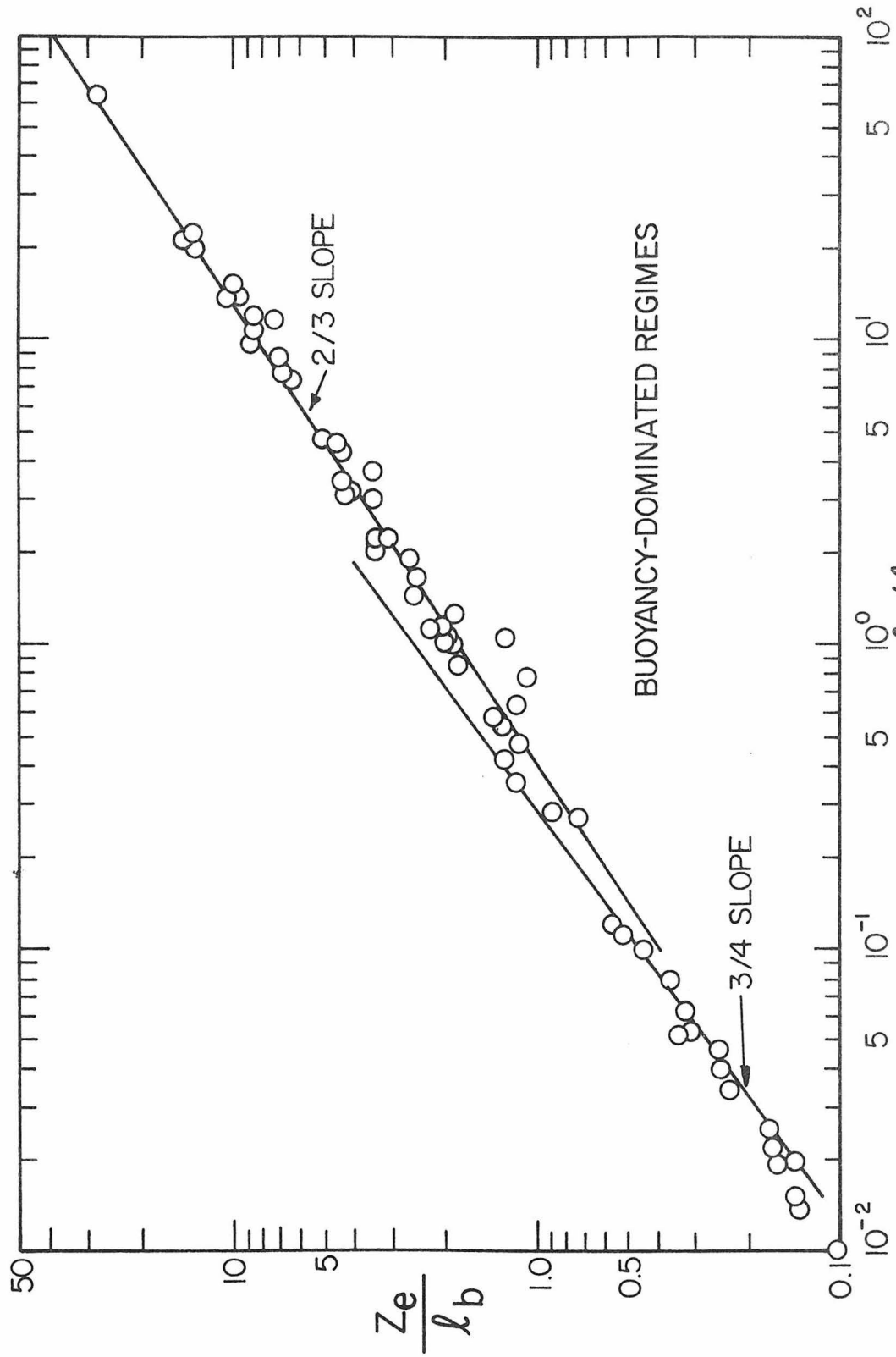

Fig. 5.28 Equilibrium heights of rise for buoyancy-dominated flow.

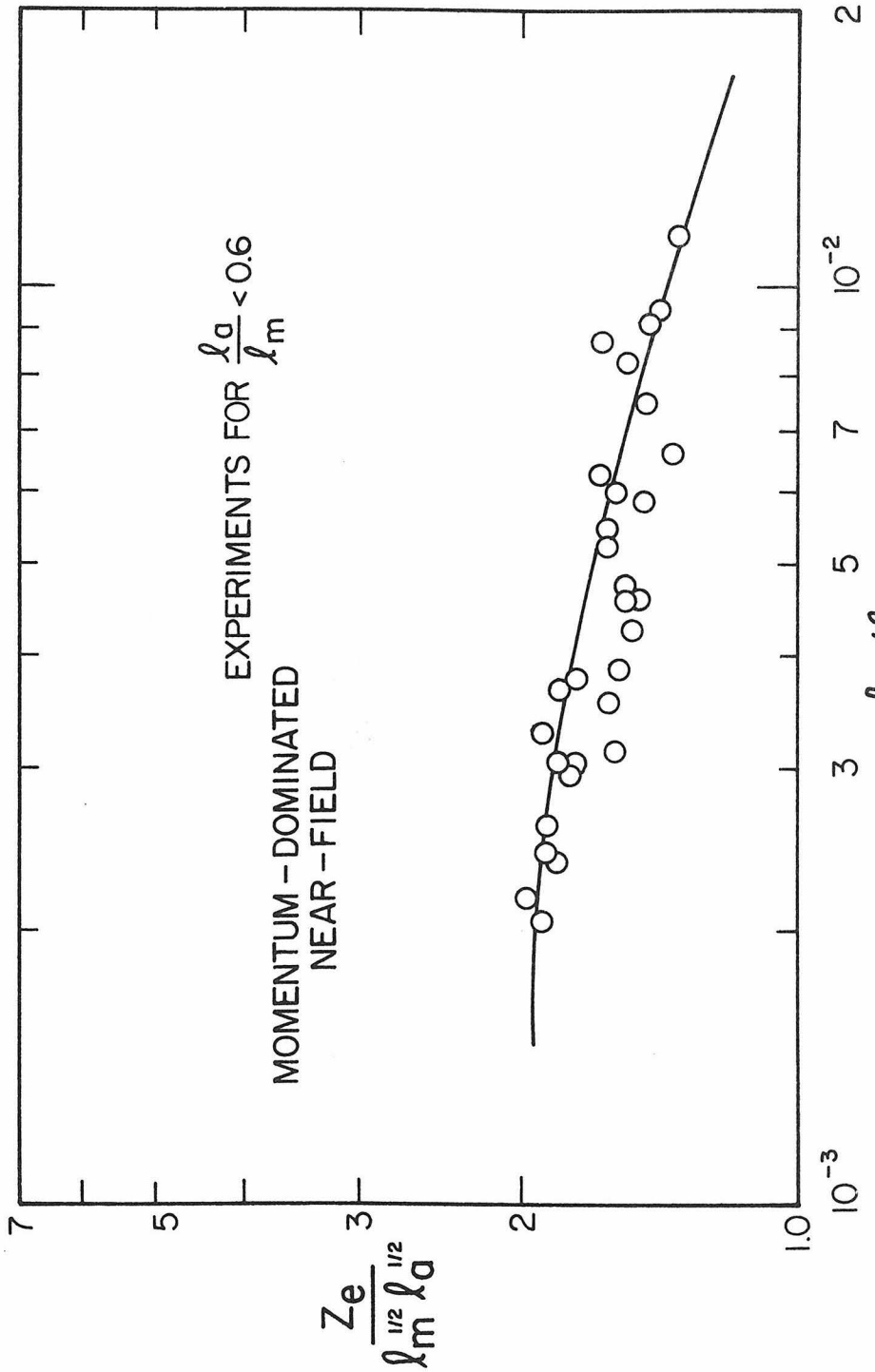

Fig. 5.29 Equilibrium height of rise coefficient C_9 as a function of ℓ_Q/ℓ_m.

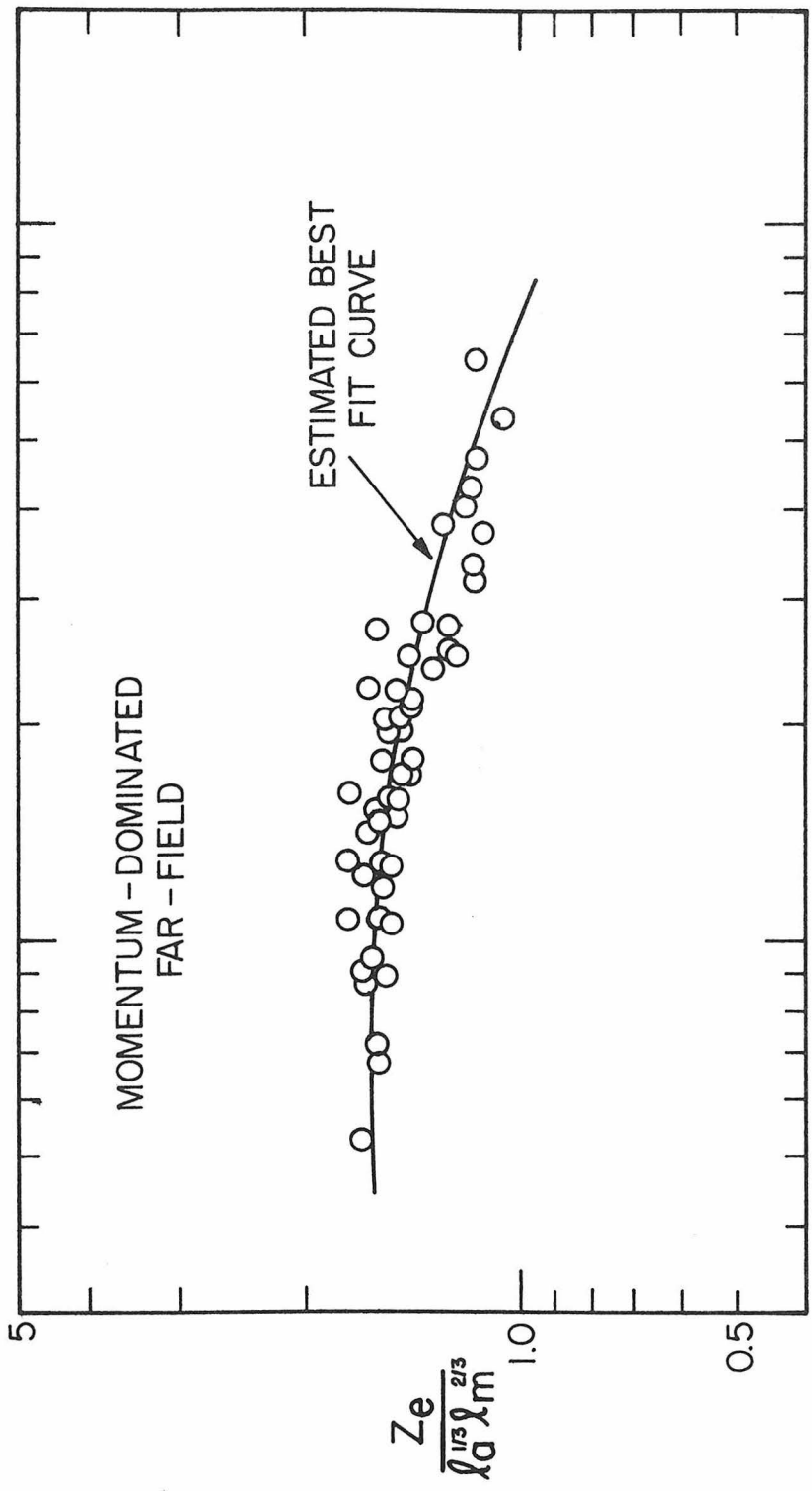

Fig. 5.30 Equilibrium height of rise coefficient C_{10} as a function of ℓ_Q/ℓ_m.

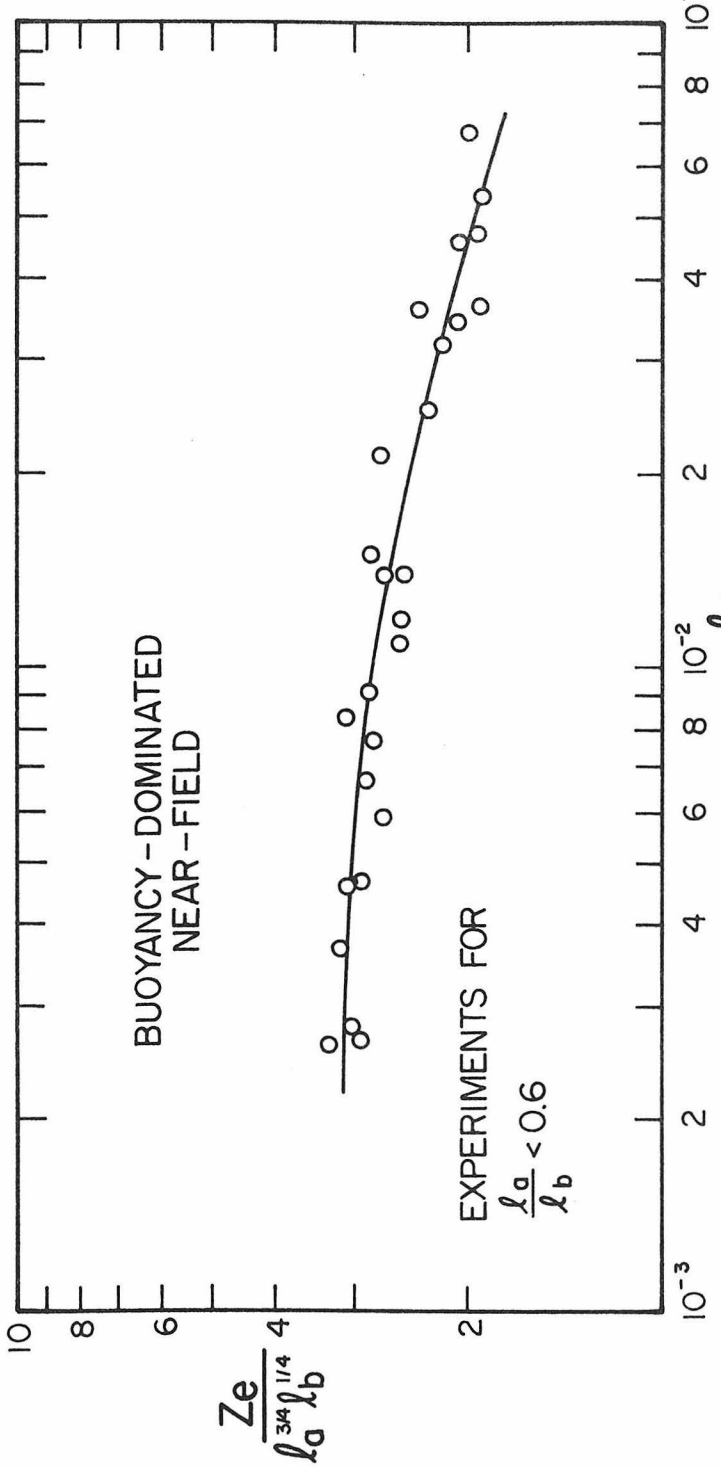

Fig. 5.31 Equilibrium height of rise coefficient C_{11} as a function of ℓ_Q/ℓ_b.

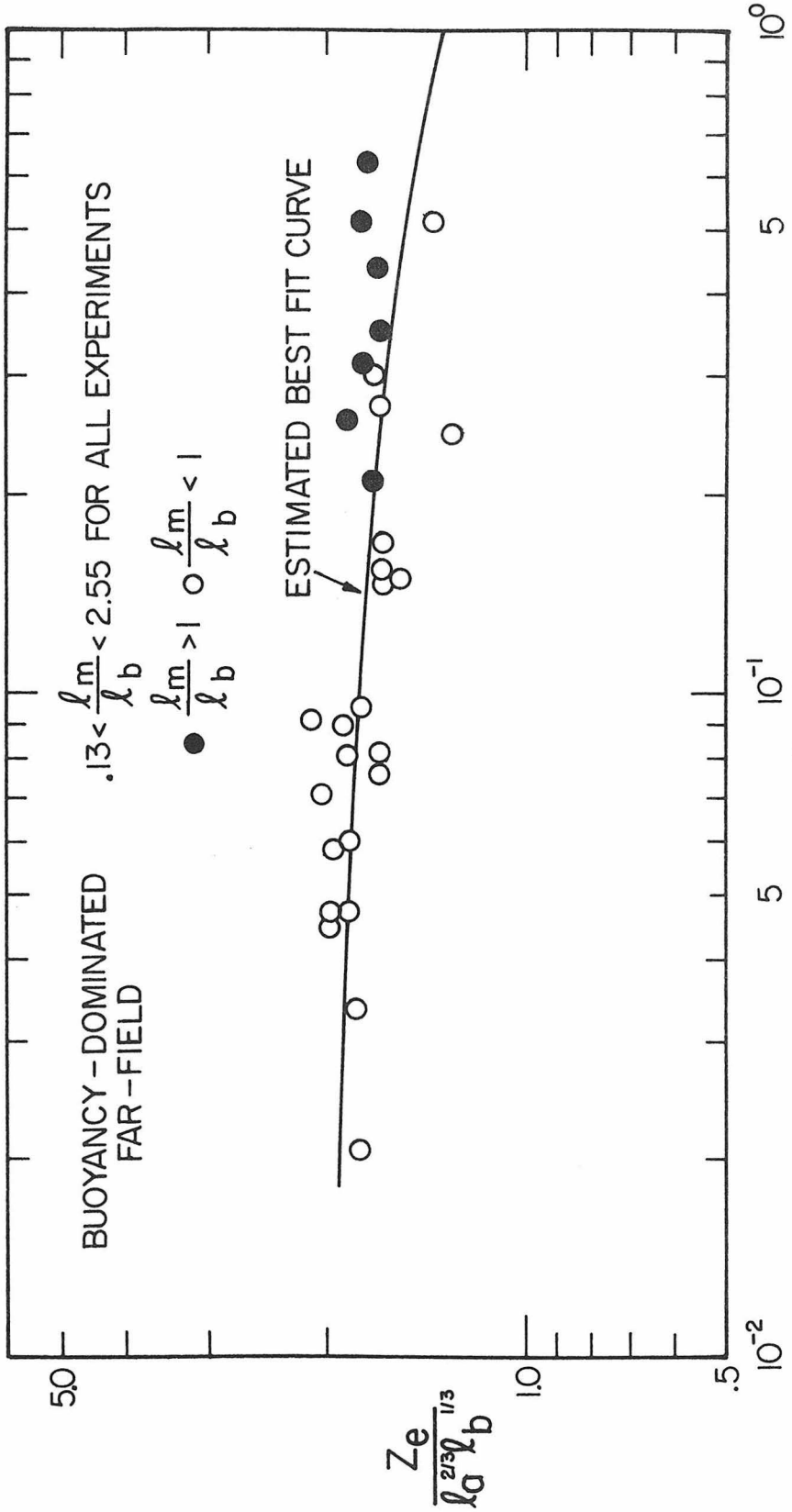

Fig. 5.32 Equilibrium height of rise coefficient C_{12} as a function of ℓ_Q/ℓ_b.

unstratified flow and it does appear that the values of the coefficient in Fig. 5.32 for the experiments where $\ell_m/\ell_b > 1$ are slightly higher than the experiments with $\ell_m/\ell_b < 1$.

The experimental data in Figs. 5.29 and 5.31 indicate that the height of rise Z_e for a jet in the near-field will decrease with increasing crossflow velocity for the same jet and stratification conditions. The theoretical considerations imply that the height of rise of a jet in the near-field will not be affected by the crossflow velocity U_A. However, the results in Figs. 5.29 and 5.31 indicate that the height of rise coefficient is affected such that the equilibrium height of rise does decrease with increasing U_A. If all other parameters are fixed, increasing the value of U_A increases the value of $\frac{\ell_Q}{\ell_m} = \frac{U_A}{V_j}$ or $\frac{\ell_Q}{\ell_b} = \frac{U_A^3}{g_o' \frac{\pi}{4} D V_j}$. Thus, the trend of decreasing height of rise coefficient implies that Z_e decreases with increasing U_A. This also can be seen from a set of experiments in which all conditions were held constant except the towing velocity. The results are summarized below:

$Q = 11.8$ mℓ/sec $\quad \frac{\Delta\rho}{\rho_o} = .108 \quad D = 1.0$ cm $\quad \varepsilon = .209$ sec^{-2}

Run no.	32	31	33	34
U_A (cm/sec)	1.19	1.66	1.82	2.72
Z_e (cm)	37.8	36.3	36.0	31.5

All of these experiments were determined to correspond to the buoyancy-dominated near-field, and the above observation of decreasing Z_e with increasing U_A is clearly indicated.

The effect of the crossflow velocity for the far-field flows is even more pronounced since the height of rise relations depend directly

on U_A ($Z_e \sim U_A^{-1/3}$ for both the mdff and the bdff). The additional dependence on the ℓ_Q/ℓ_m or ℓ_Q/ℓ_b ratios increases this effect, since the general trend of decreasing height of rise constant with increasing ℓ_Q/ℓ_m or ℓ_Q/ℓ_b is also observed for the far-field flows.

5.2.3 Measurements of Maximum Height of Rise

Estimates of the maximum heights of rise for buoyant jets in a stratified crossflow were obtained from concentration profiles measured with the light probe described in Chapter 4. The measurements made with the light probe consisted of vertical concentration profiles obtained at the horizontal location of the maximum penetration of the dyed jet discharge as indicated in Fig. 5.33.

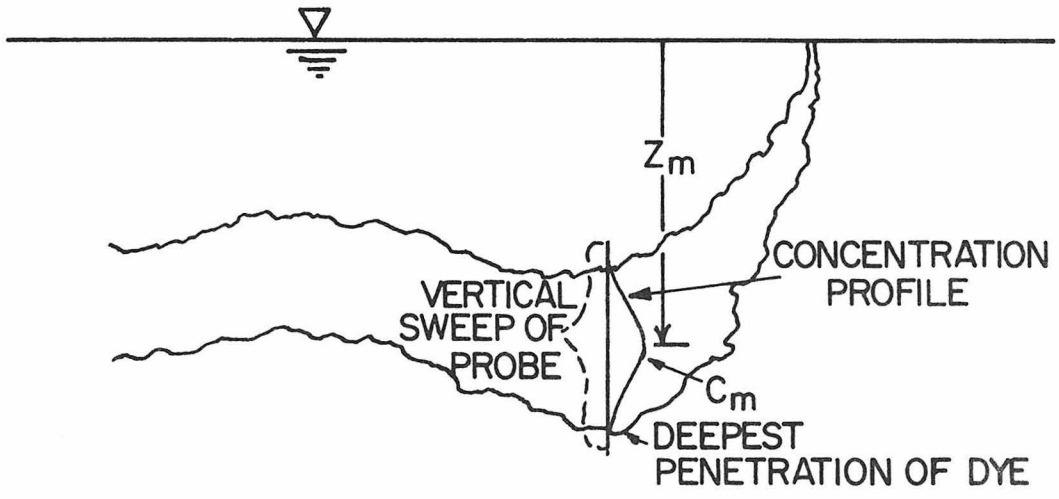

Fig. 5.33 Definition sketch of measurements of maximum height of rise.

The exact horizontal location of this point is somewhat imprecise due to the fluctuating nature of the turbulent flow. Another difficulty was that the experimental setup required that the horizontal probe position

be preset before the beginning of any experiment. The positioning of the probe was accomplished by performing a test run with the experimental conditions to be modeled, visually determining the proper horizontal alignment, and then performing the actual experiment.

The position of the maximum height of rise was defined as the elevation of the maximum time-average concentration in the vertical profile measured with the light probe. The concentration profile was determined as discussed in Chapter 4. The vertical sweep of the light probe was divided into 25 equally spaced cells and all instantaneous measurements with vertical positions corresponding to a cell were combined to form a time-average concentration for the average vertical position of that cell. The cell with the maximum time-average concentration was defined as the location of the maximum height of rise. This procedure was repeated for various jet and ambient conditions which are summarized in Appendix A.

The results of these measurements are presented in Fig. 5.34 for the jets that reached their maximum rise while in a momentum-dominated regime, while Fig. 5.35 presents the data for buoyancy-driven jets. The data were assigned to these figures on the same basis as the measurements for equilibrium height of rise which were discussed in the preceding section. Since the jet trajectories in a stratified fluid are nearly the same as in an unstratified fluid up to the maximum height of rise, the use of the unstratified experimental results to assign a given jet to a particular flow regime is a fairly accurate approach.

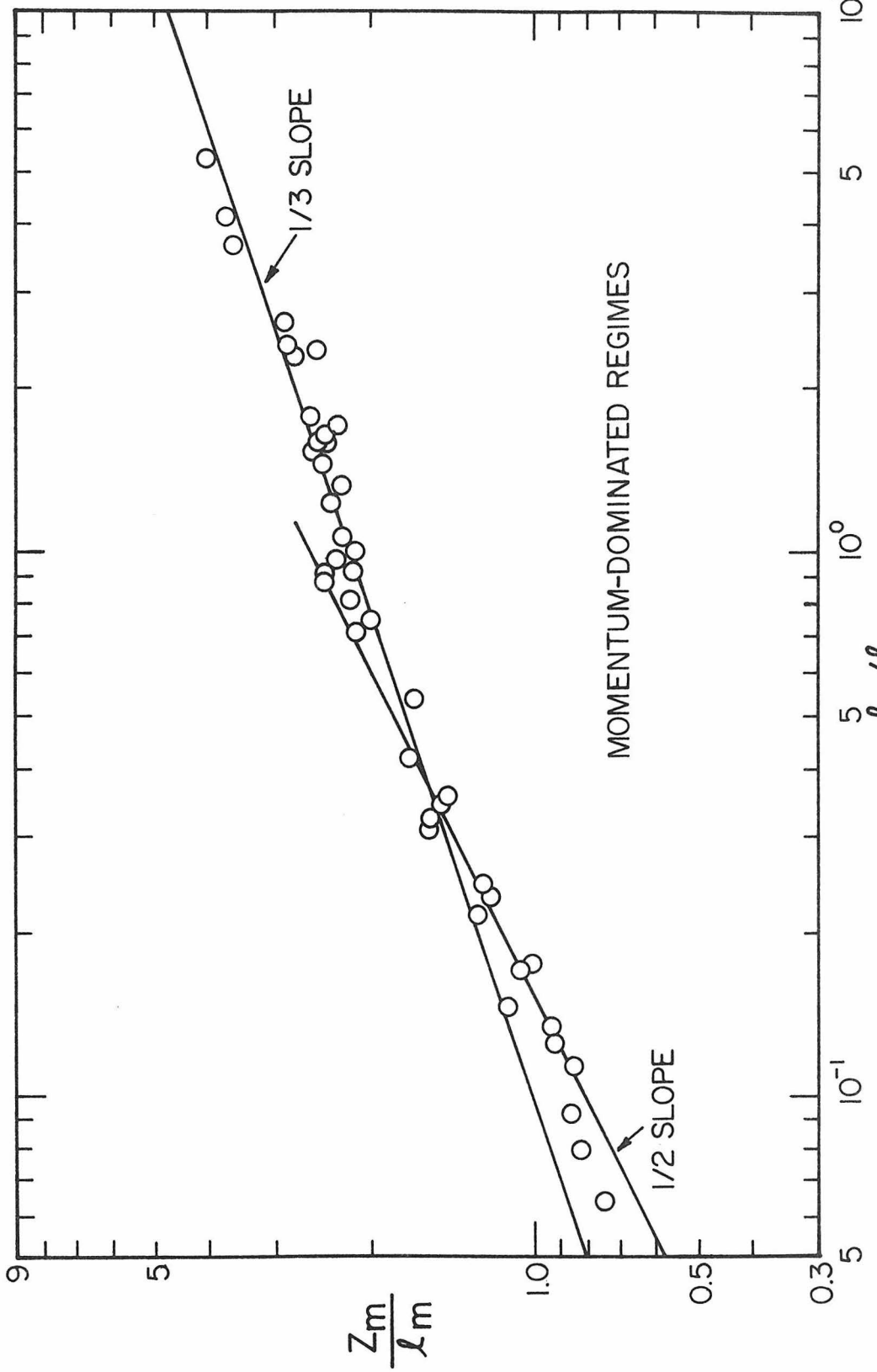

Fig. 5.34 Maximum heights of rise for momentum-dominated flow.

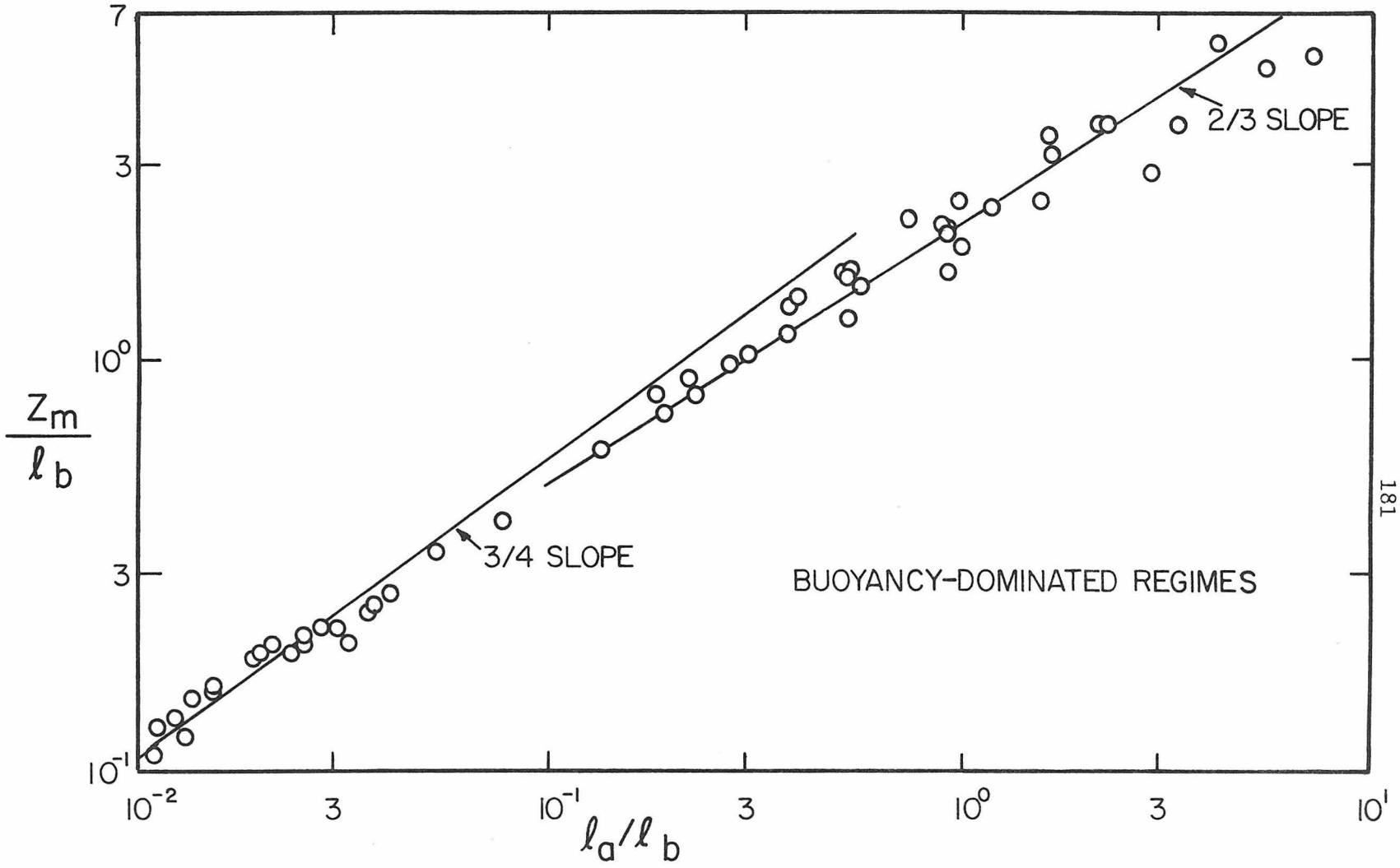

Fig. 5.35 Maximum heights of rise for buoyancy-dominated flow.

Scatter in the data similar to that observed in previous experimental results is evident in these figures. Much of this scatter can be related to the effect of the initial volume flux as discussed previously. Figs. 5.36-5.39 indicate the variation of the height of rise coefficients defined by Table 5.3 as a function of the initial volume flux. The previously observed trend of decreasing values for the various coefficients with increasing relative values of ℓ_Q is also observed in all of these figures. The bdff data were performed for a limited range of ℓ_m/ℓ_b and no effect of this ratio on the values for the corresponding coefficient is apparent.

The presentation of the experimental measurements of maximum and equilibrium heights of rise is summarized in Table 5.3.

Table 5.3 Summary of experimental results presented for the measurement of maximum and equilibrium heights of rise.

Flow Regime	Relation	Data Presented in Figure		Values for Coefficient Presented in Figure	
		Z_e	Z_m	Z_e	Z_m
Momentum-dominated near-field	$\frac{Z_m}{\ell_m}, \frac{Z_e}{\ell_m} \propto \left(\frac{\ell_a}{\ell_m}\right)^{1/2}$	5.27	5.34	5.29	5.36
Momentum-dominated far-field	$\frac{Z_m}{\ell_m}, \frac{Z_e}{\ell_m} \propto \left(\frac{\ell_a}{\ell_m}\right)^{1/3}$	5.27	5.34	5.30	5.37
Buoyancy-dominated near-field	$\frac{Z_m}{\ell_b}, \frac{Z_e}{\ell_b} \propto \left(\frac{\ell_a}{\ell_b}\right)^{3/4}$	5.28	5.35	5.31	5.38
Buoyancy-dominated far-field	$\frac{Z_m}{\ell_b}, \frac{Z_e}{\ell_b} \propto \left(\frac{\ell_a}{\ell_b}\right)^{2/3}$	5.28	5.35	5.32	5.39

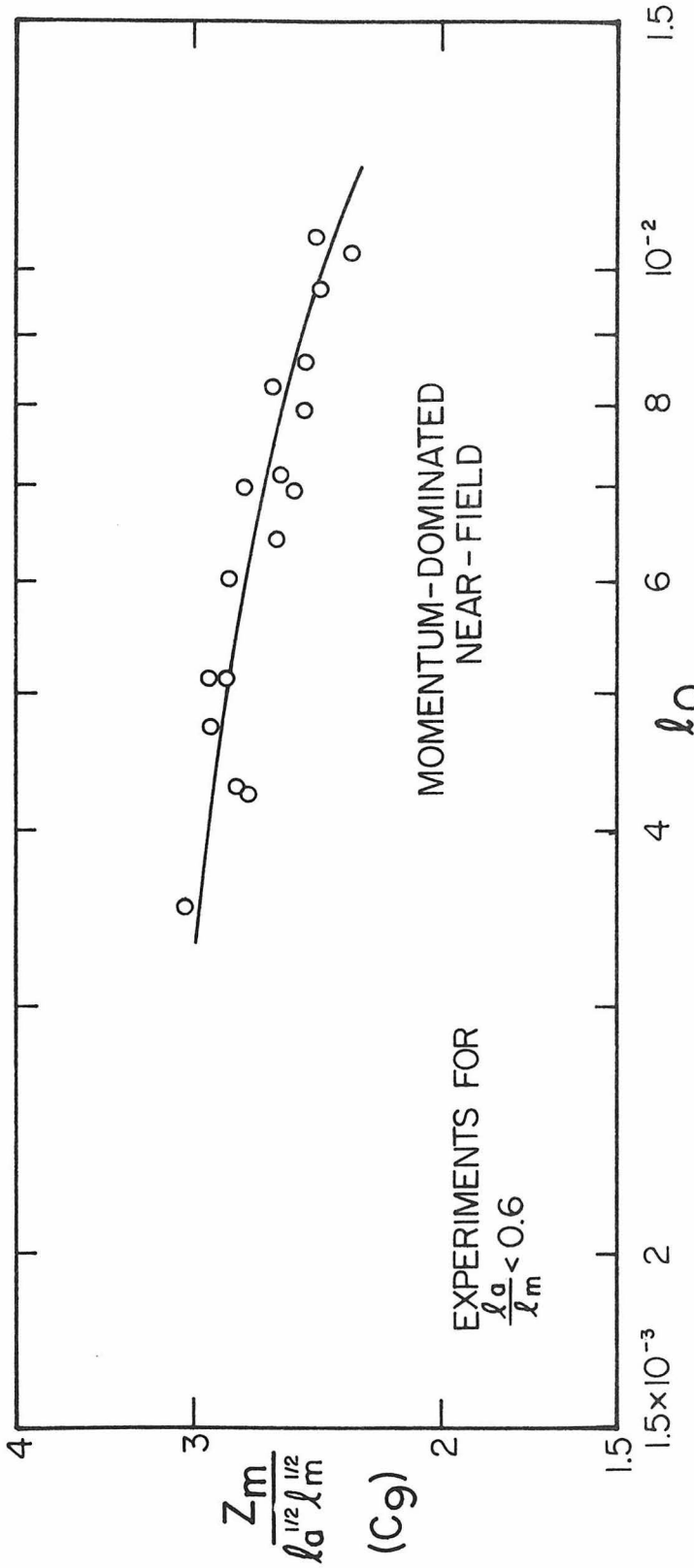

Fig. 5.36 Maximum height of rise coefficient C_9 as a function of ℓ_Q/ℓ_m.

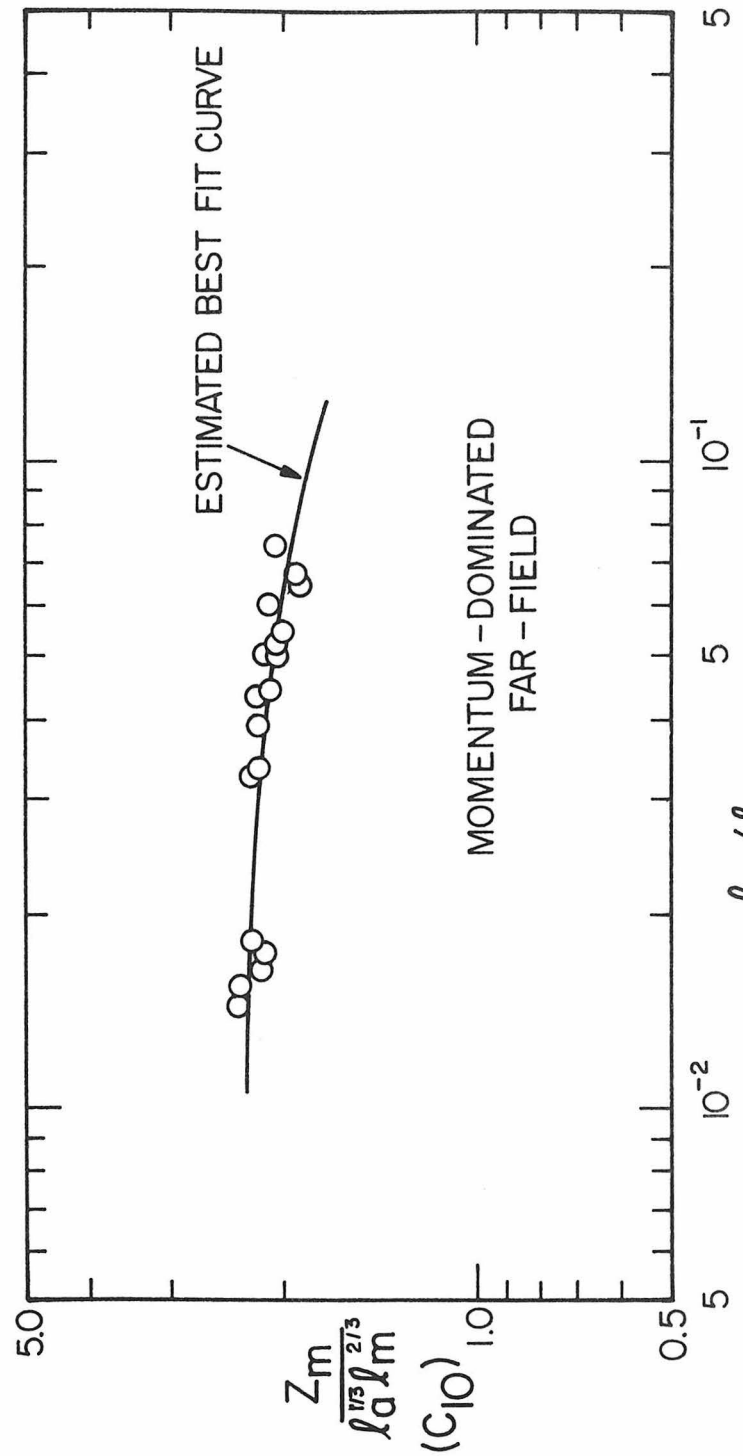

Fig. 5.37 Maximum height of rise coefficient C_{10} as a function of ℓ_Q/ℓ_m.

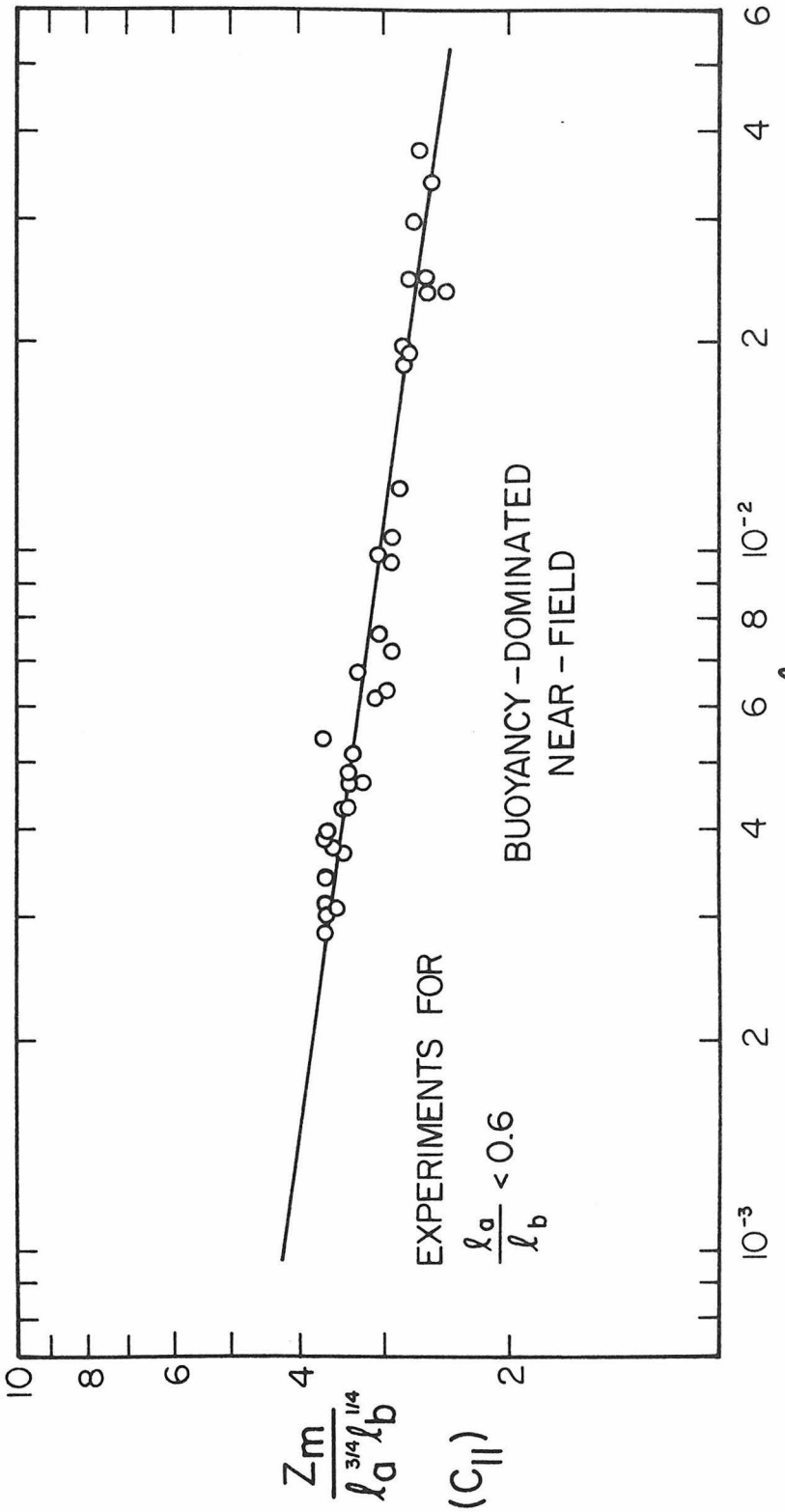

Fig. 5.38 Maximum height of rise coefficient C_{11} as a function of ℓ_Q/ℓ_b.

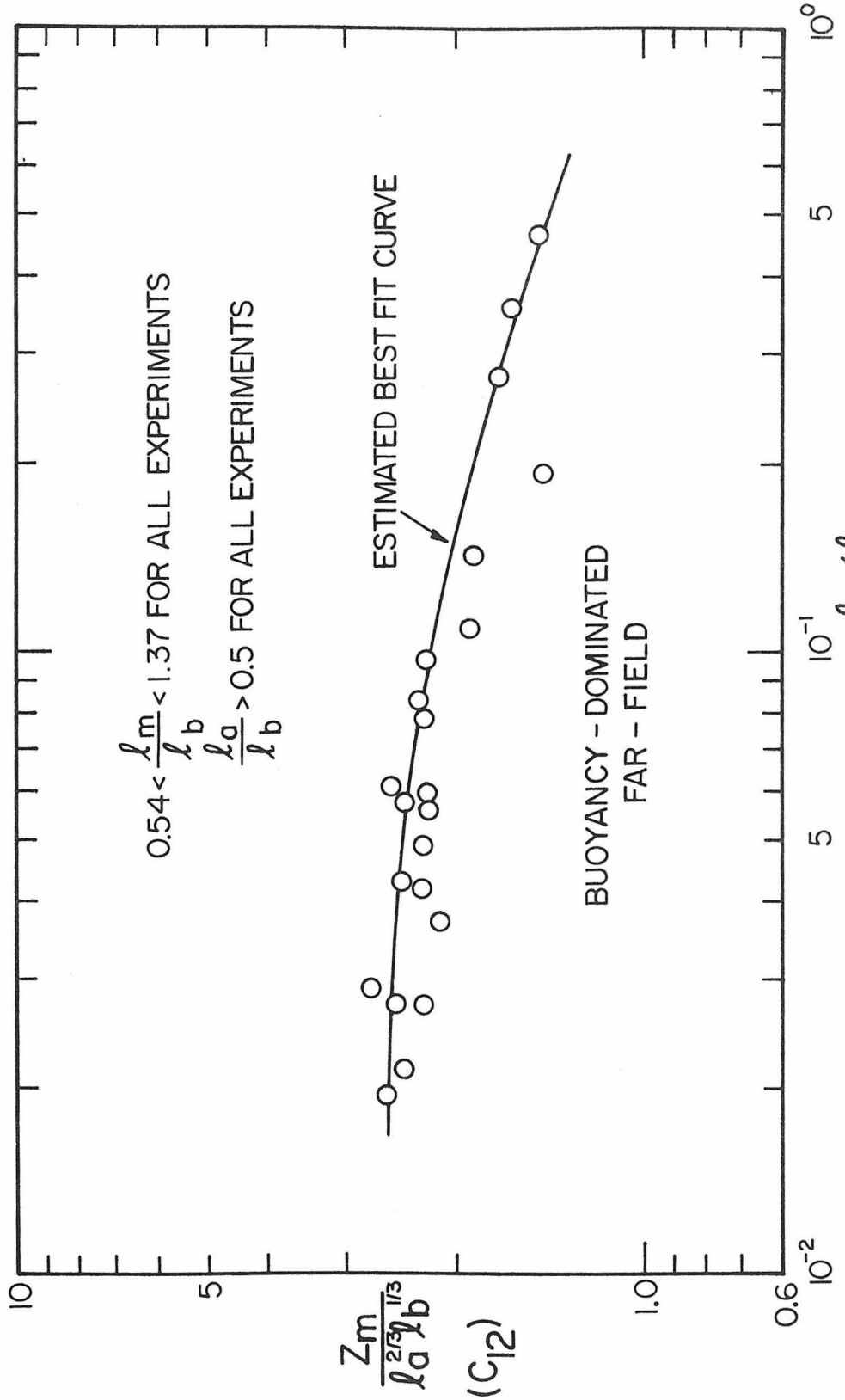

Fig. 5.39 Maximum height of rise coefficient C_{12} as a function of ℓ_Q/ℓ_b.

5.2.4 Concentration Measurements

5.2.4.1 Measurements at the maximum height of rise

The concentration measurements described in the preceding section were also analyzed to observe the characteristic dilution of a tracer at the maximum height of rise. Instantaneous concentration measurements were obtained from the output from the light probe and were analyzed by dividing the vertical probe sweep into 25 cells as described previously. The data for each cell thus consisted of a number of instantaneous concentration values. The total sample could then be processed in a number of different ways depending upon the information desired.

Several of the experiments were analyzed to determine the minimum dilution at the maximum height of rise. The minimum dilution (or maximum concentration, $S = C_o/c$) was taken as the minimum time-average value measured in the vertical cross-section which is also the value used to define the location of the maximum height of rise. Some of the earlier experiments were apparently affected by the oxidation of the dye by the chlorine added to the towing tank. This resulted in apparent dilutions which were on the order of one to two orders of magnitude larger (lower dye concentrations) than expected. These experiments were still used for the description of maximum heights of rise since it was believed that the position of the maximum dye concentration was not affected although its magnitude was incorrect. The later experiments using Rhodamine B-Extra dye as a tracer were assumed to be correct as it took much longer for this dye to be

oxidized by the chlorine (approximately 45 minutes). The results of these experiments are presented in Fig. 5.40 for momentum-dominated jets and in Fig. 5.41 for buoyancy-dominated flows. Since there were only a few experiments for each flow regime, it was difficult to establish a value for the constant in the dilution relations presented in Table 3.3. However, these dilutions can be compared to those for the same vertical rise in an unstratified flow. The lines in the figures correspond to the average experimental results for unstratified flow presented in Table 5.2. The dilutions for the stratified flow experiments follow these relations to within experimental scatter. This can be taken as a verification of the assertion that the unstratified flow model can be used quite adequately up to the maximum height of rise for the prediction of jet trajectories and dilutions.

Time-average concentration profiles were determined by computing the average concentration for all of the instantaneous readings for each vertical cell. Typical concentration profiles for several experiments are presented in Figs. 5.42 and 5.43. These experiments were selected to correspond to each of the various flow regimes; run 146 to the mdnf, run 153 to the mdff, run 095 to the bdnf, and run 144 to the bdff. The complete experimental variables for these different figures are presented in Appendix A. The variable r in these figures denotes vertical distance from the maximum height of rise Z_m (positive r implies greater vertical distance z), c denotes the average concentration for a vertical position and C_m is the maximum value measured for that profile (or the value at $z = Z_m$). The above data were taken from vertical profiles obtained at the maximum height of rise.

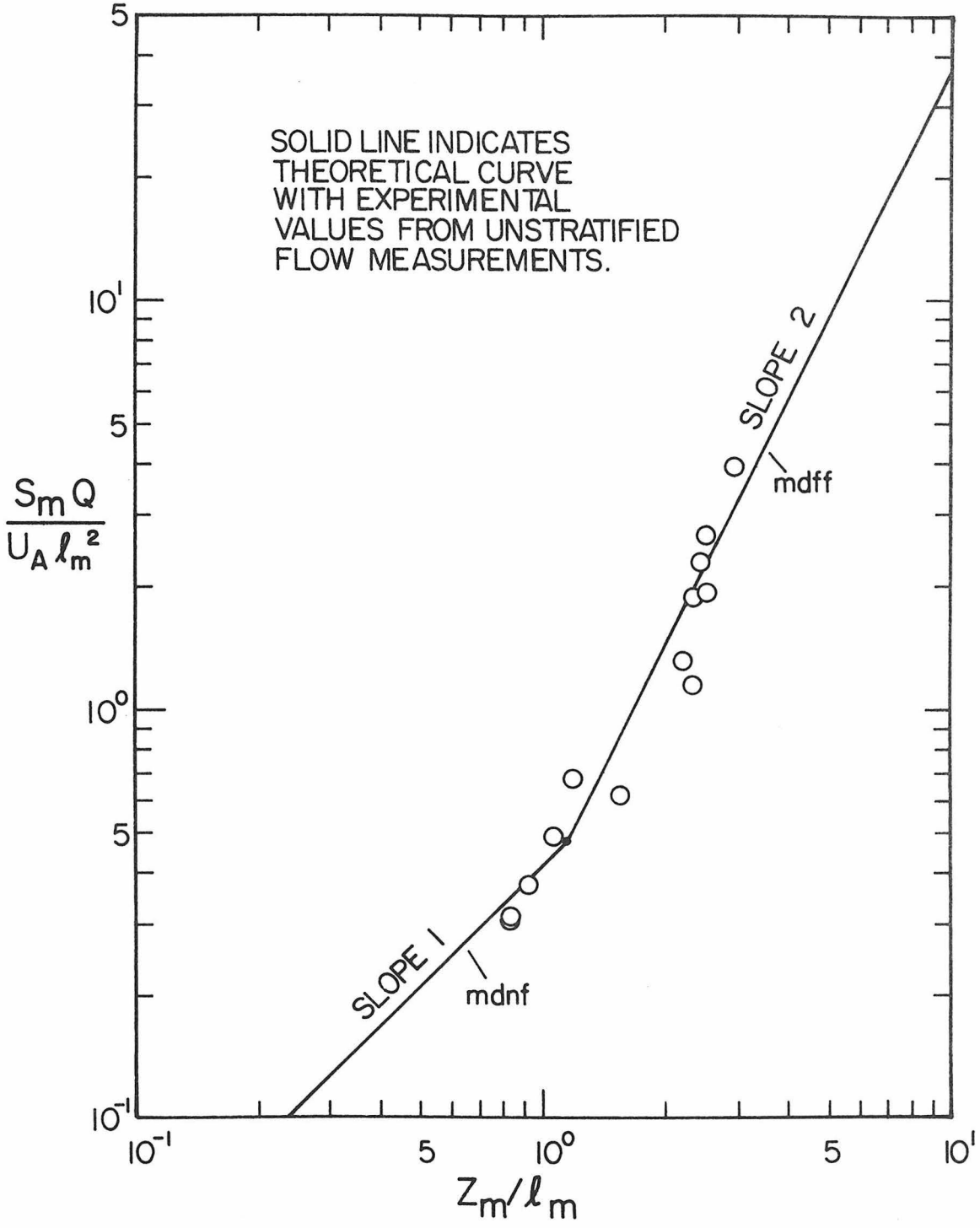

Fig. 5.40 Comparison of dilutions at maximum height of rise to unstratified flow results (momentum-dominated flow).

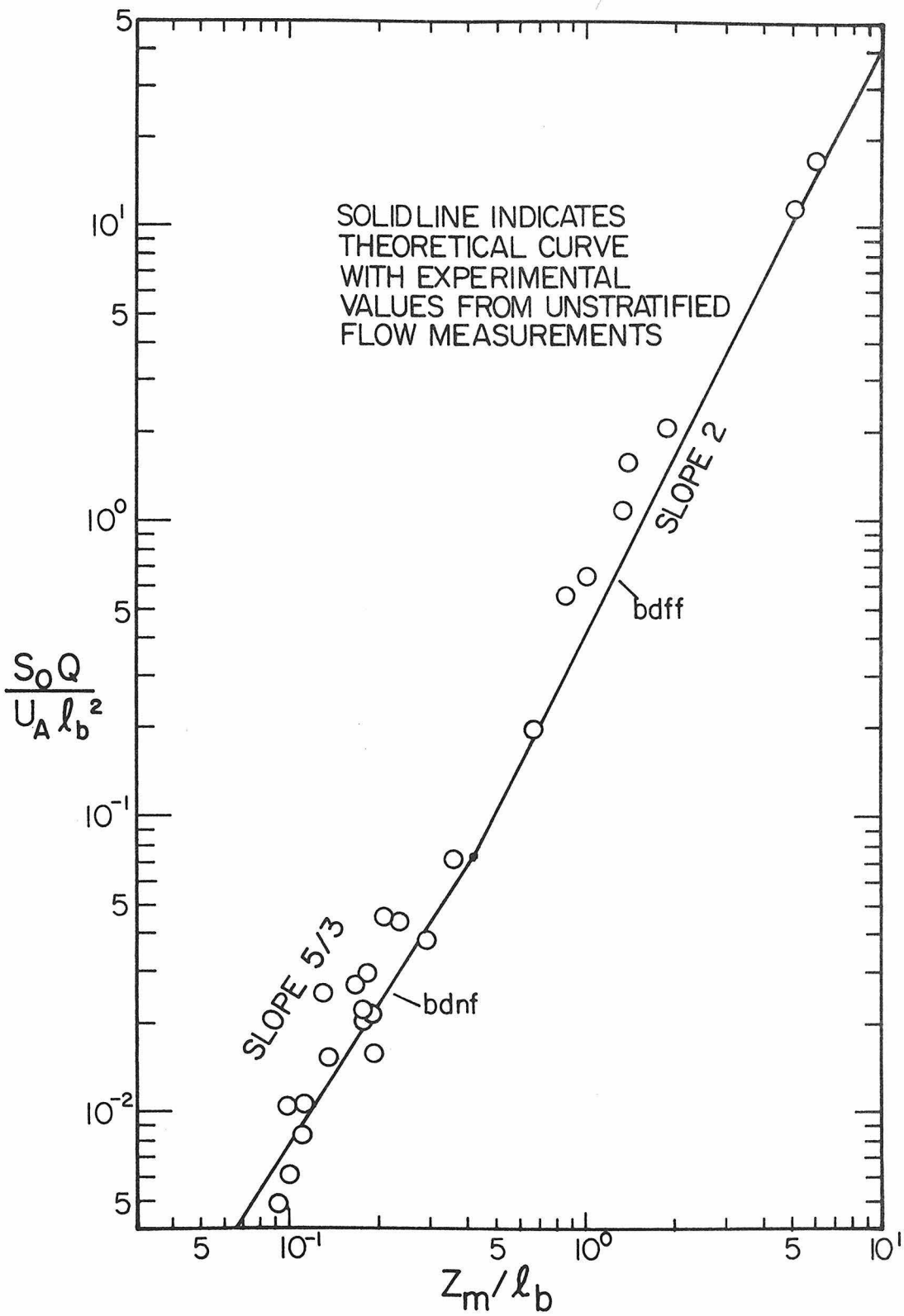

Fig. 5.41 Comparison of dilutions at maximum height of rise to unstratified flow results (buoyancy-dominated flow).

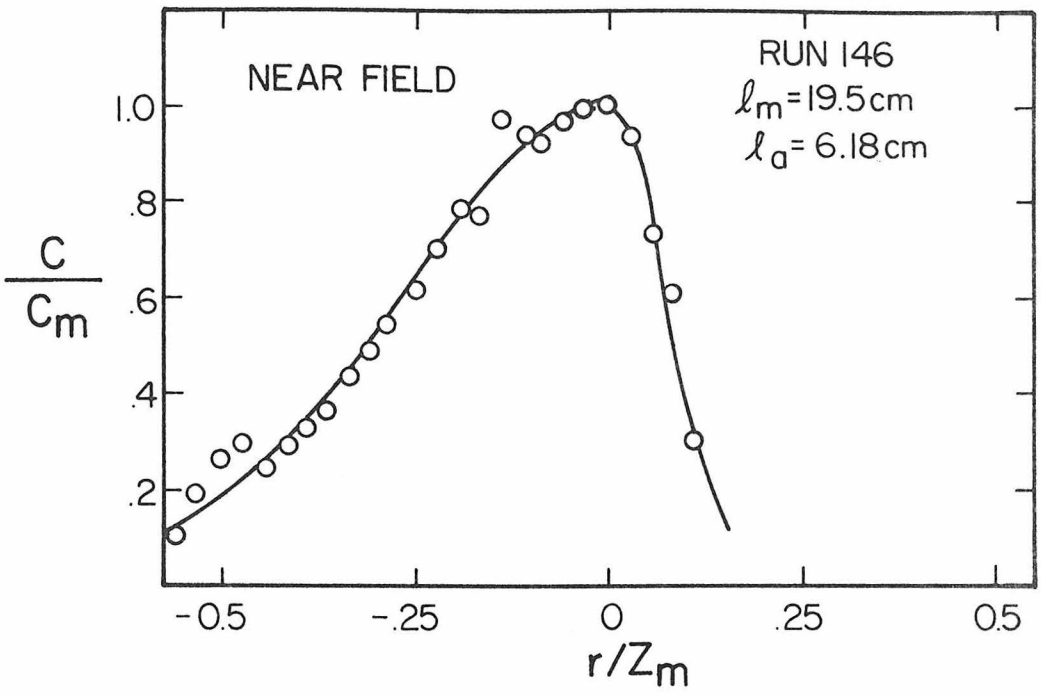

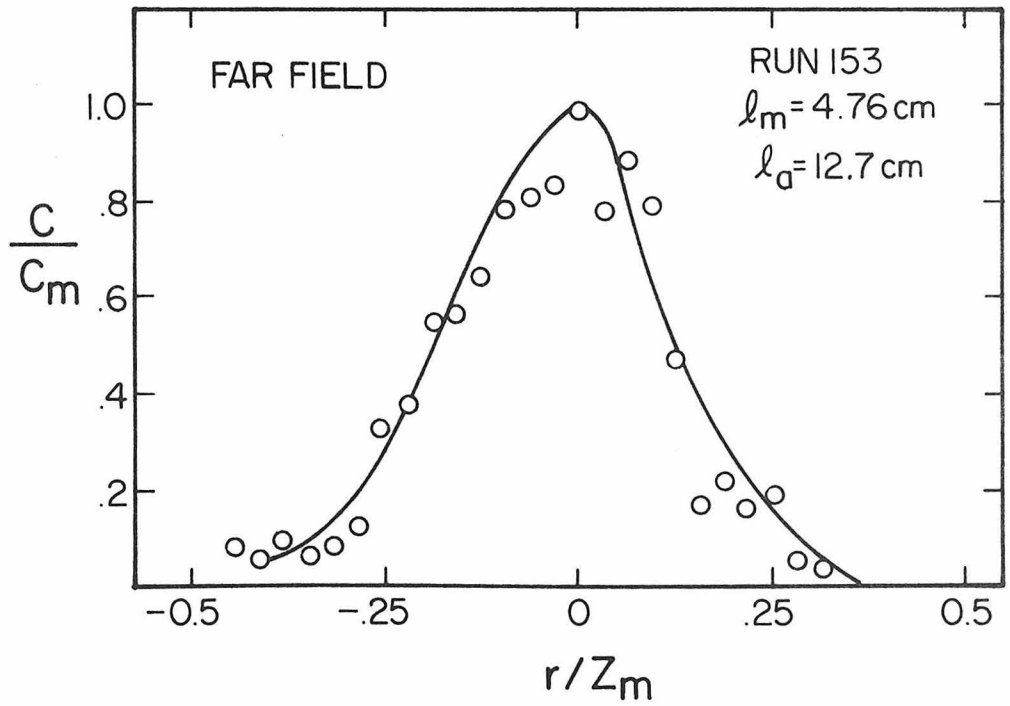

Fig. 5.42 Time average vertical concentration profiles (momentum-dominated flow).

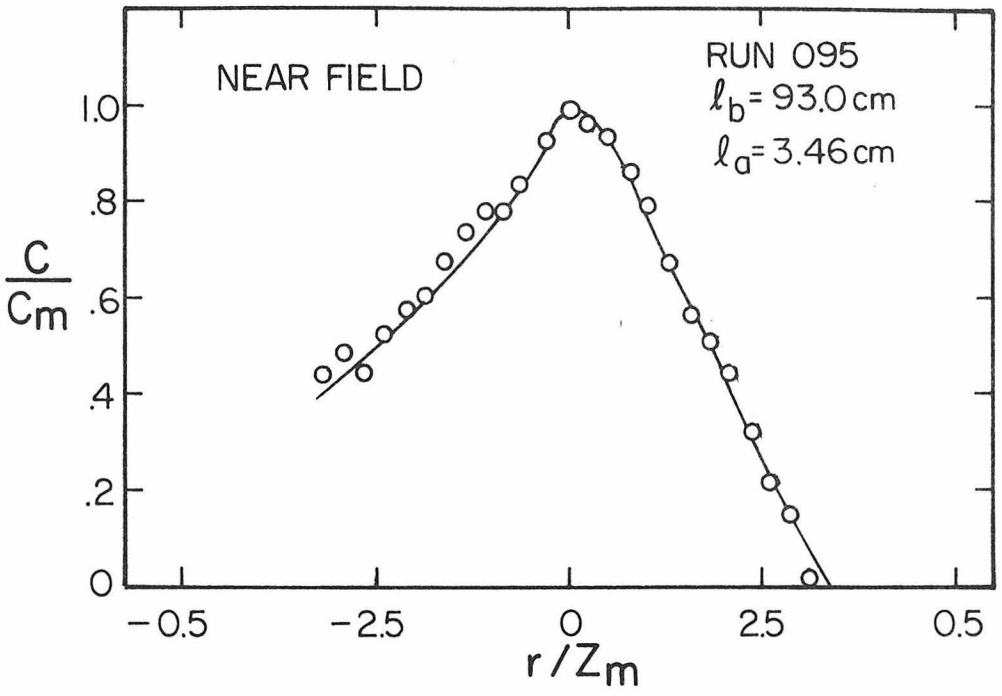

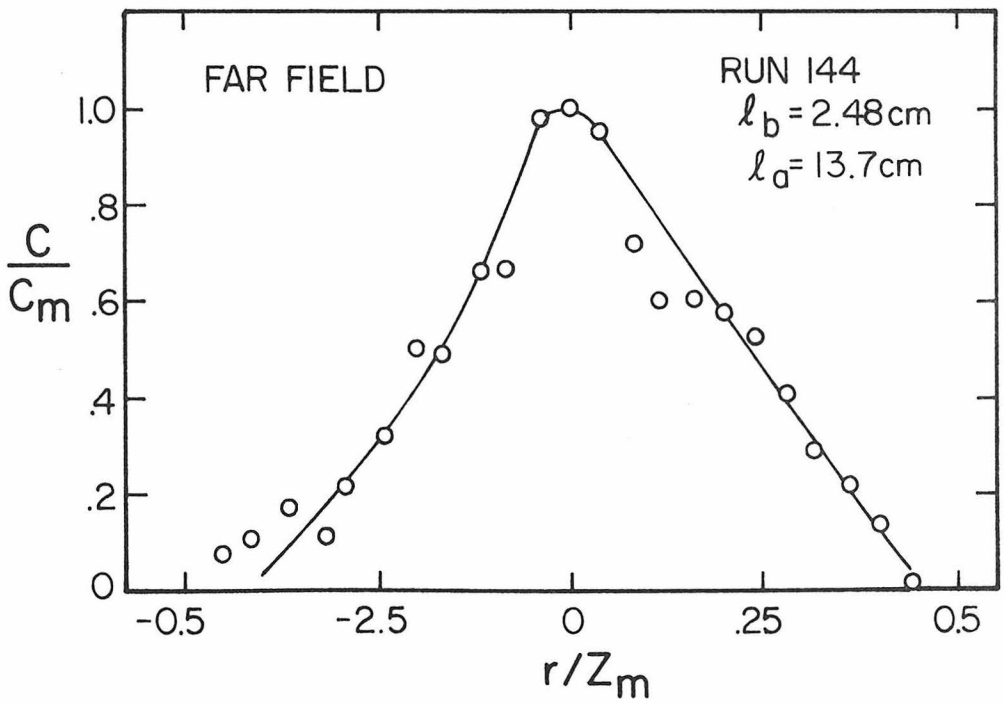

Fig. 5.43 Time average vertical concentration profiles (buoyancy-dominated flow).

The far-field profiles (runs 144 and 153) were measured with relatively short sample times and indicate the greatest uncertainty in the sample averages. These experiments have the greatest apparent scatter in the concentration profiles which is believed to be due to the lack of adequate sample time.

The shapes of the profiles for the near-field flows (run 146 for the mdnf and 095 for the bdnf) are not symmetrical which is probably due to the rapid change in curvature for near-field jets at the maximum height of rise. The nearly vertically-rising jet changes direction fairly abruptly at its maximum rise which results in the asymmetric profile at that point. The far-field flows, which are well bent over at the maximum rise, tend to have more symmetric concentration profiles.

If the jet width is defined as the vertical distance between the two locations where c is equal to $C_m/2$, the jet widths in Figs. 5.42 and 5.43 are approximately 0.4, 0.35, 0.4 and 0.42 of the corresponding value of Z_m for experiments 146, 153, 095 and 144 respectively. Thus, the jet widths are nearly the same for all cases.

The instantaneous concentration measurement for each of the above experiments were also analyzed in several different ways to examine the nature of the turbulent fluctuations. The standard deviations $\sqrt{\overline{c'^2}}$ of the instantaneous samples at each vertical position were computed for each experiment and are presented in Figs. 5.44 and 5.45 normalized by the concentration C_m. These figures also indicate that the far-field flows are more symmetric than the near-field flows. The normalized r.m.s. values ($\sqrt{\overline{c'^2}}/C_m$) for the far-field flows (runs 153 and 144)

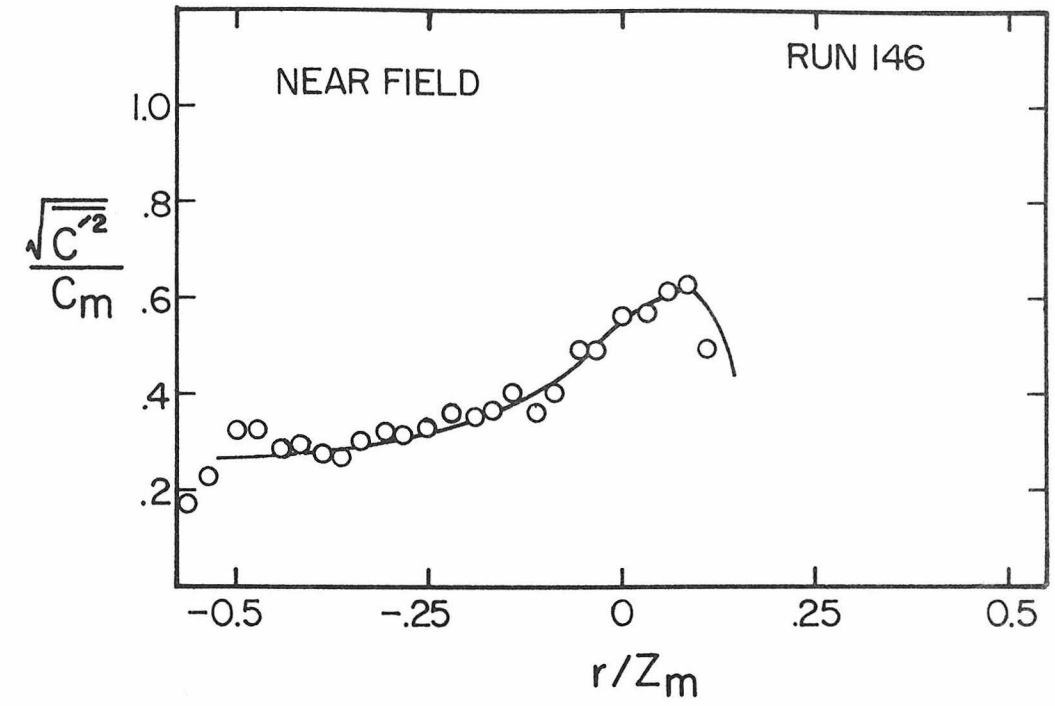

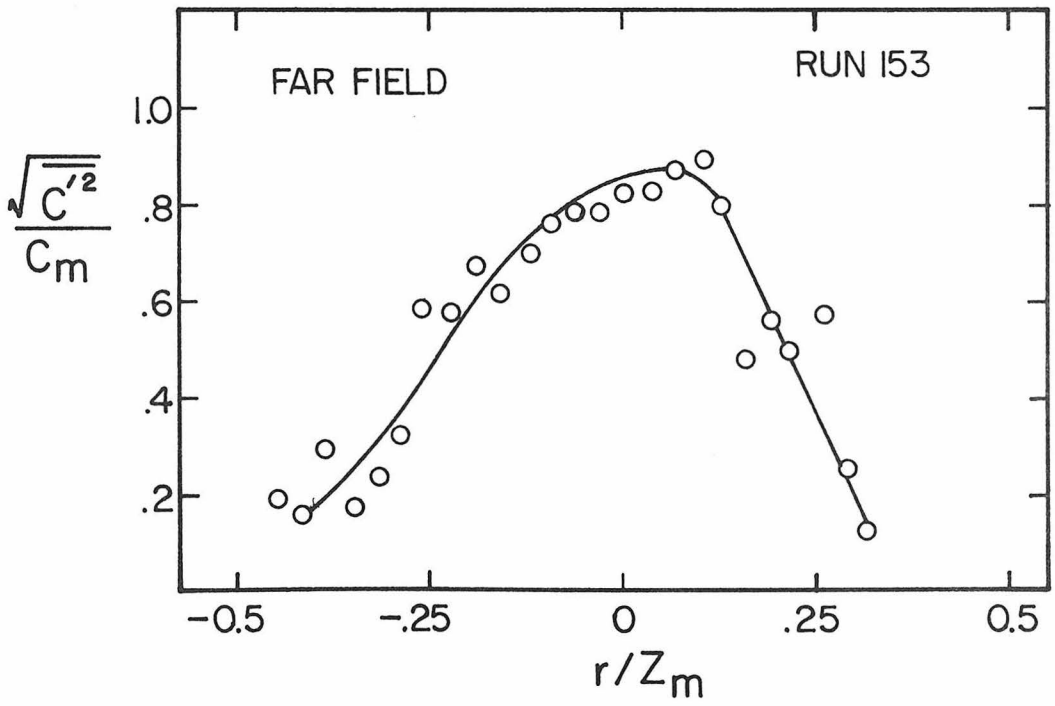

Fig. 5.44 Vertical distribution of $\sqrt{\overline{C'^2}}/C_m$ (momentum-dominated flow).

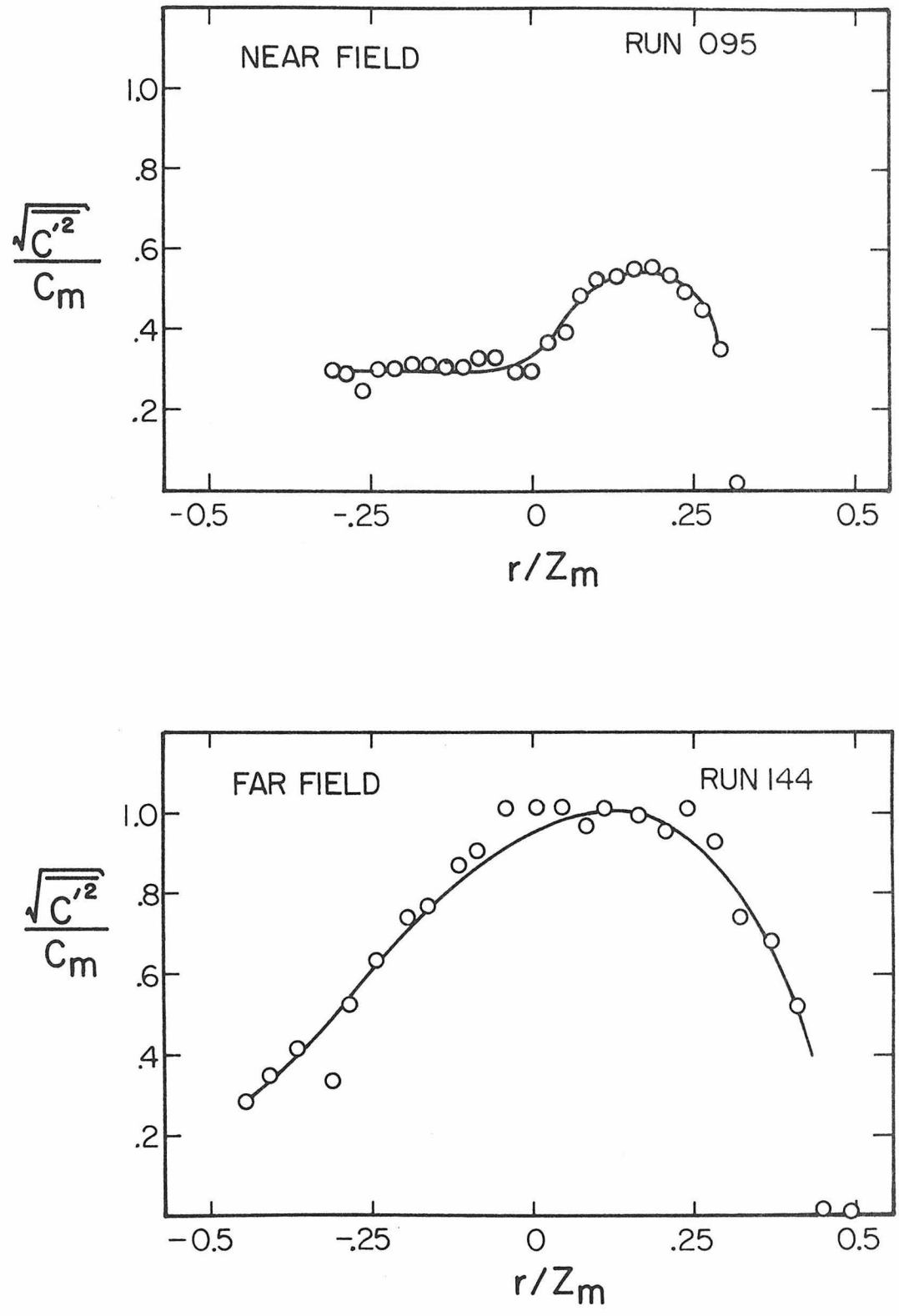

Fig. 5.45 Vertical distribution of $\sqrt{\overline{C'^2}}/C_m$ (buoyancy-dominated flow)

also have greater maxima than the near-field flows (approximately 1.0 vs. 0.6 for runs 095 and 146). These maxima are located at greater vertical rises (r positive) than the position of C_m in all cases.

The maximum and minimum instantaneous concentrations measured at each vertical location were also determined. The values of the instantaneous maxima C_{max} for the four jet flows are presented in Figs. 5.46 and 5.47. The minimum values were essentially zero at all vertical positions for all four cases and are not indicated in the figures. The results for runs 144 and 153 are believed to be influenced by the limited sampling times and may not indicate accurate values for C_{max}. It would be expected that a longer sample time might indicate greater values of C_{max}. The near-field flows appear to have instantaneous maxima on the order of 1.5 to 2.0 times the time-average maximum concentration C_m while the far-field flows indicate somewhat larger values. Even if the very large values observed for run 144 (C_{max}/C_m on the order of 5) are ignored as instrumental error, the implication is that instantaneous maxima on the order of 3 to 4 times the time-average maximum concentration can occur. Kotsovinos (1975) noted instantaneous maxima on the order of 2.2 C_m for a two-dimensional jet in a stagnant ambient fluid, so the values noted above would appear to be of the correct magnitude.

These measurements indicate that the average concentration recorded at a point is not necessarily a good indicator of the instantaneous peak values that occur. This may be an important consideration if the tracer present in a buoyant jet discharge is toxic to organisms present

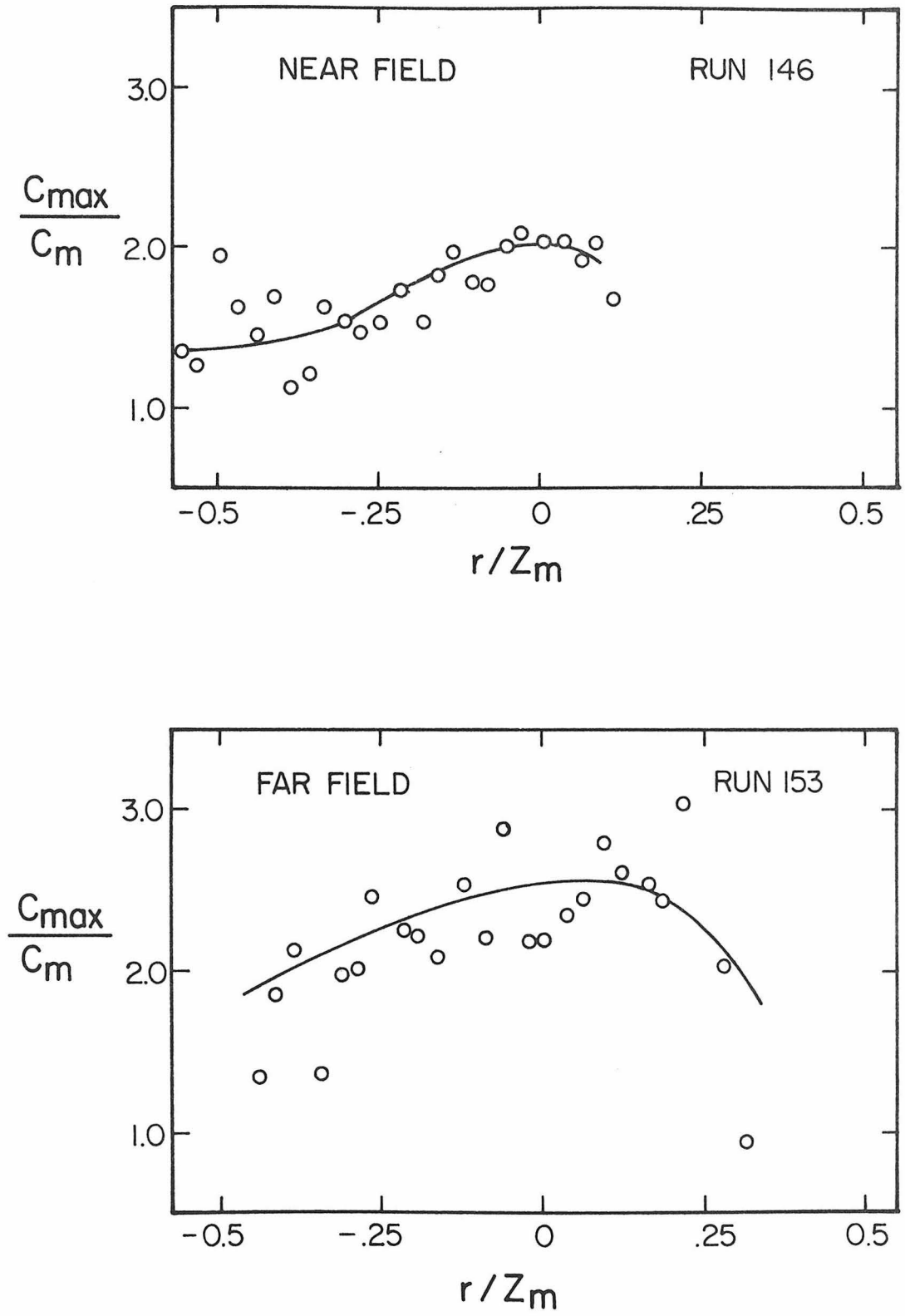

Fig. 5.46 Vertical distributions of instantaneous concentration maxima (momentum-dominated flow).

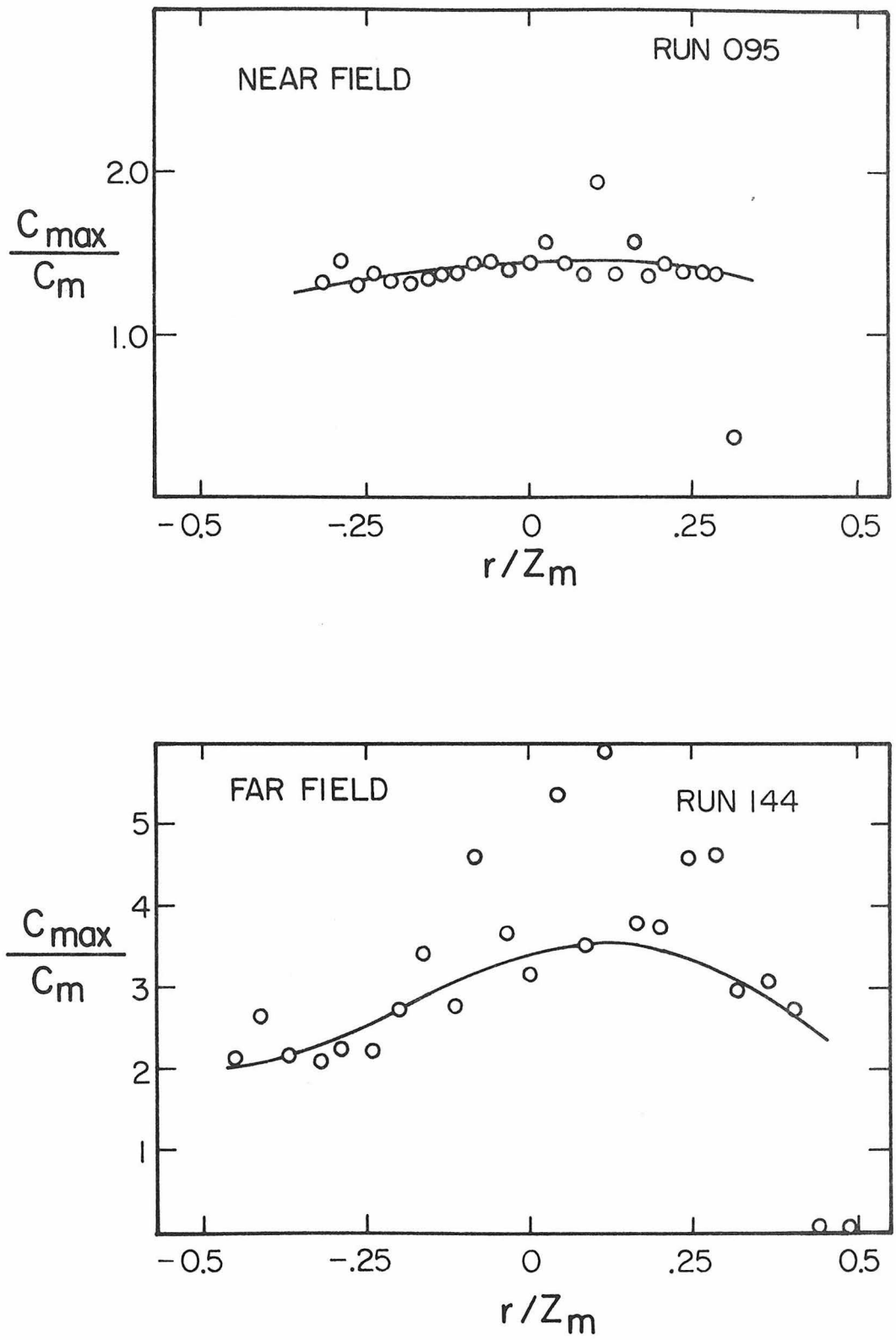

Fig. 5.47 Vertical distribution of instantaneous concentration maxima (buoyancy-dominated flow).

in the ambient fluid. The organism can encounter instantaneous peak concentrations which can be much larger than the time-averaged concentration. The intermittent nature of the flow will also expose the organism to rapid rates of change of contaminant concentration.

Intermittency profiles were also computed for each of the jet flows. The intermittency I was defined as

$$I = \frac{1}{n}\sum_{k=1}^{n} I_k$$

where

$$I_k = \begin{cases} 1 \text{ if } c' \geq 0.001 \\ 0 \text{ if } c' < 0.001 \end{cases}$$

where n is the total number of samples for a given vertical position and c' represents instantaneous concentration values (relative to the concentration at the jet source). The threshold value of 0.001 was chosen as an estimate of the lowest concentration that could accurately be measured with the light probe. The intermittency profiles computed on this basis are presented in Figs. 5.48 and 5.49 for the four experiments. These results again indicate that there is a fundamental difference between the nature of the near- and far-field flows as the shapes of the intermittency profiles are substantially different for these two cases.

5.2.4.2 Measurements beyond the point of maximum jet rise

Four sets of experiments were performed to observe the variation of jet dilution beyond the point of maximum jet rise in a stratified crossflow. These experiments were selected so that one

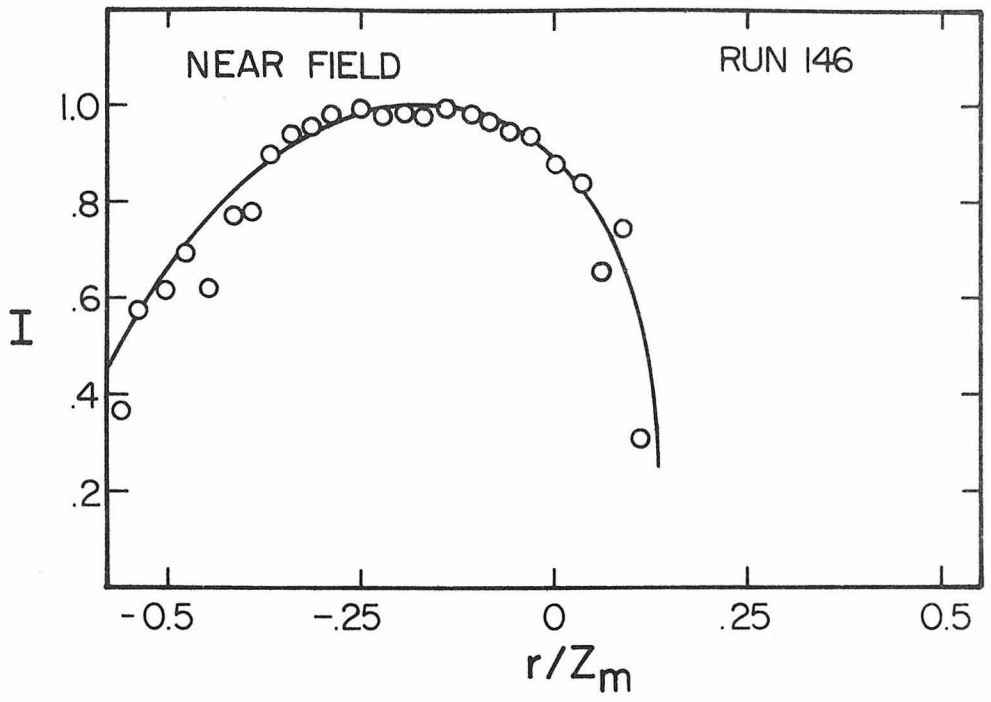

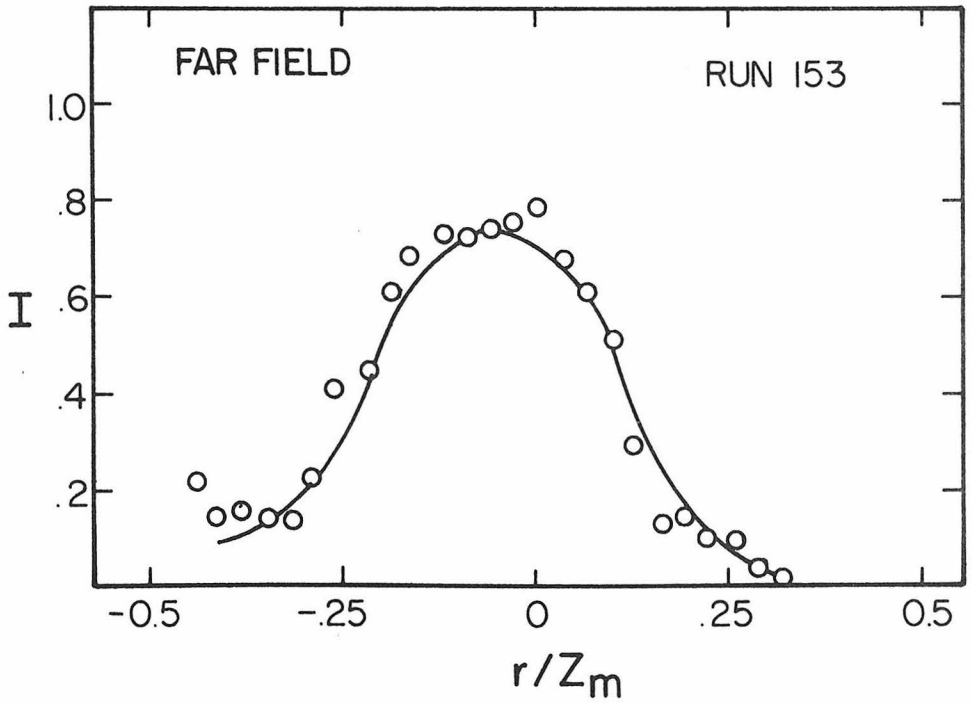

Fig. 5.48 Vertical distribution of intermittency (momentum-dominated flow).

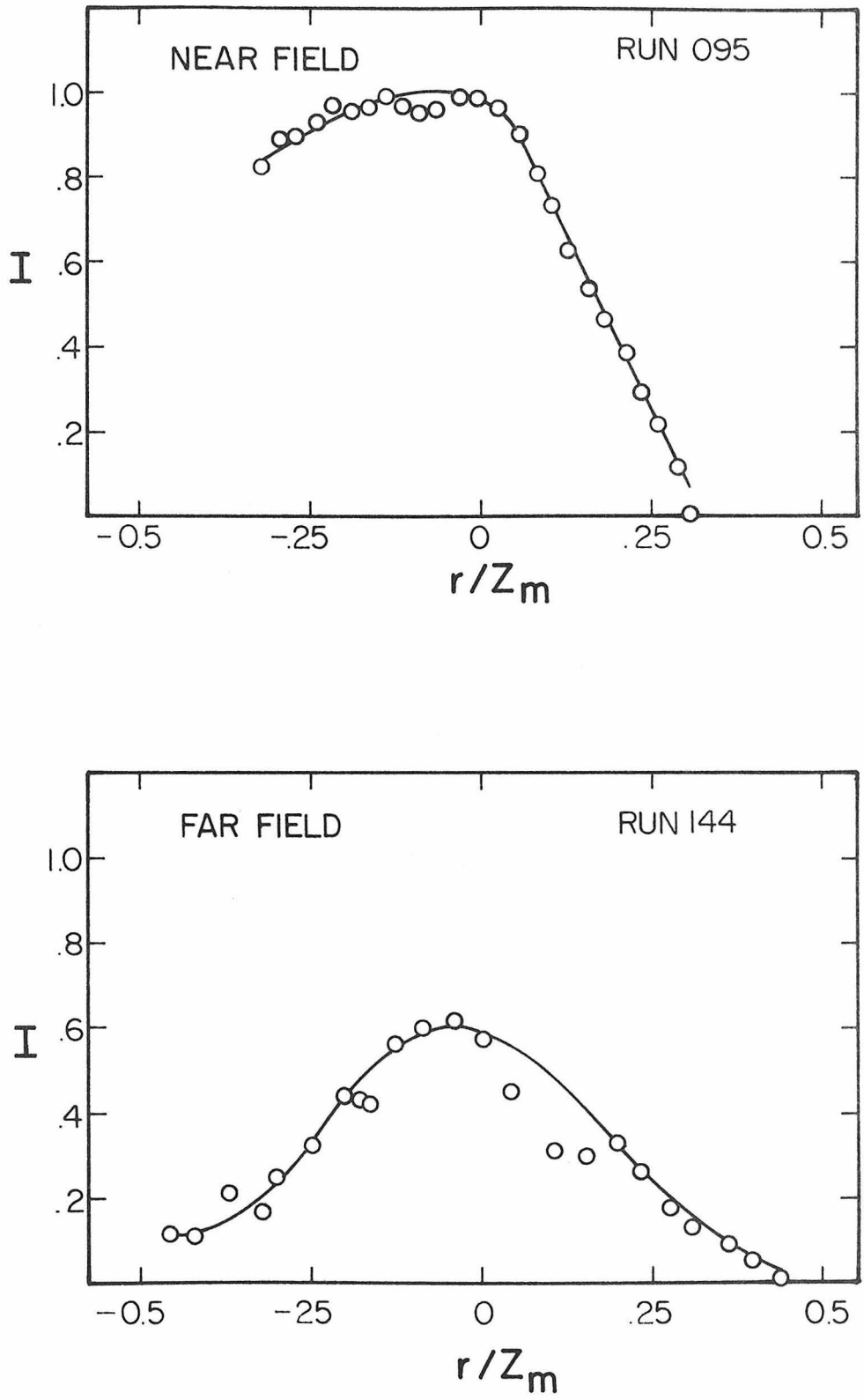

Fig. 5.49 Vertical distribution of intermittency (buoyancy-dominated flow).

set corresponded to each of the four flow regimes (the mdnf, mdff, bdnf, and bdff). Concentration measurements of the type discussed in Section 5.2.4.1 were taken at the maximum height of rise and for several downstream locations with the jet and ambient conditions repeated as closely as possible for each experiment. The minimum dilution S measured for each horizontal position normalized by the dilution S_m at the maximum height of rise is presented in Fig. 5.50 as a function of horizontal distance. The distance x_m is the horizontal location of the maximum height of rise and the length scale ℓ_a was previously defined equal to $U_A/\varepsilon^{1/2}$.

A buoyant jet at its maximum height of rise will have zero vertical momentum but will not be at its neutrally buoyant position and will tend to fall back from its maximum height of rise toward its equilibrium position. The resulting flow will be similar to that described previously for a cylindrical thermal since the flow will be nearly horizontal. The dilution of a thermal has been shown to be related to the square of the vertical rise. Thus it can be expected that to a first approximation, the dilution of a buoyant jet beyond its point of maximum rise will be dependent upon the overshoot $(Z_m - Z_e)$ of the jet beyond its equilibrium height of rise:

$$\frac{S_e - S_m}{S_m} \propto \left[\frac{(Z_m - Z_e)}{Z_m}\right]^2$$

where S_e is the characteristic dilution within the jet at its equilibrium height of rise.

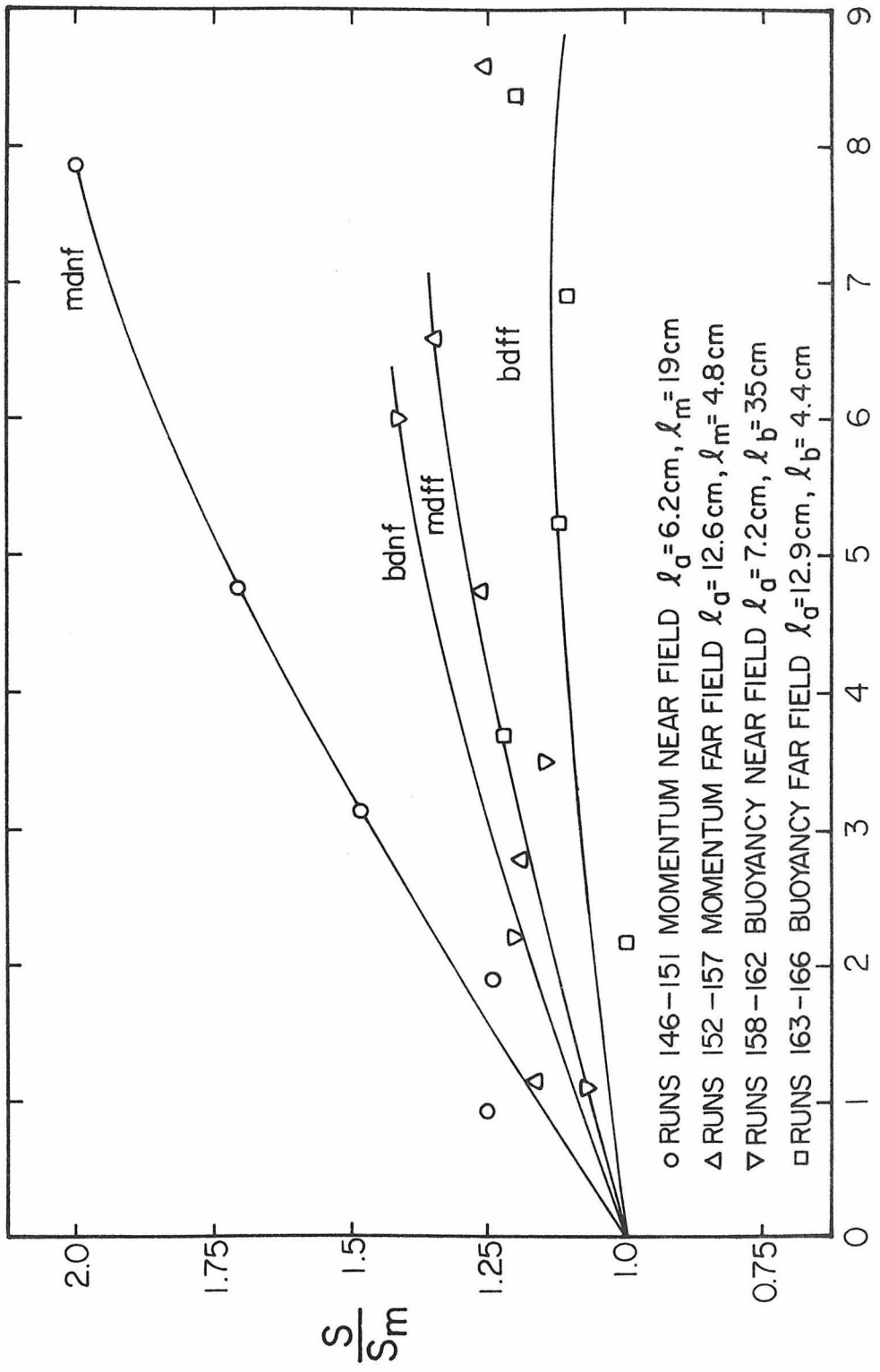

Fig. 5.50 Further dilution beyond the maximum height of rise.

It can be anticipated on the basis of this reasoning that further jet dilution is related to the relative difference between Z_m and Z_e. The results in Fig. 5.50 can be explained qualitatively on this basis. That is, the momentum-dominated near-field flow indicates the greatest amount of overshoot and thus should experience the greatest amount of further dilution. The mdnf has a relatively greater overshoot than the bdnf and each near-field flow has a greater overshoot than the corresponding far-field flow (mdnf compared to the mdff and bdnf compared to the bdff). Thus, the qualitative results in Fig. 5.50 that the mdnf flow dilutes more than the mdff and the bdnf more than the bdff are to be expected. Additional experiments need to be performed to establish the exact nature of this phenomena. The width of the flume and other experimental limitations prevented a more thorough examination of this flow behavior.

CHAPTER 6

DISCUSSION

6.1 Application of the Experimental Results

The results of the experimental investigation can be presented in a unified manner such that the trajectories and dilutions for a general buoyant jet in a crossflow can be readily determined. The qualitative presentation in Figs. 3.4 and 3.6 can be combined with the measured values of the various trajectory and dilution coefficients to develop figures which reflect the combined experimental results for the different flow regimes. Figures similar to Fig. 3.7 can also be used to present the experimental results for the measurements of maximum and equilibrium heights of rise. These figures must also reflect the additional effect of the initial volume flux, since it was observed that the experimental results were dependent upon this parameter.

The results from the trajectory measurements are presented in Figs. 6.1 and 6.2, which are alternate presentations of the same information. Fig. 6.1 is essentially the same as Fig. 3.4 with the additional effect of the jet volume flux included, while Fig. 6.2 presents the trajectories scaled with the length scale ℓ_m. When the density difference between the jet and the ambient fluid becomes small, ℓ_b also becomes small and the normalized trajectories may fall outside the range of variables in Fig. 6.1, and an alternate plot scaled with ℓ_m is useful. Therefore, the information in Fig. 6.2 should be used for situations where the jet buoyancy is relatively small since the

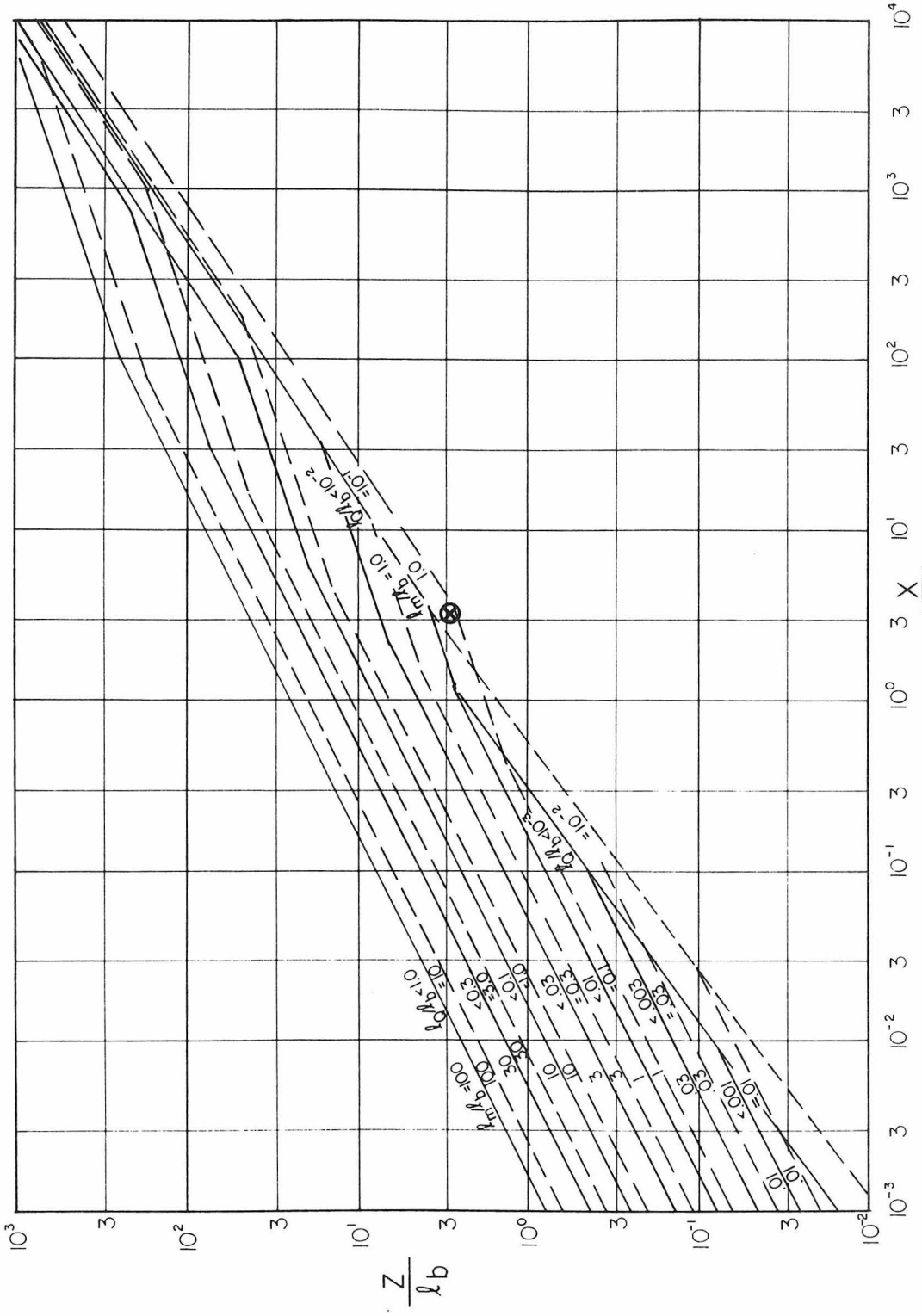

Fig. 6.1 Buoyant jet trajectories normalized with ℓ_b.

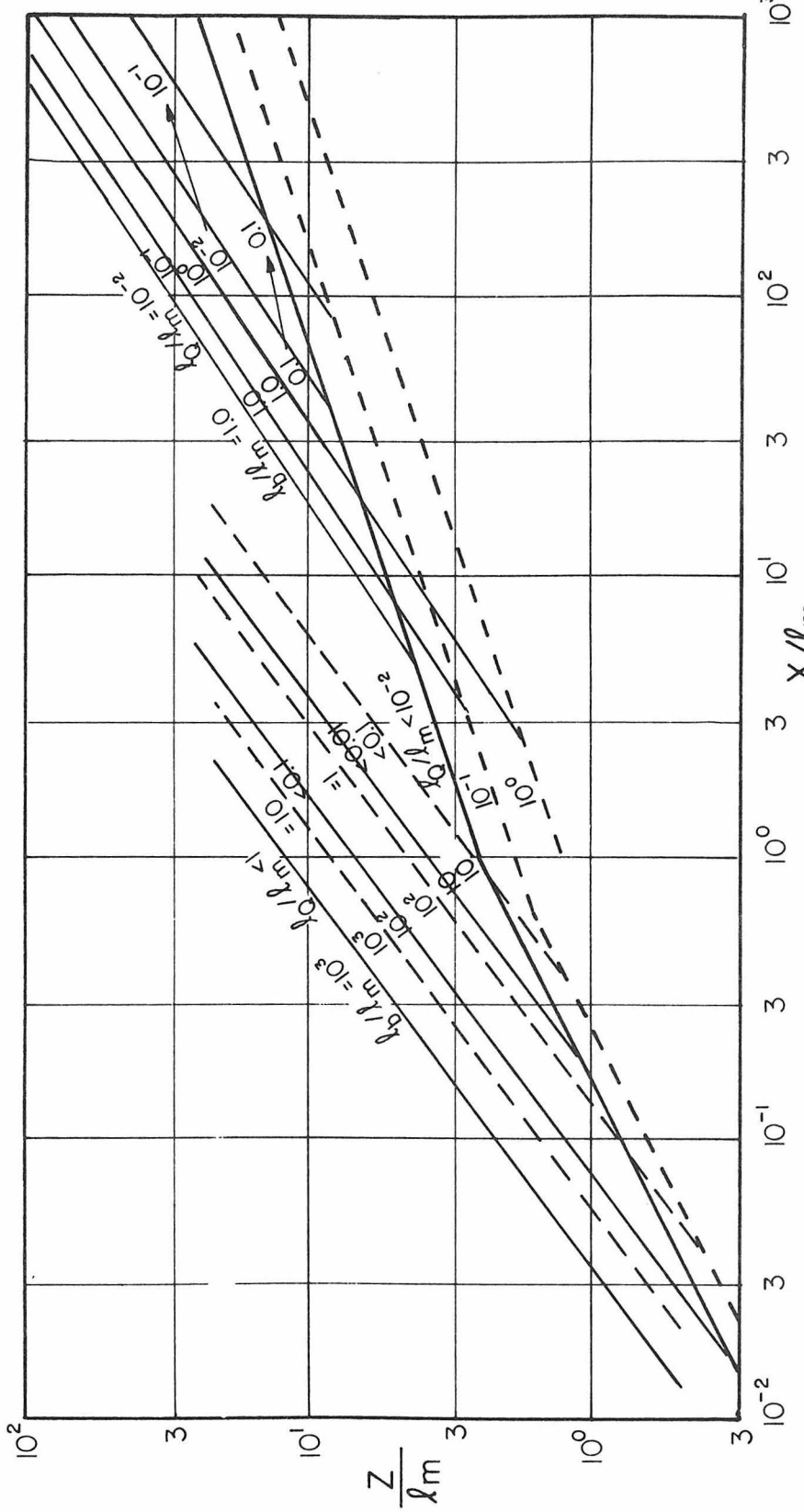

Fig. 6.2 Bucyant jet trajectories normalized with ℓ_m.

trajectories collapse to the momentum-dominated results in this figure. Similarly, since Fig. 6.1 presents the trajectories scaled with ℓ_b, the curves collapse to the buoyancy-dominated results when the jet momentum flux becomes small.

The information in these figures is the vertical location of the maximum centerline concentration, since this will generally be the result of interest in the application to a design problem. The values of the trajectory coefficients were obtained from Figs. 5.16-5.19 which is the data from the concentration measurements. The experimental data were extrapolated beyond the range of conditions investigated by referring to the results of the trajectory measurements from the photographs presented in Figs. 5.8-5.12. Although the trajectory definitions are not equivalent for these two cases, the dependence upon the initial volume flux (and the momentum flux for the buoyancy-dominated far-field) should be qualitatively the same. The shapes of the curves in Figs. 5.8-5.12 were used to extrapolate values for the trajectory coefficients in Figs. 5.16-5.19 beyond the ranges for which they were directly determined.

The information for jet dilution as a function of vertical rise is presented in Figs. 6.3 and 6.4. The values for the dilution constants were obtained from Table 5.2. There was no apparent dependence of these data on the jet volume flux so this effect is not indicated in the figures. These two figures which are alternate presentations of the same information, have been developed on the basis of reasoning similar to that for the presentation of the trajectory results. Fig. 6.3

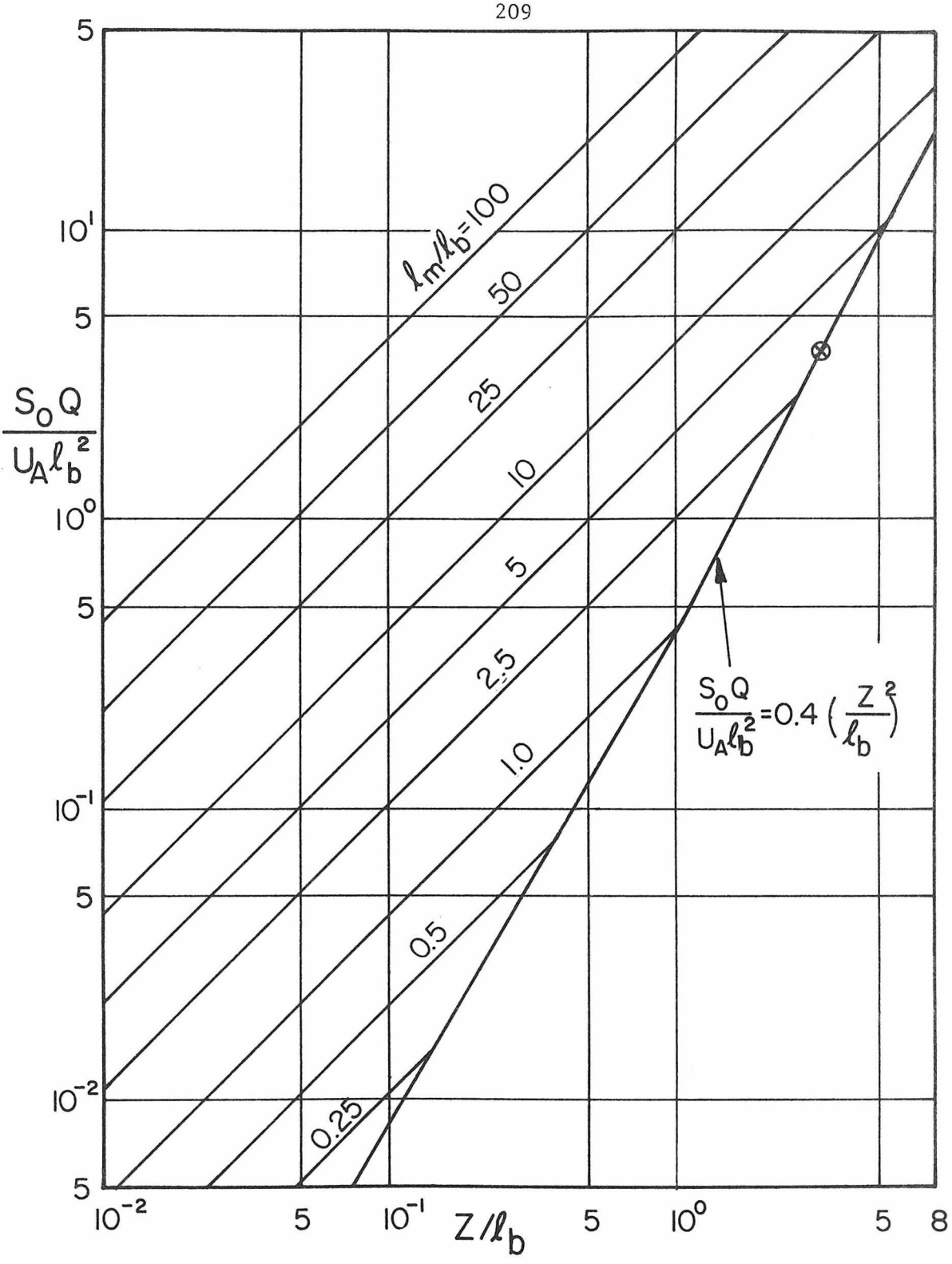

Fig. 6.3 Buoyant jet dilution normalized with ℓ_b.

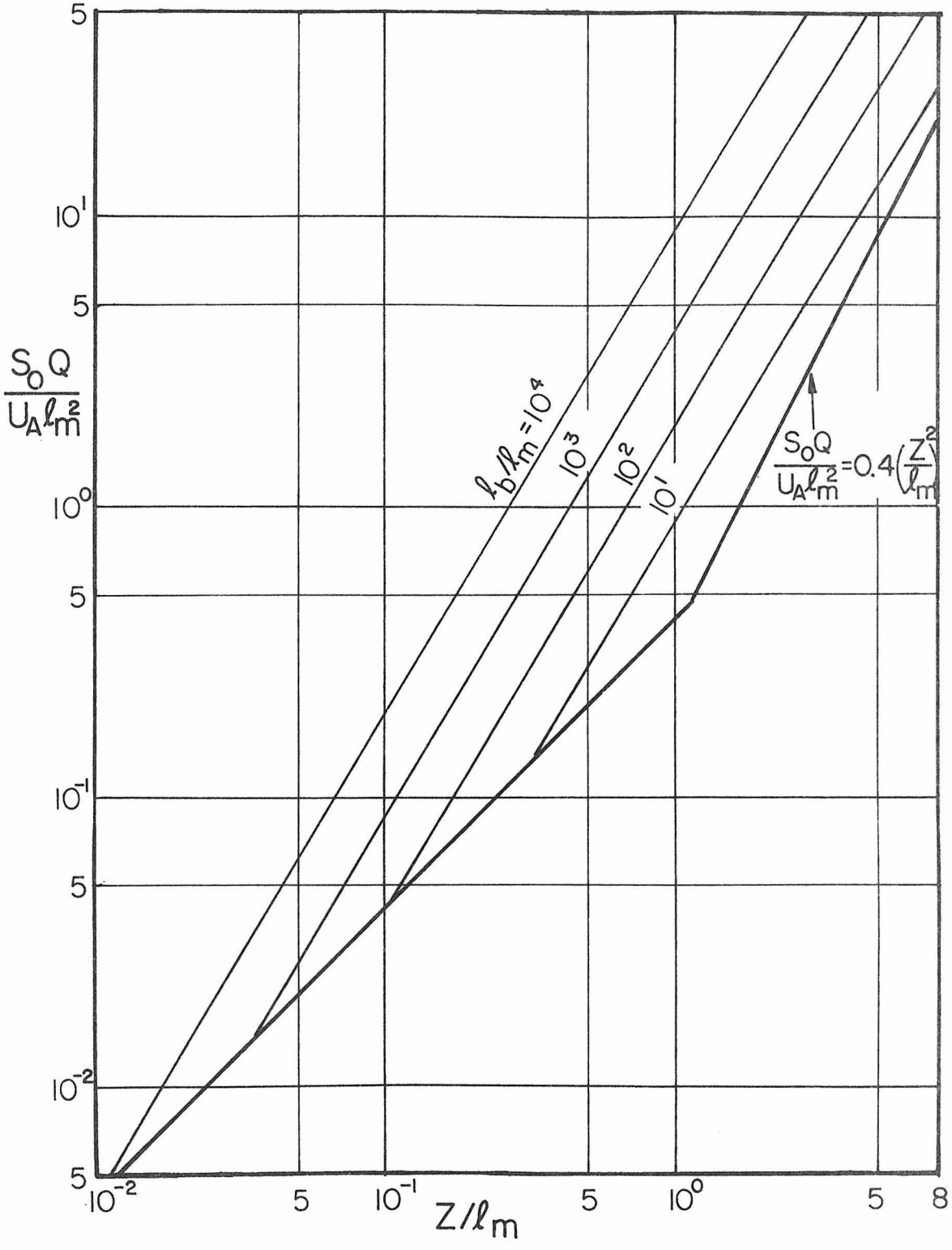

Fig. 6.4 Buoyant jet dilution normalized with ℓ_m.

gives the dilutions scaled with ℓ_b, and can be more easily applied to jets with significant buoyancy than Fig. 6.4 which is scaled with ℓ_m.

The figures discussed above can also be used to estimate the trajectories and dilutions of buoyant jets in a stratified crossflow up to the point of the maximum height of rise. The maximum height of rise can be estimated from Fig. 6.5 which is a presentation of the experimental results in a form similar to Fig. 3.7, with the additional consideration of the effect of the initial jet volume flux. A similar figure scaled with the length scale ℓ_m could be developed for this case, but Fig. 6.5 adequately describes all of the experimental results and the alternate presentation is not displayed. A similar presentation of the results from the measurements of equilibrium heights of rise is given in Fig. 6.6. The experimental results used to develop these figures are summarized in Table 5.3.

The general procedure for the use of Figs. 6.1-6.6 is as follows:

Compute the flux variable;

$$\text{Discharge} \quad Q = \frac{\pi}{4} D^2 V_j$$

$$\text{Momentum} \quad M = QV_j$$

$$\text{Buoyancy} \quad B = g \frac{\Delta\rho}{\rho_o} Q$$

The computation of the buoyancy flux for cases where the density difference is caused by temperature effects is performed by relating the temperature difference to the density difference as in Eq. 2.8

$$\frac{\Delta\rho}{\rho_o} = k_1 (T_j - T_o)$$

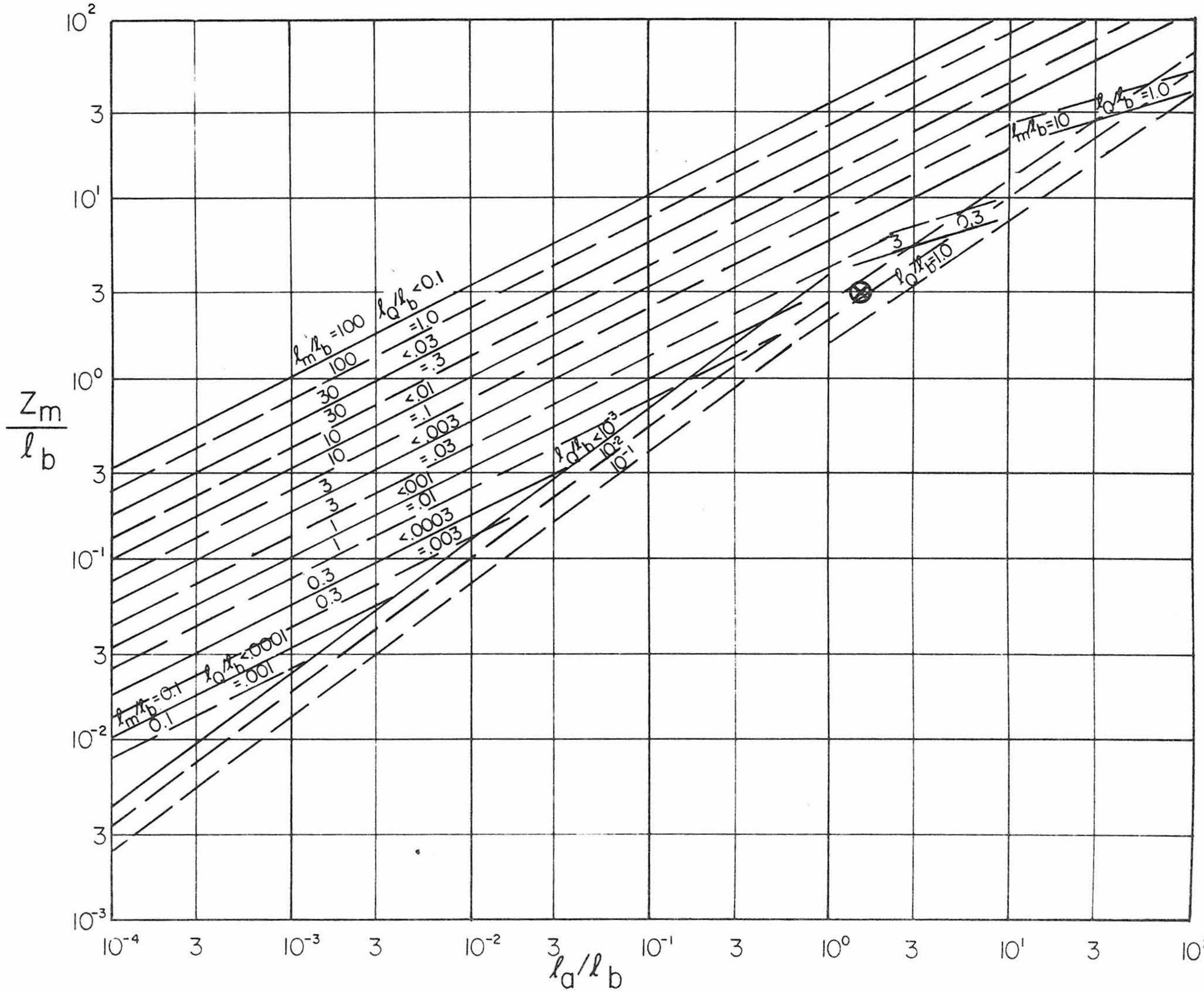

Fig. 6.5 Maximum heights of rise for buoyant jets in a stratified crossflow.

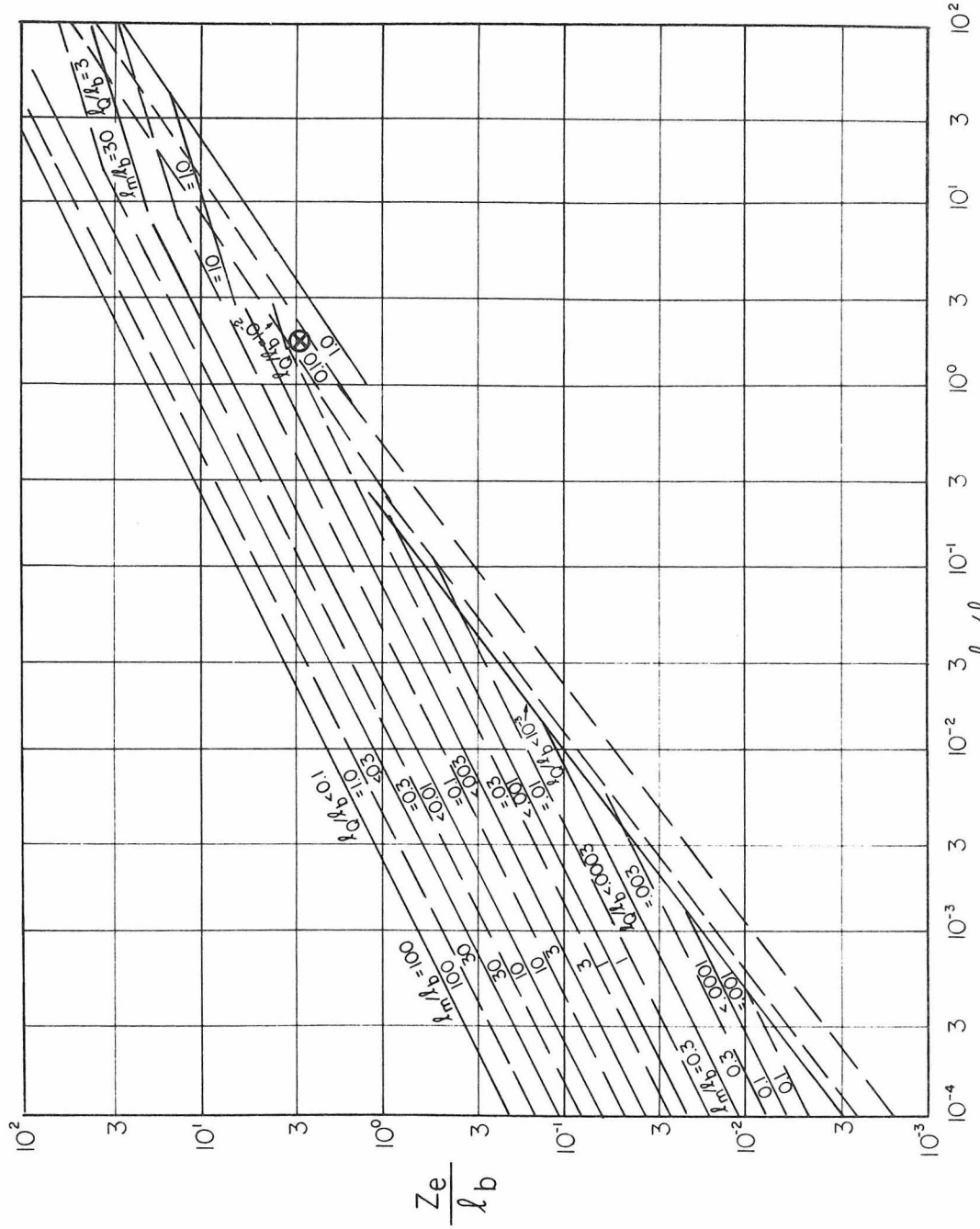

Fig. 6.6 Equilibrium heights of rise for buoyant jets in a stratified crossflow.

where T_j is the temperature of the jet discharge, k_1 is the appropriate thermal expansion coefficient, and ρ_o and T_o refer to the ambient conditions at the elevation of the jet discharge.

Compute the flow variables;

U_A (measured)

$$\varepsilon = \frac{-g}{\rho_o} \frac{d\rho_a}{dz}$$

In the atmosphere, the stratification parameter should be expressed in terms of the potential temperature gradient $\frac{d\theta_a}{dz}$;

$$\varepsilon = \frac{g}{T_o} \frac{d\theta_a}{dz}$$

Compute the magnitude of the various length scales;

$$\ell_Q = Q/M^{1/2} = \sqrt{\pi/4}\, D$$

$$\ell_m = M^{1/2}/U_A$$

$$\ell_b = B/U_A^3$$

$$\ell_a = U_A/\varepsilon^{1/2}$$

Further calculations depend upon the information desired. Figs. 6.1-6.6 present the different types of information as a function of the length scales computed above. The relevant non-dimensional ratios are calculated and the appropriate figure is consulted to estimate the parameter of interest. These figures can be used to easily obtain estimates of buoyant jet behavior if the results are only desired to

within about 15%. Otherwise, the basic data summarized in Tables 5.1-5.3 should be consulted. The use of the figures can best be demonstrated with a sample calculation. Consider the following conditions:

> A discharge of 0.5 m^3/sec from a 0.5 m port is released into the ocean. The discharge is essentially fresh water, therefore $\frac{\Delta\rho}{\rho_o}$ is approximately 0.025. The current speed is 0.025 m/sec and the ambient density difference over 50 m depth, $\frac{\Delta\rho_a}{\rho_o}$ is 0.002.

The flow variables are first computed:

$$Q = 0.5 \text{ m}^3/\text{sec}$$

$$M = QV_j = Q^2/A = 1.27 \text{ m}^4\text{sec}^{-2}$$

$$B = g'Q = g\frac{\Delta\rho}{\rho_o}Q = .123 \text{ m}^4\text{sec}^{-3}$$

$$U_A = 0.25 \text{ m/sec}$$

$$\varepsilon = \frac{-g}{\rho}\frac{d\rho_a}{dz} = g\frac{\Delta\rho_a}{\rho_o \Delta z} = 3.9 \times 10^{-4}$$

The various length scales are calculated:

$$\ell_Q = \sqrt{\pi/4}\, D = .44 \text{ m}$$

$$\ell_m = M^{1/2}/U_A = 5.1 \text{ m}$$

$$\ell_b = B/U_A^3 = 7.9 \text{ m}$$

$$\ell_a = U_A/\varepsilon^{1/2} = 12.6 \text{ m}$$

$$\frac{\ell_Q}{\ell_b} = 0.056 \quad \frac{\ell_a}{\ell_b} = 1.60 \quad \frac{\ell_m}{\ell_b} = 0.65$$

The maximum height of rise can be estimated from Fig. 6.5 for the given values of $\frac{\ell_a}{\ell_b}$ and $\frac{\ell_Q}{\ell_b}$. The estimate from the figure is $\frac{Z_m}{\ell_b} \approx 3.0$ (marked with an ⊗ in Fig. 6.5). The flow corresponds to the buoyancy-dominated far-field, but is near to the transition from the momentum-dominated far-field. The maximum height of rise of approximately 24 m can be compared to the result indicated for the bdff in Fig. 5.39 for the given values of the flow variables. The estimated maximum height of rise from Fig. 5.39 is on the order of 25 m.

The dilution for this case is estimated from Fig. 6.3 for $\frac{\ell_m}{\ell_b} = 0.65$ and $\frac{z}{\ell_b} \approx 3.0$. The point marked with an ⊗ on the figure is $\frac{S_o Q}{U_A \ell_b^2} \approx 3.6$ which indicates a characteristic minimum dilution of 112 on the jet axis. The equilibrium height of rise is estimated from Fig. 6.6. For the appropriate values of $\frac{\ell_Q}{\ell_b}$ and $\frac{\ell_a}{\ell_b}$, the estimated value of $\frac{Z_e}{\ell_b}$ is 2.8 (indicated with an ⊗ in Fig. 6.6) yielding an equilibrium height of rise of approximately 22 m. The horizontal location of Z_m can be determined from Fig. 6.1 as approximately 26 m downstream from the source for the given flow variables. (This point is approximately indicated in the figure.) This compares with the value of 23 m obtained from the trajectory coefficient indicated in Fig. 5.19 for the flow conditions indicated.

6.2 Comparison of Experimental Results to Previous Studies

There have been several previous experimental investigations to which certain portions of the data obtained in this study can be compared. The comparisons will be made for each flow regime (the mdnf, mdff, bdnf, and the bdff) separately. Experimental results for both unstratified and stratified flow measurements will be presented, if available. An important consideration is that the initial volume flux must be considered in any comparison since it was established that this would influence the values of the various trajectory coefficients. Experimental results of others can only be compared with the present investigation for values of ℓ_Q/ℓ_m (for momentum-dominated flow) or ℓ_Q/ℓ_b (for buoyancy-dominated flow) that are comparable with the range of values examined in this study. There have been no major experimental investigations of jet dilutions other than that by Fan (1967), so the following comparisons are for trajectories and heights of rise.

6.2.1 The Momentum-Dominated Near-Field

The value of the trajectory coefficient C_1 defined by

$$\frac{z}{\ell_m} = C_1\left(\frac{x}{\ell_m}\right)^{1/2}$$

can be estimated from the experimental results for a nonbuoyant jet in a stagnant ambient fluid presented by Albertson, et al. (1950). Their experimental observation of the variation of the maximum jet velocity beyond the zone of flow establishment is

$$V_{max} = 7.0\,\frac{M^{1/2}}{z}$$

The average jet velocity can be computed over a jet cross-section by assuming that the velocity profile is given by a Gaussian distribution:

$$\overline{V} = \frac{\int y^2 dA}{\int V dA} = \frac{V_{max}}{2} = 3.5 \frac{M^{1/2}}{z}$$

This can be substituted directly into the kinematic relation in Eq. 3.5 and integrated. The resulting value for the coefficient C_1 is

$$C_1 = \sqrt{2(3.5)} = 2.65$$

This value should be compared with the experimental results in Fig. 5.16 since it is likely that the position of maximum jet velocity should also correspond to the position of maximum concentration. The value of 2.65 corresponding to the limiting case of $\ell_Q/\ell_m = U_A/V_j = 0$ compares favorably with the extrapolated value of approximately 2.5 for small values of ℓ_Q/ℓ_m.

Measurements of the maximum height of rise in the momentum-dominated near-field can also be compared with three experiments by Fan (1967) for momentum-driven jets in a stagnant stratified fluid. The results of these three experiments would indicate an average value of 3.27 for the coefficient C_9 which is defined by

$$z_m/\ell_m = C_9 \, (\ell_a/\ell_m)^{1/2}$$

in the limit as $\ell_Q/\ell_m \to 0$. This compares with the value of approximately 3.0 determined for the lowest value of ℓ_Q/ℓ_m (0.0036) examined in the

present investigation. Fan's heights of rise were determined visually from photographs and his definition of Z_m may not correspond directly to that used in this study (Z_m is the location of the concentration maximum C_m).

There have been several studies of nonbuoyant jets in an unstratified crossflow. Hoult and Weil (1972) summarize the results of several experimental investigations including those of Keffer and Baines (1963) and Jordinson (1956) which considered several values of ℓ_Q/ℓ_m. Those data were determined from the examination of photographs taken of the jet flows and should correspond to the data of the present study in Fig. 5.5 and 5.8. The apparent values of the coefficient C_1 from the data of Keffer and Baines and Jordinson are plotted in Fig. 6.7 as a function of ℓ_Q/ℓ_m. The variation of the trajectory coefficient is approximately the same as that observed in this study. Hoult and Weil (1972) explained this variation of the data as caused by a wake from the discharge structure or nonuniform crossflow velocity, but the present results indicate that this variation is probably due to the effect of the initial volume flux. So far as this writer is aware, there have been no measurements of the maximum height of rise in a stratified crossflow that would correspond to the momentum-dominated near-field regime.

6.2.2 The Buoyancy-Dominated Near-Field

Although no experiments corresponding to the buoyancy-dominated near-field have been performed for buoyant jets in a crossflow to the best of this writer's knowledge, experimental results for

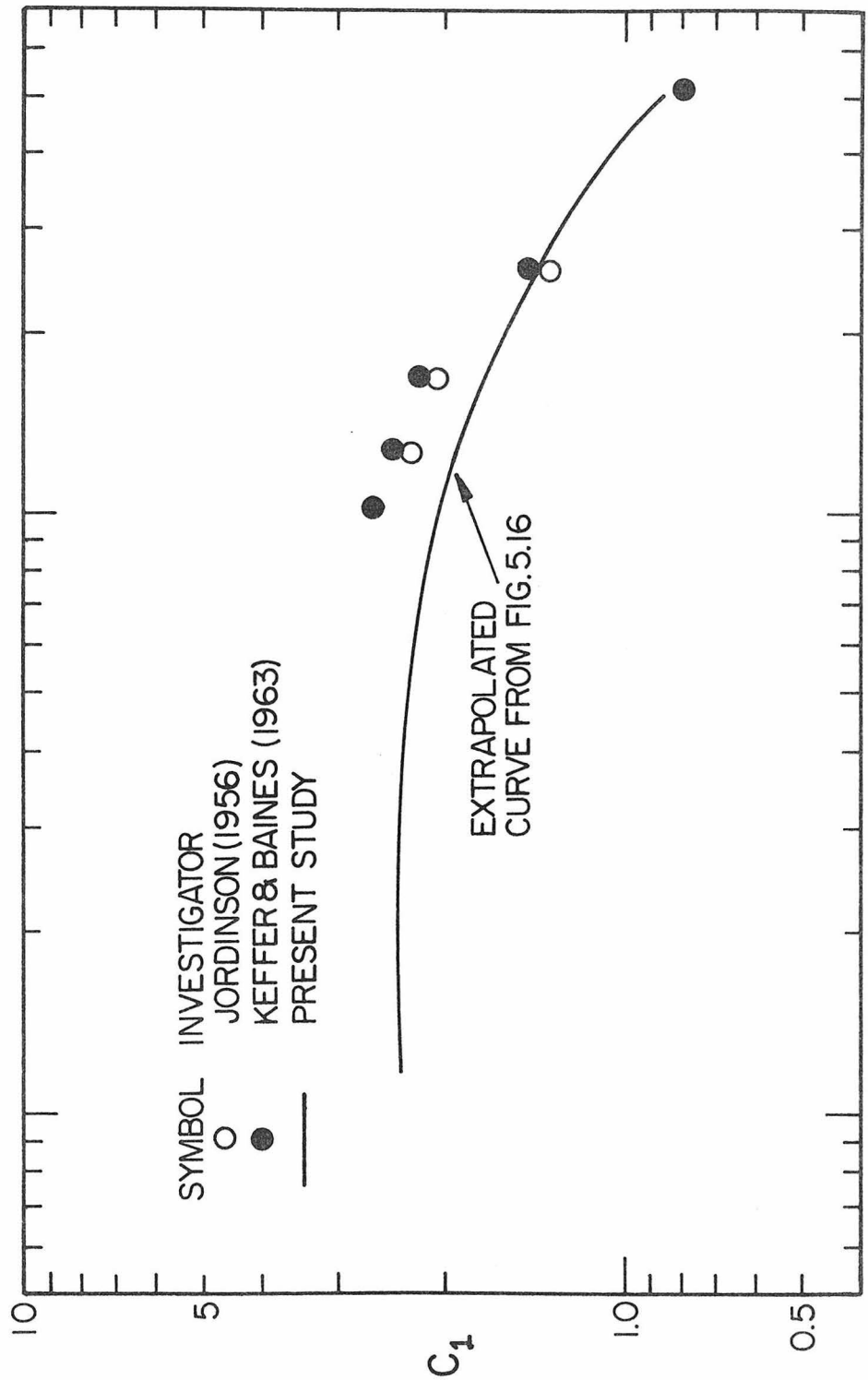

Fig. 6.7 Comparison of momentum-dominated near-field trajectories measured by Keffer and Baines (1963) and Jordinson (1956) with the present results.

buoyant plumes in a stagnant fluid can be compared to the present data. The experimental study of Rouse, et al. (1952) presents the maximum velocity variation for a buoyant plume in an unstratified fluid:

$$V_{max} = 4.7\left(\frac{B}{z}\right)^{1/3}$$

The average velocity will again be one-half the maximum velocity if the velocity profiles are assumed to be Gaussian in form as was indicated by the experimental results of Rouse. Substitution of the relation for the average velocity into the kinematic relation indicates that the constant C_5 is given by:

$$C_5 = \left(\frac{2}{3}\,(4.7)\right)^{3/4} = 2.36$$

where C_5 is defined by the relation

$$\frac{z}{\ell_b} = C_5\left(\frac{x}{\ell_b}\right)^{3/4}$$

This value should be the limiting value of C_5 as $\ell_Q/\ell_b \to 0$ in Fig. 5.18 for the same reasons as discussed for momentum-dominated flow. Although the maximum value for C_5 was measured to be only 1.8, extrapolation indicates a value of approximately 2.3 for ℓ_Q/ℓ_b less than about 10^{-3}, which agrees with the limiting value predicted from the simple plume results of Rouse, et al.

Similar results for the maximum height of rise of a buoyant plume in a stagnant stratified flow can be compared to the present data.

Briggs (1969) summarizes the experiments of Morton, et al. (1956), Crawford and Leonard (1962) and some large-scale field measurements with an approximate value for the height of rise relation:

$$\frac{z_m}{\ell_b} = 3.76 \left(\frac{\ell_a}{\ell_b} \right)^{3/4}$$

This value for the coefficient C_{11} agrees almost exactly with the value of 3.74 for the experiments in the present study for $\ell_Q/\ell_b \approx 0.003$. Thus, experimental results for the case of a stagnant ambient fluid agree very well with the experimental results from this study with very small values of ℓ_Q.

6.2.3 The Momentum-Dominated Far-Field

The only experimental results that correspond to the momentum-dominated far-field are several determinations of jet trajectories, primarily from photographs by Chu and Goldberg (1974), Pratte and Baines (1967) and others. These sets of experiments can be compared to the present data in Figs. 5.5 and 5.9, as these results were also from the examination of photographs.

Chu and Goldberg present a value of 1.44 for the coefficient C_2 defined by

$$\frac{z}{\ell_m} = C_2 \left(\frac{x}{\ell_m} \right)^{1/3}$$

from the results of their photographic study. Their experiments were performed for values of ℓ_Q/ℓ_m between 0.02 and 0.12. For the

present study, Fig. 5.9 indicates values of the coefficient between 1.3 and 1.6 for the same range of ℓ_Q/ℓ_m. The two studies thus indicate equivalent results as the range of ℓ_Q/ℓ_m values was probably insufficient for Chu and Goldberg to observe the ℓ_Q dependence.

Chan, et al. (1976) present a value of $C_2 = 1.5$ to best describe similar experiments by Pratte and Baines (1967) which were for ℓ_Q/ℓ_m between 0.03 and 0.2. Since this range of variables is slightly larger than for the Chu and Goldberg study, a slightly higher value of C_2 would be expected on the basis of the data in Fig. 5.9. This is the case and these experimental results also agree quite well with the present experiments.

There are apparently no measurements for the maximum height of rise of a nonbuoyant jet in a stratified fluid corresponding to the far-field case. Thus, no direct comparisons of the present experimental results for this case can be compared.

6.2.4 The Buoyancy-Dominated Far-Field

There have been several experimental studies for buoyant jet trajectories in the buoyancy-dominated far-field and some additional measurements of maximum height of rise. These can be compared directly to the results from the present experimental investigation.

The study by Hewett, et al. (1971) presents the trajectories for heated air plumes and plumes of a mixture of helium and air in a stratified crossflow. All of these experiments were for conditions where $\ell_m/\ell_b = 2.3$ and $\ell_Q/\ell_b = 1.1$. Hewett's data can be compared with the present unstratified trajectory results since it was

demonstrated in Chapter 5 that the trajectory in a stratified flow would be equivalent up to the maximum height of rise. The value for the trajectory coefficient C_6 defined by

$$\frac{z}{\ell_b} = C_6 \left(\frac{x}{\ell_b} \right)^{2/3}$$

that was determined by Hewett was 0.98 for the definition of the length scale ℓ_b corresponding to that used in this investigation. This agrees almost exactly with the value of 1.0 that is extrapolated from Fig. 5.19 for the same conditions. Since Hewett defined the trajectory as the location of the temperature maximum above ambient levels in the vertical plane of jet symmetry, the appropriate comparison is to the data in Fig. 5.19 for which the trajectories were determined from maximum dye concentrations in the same plane.

Hoult and Weil (1972) have compiled the results of several experimental investigations including those by Vadot (1965) and Barilla (1968) which were each for several experiments at different values of ℓ_m/ℓ_b and ℓ_Q/ℓ_b. These investigations measured jet trajectories from photographs taken of the flow pattern, which indicates that the results in Figs. 5.11 and 5.12 should be compared with these data. The experimental results from the studies from Vadot and Barilla are indicated in Fig. 6.8. The apparent values of the trajectory coefficient C_6 for the different experiments are indicated on the figure along with the approximate results from the present study. Lines of constant values of C_6 indicated from the present study are indicated on the figure and the

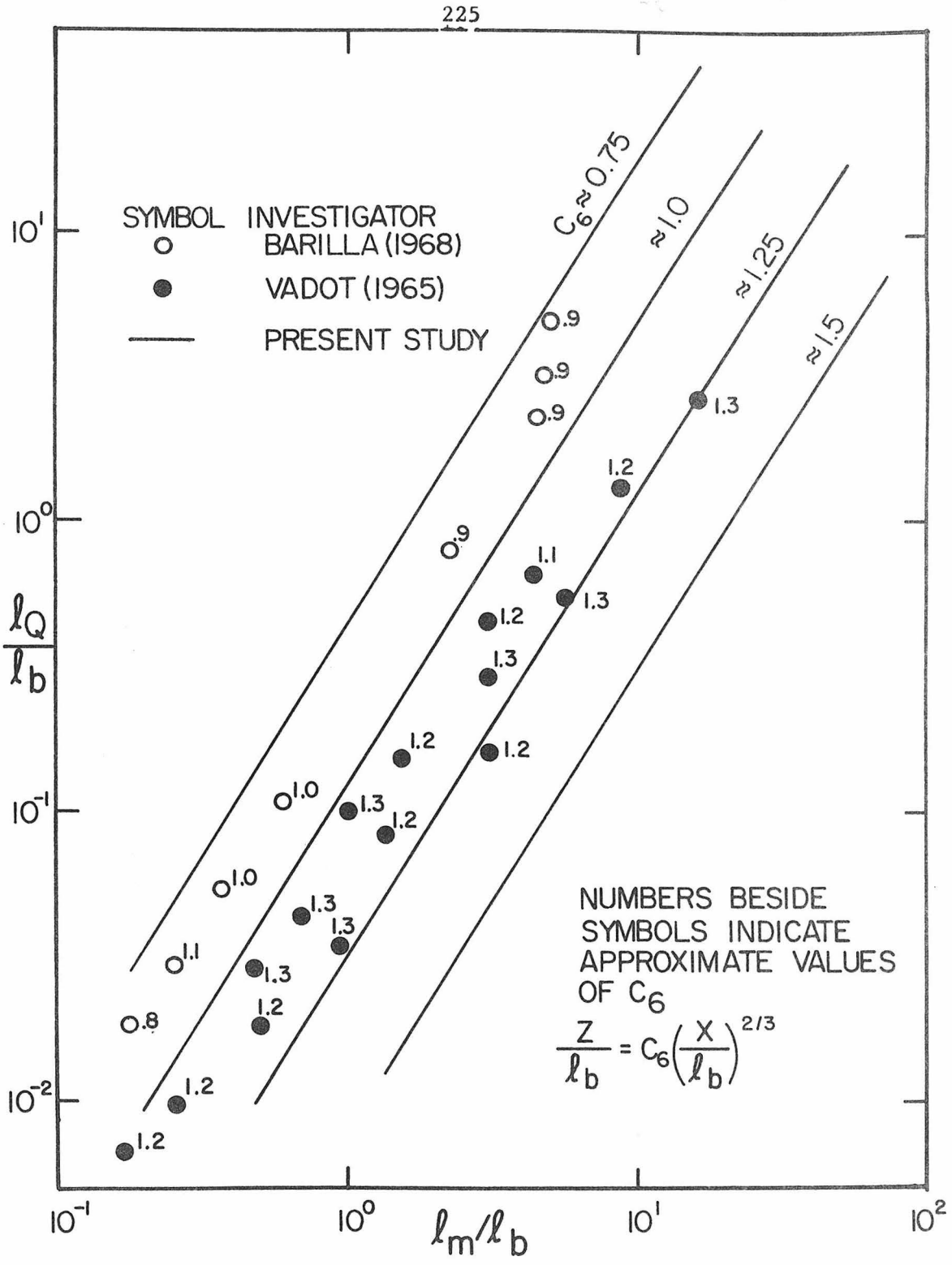

Fig. 6.8 Comparison of buoyancy-dominated far-field trajectories measured by Vadot (1965) and Barilla (1968) with the present results.

experiments of Vadot and Barilla are labeled as to the approximate values of the coefficient. The general trend of the data is in fairly good agreement with the present results and indicates that each of these experimental investigations was conducted such that the values of ℓ_m/ℓ_b and ℓ_Q/ℓ_b fall nearly along lines of constant C_6.

The measurements by Hewett, et al. (1971) described above were made in a stratified crossflow and maximum heights of rise were also measured. However, these results do not correspond to the range of ℓ_Q/ℓ_b (0.02-0.5) covered for the present measurements of maximum height of rise and cannot be compared directly. The maximum height of rise measured by Hewett was determined to follow the relation

$$\frac{Z_m}{\ell_b} = 1.7\left(\frac{\ell_a}{\ell_b}\right)^{2/3}$$

The value of 1.7 for the coefficient C_{12} is slightly greater than the value of 1.5 measured for the greatest value of ℓ_Q/ℓ_b (0.5) examined in this study which would indicate that the present data indicate slightly lower heights of rise. This apparently is due to the fact that Hewett studied a higher value of ℓ_m/ℓ_b (2.3) than the range considered in the present study (0.5 to 1.4). The possibility of a higher value of the coefficient C_{12} for larger values of ℓ_m/ℓ_b is clearly suggested by the trajectory data in Figs. 5.11 and 5.19.

The results from several sets of field measurements by the TVA (1968), Bringfelt (1968), and others also cannot be directly compared to the present experimental results because the range of values of

ℓ_m/ℓ_b and ℓ_Q/ℓ_b do not entirely correspond to the experimental conditions in the present study. There is also a considerable amount of scatter in the data from the field measurements due to the difficulty in accurately defining experimental variables. The field measurements presented by Bringfelt correspond most directly to the present experiments. Shwartz and Tulin (1972) have analyzed several of these experiments (with $\ell_Q/\ell_b \approx$ 0.5-5.0 and $\ell_m/\ell_b \approx$ 1.0-10.0) and have concluded that the appropriate value of the height of rise constant is 1.6. This would agree fairly closely with the experimental value of approximately 1.5 observed for the experiments in the present study that correspond to these ranges of parameters. Experimental measurements need to be performed with larger crossflow velocities to cover the typical range of variables observed at many industrial chimneys. However, the experimental technique in the present study prevented the examination of larger crossflow velocities in the measurements of maximum heights of rise. This was primarily due to the difficulties associated with the limited sampling times discussed previously.

6.3 Entrainment Relations

The results from the experimental investigation can be interpreted along with the analysis in Chapter 3 to make some general observations regarding the integral solution method and the associated entrainment relation. Since some of the models proposed by other researchers agree qualitatively with portions of the present analysis, their entrainment functions can be viewed as adequate to predict the

corresponding asymptotic solution. These entrainment relations can then be interpreted in light of the experimental results.

All models proposed by other researchers which predict closed form solutions agreeing with one of the asymptotic solutions in the present analysis indicate the following entrainment relation E (defined previously in Eq. 2.31):

$$\frac{d}{ds}\left[U_A \cos\theta + u_s)R^2\right] \equiv E = \alpha VR$$

Here V is the local characteristic vertical jet velocity, R is the characteristic radius and α is the entrainment coefficient. This form of the entrainment relation can be anticipated from the present description of buoyant jet flows since the flow descriptions used to develop the asymptotic models (jet or plume in a stagnant fluid for near-field flows and puff or thermal for far-field flows) consider motion only in the vertical direction. There is, however, a substantial difference between the near- and far-field cases in that the vertical velocity V is parallel to the jet axis in the near-field while it is perpendicular to the jet axis in the far-field. Thus, it would appear that a general entrainment relation that would predict all of the present asymptotic models should be composed of a term that corresponds to motion parallel to the jet axis and another component perpendicular to the jet axis. Abraham (1971), Hewett, et al. (1971), and others, propose entrainment relations of this type.

There is an additional consideration that is suggested by the present analysis. Fox (1970), List and Imberger (1973), and others

have indicated that there is not a single entrainment coefficient α that is valid for general buoyant jets in a stagnant ambient fluid. This is physically reasonable when the general problem is viewed from the standpoint of the limiting cases of a pure jet or a pure plume in a stagnant fluid. In these two cases, there is clearly a different mechanism generating the turbulence (the initial momentum for a nonbuoyant jet and the buoyancy for a plume) and hence regulating the entrainment. Thus, an entrainment relation similar to that proposed by Fox (1970) (given in Eq. 2.27)

$$E = (\alpha_1 + \alpha_2/F_\ell^2)VR$$

would be expected to be more nearly correct than a single entrainment coefficient. The same reasoning can be applied to the case of a buoyant jet in a crossflow. Since there are four different asymptotic solutions suggested by the present analysis, it would seem reasonable that there should be independent mechanisms regulating the entrainment of ambient fluid in each limiting case. Thus, an entrainment relation capable of describing the entrainment of a general buoyant jet in a crossflow should reduce to four limiting entrainment coefficients, much as Fox's entrainment relation involves two limiting coefficients.

An additional complication is due to the fact that the asymptotic flow descriptions are only approximately correct for a general buoyant jet. This is readily apparent from the experimental results which indicate that the various trajectory and height of rise coefficients depend upon the initial volume flux. The same observation must

therefore hold for an entrainment coefficient. It is instructive to consider a typical closed form solution of the integral equations. Slawson and Csanady (1967) assume an entrainment relation of the form:

$$E = 2\alpha VR$$

They make additional assumptions that make their solution correspond to a buoyant plume in the far field. Their resulting trajectory relation, assuming that α is constant, is

$$\frac{z}{\ell_b} = \left(\frac{3}{2\alpha^2}\right)^{1/3} \left(\frac{x}{\ell_b}\right)^{2/3}$$

Thus, the trajectory coefficient C_6 is related to α by

$$C_6 = \left(\frac{3}{2\alpha^2}\right)^{1/3}$$

However, the dimensional analysis in Eq. 5.1 and the experimental results in Figs. 5.11 and 5.12 imply that

$$C_6 = f\left(\frac{\ell_Q}{\ell_b}, \frac{\ell_m}{\ell_b}\right)$$

and therefore, that the coefficient α describing the entrainment in the buoyancy-dominated far-field is a function of the same variables. The same type of argument can be applied to any other entrainment coefficient which is used to determine a closed form solution corresponding to one of the present asymptotic models.

These considerations indicate the difficulty of using the integral

approach for solving the general problem of a buoyant jet in a crossflow. The difficulty of defining a conceptually correct entrainment relation poses a fundamental restriction in obtaining exact solutions to the integrated equations. While the models proposed by some researchers may be sufficiently accurate to be used for design purposes, none of the closed form solutions that have been proposed are adequate to describe the results of the present experimental investigation.

6.4 Suggestions for Future Research

There are several areas where further research is indicated in order to extend the present results for general application. The objective of this investigation was to develop a sufficient understanding of a buoyant jet in a stratified crossflow such that adequate predictions of jet behavior could be obtained for actual design problems. There are several phenomena associated with buoyant jets in a crossflow that have not been resolved by this investigation.

A major area requiring study is the effect of the ambient turbulence on the buoyant jet behavior. The self-generated turbulence within the jet decays along its trajectory and will ultimately become sufficiently small that the level of turbulence will be of the same order as the ambient turbulence. The model developed in this study will no longer accurately describe the flow behavior beyond this point. The present experiments were conducted in a towing tank and there was no ambient turbulence. Fan (1967) made similar towed jet experiments and experiments for a stationary jet in an actual crossflow and found no apparent differences in the jet behavior over trajectory distances greater than

those considered in this study. It appears likely that the effect of the ambient turbulence can be considered in the sense of a limiting case where the diffusion is essentially equivalent to that of a continuous source released into a field of ambient turbulence. This problem has been studied extensively, so it may only be necessary to examine the decay of the jet turbulence in order to obtain an estimate of the transition behavior to flow dominated by the ambient turbulence.

Another area of indicated research is the study of the concentration profiles over the entire jet cross-section. Fan (1967) noted that the points of maximum relative concentration at any cross-section along the jet trajectory occur to either side of the plane of symmetry of the jet. The average concentration peaks were on the order of one-and-a-half to two times the maximum concentration on the jet centerline plane. The location and values of these minimum dilutions need to be determined experimentally as the absolute minimum dilutions may be of more interest in engineering applications.

Another consideration is that some jet discharges, such as those from sewage outfall diffusers, are often released horizontally. This is a substantially different problem than a vertical jet discharge, particularly when the exit momentum is significant. The presence of horizontal momentum instead of vertical momentum will result in greater distances of travel for a given vertical rise and hence greater dilutions than for a vertically discharged jet. Also, the angle of the discharge with respect to the direction of the ambient flow becomes an additional parameter that must be considered, so the overall problem is more complicated.

The jet behavior beyond the point of the maximum height of rise in a stratified fluid needs to be studied further. Although the present experimental results are adequate to predict the final equilibrium height of rise, the flow behavior between the maximum rise and that point was not studied in detail. The general jet behavior in this region is substantial spreading in the horizontal plane and a decrease in the vertical extent of the jet fluid. A better understanding of this behavior would be helpful in predicting the horizontal spread of a contaminant in the jet discharge.

Finally, it may be desirable to perform additional experiments which more nearly model the conditions observed for the rise of smoke plumes from industrial chimneys. Some of these jet discharges have relatively greater mass fluxes than most of the experiments performed in this investigation. Typical values for the ratio ℓ_Q/ℓ_b for the field measurements by the TVA (1968) for plume discharges from large power plants were in the range of approximately 1-1000 and corresponding values for ℓ_m/ℓ_b were in the range of 1-100. These are somewhat larger values for both ratios than considered in this experimental study, particularly for that portion of the investigation involving the measurement of maximum heights of rise. It is therefore suggested that additional experiments be performed to model these conditions, which were beyond the capability of the present experimental setup.

CHAPTER 7

SUMMARY AND CONCLUSIONS

The objective of this study was to obtain a fundamental understanding of the effects of ambient crossflows and density stratification on the time-average behavior of buoyant jets. Round, vertically discharged, turbulent jets were considered in this investigation. The jet characteristics of interest include jet trajectories and dilutions of a passive tracer present in the jet discharge. Additional characteristics of interest in a stratified crossflow are the maximum and equilibrium heights of jet rise.

Most previous investigations have considered the integrated equations for the conservation of mass, momentum, and buoyancy. The solution to these integral equations requires the specification of an assumed relation for the entrainment of ambient fluid by the jet. Since the nature of this entrainment is not physically intuitive for complex jet flows, an objective of this study was to develop an alternate approach to the solution of the general problem.

A theoretical model, based primarily on dimensional reasoning, was developed to predict jet trajectories and other mean flow characteristics. The buoyant jet behavior was analyzed by making analogies to less complex flows whose behavior is better understood. These simplified flow descriptions can be regarded as the asymptotic behavior of a buoyant jet as various effects become dominant in controlling the flow behavior. The asymptotic solutions consider the behavior of the jet to be

controlled either by the jet momentum or the buoyancy for two possible situations; either the crossflow velocity becomes very large or it approaches zero.

The various asymptotic solutions for jet trajectories and dilutions in an unstratified crossflow are summarized in Table 3.2. Similar solutions for the height of rise for a buoyant jet in a stratified crossflow and the associated characteristic dilution are presented in Table 3.3. The trajectory and dilution for a jet up to the point of maximum height of rise is assumed to be essentially the same as for a similar jet in an unstratified flow.

Portions of the general flow description developed from these asymptotic solutions can be shown to correspond to the theoretical predictions of other researchers. These other solutions were generally developed from the integral analysis, and the form of the entrainment relation and other assumptions required to obtain closed form solutions limit their applicability. Since most of these solutions can be regarded as special cases of the general flow description developed in this investigation, the analysis provides a framework for interpreting previous investigations. This also serves to clarify the differences between the solutions proposed by other researchers.

The experimental study was conducted to verify the results of the analysis and to provide a detailed examination of the effects of the various jet and ambient flow variables. The verification of the models presented in the analysis was accomplished by the experimental investigation except that the values of the various coefficients in

Tables 3.2 and 3.3 were shown to be dependent upon the initial jet volume flux. This effect, which was neglected in the analysis as being of secondary importance, can be anticipated from dimensional reasoning and can be considered as a relatively minor adjustment to the basic flow description. An additional observation was that the trajectory coefficient for the buoyancy-dominated far-field model is also dependent upon the initial jet momentum flux; an effect which also can be anticipated from dimensional reasoning.

The experimental results for an unstratified crossflow have been summarized in Table 5.1 for jet trajectories and in Table 5.2 for dilutions. Experimental results from the measurements of maximum and equilibrium heights of rise in a stratified crossflow are presented in Table 5.3, while the measurements of jet dilutions at the maximum height of rise are given in Figs. 5.40 and 5.41. Measurements of the characteristics of the turbulent concentration fluctuations are described in Section 5.2.4 along with the results from a few experiments to determine the further dilution of a buoyant jet in a stratified fluid downstream from the point of its maximum height of rise.

The results from the experimental investigation are presented in a unified manner in Section 6.1. This presentation is based upon the theoretical considerations developed in Chapter 3, and provides a useful means for examining the combined effects of up to five independent variables in defining the mean flow characteristics. This unified presentation also facilitates the application of the experimental results to design situations.

The presentation in Section 6.1 can be used to estimate the trajectories and dilutions of a buoyant jet in an unstratified crossflow up to the point where the ambient turbulence begins to control the jet behavior. Figs. 6.1-6.4 indicate the general results of the experimental investigation. Fig. 6.1 can be used to estimate the trajectory of a jet with significant buoyancy, while the trajectory of a jet with very little buoyancy can be more easily determined from Fig. 6.2. Characteristic minimum dilutions on the jet centerline can be obtained from Figs. 6.3 or 6.4.

Trajectories and dilutions for a buoyant jet in a stratified crossflow can be estimated up to the maximum height of rise from these same figures. Estimates of the maximum and equilibrium heights of rise for a general buoyant jet can be obtained from Figs. 6.5 and 6.6 respectively.

The results of this investigation can be applied to problems commonly encountered in the design of pollutant dispersion structures. The primary application would be for single point discharges such as hot gases from industrial processes, cooling tower plumes, or discharges into lakes or oceans. Although the model conditions in the experimental study may not correspond to the jet and ambient conditions encountered for all of these types of discharges, this investigation has considered a wider range of variables than any previous study.

REFERENCES

Abraham, G. (1965), "Entrainment Principle and Its Restriction to Solve Problems of Jets," J. Hydr. Res., Vol. 3(2), pp. 1-23.

Abraham, G. (1971), "The Flow of Round Buoyant Jets Issuing Vertically into Ambient Fluid Flowing in a Horizontal Direction," Delft Hydraulics Laboratory, Delft, Netherlands, Report No. 81, 7 pp.

Abraham, G. and Eysink, W. D. (1969), "Jets Issuing into Fluid with a Density Gradient," J. Hydr. Res., Vol. 7(2), pp. 145-175.

Abramovich, G. N. (1963), "The Theory of Turbulent Jets," Translation by Scripta Technica, MIT Press, Cambridge, Massachusetts.

Albertson, M. L., Dai, Y. B., Jensen, R. A., and Rouse, H. (1950), "Diffusion of Submerged Jets," Trans. ASCE, Vol. 115, pp. 639-647.

Barilla, P. A. (1968), "Dependence of Entrainment Coefficients upon Orifice Conditions in Model Studies of a Smoke Plume in a Laminar Cross Wind," S.M. Thesis, Massachusetts Institute of Technology, Cambridge, Massachusetts.

Batchelor, G. K. (1954), "Heat Convection and Buoyancy Effects in Fluids," Quarterly J. Roy. Meteor. Soc., Vol. 80, pp. 339-358.

Briggs, G. A. (1969), Plume Rise, U.S. Atomic Energy Commission, Division of Technical Information, Oak Ridge, Tennessee.

Bringfelt, B. (1968), "Plume Rise Measurements at Industrial Chimneys," Atmospheric Environment, Vol. 2, pp. 575-598.

Cannon, J. B. (1974), "Convective Flows under Conditions Applicable to Fires in High Rise Buildings," Ph.D. Thesis, California Institute of Technology, Pasadena, California.

Chan, T.-L. and Kennedy, J. F. (1972), "Turbulent Nonbuoyant or Buoyant Jets Discharged into Flowing or Quiescent Fluids," Iowa Institute of Hydraulic Research, Report No. 140, The University of Iowa, Iowa City, Iowa.

Chan, T.-L., Lin, J.-T. and Kennedy, J. F. (1976), "Entrainment and Drag Forces of Deflected Jets," J. Hydr. Div., ASCE, Vol. 102, HY5, pp. 615-635.

Chu, V. H. and Goldberg, M. B. (1974), "Buoyant Forced-Plumes in Cross Flow," J. Hydr. Div., ASCE, Vol. 100, HY9, pp. 1203-1213.

Crawford, T. V. and Leonard, A. S. (1962), "Observations of Buoyant Plumes in Calm, Stably Stratified Air," J. Appl. Meteor., Vol. 1, pp. 251-256.

Fan, L.-N. (1967), "Turbulent Buoyant Jets into Stratified or Flowing Ambient Fluids," W. M. Keck Laboratory of Hydraulics and Water Resources, Report No. KH-R-15, California Institute of Technology, Pasadena, California.

Fan, L.-N. and Brooks, N. H. (1969), "Numerical Solutions of Turbulent Buoyant Jet Problems," W. M. Keck Laboratory of Hydraulics and Water Resources, Report No. KH-R-18, California Institute of Technology, Pasadena, California.

Fay, J. A., Escudier, M. and Hoult, D. P. (1970), "A Correlation of Field Observations of Plume Rise," J. Air Poll. Control Assoc., Vol. 20, No. 6, pp. 391-397.

Fox, D. G. (1970), "Forced Plume in a Stratified Fluid," J. Geophys. Res., Vol. 75, No. 33, pp. 6818-6835.

Gordier, R. L. (1959), "Studies on Fluid Jets Discharging Normally into Moving Liquid," St. Anthony Falls Hydraulics Laboratory, Technical Paper No. 28, Series B, The University of Minnesota, Minneapolis, Minnesota.

Hewett, T. A., Fay, J. A., and Hoult, D. P. (1971), "Laboratory Experiments of Smokestack Plumes in a Stable Atmosphere," Atmos. Environ., Vol. 5, pp. 767-789.

Hirst, E. A. (1971a), "Analysis of Round, Turbulent, Buoyant Jets Discharged to Flowing Stratified Ambients," Oak Ridge National Laboratory, Report No. ORNL-4685.

Hirst, E. A. (1971b), "Buoyant Jets Discharged to Quiescent Stratified Ambients," J. Geophys. Res., Vol. 76, No. 30, pp. 7375-7383.

Hoult, D. P., Fay, J. A. and Forney, L. J. (1969), "A Theory of Plume Rise Compared with Field Observations," J. Air Poll. Control Assoc., Vol. 19, pp. 585-590.

Hoult, D. P. and Weil, J. C. (1972), "Turbulent Plumes in a Laminar Cross Flow," Atmos. Environ., Vol. 6, pp. 513-531.

Jordinson, R. (1956), "Flow in a Jet Directed Normal to the Wind," Imperial College Aeronautics Department Paper No. 35, Imperial College of Science and Technology, London, England.

Keffer, J. F. (1969), "The Physical Nature of the Subsonic Jet in a Cross Stream," Analysis of a Jet in a Subsonic Crosswind, National Aeronautics and Space Administration SP-218, pp. 19-36.

Keffer, J. F. and Baines, W. D. (1963), "The Round Turbulent Jet in a Cross-Wind," J. Fluid Mech., Vol. 15, pp. 481-496.

Kotsovinos, N. E. (1975), "A Study of the Entrainment and Turbulence in a Plane Buoyant Jet," W. M. Keck Laboratory of Hydraulics and Water Resources, Report No. KH-R-32, California Institute of Technology, Pasadena, California.

Lin, J.-T. (1971), "Three Theoretical Investigations of Turbulent Jets, Part 3A Logarithmic Trajectory for Round Nonbuoyant Jets Discharging Perpendicularly into Cross Streams," Iowa Institute of Hydraulic Research Report No. 127, The University of Iowa, Iowa City, Iowa.

List, E. J. and Imberger, J. (1973), "Turbulent Entrainment in Buoyant Jets and Plumes," J. Hydr. Div., ASCE, Vol. 99, HY9, pp. 1461-1474.

List, E. J. (1976), Private Communication (unpublished manuscript).

Moore, D. J. (1974), "A Comparison of the Trajectories of Rising Buoyant Plumes with Theoretical/Empirical Models," Atmos. Environ., Vol. 8, pp. 441-457.

Morton, B. R., Taylor, G. I. and Turner, J. S. (1956), "Turbulent Gravitational Convection from Maintained and Instantaneous Sources," Proc. Roy. Soc. London, A234, pp. 1-23.

Morton, B. R. (1959), "Forced Plumes," J. Fluid Mech., Vol. 5, pp. 151-163.

Morton, B. R. (1971), "The Choice of Conservation Equations for Plume Models," J. Geophys. Res., Vol. 76, No. 30, pp. 7409-7416.

Pratte, B. D. and Baines, W. D. (1967), "Profiles of the Round Turbulent Jet in a Crossflow," J. Hydr. Div., ASCE, Vol. 93, HY6, pp. 53-64.

Priestley, C.H.B. and Ball, F. K. (1955), "Continuous Convection from an Isolated Source of Heat," Quarterly J. Roy. Meteor. Soc., Vol. 81, pp. 144-157.

Priestley, C.H.B. (1956), "A Working Theory of the Bent-Over Plume of Hot Gas," Quarterly J. Roy. Meteor. Soc., Vol. 82, pp. 165-176.

Prych, E. A. (1970), "Effects of Density Differences on Lateral Mixing in Open Channel Flows," W. M. Keck Laboratory of Hydraulics and Water Resources, Report No. KH-R-21, California Institute of Technology, Pasadena, California.

Roberts, P. J. W. (1977), "Dispersion of Buoyant Waste Water Discharged from Outfall Diffusers of Finite Length," Ph.D. Thesis, California Institute of Technology, Pasadena, California.

Rouse, H., Yih, C. S. and Humphreys, H. W. (1952), "Gravitational Convection from a Boundary Source," Tellus, Vol. 4, pp. 201-210.

Schatzmann, M. (1977), "A Mathematical Model for the Prediction of Plume Rise in Stratified Flows," Symposium on Turbulent Shear Flows, Pennsylvania State University, University Park, Pennsylvania, April 18-20, 1977, pp. 6.39-6.49.

Schlichting, H. (1968), Boundary Layer Theory, McGraw-Hill, 4th Edition.

Scorer, R. S. (1959), "The Behaviour of Chimney Plumes," International J. Air Poll., Vol. 1, pp. 198-220.

Shwartz, J. and Tulin, M. P. (1972), "Chimney Plumes in Neutral and Stable Surroundings," Atmos. Environ., Vol. 6, pp. 19-36.

Slawson, P. R. and Csanady, G. T. (1967), "On the Mean Path of Buoyant, Bent-Over Chimney Plumes," J. Fluid Mech., Vol. 28, No. 2, pp. 311-322.

Slawson, P. R. and Csanady, G. T. (1971), "The Effect of Atmospheric Conditions on Plume Rise," J. Fluid Mech., Vol. 47, No. 1, pp. 33-49.

Tennessee Valley Authority (1968), "Full-Scale Study of Plume Rise at Large Electric Generating Stations," TVA, Knoxville, Tennessee.

Vadot, L. (1965), "Study of Diffusion of Smoke Plumes into the Atmosphere (in French, Centre Interprofessionnel Technique d'Etudes de la Pollution Atmospherique, Paris, France).

Vizel, Y. M. and Mostinskii, I. L. (1965), "Deflection of a Jet Injected into a Stream," J. Eng. Phys., Vol. 8, No. 2, pp. 160-163.

Weil, J. C. (1968), "Model Experiments of High Stack Plumes," S.M. Thesis, Massachusetts Institute of Technology, Cambridge, Massachusetts.

Wood, R. W. (1934), Physical Optics, McMillan Company, 3rd Edition.

APPENDIX A

SUMMARY OF EXPERIMENTAL DATA

Table A.1 Summary of experiments to measure jet trajectories from photographs.

Run Number	Q cm^3/sec	D (cm)	$\Delta\rho/\rho_o$	U_A cm/sec	C_1	C_2	C_5	C_6
27	4.9	0.4	.0300	4.75	1.57	1.53		0.78
28	17.6	0.4	.0300	4.78	1.68	1.69		
29	8.2	0.4	.0300	6.76		1.58		0.81
30	16.1	0.4	.0300	6.28		1.52		
33	4.5	0.2	.0300	3.06	1.57	1.56		0.89
34	4.3	0.2	.0300	6.73		1.50		
35	7.2	0.2	.0300	6.76		1.70		
37	11.4	0.2	.0300	4.56	1.92	1.95		
2-0	8.6	0.2	.0334	2.37	1.88	1.77		
2-1	5.1	0.2	.0334	2.36	1.85			
2-2	5.4	0.2	.0334	4.57	1.70	1.52		1.20
2-3	5.2	0.2	.0334	8.02	1.51	1.42		1.43
2-4	10.0	0.2	.0334	8.12	1.92	1.62		
2-5	9.7	0.2	.0334	12.63		1.34		
2-6	15.3	0.2	.0334	12.63	1.61	1.48		
2-7	5.8	0.2	.0334	12.5		1.43		1.47
2-8	5.8	0.2	.0334	20.2		1.10		1.62
2-9	13.9	0.2	.0334	20.2	1.62	1.48		
2-10	18.3	0.2	.0334	20.2	1.93	1.76		
2-11	18.5	0.2	.0334	42.3		1.24		2.74
2-13	21.6	0.4	.0334	25.3	1.30	1.25		1.44
2-14	33.2	0.4	.0334	25.3	1.56	1.42		
2-15	7.5	0.4	.0334	12.1		1.37		1.28
2-16	13.9	0.4	.0334	12.0	1.61	1.43		1.38
2-17	29.5	0.4	.0334	12.0	1.65	1.54		
2-18	29.6	0.4	.0334	7.68	1.96	1.83		
2-19	5.8	0.4	.0334	2.69	1.80			
2-20	25.7	0.4	.0334	6.77	2.03	1.76		
2-21	6.3	0.4	.0334	16.9		1.14		1.14
2-22	8.7	0.4	.0334	37.2		1.04		1.36
2-23	17.1	0.4	.0334	37.2		0.99		1.49
2-24	25.2	0.8	.0334	19.8	0.82	0.94		0.97
2-25	39.3	0.8	.0334	19.9	1.02	0.95		1.40
2-26	15.8	0.8	.0334	12.0	0.83	0.96		1.04
2-27	6.4	0.8	.0334	16.18				0.85
2-29	33.7	0.8	.0334	9.64	1.38	1.33		1.13
2-30	40.1	0.8	.0540	35.6		0.74		1.07
2-31	38.3	0.8	.0540	19.1		1.07		1.01
2-32	19.8	0.8	.0540	12.7		1.04		0.97
2-33	32.1	0.8	.0540	12.8	1.29	1.23		1.13
2-34	6.5	0.8	.0540	7.22		1.09		0.86
2-35	6.4	0.8	.0540	5.15				0.73
2-36	7.0	0.8	.0540	2.45	1.30		0.74	0.76

Table A.1 (Continued)

Run Number	Q cm^3/sec	D (cm)	$\Delta\rho/\rho_o$	U_A cm/sec	C_1	C_2	C_5	C_6
4-1	10.7	1.0	.107	1.94			1.30	
4-2	9.3	1.0	.107	1.66			1.43	
4-3	12.2	1.0	.107	1.78			1.42	
4-4	9.0	1.0	.107	1.75			1.33	
4-5	7.0	1.0	.107	2.10			0.88	
4-6	12.0	1.0	.107	2.08			1.14	
4-7	12.0	1.0	.107	1.07			1.53	
4-8	10.2	1.0	.152	1.55			1.56	
4-9	7.5	1.0	.152	1.65			1.39	
4-10	20.3	1.0	.152	1.60			1.48	
4-11	11.2	1.0	.152	2.92			0.96	
4-12	11.2	1.0	.152	1.91			1.29	
4-13	18.9	1.0	.152	1.99			1.47	
4-14	9.9	1.0	.152	0.94			1.64	
4-15	9.4	1.0	.152	1.25			1.60	

Table A.2 Summary of experiments to measure jet trajectories and dilutions from concentration measurements with suction sampling system.

Run Number	Q cm^3/sec	D cm	$\Delta\rho/\rho_o$	U_A cm/sec	x cm	z cm	S_o
1	11.8	0.4	.0963	2.57	12.5	30	36.3
2	12.8	0.4	.0963	2.58	15	35	37.0
3	12.4	0.4	.0963	2.66	10	27	29.7
4	11.8	0.4	.0963	2.54	7.5	22	20.7
5	11.7	0.4	.0963	2.58	5	17	15.8
6	12.3	0.4	.0963	2.63	2.5	10	8.5
7	16.1	0.4	.0963	3.58	2.5	8	4.1
8	14.9	0.4	.0963	3.63	5	12	7.8
9	15.0	0.4	.0963	3.43	7.5	18	16.5
10	14.0	0.4	.0963	3.40	10	22	25.0
11	13.1	0.4	.0963	3.46	12.5	25	31.0
12	12.9	0.4	.0963	3.50	15	28	62.9
13	13.4	0.4	.0963	3.62	20	33	88.9
14	12.9	0.4	.0963	3.63	25	35	103.4
15	11.4	0.4	.102	2.42	2.5	10	10.8
16	12.1	0.4	.102	2.34	5	17	17.9
17	11.6	0.4	.102	2.50	7.5	21	23.4
18	11.2	0.4	.102	2.47	10	25	29.0
19	11.3	0.4	.102	2.55	12.5	33	52.5
20	13.0	0.4	.102	2.58	15	36	55.9
21	13.2	0.4	.102	2.58	20	39	71.6
22	13.4	0.4	.102	2.72	25	44	90.9
23	13.3	0.4	.102	3.40	25	33	62.0
24	12.7	0.4	.102	3.43	20	34	62.0
25	11.7	0.4	.102	3.40	15	32	68.2
26	12.0	0.4	.102	3.50	12.5	27	56.8
27	11.6	0.4	.102	3.59	10	23	48.7
28	11.8	0.4	.102	3.49	7.5	20	32.5
29	10.2	0.4	.102	3.46	5	14	18.2
30	10.3	0.4	.102	3.63	2.5	8	11
31	11.9	0.4	.102	2.38	2.5	11	12.1
32	10.3	0.4	.102	2.01	2.5	13	18.4
33	19.3	0.4	.102	1.95	2.5	16	13.9
34	7.5	0.4	.102	.994	2.5	17	19.5
35	15.1	0.4	.102	.939	2.5	23	18.4
36	14.5	0.4	.102	.918	2.5	23	19.5
37	23.4	0.4	.102	2.41	2.5	18	15.0
38	15.4	0.4	.102	1.33	2.5	21	16.8
39	6.7	0.4	.0980	2.63	5.0	13	33.0
40	17.5	0.4	.0980	2.71	5.0	19	18.9
41	8.18	0.4	.0980	1.84	5.0	21	44.0
42	16.6	0.4	.0980	1.93	5.0	26	23.3
43	4.8	0.4	.0980	1.36	5.0	21	41.7
44	8.0	0.4	.0980	.909	5.0	29	48.0
45	5.0	0.4	.0980	.813	5.0	35	58.7
46	8.7	0.4	.0980	2.28	5.0	18	28.3

Table A.2 (Continued)

Run Number	Q cm^3/sec	D cm	$\Delta\rho/\rho_o$	U_A cm/sec	x cm	z cm	S_o
47	14.0	0.4	.0980	1.92	5	24	27.3
48	13.5	0.4	.0980	2.16	5	22	22
49	6.0	0.4	.0980	2.25	5	14	28.8
50	9.7	0.4	.0980	2.29	5	17	23.0
51	14.8	0.4	.0980	2.95	5	17	19.8
52	8.4	0.4	.0980	2.90	5	13	21.6
53	12.4	0.4	.0980	3.30	5	15	25.1
54	9.6	0.4	.0980	3.31	5	13	22.6
55	12.4	0.4	.0980	3.98	5	13	22.6
56	6.7	0.4	.0980	3.93	5	10	25.9
57	15.5	0.4	.0980	2.91	5	20	20.3
58	18.8	0.4	.0980	2.99	5	22	19.6
59	12.5	0.4	.0980	2.45	5	21	23.3
60	5.2	0.4	.0980	1.84	5	18	31.7
61	12.8	0.4	.0980	3.93	5	13	16.1
62	14.6	0.4	.0980	1.82	5	22	24.4
63	3.9	0.4	.0251	2.11	7.5	15	49.5
64	3.9	0.4	.0251	2.12	15.0	19	102
65	3.9	0.4	.0251	2.04	22.5	25	149
66	3.9	0.4	.0251	2.08	30.0	28	234
67	3.9	0.4	.0251	2.04	37.5	30	269
68	3.9	0.4	.0251	2.18	45.0	32	389
69	5.6	0.4	.0503	4.26	7.5	12	47.4
70	5.6	0.4	.0503	4.20	15.0	14	77.4
71	5.6	0.4	.0503	4.19	22.5	17	167
72	5.6	0.4	.0503	4.26	30.0	17	202
73	5.6	0.4	.0503	4.18	37.5	23	249
74	5.6	0.4	.0503	4.11	45.0	24	268
75	11.1	0.4	.0497	3.00	5	17	27.5
76	11.1	0.4	.0497	2.92	10	23	53.2
77	11.1	0.4	.0497	2.93	15	28	90.0
78	11.1	0.4	.0497	2.93	20	30	143
79	11.1	0.4	.0497	2.81	25	34	142
80	7.9	0.4	.0249	2.91	7.5	15	32.3
81	7.9	0.4	.0249	2.83	15	22	54.4
82	7.9	0.4	.0249	2.91	22.5	24	128
83	7.9	0.4	.0249	2.93	30	26	137
84	7.9	0.4	.0249	2.92	37.5	29	157
85	7.9	0.4	.0249	2.91	45.0	30	204
86	7.9	0.4	.0254	2.95	30	26	80.8
87	7.9	0.4	.0254	2.94	37.5	30	95.4
88	7.9	0.4	.0254	2.93	45	31	108
89	44.5	0.8	.0246	3.98	4.0	18	12.2
90	44.5	0.8	.0246	3.97	8.0	26	16.2

Table A.2 (Continued)

Run Number	Q cm^3/sec	D cm	$\Delta\rho/\rho_o$	U_A cm/sec	x cm	z cm	S_o
91	44.5	0.8	.0246	3.99	12.0	32	26.2
92	44.5	0.8	.0246	3.97	16.0	33	30.7
93	44.5	0.8	.0246	3.84	20.0	37	40.3
94	44.5	0.8	.0247	5.05	4.0	16	--
95	44.5	0.8	.0247	5.06	16.0	31	--
96	7.9	0.4	.0249	5.73	7.5	9	26.4
97	7.9	0.4	.0249	5.68	15	12	39.3
98	7.9	0.4	.0249	5.74	22.5	13	59.7
99	7.9	0.4	.0249	5.80	30.0	15	74.8
100	7.9	0.4	.0249	5.94	37.5	16	80.6
101	7.9	0.4	.0249	5.67	45.0	17	88.2
102	15.7	0.4	.0254	2.10	3	20	14.7
103	15.7	0.4	.0254	2.05	6	26	22.5
104	15.7	0.4	.0254	2.08	9	30	33.2
105	15.7	0.4	.0254	2.11	12	35	37.6
106	15.7	0.4	.0254	2.11	15	39	46.9
107	20.1	0.8	0	2.00	2	12.6	6.46
108	20.1	0.8	0	2.04	4	16.7	8.80
109	20.1	0.8	0	1.89	6	19.6	11.0
110	20.1	0.8	0	1.84	8	21.9	14.9
111	40.2	0.8	0	3.87	2	12.6	5.13
112	40.2	0.8	0	4.00	4	17.7	7.06
113	40.2	0.8	0	3.68	6	22.6	13.5
114	40.2	0.8	0	4.05	8	22.9	15.4
115	30.2	0.8	0	2.50	3	17.8	20.6
116	30.2	0.8	0	1.97	6	24.4	23.7
117	30.2	0.8	0	1.66	9	31.2	26.8
118	30.2	0.8	0	2.12	12	34.2	35.9
119	45.2	0.8	0	3.06	3	17.8	7.94
120	45.2	0.8	0	3.04	6	26.4	12.2
121	45.2	0.8	0	2.97	9	30.2	15.9
122	45.2	0.8	0	2.91	12	36.2	18.2
123	40.2	0.8	0	2.17	2	15.7	5.53
124	40.2	0.8	0	2.34	4	21.9	10.3
125	40.2	0.8	0	2.16	6	28.4	12.5
126	40.2	0.8	0	2.18	8	33.1	15.7

Table A.3 Summary of experiments to measure equilibrium heights of rise from photographs.

Run Number	Q cm^3/sec	D (cm)	$\Delta\rho/\rho_o$	U_A cm/sec	ε (sec^{-2})	Z_e cm
1	24.2	0.4	~0	3.76	.112	22.1
2	40.3	0.4	~0	8.69	.112	26.3
3	45.6	0.4	~0	8.67	.112	25.1
4	35.9	0.4	~0	4.88	.112	27.5
6	32.1	0.4	~0	4.40	.112	29.0
7	18.7	0.4	~0	2.70	.112	17.9
8	19.2	0.4	~0	1.04	.112	21
9	18.4	0.4	~0	1.37	.112	22
10	18.7	0.4	~0	1.91	.112	23
11	18.7	0.4	~0	4.86	.112	14
12	18.9	0.4	~0	9.80	.112	11
13	34.4	1.0	.1096	7.19	.103	32.3
14	54.0	1.0	.1096	7.22	.103	39.3
15	18.2	1.0	.1096	4.70	.103	20
16	11.2	1.0	.1096	4.68	.103	22.1
17	23.2	1.0	.1096	2.82	.103	40
18	8.6	1.0	.1096	2.39	.103	35
19	7.5	1.0	.1096	1.93	.103	35.5
25	49.8	1.0	.1076	13.7	.209	20.5
26	50.3	1.0	.1076	9.55	.209	22.5
27	50.4	1.0	.1076	7.04	.209	29.8
28	33.7	1.0	.1076	4.63	.209	31.8
29	26.2	1.0	.1076	3.52	.209	35.3
30	15.6	1.0	.1076	2.50	.209	35.8
31	12.2	1.0	.1076	1.68	.209	36.3
32	12.3	1.0	.1076	1.20	.209	37.8
42	9.3	1.0	.0648	1.83	.123	30
43	9.2	1.0	.0648	1.46	.123	31.5
44	9.3	1.0	.0648	3.15	.123	21
45	9.2	1.0	.0648	3.76	.123	20
46	9.2	1.0	.0648	5.47	.123	12
47	9.2	1.0	.0648	7.0	.123	12
48	46.7	1.0	.0648	10.2	.123	23
49	46.7	1.0	.0648	12.0	.123	22.5
50	47.1	1.0	.0648	4.12	.123	31.5
57	27.7	1.0	.0652	4.64	.0636	22.5
58	11.1	1.0	.0652	7.93	.0636	19.5
59	17.2	1.0	.0652	7.58	.0636	21.5
60	9.8	1.0	.0652	7.58	.0636	20.5
61	7.6	1.0	.0652	4.85	.0636	19.5
62	11.2	1.0	.0652	4.86	.0636	27.5
63	17.7	1.0	.0652	3.51	.0636	34
64	8.6	1.0	.0652	3.53	.0636	26

Table A.3 (Continued)

Run Number	Q cm^3/sec	D (cm)	$\Delta\rho/\rho_o$	U_A cm/sec	ε (sec^{-2})	Z_e cm
71	12.3	0.2	.0303	5.08	.215	22
72	17.6	0.2	.0303	5.04	.215	26.5
73	11.7	0.2	.0303	3.50	.215	22.5
74	21.4	0.2	.0303	7.30	.215	25.5
75	20.8	0.2	.0303	11.2	.215	20.5
76	10.8	0.2	.0303	3.67	.215	22.5
77	7.0	0.2	.0303	2.86	.215	16.5
78	13.4	0.2	.0303	3.85	.215	25.5
79	13.0	0.2	.0303	2.17	.215	29
91	18.1	0.2	.0138	6.80	.0824	27
92	8.5	0.2	.0138	6.80	.0824	15
93	7.7	0.2	.0138	9.34	.0824	11.5
94	20.2	0.2	.0138	9.29	.0824	26.5
95	19.8	0.2	.0138	12.9	.0824	22
96	8.6	0.2	.0138	12.9	.0824	10
97	9.2	0.2	.0138	4.56	.0824	22
98	16.2	0.2	.0138	5.47	.0824	30
99	6.6	0.2	.0138	5.45	.0824	14.5
100	20.7	0.2	.0138	11.7	.0824	22.5
101	7.1	0.2	.0138	3.56	.0824	17.5
102	13.1	0.2	.0138	2.97	.0824	29.5
103	7.6	0.2	.0138	2.97	.0824	21.5
104	7.2	0.2	.0138	2.05	.0824	23.5
105	7.6	0.2	.0138	1.43	.0824	24
106	18.8	0.2	.0058	1.42	.330	25
107	12.4	0.2	.0058	1.40	.330	17.5
108	8.2	0.2	.0058	1.40	.330	14.5
109	4.8	0.2	.0058	1.39	.330	10
110	4.3	0.2	.0058	1.13	.330	10
111	17.5	0.2	.0058	1.15	.330	25
112	15.0	0.2	.0058	1.15	.330	22.5
113	6.2	0.2	.0058	1.15	.330	11.5
114	9.4	0.2	.0058	1.15	.330	15
115	12.1	0.2	.0058	1.17	.330	19
116	12.2	0.2	.0058	1.66	.330	19
117	16.0	0.2	.0058	1.65	.330	24
118	9.8	0.2	.0058	1.65	.330	16
119	16.8	0.2	.0058	1.64	.330	30
120	7.0	0.2	.0058	1.64	.330	12
121	4.6	0.2	.0058	1.65	.330	9
122	5.6	0.2	.0039	1.57	.227	13.5
123	16.6	0.2	.0039	1.57	.227	25
124	12.8	0.2	.0039	1.51	.227	21.5
125	10.5	0.2	.0039	1.53	.227	16.5
126	8.0	0.2	.0039	1.53	.227	15.5
127	7.0	0.2	.0039	1.39	.227	15
128	4.7	0.2	.0039	1.39	.227	10.5
129	9.2	0.2	.0039	1.39	.227	16
130	11.8	0.2	.0039	1.38	.227	21.5

Table A.3 (Continued)

Run Number	Q cm^3/sec	D (cm)	$\Delta\rho/\rho_o$	U_A cm/sec	ε (sec^{-2})	Z_e cm
131	14.4	0.2	.0039	1.39	.227	24
132	13.4	0.2	.0039	1.10	.227	23.5
133	16.4	0.2	.0039	1.11	.227	27.5
134	5.4	0.2	.0039	1.11	.227	10
135	7.6	0.2	.0039	1.10	.227	14.5
136	11.1	0.2	.0039	1.11	.227	18
137	21.1	0.2	.0039	8.05	.227	23.5
138	20.9	0.2	.0039	5.80	.227	28
139	21.0	0.2	.0039	10.0	.227	21.5
140	6.9	0.2	.0039	2.87	.227	14
141	15.8	0.2	.0039	4.42	.227	24
142	8.8	0.2	-.0011	4.48	.151	16
143	5.6	0.2	-.0011	4.49	.151	10
144	12.8	0.2	-.0011	5.18	.151	21
145	9.7	0.2	-.0011	5.16	.151	17
146	4.4	0.2	-.0011	5.18	.151	7.5
147	4.3	0.2	-.0011	5.88	.151	7.5
148	6.96	0.2	-.0011	5.88	.151	12
149	9.1	0.2	-.0011	5.89	.151	16
150	12.3	0.2	-.0011	5.89	.151	20
151	14.4	0.2	-.0011	5.88	.151	22.5
152	14.9	0.2	-.0011	7.46	.151	20
153	10.9	0.2	-.0011	7.46	.151	15.5
154	5.8	0.2	-.0011	7.46	.151	8.5
155	5.8	0.2	-.0011	8.67	.151	8.0
156	10.7	0.2	-.0011	9.26	.151	12.5
157	16.4	0.2	-.0011	9.26	.151	21.0
158	20.8	0.2	-.0011	9.29	.151	25.5
159	20.7	0.2	-.0011	12.7	.151	21.5
160	7.5	0.2	-.0011	12.7	.151	7.5
161	12.5	0.2	-.0011	12.7	.151	11.5
162	14.8	1.0	.1249	1.75	.273	35
163	8.8	1.0	.1249	1.50	.273	28
164	8.8	1.0	.1249	1.48	.273	27.5
165	3.9	1.0	.1249	1.50	.273	19.5
166	14.8	1.0	.1249	1.48	.273	38.5
167	14.3	1.0	.1249	2.37	.273	30
182	39.2	1.0	.1260	9.29	.125	26.5
183	21.2	1.0	.1260	9.31	.125	22
184	19.6	1.0	.1260	7.41	.125	21.5
185	9.5	1.0	.1260	7.41	.125	18.5
186	35.9	1.0	.1260	7.41	.125	28
187	36.5	1.0	.1260	5.54	.125	33.5
188	20.3	1.0	.1260	5.54	.125	27.5
189	12.8	1.0	.1260	5.53	.125	23
190	7.2	1.0	.1260	5.54	.125	18
191	16.5	1.0	.1260	4.62	.125	23.5
201	11.1	1.0	.0741	1.92	.169	29

Table A.3 (Continued)

Run Number	Q cm^3/sec	D (cm)	$\Delta\rho/\rho_o$	U_A cm/sec	ε (sec^{-2})	Z_e cm
202	7.17	1.0	.0741	1.90	.169	24
203	4.33	1.0	.0741	1.89	.169	20.5
204	4.12	1.0	.0741	1.54	.169	20.5
205	7.44	1.0	.0741	1.53	.169	25.5
206	9.74	1.0	.0741	1.54	.169	31
207	11.9	1.0	.0741	1.53	.169	34
216	7.0	1.0	.0761	4.66	.185	17.5
217	4.7	1.0	.0761	4.67	.185	14
218	13.4	1.0	.0761	4.68	.185	22
219	17.6	1.0	.0761	4.69	.185	23
220	26.6	1.0	.0761	4.69	.185	26
221	36.9	1.0	.0761	4.71	.185	34
222	43.9	1.0	.0761	4.71	.185	36
223	43.9	1.0	.0761	7.51	.185	24.5
224	32.2	1.0	.0761	7.53	.185	23
225	21.1	1.0	.0761	7.53	.185	18.5
226	11.5	1.0	.0761	7.53	.185	14
227	7.0	1.0	.0761	7.51	.185	12
228	6.6	1.0	.0761	10.8	.185	11
229	44.4	1.0	.0761	10.8	.185	23
230	33.0	1.0	.0761	10.9	.185	20.5

Table A.4 Summary of experiments to measure maximum heights of rise and associated dilution from measurements with light probe,

Run Number	Q cm^3/sec	D cm	$\Delta\rho/\rho_o$	U_A cm/sec	ε sec^{-2}	Z_m cm	S_m
004	6.1	1.0	.0265	1.63	.110	22.6	--
012	4.8	0.2	.0046	1.32	.0775	24.5	77.2
013	6.5	0.2	.0046	1.32	.0775	29.8	76.0
014	8.0	0.2	.0046	1.30	.0775	32.5	72.5
015	9.6	0.2	.0046	1.31	.0075	35.0	71.9
016	4.9	0.2	.0047	1.67	.0354	27.9	--
017	6.3	0.2	.0047	1.66	.0354	36.4	--
018	7.5	0.2	.0047	1.66	.0354	37.8	--
019	8.5	0.2	.0047	1.66	.0354	45.1	--
020	4.6	0.2	.0042	1.42	.203	18.5	43.4
021	6.1	0.2	.0042	1.39	.203	22.7	53.5
022	8.9	0.2	.0042	1.45	.203	29.7	48.8
023	10.6	0.2	.0042	1.45	.203	34.0	54.9
024	12.8	0.2	.0042	1.44	.203	37.5	61.9
025	4.2	0.2	.0047	1.53	.079	22.6	--
026	6.1	0.2	.0047	1.54	.079	27.6	--
027	7.0	0.2	.0047	1.55	.079	32.8	--
029	10.1	0.2	.0047	1.52	.079	41.5	--
030	4.3	1.0	.1061	1.53	.0871	33.6	--
031	5.4	1.0	.1061	1.58	.0871	35.8	--
032	6.9	1.0	.1061	1.56	.0871	43.1	--
034	4.3	1.0	.1061	1.45	.0935	30.2	--
035	4.8	1.0	.1061	1.38	.0935	36.9	--
036	5.3	1.0	.1061	1.44	.0935	40.1	--
037	5.9	1.0	.1061	1.39	.0935	44.9	--
038	5.1	1.0	.1061	1.33	.0935	42.5	--
040	5.9	1.0	.1122	1.31	.167	31.6	3120
041	4.3	1.0	.1122	1.31	.167	33.0	1430
042	4.8	1.0	.1122	1.31	.167	35.0	1220
043	5.4	1.0	.1122	1.31	.167	34.6	1000
044	5.9	1.0	.1122	1.31	.167	37.0	862
061	4.3	1.0	.0528	1.91	.068	26.2	--
069	5.2	0.4	.0524	1.99	.105	27.9	--
070	5.3	0.4	.0524	2.10	.105	27.2	--
071	5.9	0.4	.0524	2.51	.105	27.2	--
072	5.7	0.4	.0524	2.89	.105	27.2	--
073	8.5	0.4	.0524	2.96	.105	27.4	--
077	6.5	0.4	.0230	2.01	.0864	24.6	--
078	4.7	0.4	.0230	2.01	.0864	21.2	--
079	5.1	0.4	.0230	2.40	.0864	20.1	--
080	5.5	0.4	.0230	2.77	.0864	20.5	--
081	7.1	0.4	.0230	1.95	.0864	22.6	--
086	5.6	1.0	.0233	2.17	.104	14.8	--
087	6.4	1.0	.0233	2.62	.104	15.4	--
088	8.0	1.0	.0233	3.08	.104	15.4	--

Table A.4 (Continued)

Run Number	Q cm^3/sec	D cm	$\Delta\rho/\rho_o$	U_A cm/sec	ε sec^{-2}	Z_m cm	S_m
089	13.4	1.0	.0233	3.06	.104	22.8	--
090	12.3	1.0	.0233	2.63	.104	24.6	746
091	11.9	1.0	.0233	2.22	.104	24.6	585
092	16.1	1.0	.0233	2.59	.104	24.1	422
093	17.7	1.0	.0233	2.94	.104	24.1	422
094	19.3	1.0	.0233	3.39	.104	24.1	422
095	3.9	1.0	.0709	1.43	.171	23.2	128
096	5.4	1.0	.0709	1.41	.171	28.1	122
097	7.2	1.0	.0709	1.45	.171	33.5	107
098	9.7	1.0	.0709	1.44	.171	35.7	101
099	12.3	1.0	.0709	1.44	.171	38.1	93.3
100	4.7	0.2	.0232	2.44	.0890	21.6	--
101	4.8	0.2	.0232	2.73	.0890	21.6	--
102	5.4	0.2	.0232	3.02	.0890	21.6	--
103	6.8	0.2	.0232	3.33	.0890	26.7	--
104	6.4	0.2	.0232	2.95	.0890	26.7	--
105	5.4	0.2	.0232	2.55	.0890	25.5	--
106	7.5	0.2	.0232	3.39	.0890	30.8	--
107	8.6	0.2	.0232	3.57	.0890	33.0	--
108	4.2	0.4	.0236	2.53	.0371	22.4	--
109	4.3	0.4	.0236	3.01	.0371	21.7	--
110	4.2	0.4	.0236	2.17	.0371	22.4	--
111	5.9	0.4	.0236	2.21	.0371	25.7	--
112	5.9	0.4	.0236	2.76	.0371	24.5	--
113	7.6	0.4	.0236	2.74	.0371	27.2	--
114	7.4	0.4	.0236	2.35	.0371	27.8	--
115	17.1	1.0	.0286	1.60	.202	26.0	23.8
116	6.4	1.0	.0286	1.58	.202	18.6	33.1
122	4.6	0.4	.0114	2.46	.075	12.1	--
123	6.4	0.4	.0114	2.55	.075	16.0	--
124	5.7	0.4	.0114	3.18	.075	14.0	--
125	7.9	0.4	.0114	3.14	.075	17.1	--
126	7.9	0.4	.0114	3.79	.075	16.5	--
127	12.3	0.4	.0114	3.81	.075	23.0	--
128	9.4	0.4	.0114	3.23	.075	20.3	--
129	7.5	0.4	.0117	3.05	.0700	16.9	44.6
130	12.0	0.4	.0117	3.10	.0700	24.7	39.4
131	13.9	0.4	.0117	3.61	.0700	25.8	35.3
132	10.7	0.4	.0117	3.72	.0700	20.8	36.7
133	6.7	0.4	.0117	3.41	.0700	13.8	41.6
134	6.5	0.4	.0117	2.77	.0700	15.6	35.0
141	17.1	1.0	.0117	1.30	.0742	30.5	21.2
142	6.5	1.0	.0117	1.41	.0742	19.9	27.8
143	8.6	1.0	.0117	3.73	.0742	10.5	56.2
144	11.2	1.0	.0117	3.73	.0742	12.5	58.0
145	6.7	1.0	.0117	2.89	.0742	12.0	47.0
146	5.4	0.2	.0144	1.55	.0630	30.5	68.4
152	5.4	0.4	.0143	3.15	.0623	13.9	54.0

Table A.4 (Continued)

Run Number	Q cm^3/sec	D cm	$\Delta\rho/\rho_o$	U_A cm/sec	ϵ sec^{-2}	Z_m cm	S_m
158	9.6	1.0	.0144	1.56	.0470	14.4	31.3
163	9.9	1.0	.0141	3.11	.0595	13.2	52.9
153	5.4	0.4	.0143	3.17	.0623	15.4	62.3